

Alma Mater Studiorum – Università di Bologna

**DOTTORATO DI RICERCA IN  
SCIENZE BIOMEDICHE E NEUROMOTORIE**

Ciclo XXXI

**Settore Concorsuale: 05/E1 – Biochimica generale e biochimica clinica  
Settore Scientifico Disciplinare: BIO/10**

**Bioenergetics of cancer cells in anoxia  
and  
role of the miRNAs in melanoma resistance to targeted therapies**

**Presentata da: Dott.ssa Anna Costanzini**

**Coordinatore Dottorato**

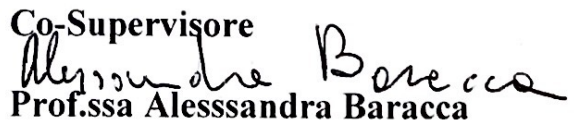
**Prof. Pietro Cortelli**

**Supervisore**



**Prof. Giancarlo Solaini**

**Co-Supervisore**



**Prof.ssa Alessandra Baracca**

**Esame finale anno 2019**



## Abstract

Tumours are characterized by a metabolic rewiring that helps transformed cells to survive in harsh conditions.

The endogenous inhibitor of the ATP-synthase  $IF_1$  is overexpressed in several tumours and it has been proposed to drive metabolic adaptation. In ischemic normal-cells,  $IF_1$  acts limiting the ATP consumption by the reverse activity of the ATP-synthase, activated by  $\Delta\Psi_m$  collapse. Conversely,  $IF_1$  role in cancer cells is still unclear. It has been proposed that  $IF_1$  favours cancer survival by preventing energy dissipation in low oxygen availability, a frequent condition in solid tumours. Our previous data proved that in cancer cells hypoxia does not abolish  $\Delta\Psi_m$ , avoiding the ATP-synthase reversal and  $IF_1$  activation. In this study, we investigated the bioenergetics of cancer cells in conditions mimicking anoxia to evaluate the possible role of  $IF_1$ . Data obtained indicate that also in cancer cells the  $\Delta\Psi_m$  collapse induces the ATP-synthase reversal and its inhibition by  $IF_1$ . Moreover, we demonstrated that upon uncoupling conditions,  $IF_1$  favours cancer cells growth preserving ATP levels and energy charge. We also showed that in these conditions  $IF_1$  favours the mitochondrial mass renewal, a mechanism we proposed driving apoptosis-resistance.

Cancer adaptability is also associated with the onset of therapy resistance, the major challenge for melanoma treatment. Recent studies demonstrated that miRNAs dysregulation drive melanoma progression and drug-resistance by regulating tumour-suppressor and oncogenes. In this context, we attempted to identify and characterize miRNAs driving resistance to vemurafenib in patient-derived metastatic melanoma cells BRAFV600E-mutated. Our results highlighted that several oncogenic pathways are altered in resistant cells, indicating the complexity of both drug-resistance phenomena and miRNAs action. Profiling analysis identified a group of dysregulated miRNAs conserved in vemurafenib-resistance cells from distinct patients, suggesting that they ubiquitously drive drug-resistance. Functional studies performed with a first miRNA confirmed its pivotal role in resistance towards vemurafenib.



# Index

<b>1</b>	<b>INTRODUCTION .....</b>	<b>1</b>
<b>1.1</b>	<b>Mitochondria .....</b>	<b>1</b>
1.1.1	Ultrastructure of the mitochondria .....	2
1.1.2	Mitochondrial genome .....	5
<b>1.2</b>	<b>The oxidative phosphorylation.....</b>	<b>7</b>
1.2.1	The Electron Transport Chain (ETC) .....	7
1.2.2	The F <sub>1</sub> F <sub>0</sub> -ATP synthase .....	9
1.2.2.1	Structure of the F <sub>1</sub> F <sub>0</sub> -ATP synthase .....	10
1.2.2.2	F <sub>1</sub> F <sub>0</sub> -ATP synthase and ATP synthesis process .....	12
1.2.2.3	Modulation of the F <sub>1</sub> F <sub>0</sub> -ATP synthase activity .....	14
<b>1.3</b>	<b>Mitochondria and cancer .....</b>	<b>15</b>
<b>1.4</b>	<b>The ATPase Inhibitory Factor 1 IF<sub>1</sub> .....</b>	<b>16</b>
1.4.1	IF <sub>1</sub> and cancer.....	19
<b>1.5</b>	<b>Mitochondria membrane potential and homeostasis.....</b>	<b>21</b>
<b>1.6</b>	<b>Mitochondria quality control.....</b>	<b>24</b>
1.6.1	Biogenesis of Mitochondria.....	25
1.6.2	Mitochondria dynamics: Fusion and Fission .....	27
1.6.3	Mitochondrial degradation.....	28
1.6.3.1	The PINK1/Parkin mediated mitophagy.....	30
1.6.3.2	BNIP3 and BNIP3L/NIX mediated mitophagy.....	32
<b>1.7</b>	<b>Cutaneous malignant melanoma.....</b>	<b>33</b>
1.7.1	B-raf signalling and BRAFV600E melanoma.....	35
1.7.2	Melanoma treatment.....	36
1.7.2.1	Immunotherapeutic antibodies .....	37
1.7.2.2	MAPK pathway-targeted therapy and vemurafenib .....	38
1.7.2.3	Limitation of the melanoma therapies and drug resistance.....	39
1.7.3	miRNAs and the plasticity of melanoma .....	41
<b>1.8</b>	<b>Intracellular pathways related to cancer progression .....</b>	<b>44</b>
1.8.1	Wnt/ $\beta$ -catenin canonical pathway .....	44

1.8.2	TGF- $\beta$ pathway.....	46
1.8.3	Hedgehog pathway.....	47
1.8.4	p53 pathway.....	49
<b>2</b>	<b>AIMS OF THE STUDY.....</b>	<b>50</b>
<b>3</b>	<b>MATERIALS AND METHODS.....</b>	<b>53</b>
<b>3.1</b>	<b>Cell cultures.....</b>	<b>53</b>
3.1.1	Human Osteosarcoma cell lines.....	53
3.1.2	Human Melanoma cell lines.....	53
3.1.3	Phoenix retrovirus-producer cell line.....	54
<b>3.2</b>	<b>Bacterial transformation and plasmids purification.....</b>	<b>54</b>
<b>3.3</b>	<b>Production of stably IF<sub>1</sub>-silenced GFP-negative osteosarcoma clones.....</b>	<b>55</b>
3.3.1	Phoenix cell line transfection and collection of viruses.....	55
3.3.2	143B cell line infection and selection of clones.....	56
<b>3.4</b>	<b>Generation of mtRFP-positive osteosarcoma clones.....</b>	<b>56</b>
3.4.1	Osteosarcoma cell lines transfection and selection of mtRFP-positive clones.....	56
3.4.2	mtRFP-fluorescence intensity fluorometric analysis.....	57
<b>3.5</b>	<b>miRNA mimic and miRNA inhibitor transfection.....</b>	<b>57</b>
<b>3.6</b>	<b>Cell growth evaluation.....</b>	<b>58</b>
<b>3.7</b>	<b>Cell viability assessment.....</b>	<b>59</b>
<b>3.8</b>	<b>Biochemical assays.....</b>	<b>59</b>
3.8.1	Glucose consumption and lactate release measurements.....	59
3.8.2	Cellular ATP content assay.....	60
3.8.3	ADP/ATP ratio assay.....	60
3.8.4	Mitochondrial ATP hydrolysis assay.....	61
3.8.5	Citrate synthase activity assay.....	62
<b>3.9</b>	<b>Flow cytometry assay of mitochondrial membrane potential.....</b>	<b>63</b>
<b>3.10</b>	<b>Fluorescence microscopy.....</b>	<b>63</b>
<b>3.11</b>	<b>SDS-PAGE and Western blot analysis.....</b>	<b>64</b>
<b>3.12</b>	<b>Evaluation of mtRFP and LC3-YFP colocalization in fluorescence microscopy to asses mitophagy activation.....</b>	<b>65</b>

<b>3.13</b>	<b>IC50 calculation by MTT assay .....</b>	<b>66</b>
<b>3.14</b>	<b>Dual-luciferase reporter assay .....</b>	<b>68</b>
<b>3.15</b>	<b>RNA extraction.....</b>	<b>69</b>
<b>3.16</b>	<b>miRNAs profiling with Nanostring array.....</b>	<b>70</b>
<b>3.17</b>	<b>Quantitative reverse transcription PCR.....</b>	<b>70</b>
3.17.1	Quantification of miRNAs .....	71
3.17.2	Quantification of mRNAs .....	71
<b>3.18</b>	<b>Bioinformatic analysis.....</b>	<b>72</b>
<b>3.19</b>	<b>Cell cycle determination.....</b>	<b>72</b>
<b>3.20</b>	<b>Statistical analysis.....</b>	<b>73</b>
<b>4</b>	<b>RESULTS .....</b>	<b>74</b>
<b>4.1</b>	<b>Role of IF<sub>1</sub> in the bioenergetics of cancer cells in anoxia.....</b>	<b>74</b>
4.1.1	Production of IF <sub>1</sub> -silenced and GFP-negative stable clones from 143B cells.....	75
4.1.2	Production of osteosarcoma clones stably expressing the mtRFP.....	77
4.1.2.1	Characterization of mtRFP osteosarcoma clones.....	78
4.1.2.1.1	Assessment of the relation between measured fluorescence intensity and quantity of mtRFP expressed.....	78
4.1.2.1.2	Monitoring of the mtRFP fluorescence intensity and correlation with citrate synthase activity .....	80
4.1.2.1.3	Assessments of the mtRFP response in conditions inducing variations of the mitochondrial mass.....	82
4.1.2.1.4	Cell growth, CS activity and IF <sub>1</sub> protein levels assessment in mtRFP-clones .....	84
4.1.3	Evaluation of the IF <sub>1</sub> impact on the biology and bioenergetics of osteosarcoma cells in anoxia-mimicking conditions.....	86
4.1.3.1	Cell growth and viability assays .....	87
4.1.3.2	Glycolytic flux assessment and intracellular ATP levels.....	89
4.1.3.2.1	Mitochondrial membrane potential evaluation in cell in anoxia-mimicking conditions.....	91
4.1.3.3	Steady-state ATP levels and F <sub>1</sub> F <sub>0</sub> -ATP synthase ATPase activity assessments.....	95
4.1.3.4	Mitochondrial mass assessments.....	96
4.1.3.5	Mitochondrial turnover evaluation.....	98
4.1.3.6	Cellular energy charge assessment.....	104
4.1.3.7	OXPHOS complexes and IF <sub>1</sub> protein levels assessment.....	105

<b>4.2</b>	<b>Role of the miRNAs in the resistance to BRAF-inhibitors in metastatic melanoma.....</b>	<b>109</b>
4.2.1	Characterization of M21 and M21R melanoma cells .....	110
4.2.2	Assessment of the signalling pathways related to cancer progression.....	112
4.2.2.1	Wnt/ $\beta$ -catenin signalling pathway.....	112
4.2.2.2	TGF- $\beta$ signalling pathway .....	116
4.2.2.3	Sonic-Hedgehog signalling pathway.....	118
4.2.2.4	p53 signalling pathway.....	119
4.2.3	Identification of the miRNAs differentially expressed in melanoma cells resistant to vemurafenib.....	121
4.2.4	Assessment of the effect of mir-425-5p levels on the tolerance to vemurafenib in M21 and M21R cells.....	122
4.2.4.1	Effect of mir-425-5p overexpression in vemurafenib-sensitive cells .....	125
4.2.4.1.1	Cell growth assessment.....	125
4.2.4.1.2	Cell cycle evaluation .....	126
4.2.4.1.3	Metabolic activity assay and IC <sub>50</sub> calculation .....	128
4.2.4.1.4	Signalling of cancer-related pathways in M21 cells upon mir-425-p overexpression.....	129
4.2.4.2	Effect of mir-425-5p inhibition in vemurafenib-resistant melanoma cells .....	131
4.2.4.2.1	Cell growth assessment.....	131
4.2.4.2.2	Cell cycle evaluation .....	132
4.2.4.2.3	Metabolic activity assay and IC <sub>50</sub> calculation.....	134
4.2.4.2.3	Signalling of cancer-related pathways in M21R cells upon mir-425-p inhibition ...	135
<b>5</b>	<b>DISCUSSION.....</b>	<b>137</b>
<b>6</b>	<b>BIBLIOGRAPHY .....</b>	<b>151</b>
<b>7</b>	<b>IMAGES SOURCES .....</b>	<b>170</b>





# 1 Introduction

## 1.1 Mitochondria

Mitochondria are double-membraned organelles frequently named the "power-houses" of the cells, because of their crucial role in cellular energy production by synthesizing ATP [1]. The organelles were cytologically described for the first time in 1890 by Richard Altmann, whose proposed that the observed "granules" were elementary organism living inside cells, accomplishing metabolic processes. Altmann's intuition anticipated the now almost fully accepted endosymbiotic theory, positing that mitochondria derive from a proteobacterium internalized by a pre-eukaryotic cell as a symbiont then coevolved to originate a single organism, the eukaryotic cell [2]. A few years later, in 1898, Carl Benda coined the "mitochondrion" term, derived from the Greek "mitos," meaning "thread", and "chondros," signify "granule," referring to the shapes of the organelles visible by the light microscope as strands or small singular grains [3]. Benda's definition already reflected the highly-dynamic nature of the mitochondria, whose size, ultrastructure, number and network morphology, are constantly modified in response to the metabolic and pathologic conditions undergone by the organelles and the whole cell. This morphological plasticity feature gives mitochondria great functional flexibility useful to satisfy cellular requirements [4]. Besides their pivotal role in ATP production via oxidative phosphorylation, mitochondria drive a wide spectrum of other essential cellular functions, controlling energy expenditure and nutrient usage [5], intracellular  $\text{Ca}^{2+}$  reservoirs [6], cell death [7] and several pathways by regulating their key mediators, such as reactive oxygen species (ROS) [8]. All these processes are finely coordinated and modulated to ensure the cellular homeostasis and the adaptation to environmental conditions. Therefore, due to the cellular pleiotropic role of these organelles, the occurrence of dysfunctions of mitochondrial structure and biology have harmful impacts to the health. Severe pathological conditions have been related to mitochondria aberration, among others, neurodegenerative and cardiovascular diseases, obesity, diabetes and also cancer [9].

Many studies over the past years focused their attention on the comprehension of cell transformation process and tumour progression, underlying the complexities and the multifactorial nature of the cancer disease. The biological capabilities acquired by tumour cells include metabolic rewiring, adaptation to stress conditions, aberrant signalling pathway and resistance to cell death. All these processes are strongly related to mitochondrial biology [10]. Indeed, many evidence proved that mitochondria actively contribute to tumorigenesis because of the ability of malignant cells to exploit mitochondria flexibility to adapt to the tumour microenvironment [11], [12]. Therefore, shedding light on the functions and dynamics of mitochondria supporting cancer onset and progression may contribute to the development of new approaches for the targeted cancer therapy.

### 1.1.1 Ultrastructure of the mitochondria

The mitochondria have a complex structure and a characteristic internal architecture, which are essential for the functional state of these organelles.

Shape, number, and size of mitochondria vary among cell types and tissues in relation to their energy demand and functional state. When the organelles network is poorly interconnected, mitochondria are visible in the cytoplasm in a round, rod or bean-like shape, with a medium diameter in the range of 0.05-1  $\mu\text{m}$  and up to 10  $\mu\text{m}$  in length.

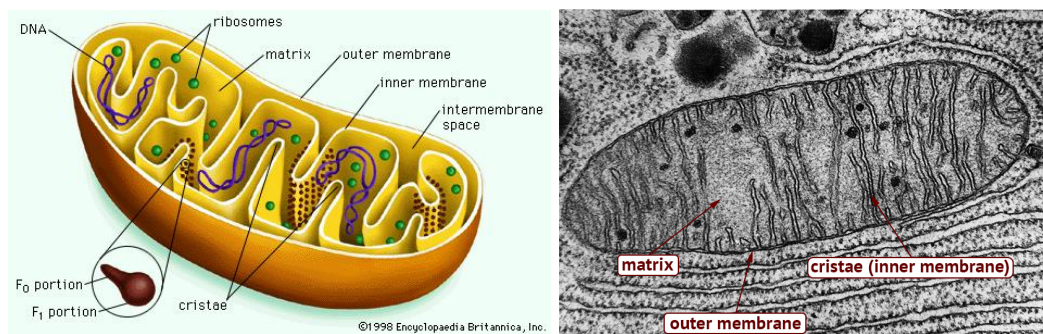


**Figure 1: The mitochondrion:** (A) Schematic representation of a mitochondrion (B) Transmission electron microscopy image of a mitochondrion.

Structurally, the mitochondria are bounded by two distinct membranes enclosing a dense matrix. The external surface consists of the outer mitochondria membrane (OMM), a porous phospholipid bilayer passively permeable by ions, and small molecules up to ~5 kDa through voltage-dependent anion channels (VDACs) also named mitochondrial porins [13]. Larger molecules, such as proteins synthesized in the cytosol, are imported by the translocases of the mitochondrial outer membrane (TOM complexes), consisting of surface receptors recognizing the mitochondrial-targeting signal of proteins, and the import pore [14], [15]. Because of the low selectivity in molecules trafficking, there is no membrane potential across the outer mitochondrial membrane. A small lumen of around 20 nm named the intermembrane space (IMS) separates the OMM from the inner mitochondrial membrane (IMM), the innermost phospholipid bilayer. The IMS is an aqueous compartment, whose content is defined by the molecules exchange between the cytosol and the mitochondrial matrix managed by the outer and the inner membranes. As effects of this transportation and the discard of the processes taking place in IMM and matrix, IMS compartment is more acidic than the cytosol by 0.2-0.7 pH units [16].

Unlike the outer membrane, the inner mitochondrial membrane is a highly selective diffusion barrier. Ions and molecules cross this boundary only carried by specific membrane transporters mostly members of the mitochondrial carrier family (MCF), of bacterial-type ion transporters, and of ABC transporters [17]. Here, the inner translocase mitochondrial protein (TIM) is connected to the TOM forming supercomplexes that allow the delivery of precursor to the matrix and the insertion of proteins in the inner membrane [18]. The carrier proteins together finely regulate the transit of metabolites, ions, cofactors, biosynthetic precursors to and from the matrix, allowing the maintenance of the electrochemical gradient established across the IMM by the electron transport chain (ETC) that drives the oxidative phosphorylation in the synthesis of ATP. Moreover, the inner membrane is folded to forms invaginations called cristae, that project to the mitochondrial matrix, with a prominent increase of the IMM surface. The cristae are considered the hubs of the energy production. In these sub-compartments, indeed, are concentrated most of the complexes of electron transport chain, the ATP synthases and soluble electron carriers [19].

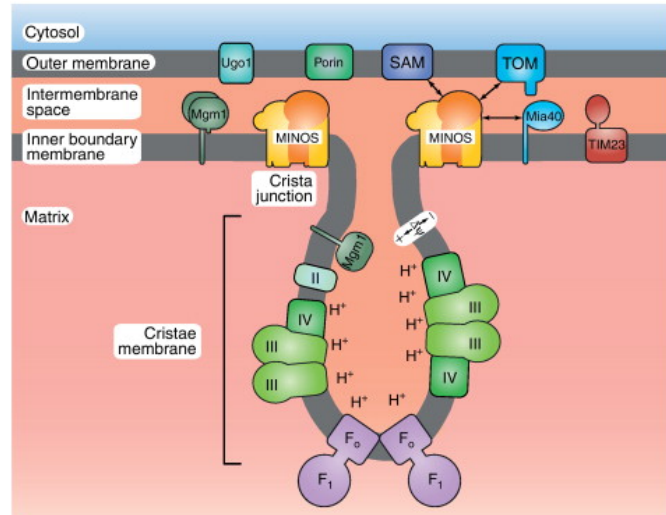


**Figure 2: The *crista*:** Schematic representation of the mitochondrial *crista*. Electron transport chain complexes are represented in green, the ATP-synthase in purple.

Membrane walls forming the cristae lumen are connected to the planar inner membrane by the cristae junctions, structures that form a constriction at the base of the invaginations. This sub-mitochondrial architecture optimizes the ATP-synthesis performance by restricting the diffusion of protons through the cristae junctions and then limiting proton-leakage toward the cytosol. Furthermore, cristae junctions limit the diffusion of molecules and reactive species toward the intermembrane spaces, such as the ROS produced by the respiratory chain, bordered into the cristae lumen to decrease the risk of damage of other cellular compartments. The number and deepness of cristae reflect the bioenergetic activity of the mitochondria. Indeed, cristae surface and lumen volume are increased in cells with high ATP demand, whereas IMM is less folded in mitochondria of cells at low energy need, increasing the matrix component. Therefore, a mitochondrial crista can be considered as a dynamic biochemical reactor, from whose shape and dimensions depend both the efficiency of the oxidative phosphorylation (OXPHOS) process and the cell homeostasis [20]. The peculiar lipid composition of the inner membrane of mitochondria, enriched in cardiolipin, also contributes to the efficiency of the mitochondrial functionality. Indeed, the cardiolipin stabilizes the supercomplexes of the ETC and OXPHOS, and its biochemical characteristics favour the cristae folding [21], [22].

Surrounded by the IMM, the deepest mitochondrial compartment is the mitochondrial matrix, displaying a viscous texture due to the high number of soluble proteins contained. In particular, here are located many enzymes, that catalyse reactions part of the essential biochemical pathways of the cell, such as the citric acid cycle, the fatty acids oxidation and some steps of the urea process formation. Moreover, the matrix contains the mitochondrial genome (mtDNA) and the mitoribosomes and in here the mtDNA replication, transcription and translation of a few essential proteins, take place [13], [23].

### 1.1.2 Mitochondrial genome

According to the endosymbiotic theory, mitochondria derived from prokaryotic cells. As a result of the eukaryotic cell evolution, most of the genes of the ancestral bacterial genome were lost or transferred to the nucleus, but an independent genome was left in these organelles. Indeed, mammalian mitochondria are supplied with circular, double-stranded molecule of DNA about 16.6 Kbp long, and exist in hundreds of copies per organelle in relation to the cell type [24]. The strands of the DNA duplex are distinguished on the basis of their density in relation to the nucleotides content. Most of the mtDNA information is encoded by the heavy-strand (rich in guanine). The mitochondrial DNA (mtDNA) encodes 22 tRNAs, 2 ribosomal RNAs (the 12S and 16S rRNA), and 11 messenger RNAs translated by the mitochondrial ribosome to 13 proteins, all subunits of the OXPHOS complexes.

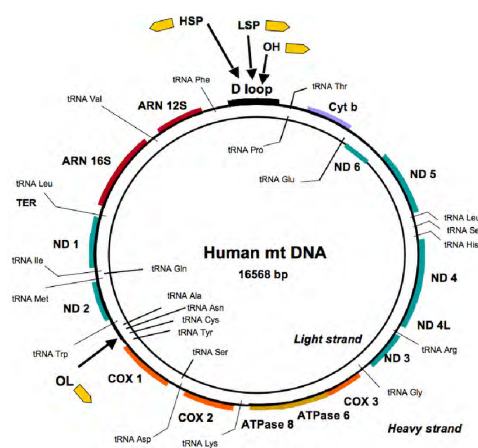


**Figure 3: The human mitochondrial genome: genomic map of the mtDNA.**

The remaining subunits of the 90 that compose the oxidative phosphorylation system are encoded by the nuclear genome, translated by cytosolic ribosomes and then imported into the mitochondria [25].

However, the mitochondrially-encoded complexes are essential, as experimentally demonstrated by the collapse of the OXPHOS process in the absence of the mtDNA expression [26]. Compared to the nuclear genome (nDNA), the mammalian mtDNA exhibits a rudimentary organization, since the genes do not have introns, intergenic sequences are absent or limited, and some of the genes overlap. The only small non-coding region of the mtDNA is the D-loop (displacement loop), that is essential for the transcription and the replication processes [27]. The mitochondria genome replicates independently from the cell cycle but in a semi-autonomous way from the cell, because a few enzymes required for the process are encoded by the nDNA and then imported into the mitochondria [28]. In the mitochondrial matrix, mtDNA is assembled into the supramolecular structure called nucleoids, each containing one or two copies of the mitochondrial DNA and a set of DNA-binding core proteins. The nucleoids core carries mature proteins involved in mtDNA maintenance and transcription, and other factors of signalling pathways controlling mitochondrial biogenesis, metabolism, apoptosis, and retrograde mitochondria-to-nucleus signalling [29]. The organization in nucleoids represents an efficient unit for the segregation of the mtDNA during the cell division, but poorly protects the genome from the action of the external genotoxic agents. Indeed, the mutation rate is estimated to be ten times higher in mtDNA than in nDNA [30]. Alterations of the mitochondrial genome are also promoted by the high rate of the replication and the oxidative stress caused by the proximity to the respiratory chain, one of the major intracellular sources of ROS [31]. Due to the coexistence of multiple copies of mtDNA, the occurrence of mutations leads to the heterogeneity of the mitochondrial genotype within the cell. This condition is named heteroplasmy, and it is the opposite of the homoplasmy, state in which a cell or a tissue have only one mtDNA-genotype. When a pathogenic mutation occurs in the mtDNA, may be introduced in the newly-replicated genomes, increasing the heteroplasmy level. To cause a pathologic condition, heteroplasmy for the aberrant mutations must reach a certain fraction in the cell, overcoming a threshold level beyond which the mitochondrial function collapses.

Furthermore, since during the cell division mitochondria are symmetrically subdivided within daughter cells and segregate in a random manner, to predict the impact of an aberrant mutation occurring in the mtDNA is extremely difficult [32]. Moreover, the mitochondrial genome is exclusively maternally inherited from the mother oocyte and does not undergo germline recombination [33]. Understanding the mechanisms underlying the maternal inheritance and the heteroplasmy dominance represents the major challenge for the diagnosis and treatment of mtDNA diseases.

## **1.2 The oxidative phosphorylation**

By operating the cellular respiration, the cells release the biochemical energy stored in nutrient and turn it into adenosine triphosphate (ATP), the energy-rich molecule that fuels cellular activities, such as biosynthesis, transport of molecules across the membranes and movement. Depending on the metabolic conditions, in nonphotosynthetic eukaryotes, ATP is produced by various biochemical pathways and the more relevant are the glycolysis, the citric acid cycle, the oxidative phosphorylation, and fatty acid oxidation. In aerobic conditions, ATP is efficiently produced by mitochondria via the oxidative phosphorylation (OXPHOS). In this process, the electrochemical gradient, established across the inner mitochondrial membrane by the electron transport chain, drives the ATP-synthase in the conversion of ADP into ATP. Cellular homeostasis is strictly related to the structural and functional integrity of OXPHOS system.

### **1.2.1 The Electron Transport Chain (ETC)**

The electron transport chain (ETC) is a highly efficient molecular machinery that performs a series of concatenated redox reactions, to transfer the electrons from the NADH and FADH<sub>2</sub> electron carrier molecules to the oxygen. The catabolic pathways of glycolysis, fatty acid oxidation and citric acid cycle supply the NADH and FADH<sub>2</sub> to the mitochondrial ETC. The electrons crossing the respiratory chain, progressively release energy, then used to transport hydrogen ions (H<sup>+</sup>) from the matrix toward the



mitochondrial intermembrane space. This process leads to the generation of the electrochemical proton gradient across the inner mitochondrial membrane, later exploited for the synthesis of ATP by chemiosmosis. Electron-transfer reactions are coupled to the  $H^+$  pumping by the activity of the ETC multiprotein complexes, embedded in the IMM, and two diffusible electron transporters, that shuttle electrons between them. The Complex I also named NADH:ubiquinone oxidoreductase or NADH dehydrogenase, is the first actor of the respiratory chain.

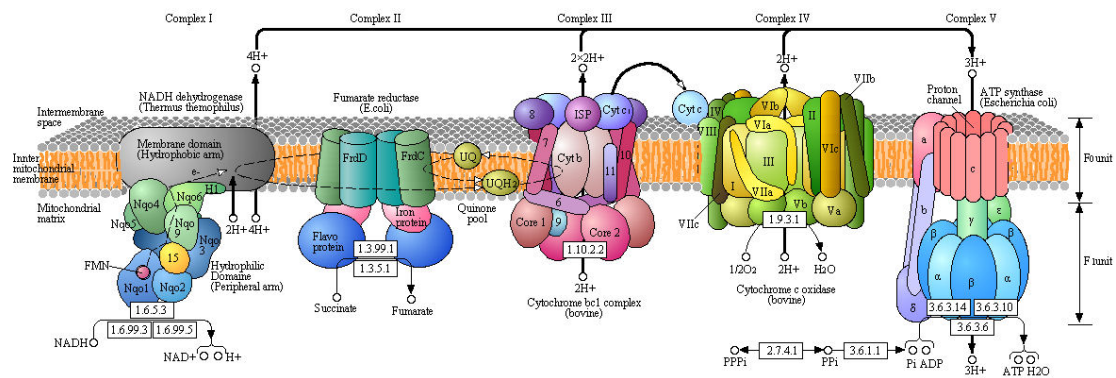


**Figure 4: The Oxidative phosphorylation (OXPHOS)** Schematic representation of the OXPHOS complexes embedded in the inner mitochondrial membrane. Protons flux and complexes subunits are shown.

This complex consists of 46 polypeptides assembled in the IMM to form a proton-pump with a characteristic L-shape that protrudes towards the matrix. In the first step of the ETC, two electrons are received from an NADH molecule to Complex I and transferred to the prosthetic group consisting of a flavin mononucleotide (FMN), thus reduced to  $FMNH_2$ . Electrons subsequently pass to the iron-sulfur (Fe-S)-containing proteins, through a new redox reaction.

Finally, the passage of the two electrons to the coenzyme Q induces the pumping of  $4 H^+$  across the Complex I towards the inner membrane space. Coenzyme Q (Q), or ubiquinone is a small lipid molecule free to moves through the hydrophobic core of the inner mitochondrial membrane. The Q molecule once is reduced to ubiquinol ( $QH_2$ ) delivers electrons to the Complex III of the respiratory chain [33].

The Complex II of the ETC is the succinate dehydrogenase enzyme also involved in the TCA cycle and alternatively named succinate-coenzyme Q reductase. This enzyme catalyses the transformation of succinate to fumarate, producing FADH<sub>2</sub> that carries electrons to Fe-S centres of the complex. Eventually, electrons reduce the ubiquinone to ubiquinol. The Complex II activity is not coupled to protons-pumping so FADH<sub>2</sub> leads to a less efficient yield in the ATP synthesis [34]. Thus, ubiquinone receives the electrons both from the NADH via the complex I, and from FADH<sub>2</sub> through the complex II, bypassing the Complex I. The Complex III, or Q-cytochrome c oxidoreductase, represents the second proton pump of the respiratory chain. Due to its composition, the Complex III is also called cytochrome bc<sub>1</sub> complex, consisting of cytochrome b, Fe-S proteins, Rieske center (2Fe-2S center), and cytochrome c proteins. This complex transfers the electrons carried by the ubiquinol to oxidized cytochrome c (cyt c), a water-soluble protein that lately transports electrons to the Complex IV. The transfer of electrons through the Complex III results in the pumping of four protons out of the mitochondrial matrix in the IMS [35]. The cyt c provides electrons to the last complex of the ETC: the cytochrome c oxidases (COX). Due to its structure, the Complex IV is capable of trapping oxygen allowing its complete reduction using the electrons derived by the ETC. The reduced oxygen is then bound to hydrogen ions and released as water (H<sub>2</sub>O), together with the flux of protons towards the intermembrane space. The overall reaction catalysed by the complex IV leads to the pumping of 4 H<sup>+</sup> and the removal of other 4 H<sup>+</sup> for the release of H<sub>2</sub>O for each oxygen molecules reduced [36]. The concatenated reactions of the electron transport chain cooperate together to establish a proton electrochemical gradient ( $\Delta\tilde{\mu}_{H^+}$ ) across the IMM by extruding protons from the mitochondrial matrix into the intermembrane space [37].

### **1.2.2 The F<sub>1</sub>F<sub>0</sub>-ATP synthase**

The fifth and last complex of the oxidative phosphorylation is the ATP-synthase, the molecular motor specialized in the energy interconversion by synthesizing ATP. Related to its functional structure, the Complex V is also named F<sub>1</sub>F<sub>0</sub>-ATP synthase.

According to Michell's chemiosmotic theory, the  $F_1F_0$ -ATP synthase catalysis is driven by the proton electrochemical gradient ( $\Delta\tilde{\mu}_{H^+}$ ) built by the ETC.  $\Delta\tilde{\mu}_{H^+}$  consists of an electrical component, the mitochondrial membrane potential ( $\Delta\Psi_m$ ), and the pH gradient between the two sides of the inner membrane ( $\Delta pH_m$ ) [38]. In functional mitochondria, the inner membrane side facing the matrix display a negative charge and an alkaline pH [39]. Experimental evidence proved that efficient synthesis of ATP by OXPHOS requires both high protons driving force and a low pH within the cristae lumen of the mitochondria [40][41]. The ATP-synthase is expressed by the energy-producing membranes of bacteria, chloroplasts and eukaryotic mitochondria and its architecture is mostly conserved among the species. The overall structure of the mammalian  $F_1F_0$ -ATP synthase is essentially well defined, whereas the regulatory mechanisms are still in part unclear [42].

#### **1.2.2.1 Structure of the $F_1F_0$ -ATP synthase**

Mammalian  $F_1F_0$ -ATP synthase is a large heterooligomeric complex (up to 650 kDa), with a mushroom-like shape, partially located within in the inner mitochondrial matrix, that produces ATP via a stepwise rotational mechanism. The  $F_1F_0$ -ATP synthase consists of two functional portions, the membrane-extrinsic  $F_1$  domain and a membrane-intrinsic  $F_0$  sector, connected with each other by central and peripheral stalks. The  $F_1$  domain represents the cap of the mushroom and protrudes in the mitochondrial matrix.  $F_1$  is responsible for the catalytic activity of the complex, where ATP is produced from ADP and inorganic phosphate ( $P_i$ ). On the other hand, the  $F_0$  domain acts as the motor, generating rotation using the energy stored in the proton-motive force. The central stalk, connected to the  $F_0$  motor, transmits the rotational energy to the  $F_1$  catalytic domain [42]. In all eukaryotic cells, the  $F_1$  portion is a complex of five types of polypeptides, named  $\alpha$ ,  $\beta$ ,  $\gamma$ ,  $\delta$  and  $\epsilon$ . Both the  $\alpha$  and  $\beta$  subunits occur in 3 copies, and are arranged in alternation to form a hexameric ring named the  $\alpha_3\beta_3$  domain, with a spherical structure [43]. Beneath the  $\alpha_3\beta_3$  ring, the  $\gamma$ ,  $\delta$  and  $\epsilon$  form the central stalk.

The  $\gamma$ -subunit display an extended  $\alpha$ -helical structure that in part develops in the core of the hexameric ring, occupying the central axis [44].

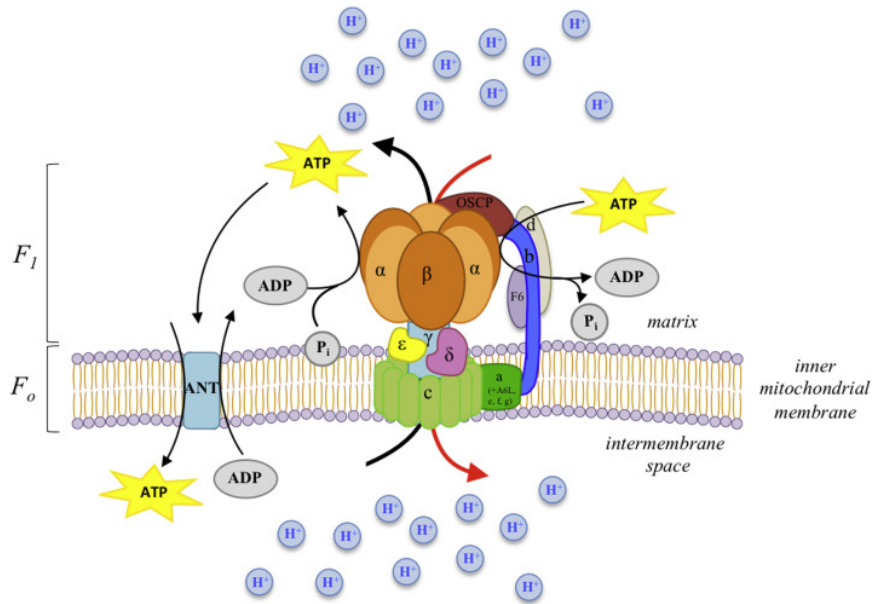


**Figure 5: Mammalian F<sub>1</sub>F<sub>0</sub>-ATP synthase.**

The rest of the  $\gamma$ -subunit form a “foot” that with the help of  $\delta$ -and  $\epsilon$ -subunits binds the F<sub>0</sub> domain and connect it to the F<sub>1</sub> portion. F<sub>0</sub> domain consists of a hydrophobic cylindrical structure made of c-subunits (the c-ring), one copy each of subunits a, b, d, F6 and the oligomycin sensitivity-conferring protein (OSCP). The OSCP protein is so called because it has been related to the sensitivity to oligomycin, a compound widely used in bioenergetics research. Oligomycin is an inhibitor of the bidirectional proton flux through the ATP synthase, irreversibly binding the channel of the F<sub>0</sub> subunit [45]. The size and the constitution of c-ring vary among species, and they are possibly related to the bioenergetic requirement [46]. The c-ring together with the central stalk subunits ( $\gamma$ ,  $\delta$ ,  $\epsilon$ ) form the rotor of the F<sub>1</sub>F<sub>0</sub>-ATP synthase whereas subunits b, d, F6 and OSCP form the peripheral stalk, placed to one side of the complex. Another protein, the a-subunit, is associated with the outside surface of the c ring and it is connected with  $\delta$ -subunit of the central stalk by the peripheral stalk [47].

The  $\alpha_3\beta_3$ , a, b, d, F6, OSCP subunits represent together the stator of the Complex V. A number of additional subunits (e, f, g, and A6L) are associated with  $F_o$  [48].

Many scientific data proved that  $F_1F_o$ -ATP synthase is mostly organized in dimers and oligomers in the mitochondrial membrane [49]. The supramolecular organization concurs to the stabilization of the Complex V, allowing a higher efficiency of the process and also protection from mechanical insults. Moreover,  $F_1F_o$ -ATP synthase oligomeric organization have been linked to the maintenance of the mitochondrial morphology by cooperating in the cristae folding favouring the membrane curvature [50], [20].

### **1.2.2.2 $F_1F_o$ -ATP synthase and ATP synthesis process**

The  $F_1$  domain of the ATP synthase synthesizes and release ATP from ADP and inorganic phosphate (Pi) exploiting the energy derived from the transit of protons through the  $F_o$  portion of the enzyme [51]. The  $H^+$  of the intermembrane space cross the inner membrane via the a-subunit of the  $F_o$  domain to the c-ring [52]. The released energy causes the rotation of the c-ring subunits along with the central stalk located in the core of the  $F_1$  portion. Rotation of subunit  $\gamma$  within the  $F_1$   $\alpha_3\beta_3$  hexamer provides energy for ATP synthesis activating a stepwise process named “rotary catalysis” exploiting the “binding-change” mechanism, first proposed by Boyer [48], [53]. The ATP synthesis reaction starts with the formation of a bond between the terminal oxygen of the ADP and the Pi, forming a pentacovalent intermediate molecule at first, that then dissociated in ATP and water molecules. This reaction is catalysed by each of the three  $\beta$  subunits, at the interface with the adjacent  $\alpha$  subunit. Therefore, the  $F_1$  portion operates in three steps consisting in the binding of ADP and Pi to the  $\beta$  subunit, ATP formation, and then ATP release. Each site of the  $\alpha_3\beta_3$  progressively switches through three different conformations to perform one of the three stages [54].

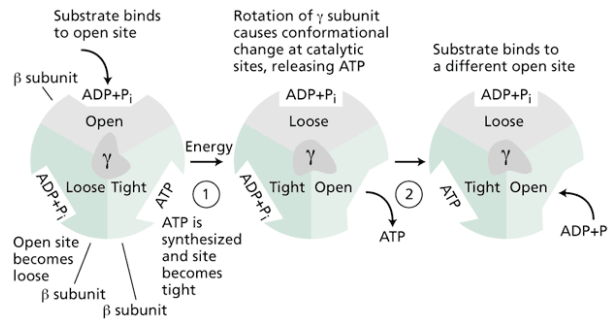


**Figure 6: The binding-change mechanism of the F<sub>1</sub>-F<sub>0</sub>-ATP synthase.** Process schematization as seen from the top of the F<sub>1</sub> portion.

The conformational changes are driven by the  $\gamma$  subunit rotation dragged by the c-ring movement, which is pushed by the energy released from the  $H^+$  transit between the compartment at the high-protons concentration and the one at low- $H^+$ . The  $360^\circ$  rotation of F<sub>0</sub> domain is performed by a flux of protons in equal number to the c-subunits composing the c-ring. Experimental observations determined that the rotation occurs always in the clockwise direction during ATP synthesis, observing the nanomotor from the bottom side of the  $\alpha_3\beta_3$ , the closest to the F<sub>0</sub> and the membrane. However, upon specific conditions, the F<sub>1</sub>F<sub>0</sub>-ATP synthase can reverse its activity to hydrolyse ATP, and this occurs when the  $\gamma$  subunit rotates in the counter-clockwise direction [55]. On the other hand, a significant drop in the ATP levels caused by insufficient ATP generation in proportion to the ATP used could be detrimental for the cell homeostasis. Indeed, when ATP levels go under a certain threshold, acidosis is observed, leading to the activation of enzymes, such as proteases, nucleases and lipases, that degrade the cellular components inducing cell death activation [56].

In order to avoid serious consequences to the cell viability, the intracellular concentration of ATP may vary only in a limited range [57]. For this purpose, both ATP synthesis and ATP hydrolysis activities performed by the F<sub>1</sub>F<sub>0</sub>-ATP synthase must be finely regulated.

### 1.2.2.3 Modulation of the F<sub>1</sub>F<sub>0</sub>-ATP synthase activity

In physiologic condition, when intracellular ATP levels are too high or too low, ATP synthesis may be inhibited or stimulated respectively. Indeed, in eukaryotic cells, the rate of ATP usage may widely vary by a factor of 5–10 depending on the activities performed (i.e. resting or exercise) and the environmental conditions (temperature and oxygen available) [58]. Therefore, F<sub>1</sub>F<sub>0</sub>-ATP synthase activity is modulated at different levels. Among these is comprised the regulation of the Complex V content in mitochondria that occurs through the modulation of the genes encoding for the F<sub>1</sub>F<sub>0</sub>-ATP synthase subunits, mediated by transcription factors in response to the metabolic stimuli. For instance, ATP depletion causes the expression of specific transcription factors, such as nuclear respiratory factor-1 (NRF-1), that induces the up-regulation of the ATP-synthase expression, but also other mitochondrial enzymes, such as cytochrome oxidase and cytochrome c of the ETC, and multiple genes involved in mitochondrial biogenesis [59]. Indeed, modification of the expressions and efficiency of the electron transport chain regulates the F<sub>1</sub>F<sub>0</sub>-ATP synthase activities, through the modulation of the electrochemical gradient. Both ETC enzyme and ATP synthase can also undergo post-transcriptional modifications, such as phosphorylation of specific residues, inducing changes in the conformation and therefore in the catalytic efficiency. In particular, the complexes phosphorylation may be driven by a cAMP-dependent pathway that activates PKA [60]. Moreover, many evidences highlighted how the ATP and ADP molecules inhibit and stimulate the OXPHOS respectively, by allosteric binding to the complexes [61]. Other regulatory proteins have been proposed to interact with the F<sub>1</sub>F<sub>0</sub>-ATP synthase, such as the oncoprotein Bcl-XL, the factor B involved in the Complex V oligomerization, and CaBI, which may up-regulate the enzyme functionality in response to Ca<sup>2+</sup> intracellular levels [60], [62], [63]. However, the most relevant regulator of the F<sub>1</sub>F<sub>0</sub>-ATP synthase is the Inhibitory Factor 1 (IF<sub>1</sub>). Several studies focused on the biochemical and functional characterization of IF<sub>1</sub> to understand the role of this protein in the cell homeostasis, and also in pathological conditions, opening great perspective also for the cancer treatment.

Despite the vast amount of information and data collected, many aspects of the IF<sub>1</sub> functionality are in part unclear [64], [65], [66].

### **1.3 Mitochondria and cancer**

With their highly dynamic nature, the mitochondria play an essential role in the rapid sensing and integration of stress signals and environmental changes, adapting their biosynthetic and signalling pathways, in order to provide appropriate responses to ensure cell homeostasis. Over the physiologic functionality, it is widely demonstrated that mitochondria have a pivotal role also in the neoplastic transformation process, providing the adequate amount of energy and biomass to cancer cells in order to sustain their uncontrolled proliferation [67]. Moreover, mitochondria plasticity allows the metabolic rewiring of cancer cells necessary for adapting to adverse environmental conditions and cooperating in the resistance to the cancer treatments [68]. Indeed, onset and progression of solid tumours are commonly characterized by conditions of inconstant blood perfusion determining variations in oxygen, nutrient availability and also pH [11]. The first observation of the metabolic reprogramming occurring in cancer cells was provided by Warburg, who noticed that some tumour cells mostly obtain energy from glycolysis instead of oxidative phosphorylation, even in the presence of oxygen [69]. This cancer trait is now known as “Warburg effect” or aerobic glycolysis and several studies were performed later to shed light on the mechanisms underlying it. In particular, it was pointed out that most of the Warburg-cancer cells showed downregulation of the OXPHOS activity rather than complete loss of activity. During the past decades, many other metabolic hallmarks of the cancer have been described. In particular, cancer cells frequently increase the flux of the pentose phosphate pathway (PPP) that provides essential molecules for nucleotide synthesis and NADPH for anti-oxidant defences necessary for the tumour growth together with the intermediates for the amino acid biosynthesis provided by the aerobic glycolysis [70], [71], [72]. The low OXPHOS activity together with the high rate of the PPP pathway, that limits pyruvate availability, contribute to the downregulation of the Krebs cycle in the cancer cell.



Moreover, cancer cells can also boost the glutamine consumption as a source of carbon and nitrogen to supply the high request of biomass [73]. Conversely, other tumour types can even increase the oxidative phosphorylation, maintaining a healthy and efficient mitochondrial mass by increasing the mitochondrial turnover. Indeed, beside the metabolic aspects, several other mitochondrial functions support cell transformation and cancer progression, including mitochondrial quality control mechanisms, fission and fusion dynamics that can also reduce the cell susceptibility to immunity, cell death and redox stress. Interestingly, the expression and regulation of many mitochondrial proteins depend on the transduction of the major cellular pathways such as HIF1, c-Myc, p53, Ras and mTOR/AMPK, whose signalling is frequently altered in cancer [74]. In transformed cells, the occurrence of new genetic mutations in either nuclear or mitochondrial genome, and the pressure of the environmental conditions lead to the development of intra-tumour heterogeneity. Moreover, the cancer progression is characterized by the change of mitochondria functionality together with the evolution of transformed cells, that develop different metabolic needs, as it occurs in the shift from adherent proliferation to metastatic invasion. The molecular and metabolic plasticity of cancer during the progression represents one of the most relevant issues for the efficiency of the therapies and disease outcomes.

## **1.4 The ATPase Inhibitory Factor 1 IF<sub>1</sub>**

As anticipated above, the F<sub>1</sub>F<sub>0</sub>-ATP synthase can reverse its activity and hydrolyse ATP to pump protons towards the intermembrane space. This event may occur when the electrochemical proton gradient is abolished, as happens when the inner membrane is damaged, or in cells experiencing low-oxygen conditions, such as in ischemia and hypoxia [75], [76]. In particular, the limited availability of the final acceptor O<sub>2</sub> determines an impairment of the ETC, resulting in the inefficient  $\Delta\Psi_m$  formation that, in turn, is insufficient to sustain the ATP synthesis. In these conditions, the ATP-hydrolytic activity of the Complex V leads to the production ADP, Pi and also protons, that cooperate to restore the electrochemical proton gradient.

Considering that, intracellular energy levels are critical for cell viability, the consumption of ATP must be prevented. With this purpose, ATP hydrolysis by the  $F_1F_0$ -ATP synthase is blocked by the action of the inhibitor protein  $IF_1$ , with a pH-dependent mechanism [77], [78]. The mitochondrial ATPase Inhibitory Factor 1 ( $IF_1$ ) was described for the first time by Pullman and Monroy in mitochondria extracted from the bovine cardiac muscles [77]. The expression and functionality of  $IF_1$  were successively identified in several other mammals but also in *C. elegans* and in plant mitochondria [79], [80], [81].

The human  $IF_1$  is constitutively expressed by the ATPF1 gene on the chromosomes 1, producing a pre-protein of around 100 amino acids in length, then targeted to the mitochondrial matrix. In the organelles,  $IF_1$  undergoes the cleavage of the 25-residues composing the mitochondrial targeting sequence, located in the N-terminal of the polypeptide. This process produces the  $IF_1$  mature form with size near to 10 kDa. In mammals,  $IF_1$  performs its inhibitory function in the dimeric form, through the organization in the antiparallel coiled-coil conformation of the  $\alpha$ -helices in the C-terminal region of two monomers [82]. The N-terminus of  $IF_1$  protein consists of the inhibitory region. The  $F_1$  domain's crystallographic structures of the Complex V repressed by  $IF_1$  showed that the inhibitor binds a site in the catalytic interface, between the  $\alpha$  and  $\beta$  subunits, and also interacts to the  $\gamma$  subunit by the N-terminus region [83], [84]. The inhibitory protein initially takes contact to the catalytic site with the  $\alpha\beta$  subunits in the open conformation. When hydrolysis of two ATP molecules occurs, the  $F_1$  domain rotates in a counter-clockwise manner, and  $\alpha\beta$  subunits undergo conformational changes, adopting the closed conformation [95]. Forced by the  $\alpha\beta$  subunits, also  $IF_1$  rearrange its organization, by adopting an  $\alpha$ -helical structure in the N-terminus, whereas the dimerization domain at the C-terminus loses its organization. In this scenario,  $IF_1$  completely blocks the progressive counter-clockwise rotation of the  $F_1F_0$ -ATP synthase, then inhibiting the hydrolase activity and ATP dissipation. Nevertheless, the  $IF_1$  inhibition is reversible, and when optimal conditions for the ATP synthesis are restored, the clockwise rotation of the  $F_1$  domain disrupts all the interactions, allowing the release of the inhibitor from the complex. The regulation of the ATPase Inhibitory Factor 1 activity is in part exerted by the pH of the mitochondrial matrix, through the modulation of the  $IF_1$  oligomerization.

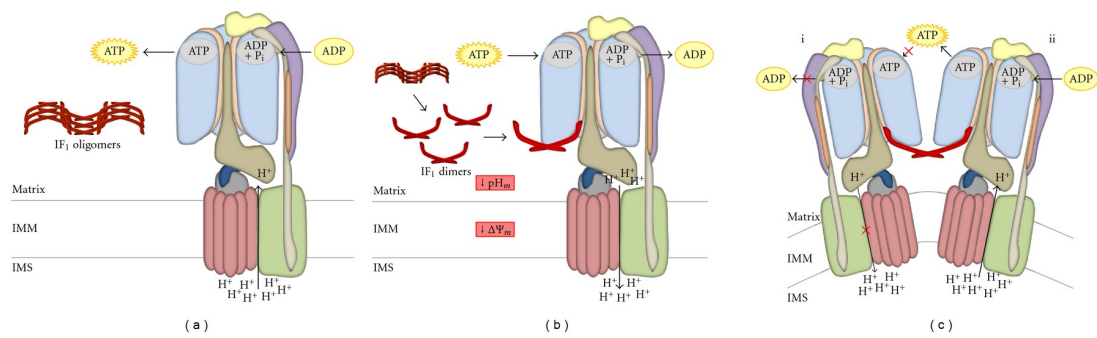


**Figure 7: Interaction of IF<sub>1</sub> with the F<sub>1</sub>F<sub>0</sub>-ATP synthase.** (A) Normal conditions. IF<sub>1</sub> is mainly inactive in the oligomeric form. (B) Collapse of the electrochemical gradient, the F<sub>1</sub>F<sub>0</sub>-ATP synthase starts hydrolysing ATP, inducing the collapse of the pH in the matrix, thus determining the disruption of IF<sub>1</sub> oligomers, freeing active dimers. (C) IF<sub>1</sub> can interact with two F<sub>1</sub> domains inducing the dimerization of the F<sub>1</sub>F<sub>0</sub>-ATP synthase.

In particular, in normal conditions, when the electrochemical proton gradient is established, the alkaline pH of the matrix induces the formation of IF<sub>1</sub> tetramers. In this conformation, the N-terminus inhibitory domains are hidden in the oligomeric core, avoiding the interaction with F<sub>1</sub>F<sub>0</sub>-ATP synthase [85]. Conversely, when the  $\Delta\mu_{H^+}$  collapses and the pH decreases, IF<sub>1</sub> is found in the active form, exposing the inhibitory domains at the two sides of the homodimer. The control of the IF<sub>1</sub> oligomerization operated by the pH occurs via the histidine residues in the C-terminus of IF<sub>1</sub> which change in protonation state defines attractive and repulsive molecular forces [66]. The evidence that IF<sub>1</sub> dimer binds two F<sub>1</sub>F<sub>0</sub>-ATP synthase complexes at the same time led to hypothesize a role of the inhibitor on the F<sub>1</sub>F<sub>0</sub>-ATP synthase oligomers formation and stabilization [82]. However, while some studies reported evidence of IF<sub>1</sub>-mediated dimerization of the ATP synthase, others pointed out that changes in the expression of the inhibitor do not cause the variation of the ATP synthase degree of oligomerization [86], [87], [88], [89]. Furthermore, a consequence of the idea that IF<sub>1</sub> may boost the ATP synthase dimerization and proved that ATP-synthase dimers concur in the curvature of the inner membrane, some studies attributes a role to IF<sub>1</sub> in cristae formation and their maintenance [90].

Literature data on this topic remain still contradictory, therefore, further investigations are needed to elucidate the role of the IF<sub>1</sub> in the ATP synthase dimerization and in the mitochondrial ultrastructure determination. Conversely, it is widely accepted that the endogenous inhibitor IF<sub>1</sub> acts to prevent of ATP depletion during ischemia and reperfusion of tissues, limiting the cellular damage and delaying the cell death [91], [92]. Indeed, it has been shown that during ischemic episodes, the cardiomyocytes boost the glycogenolysis to supply cytosolic ATP. ATP is then imported to the mitochondrial matrix by the adenine nucleotide translocator (ANT), which also works in reverse. The ATP provided is the substrate for the F<sub>1</sub>F<sub>0</sub>-ATP synthase reverse catalysis activated in order to sustain both  $\Delta\Psi_m$  and  $\Delta pH$ . In these conditions, the activation of IF<sub>1</sub> inhibits this hydrolytic activity and limits ATP depletion [93]. Moreover, the different susceptibility to cardiac ischemia among species has been related to the IF<sub>1</sub> levels and its binding affinity to the F<sub>1</sub>F<sub>0</sub>-ATP synthase [94], [95].

#### **1.4.1 IF<sub>1</sub> and cancer**

Several recent studies focused on the involvement of the ATPase inhibitory IF<sub>1</sub> in the cancer development and progression. This hypothesis is supported by the IF<sub>1</sub> overexpression found in several human tumours, such as lung carcinomas, breast cancer, colon carcinoma, Yoshida's sarcoma and hepatocellular carcinoma [90], [96].

In addition, it has been suggested that high IF<sub>1</sub> levels correlate with poor prognosis and reduced survival for some cancer types, suggesting its potential use as a predictive marker [97], [98], [99]. The capability of supporting cell viability under ischemic conditions in normal tissue argues in favour of its role as master regulator of cancer metabolic plasticity. Indeed, the low or absent availability of oxygen and nutrients is a common feature of solid tumours, in which the metabolic substrates supplied to cells varies depending on their distance from the blood vessels [100]. Interestingly, experimental evidence pointed out that IF<sub>1</sub> expression confers to cells the capability to survive longer to nutrient deprivation and oxidative phosphorylation inhibition compared to cells not expressing IF<sub>1</sub>, that quickly deplete ATP via F<sub>1</sub>F<sub>0</sub>-ATP synthase reverse activity to

preserve electrochemical proton gradients [101]. Moreover, other studies attribute to IF<sub>1</sub> a role in the determination of the Warburg phenotype in normal conditions, suggesting that this protein is able to block the ATP-synthesis by the Complex V, then inhibiting OXPHOS and favouring aerobic glycolysis [102], [90]. According to this point of view, cells expressing the inhibitor preserve higher levels of  $\Delta\Psi_m$  because it is not dissipated by F<sub>1</sub>F<sub>0</sub>-ATP synthase catalysis. Conversely, other experimental evidences support the opposite thesis, proving that IF<sub>1</sub> expression confers to cancer cells a higher oxidative phosphorylation rate, together with a decrease of the mitochondrial membrane potential compared to cells IF<sub>1</sub> non-expressing cells [87], [101]. Despite the proposed roles in cancer related to its direct interaction to the F<sub>1</sub>F<sub>0</sub>-ATP synthase, several studies also suggested that IF<sub>1</sub> may trigger a retrograde molecular signalling mediating the nucleus-mitochondria communication, directly acting as small signalling molecules or by modulating the ROS levels [66]. Indeed, slight changes in ROS levels occur in physiological conditions and act as a secondary messenger in several cellular signalling pathways, such as the NF- $\kappa$ B pathway, mitogen-activated protein kinase (MAPK), PI3K-Akt pathway, and Ubiquitination/Proteasome System [103]. On the contrary, the excessive ROS production is detrimental and can either stimulate oncogenic pathways or determines the damage of the cellular component (DNA, enzymes, lipids and proteins) up to induce the cell death. Therefore, ROS levels must be finely balanced, by orchestrating the ROS production and elimination by the antioxidant enzymatic system. Many studies recently focused on the involvement of IF<sub>1</sub> in the modulation of the redox state due to its relation with the respiratory chain, the main ROS producer in the cells. A first study suggested that in colon cancer cells in normal conditions, IF<sub>1</sub> inhibits the ATP-synthesis inducing the hyperpolarization of mitochondria, together with an increase of ROS production. This condition is proposed to trigger a ROS-mediated signalling to the nucleus, that stimulates the NF $\kappa$ B pathway enhancing the proliferation, invasion and the cell survival [102]. Other studies performed in normoxia demonstrated that IF<sub>1</sub> expression determines a lower balance of ROS, attributed to the increasing of OXPHOS efficiency by the stabilization of the F<sub>1</sub>F<sub>0</sub>-ATP synthase in super-complexes and of the cristae

formation [104], [105]. In addition, it has been suggested that IF<sub>1</sub> favours the tumorigenesis process by inhibiting the programmed cell death.

Interestingly, many scientific data suggest that IF<sub>1</sub>-expressing cancer cells have a better tolerance to apoptotic stimuli by limiting the release of the mitochondrial pro-apoptotic proteins (cytochrome c) into the cytosol and then reducing the activation of the caspase-mediated apoptosis. The IF<sub>1</sub> pro-survival effect has been ascribed to a better maintenance of the mitochondrial cristae, also by OPA1 stabilization, avoiding the inner membrane remodelling, essential for mitochondrial commitment to apoptosis [106], [107]. Moreover, some investigators stated that IF<sub>1</sub> confers a proliferative advantage to cancer cells also in physiologic conditions promoting the uncontrolled growth [102], [108]. This point of view is rejected by other studies, showing no difference in the proliferation rate between tumoral cells expressing IF<sub>1</sub> and knocked-out for it [87], [101]. Interestingly, Campanella and colleagues exclusively pointed out that the mitochondrial volume fraction positively correlates with the inhibitor levels. Moreover, it was hypothesised that IF<sub>1</sub> expression restrains ROS levels, mediating a reduction of autophagy activation via depressing retrograde signalling [104]. Moreover, the same investigators identified IF<sub>1</sub> as essential for PARK2 recruitment to initiate mitochondria autophagy upon mitophagy stimuli, then proposing IF<sub>1</sub> as a master regulator of the mitochondrial degradation system [109]. Despite the discordant data reported in the literature, IF<sub>1</sub> involvement in cancer dynamics is clearly defined further investigations are necessary to shed light on its apparently complex mechanisms of action.

## **1.5 Mitochondria membrane potential and homeostasis**

The maintenance of  $\Delta\Psi_m$  with the expense of the cytoplasmic ATP is potentially dangerous for the cellular functions, therefore the preservation of the  $\Delta\Psi_m$  is also relevant for the cell homeostasis and may represent a mechanism of protection [110]. Recent findings pointed out that the  $\Delta\Psi_m$  levels influence the mitochondria health, for instance by modulating their quality control processes and the flux of essential ions. Indeed, the negative charge provided by  $\Delta\Psi_m$  to matrix-side of the IMM allows the transport of the Ca<sup>2+</sup>, Fe<sup>2+</sup> from the cytosol to mitochondria by intrinsic electrogenic carriers [111].

These two cations are essential cofactors for proteins involved in various cellular processes, including electron transport, enzyme catalysis, biosynthesis, DNA replication, repair, transcription, and translation [112]. In physiologic conditions, cells mostly maintain the levels of  $\Delta\Psi_m$  and intracellular ATP required for normal cell activities. However, these parameters undergo transient changes due to the activity of the cells and the interactions with the environment [110]. Prolonged perturbation of either  $\Delta\Psi_m$  or ATP may compromise cell homeostasis, giving rise to pathological conditions. Among the processes induced by the instability of  $\Delta\Psi_m$ , of interest is the opening of the mitochondrial permeability transition (MPT) [113]. The MPT is a large, multiprotein channel localized in the inner membrane of the mitochondria. The depolarization ( $\Delta\Psi_m$  decrease) induces the opening of the MPT that allows the rapid release of molecules from the matrix, including ions and proteins modulating the cell-fate pathways. The period that the mitochondrion persists depolarized, and in turn, the MPT is open, represent a critical factor. Indeed, a brief event of depolarization, may not induce notable changes in mitochondrial functioning, while prolonged depolarization can lead to a “point of no return”, inducing the degradation of the organelle. Although the elimination of a single mitochondrion is not relevant for the cell viability, it induces the release of cytochrome c, AIF factors that mediate cell apoptosis. Induction of the cell death pathway depends on the total levels reached by these deadly factors in the whole cell, and it is an expression of the severity of the mitochondria damage [110]. Nevertheless, the limited  $\Delta\Psi_m$  decrease not followed by the opening of the MPT and fatal events is also possible, as it occurs in physiological processes. On the contrary, several experimental evidences strongly demonstrated that, upon prolonged and maybe complete depolarization, mitochondria are selectively eliminated by autophagy process (mitophagy), part of the mitochondrial quality control system. Through mitophagy, mitochondria are degraded and components recycled without inducing cell death [114], [115]. Furthermore, other studies highlighted the effect of the mitochondrial membrane potential on the production of ROS and in turn the role in the redox cellular stress determination. Indeed, high  $\Delta\Psi_m$  occurs when the respiratory chain, the main producer of ROS in the cell, works at a high rate. This leads to the conclusion that the generation of ROS depends exponentially on  $\Delta\Psi_m$  [116].

However, conditions of low  $\Delta\Psi_m$  have been related to the increase of ROS, suggesting that the  $\Delta\Psi_m$  control is relevant for the cell homeostasis. Finally, when the  $\Delta\Psi_m$  is nulled, and the system is defined uncoupled, the protein import is limited or even suspended [117]. The above observations about the main role of the mitochondrial membrane potential, suggest that  $\Delta\Psi_m$  could be examined as a potential prognostic factor to assess the tissue alterations or damage in pathologies. Moreover, the mechanisms of  $\Delta\Psi_m$  control and the processes controlled by the mitochondrial membrane potential are also relevant for the cancer development progression.

The studies of the oxidative phosphorylation process and in particular the role of the mitochondrial membrane potential have been possible in part by the use of the uncoupling agents [118]. As already discussed above, ATP synthesis occurs by the coupling of two processes: the electron transport chain and  $F_1F_0$ -ATP synthase catalysis. Uncoupling molecules hamper the concatenation of the two processes, dissipating the electrochemical gradient provided by the ETC and avoiding the use for the ATP synthesis. Thus, upon uncoupling conditions, electron transfer redox reaction occurs, together with the ATPase activity of the  $F_1F_0$ -ATP synthase, where ATP synthesis is inhibited. Due to their function, uncouplers are commonly employed in the experimental procedure to chemically reproduce the  $\Delta\Psi_m$  collapse typical of the ischemia (anoxia-mimicking condition). Most of the uncouplers are weak hydrophobic acids that possess a protonophoric capacity, that is the ability to perform the transport of  $H^+$  across the proton-impermeable membranes. Essentially, at the membrane interface, the anionic form of the uncoupler binds protons, becoming neutral and thus able to traverse the membrane. On the opposite side, the uncoupler then releases  $H^+$  and reverts in the anionic form, then going back to the first interface of the membrane, where it newly starts the cycle. Protonophore uncouplers commonly used are 2,4-dinitrophenol (DNP), Carbonyl cyanide-p-trifluoromethoxy phenylhydrazone (FCCP) and Carbonyl cyanide m-chlorophenyl hydrazone (CCCP). Other substances employed to uncouple mitochondria, such as gramicidin, form small pores into the membrane and then ions are free to transit. Electrochemical proton gradient can also be abolished by using molecules with high affinity to different ions species, such as valinomycin and nigericin, that allow the transit of  $K^+$  across the inner mitochondrial membrane [119].



## 1.6 Mitochondria quality control

Mitochondria play a pivotal role in several cellular processes and therefore the maintenance of a healthy and functional mitochondria mass is essential for the overall cellular homeostasis. For this purpose, cells have developed sophisticated mechanisms to regulated number, size and shape of mitochondria, in response to stress conditions and metabolic needs. Whereas mitochondrial dynamics processes of fusion and fission determine the shape and morphology of mitochondrial network, the mitochondrial quality control systems perform the turnover of the organelles, removing superfluous or damaged mitochondria and stimulating the biogenesis of the new ones. The mitochondria dynamic and the quality control systems are actually strictly related and consist of signalling pathways between cellular sensing apparatus, nucleus and mitochondria functions.

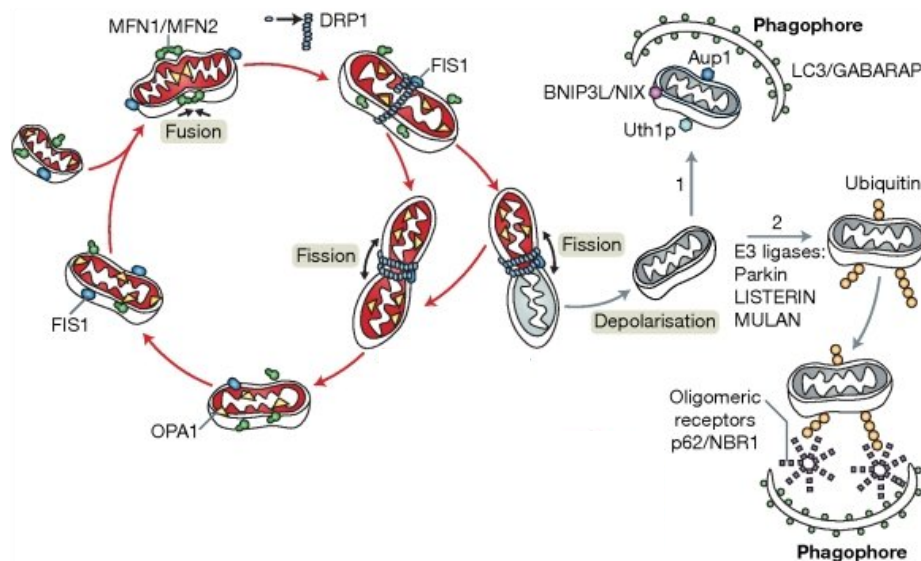


**Figure 8: Mitochondrial dynamics and quality control.** Mitochondria quantity and quality in cells depends on the cooperation of several processes: fusion and fission dynamics, biogenesis and autophagic degradation.

### 1.6.1 Biogenesis of Mitochondria

In contrast to other cellular organelles, the mitochondria are not generated de novo and therefore they arise from the already-existing ones, via the mitochondrial biogenesis process, which also entails both fusion and fission events. The formation of a new mitochondrion requires the membranes biosynthesis, the translation of mitochondrial proteins and their correct targeting, importing and folding into the proper organelle compartment [120]. Taking into account that most of the mitochondrial proteins are encoded by the nuclear genome, whereas 13 essential OXPHOS proteins are expressed by mtDNA, the biogenesis requires a strict cooperation of the two genomes. Alterations in nutrient availability, temperature, molecular stimuli concur to modulate the mitochondrial biogenesis, through the activation of hormone and growth factor-initiated intracellular signalling pathways which regulates the expression of the specific nuclear transcription factors. The peroxisome proliferator-activated receptor gamma, coactivator 1  $\alpha$ , also known as PGC-1 $\alpha$  or PPARGC1A is considered the master regulator of the mitochondrial biogenesis process, together with the nuclear respiratory factors NRF1 and NRF2, and the mitochondrial transcription factor A TFAM. Increased levels of PGC-1 $\alpha$  and PGC-1  $\beta$  are sufficient to increase the total mitochondrial mass and the related mitochondrial activity, such as ROS-scavenging enzymes, OXPHOS components, metabolic pathways, import complexes, fission and fusion proteins, and mitochondrial sirtuins [121][122][123].

Moreover, a wide range of other molecules acts to regulate the biogenesis processes at different levels. Among these, second messengers such as  $\text{Ca}^{2+}$ , cAMP, hormones, and kinase pathways (PKA, MAPK,) also acting by regulating PGC-1 $\alpha$  expression, post-translational modification and localization [124]. In order to carry out the mitochondrial adaptive response to physiological changes or to pathological stimuli, PGC-1 $\alpha$  levels are increased and most of this protein is accumulated in the cytoplasm. Then, upon phosphorylation and/or deacetylation, PGC-1 $\alpha$  translocation into the nucleus [125]. PGC-1 $\alpha$  can also enter into the mitochondria, where interacts with the TFAM to modulate mtDNA expression [126].

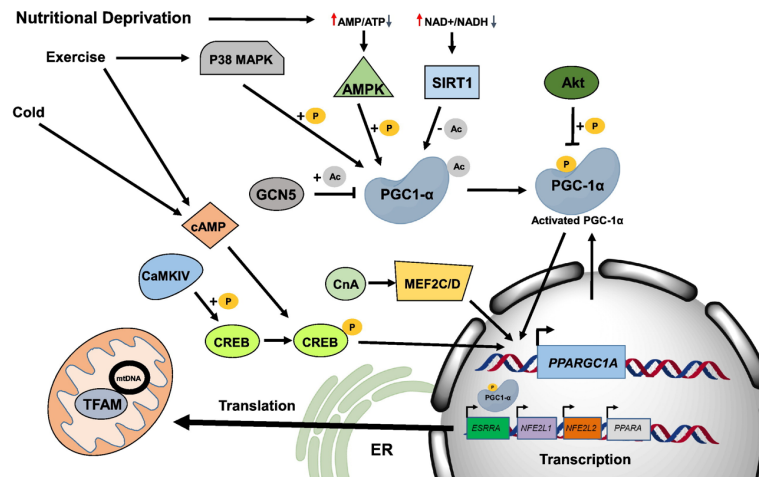


**Figure 9: Overview of the mitochondrial biogenesis process orchestrated by PGC-1 $\alpha$ .**

As co-activator, PGC-1 $\alpha$  does not interact directly with the DNA, nor it exerts enzymatic activity. Indeed, PGC-1 $\alpha$  acts by enhancing and favouring the binding of the transcription factors on the promoter of the mitochondrial genes within the nucleus. Localized in the nuclear genomic regions, PGC-1 $\alpha$  is able to boost gene expression in several ways, such as inducing the chromatin remodelling by recruiting different histone acetyltransferases (HATs) increasing the DNA accessibility to the transcriptional machinery, or removing repressors such as the histone deacetylases (HDACs) [127]. Moreover, PGC-1 $\alpha$  allows the initiation of the gene expression by recruiting some component of the molecular machinery, such as the RNA polymerase II. In this manner, PGC-1 $\alpha$  controls the expression of NRF1 and NRF2, transcriptional factor supervising the expression of the subunits of the OXPHOS complexes, proteins of the mitochondrial import machinery and the mitochondrial transcription factor TFAM. NRF factors are also post-translationally regulated by the direct interaction to PGC-1 $\alpha$  or by phosphorylation on specific residues. NRF1 stimulates the nuclear encoding of respiratory subunits, as well as the mitochondrial transcription factors TFAM and the proteins regulating the mitochondrial transcription and ribosome assembly (TFBs proteins) [128]. Conversely, NRF2 binds to a cis-acting element in the cytochrome oxidase subunit IV (COXIV) promoter and cooperates with NRF1 [129]. TFAM is the main actor of the mtDNA replication and transcription and its protein levels correlate with mtDNA copy number.

Several pathways are described to modulate PGC-1 $\alpha$  functioning, either regulating its expression and availability or by post-translational modification. Among these, the metabolic stress sensors AMPK and SIRT1 directly affect PGC-1 $\alpha$  activity through phosphorylation and deacetylation, respectively [130]. The AMP-activated protein kinase (AMPK) is a Ser/Thr kinase activated upon increase of the cellular AMP/ATP relative content that may occur in presence of defects in energy production or by increased energy consumption [131]. The AMPK activation determines a metabolic switch through the activation of the catabolic pathways to produce ATP while the inhibition of the anabolic processes, avoiding energy consumption. AMPK can quickly exploit its functionality by direct phosphorylation of metabolic enzymes, and it can also have long-term effects acting on a transcriptional level by phosphorylating PGC-1 $\alpha$ , in order to adapt gene expression to energy demands. PGC-1 $\alpha$  activity is also enhanced by the deacetylation of specific residues by the SIRT1 an NAD<sup>+</sup>-dependent deacetylase. SIRT1 is activated by the increase of the NAD<sup>+</sup>/NADH ratio, and aside from PGC-1 $\alpha$ , may acts also by direct deacetylation of many transcriptional factors, PPAR $\gamma$ , p53, and the FOXO family of transcription factors [132], [133], [134]. In contrast, GCN5 and SRC-3 acetyltransferase enzymes inactivate PGC-1 $\alpha$  by acetylation. Expression levels of deacetylases and acetyltransferases are oppositely modulated by the nutrients availability, determining together the PGC-1 $\alpha$  acetylation status and its activation [130]. Interestingly, it has been reported that the knock-out for PGC-1 $\alpha$  gene results in the increase of the oxidative stress and predispose mitochondria to the apoptosis activation [135].

In summary, PGC-1 $\alpha$  manages the mtDNA replication and the correct assembly and localization of mitochondrial proteins and membranes newly synthesized to form the daughter mitochondrion that subsequently develops by fission from the existing one.

### **1.6.2 Mitochondria dynamics: Fusion and Fission**

The shape and interconnection of the mitochondrial network are constantly modified by fusion and fission events, in response to metabolic requirements and stress stimuli. Mitochondrial dynamics processes are essential to provide the adequate mitochondrial mass to growing and dividing cells, both in terms of quantity and functionality [136].

While fission consists in the fragmentation of the mitochondria, the fusion process leads to the melting of different organelles. These processes occur through the remodelling of both outer and inner mitochondrial membranes, which division and fusion are mediated by proteins of the dynamin-like GTPase family [137]. In particular, the organelle fragmentation is achieved by Drp1, a cytosolic protein that aggregates around the mitochondrion to form a ring which strangles the organelle to split both inner and outer membranes. Although fission forms new mitochondria, it can also promote either their autophagic degradation, or the cellular apoptosis. On the contrary, the fusion process is carried out by two groups of proteins, both members of the dynamin-like family: while Mfn1 and Mfn2 act to merge the outer membranes, OPA1 activates the fusion of the inner mitochondrial membranes. Since genetic alterations easily occur in mitochondrial genomes, the fusion of organelles within the same cells can help to compensate the effect of detrimental mutation either by mixing mtDNA to maintain a degree of heteroplasmy that ensures mitochondrial functionality. Moreover, fission events also determine the exchange and mixing of proteins and lipids between mitochondria, that can mitigate the effect of structural and functional damage derived from stress insult [138], [139]. Furthermore, the increased interconnection of the mitochondrial network by enhanced fusion determines a better OXPHOS efficiency by stimulating metabolic cooperation among mitochondria, also better counteracting stress insults [140]. The OPA1, Mfn1 and Mfn2 regulation occurs by their proteolysis and post-translational modifications [137].

### **1.6.3 Mitochondrial degradation**

Stress, pathological conditions and ageing lead to the accumulation of mitochondrial damages that may be dangerous for the cell homeostasis, among other mechanisms by inducing ROS production and cellular redox stress. Therefore, the cells have developed several mechanisms to repair and to rescue injured mitochondrial component or to eliminate irrecoverable dysfunctional organelles. The misfolded and oxidized proteins of the distinct mitochondrial compartments are usually recognized and degraded by the intramitochondrial ATP-dependent proteases, such as LONP1, PARL, and HTRA2/OMI

[141]. Furthermore, altered components of the outer mitochondrial membrane are identified and eliminated by the cytosolic ubiquitin-proteasome system (UPS) [142].

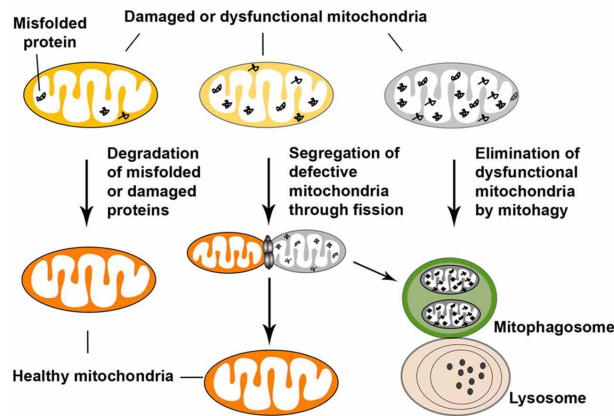


**Figure 10: Mechanisms concurring the mitochondrial quality control.**

Proteases and UPS activations are coordinated with the activation of the mitochondrial unfolded protein response ( $UPR^{mt}$ ), a retrograde signalling pathway to the nucleus that stimulates the expression of either new mitochondrial components and the mitochondrial chaperones, also named heat shock proteins (HSPs).

The HSPs cooperate to keep under control the proteolytic stress by accomplishing the transport, import and folding of the newly formed proteins [143]. Moreover, the clearance of the dysfunctional mitochondrial components may also occur through their engulfment in mitochondrial-derived vesicles (MDVs) [144]. These vesicles are developed by the mitochondrial membranes and released within the cytosol in a fission-independent mechanism. Once in the cytosol, MDVs are degraded to lysosomes activation. Whether the efforts to repair and substitute damaged component are insufficient to ensure mitochondria homeostasis, the quality control mechanism can activate pathways to degrade dysfunctional organelles stimulating the macro-autophagy. The latter is a catabolic process in which cytoplasmic organelles and constituents are degraded in vesicles to save essential metabolites and to limits the deleterious effect of dysfunctional cellular components [145].

The autophagy fulfilment involves different step. The first phase consists in the activation of the mitophagy by specific molecular signals from the organelles to induces the nucleation, that is the recruitment of the components necessary to build the autophagosomes. Subsequently, the autophagosomes are assembled around the mitochondria, starting the sequestration. Once enclosed and loaded, autophagosomes migrates and fuses with the endolysosomes to form the autolysosomes in the step of maturation. Finally, the acidification of the autolysosomes activates the hydrolases that perform the degradation of the cargo. When autophagosomes nucleation occurs, the cytosolic form of LC3 (LC3-I) is conjugated to phosphatidylethanolamine to form LC3-phosphatidylethanolamine conjugate (LC3-II), which is recruited to autophagosome membranes. The organelles directed to autophagic degradation expose specific receptors able to recognize and bind LC3-II, favouring the autophagosomes nucleation. Therefore, LC3-II is commonly considered a marker of autophagy activation [146].

The mitochondria removal via the autophagic process is named mitophagy and occurs through different receptor-mediated mechanisms. Among these, the most well-characterized are the mitophagy activation via ubiquitinated mitochondrial proteins and by molecules constitutively localized in the outer membranes, that act as mitophagy receptors. Proteomic studies reported that proteins of the inner mitochondrial membrane such as OXPHOS complexes, have degradation rate comparable to the organelles turnover, inferring that IMM proteins are principally degraded via mitophagy [147]. Other studies also revealed that proteins of the outer membrane and matrix are readily redistributed across the mitochondria when fusion and fission machinery is intact, whereas IMM components are redistributed more slowly [148].

#### **1.6.3.1 The PINK1/Parkin mediated mitophagy**

The mitophagy activation mediated by PINK1 and Parkin is the best know pathway for the elimination of mitochondria. The phosphatase and tensin homolog-induced putative kinase 1 PINK1 is a nuclear-encoded protein constitutively expressed e translocated to the mitochondria [149]. In physiologic conditions, PINK1 levels are maintained at a low level by the continuous activity of the mitochondria-specific proteases presenilin-

associated rhomboid-like protein (PARL) and the mitochondrial processing peptidase (MPP) [150]. The PARL and MPP enzymes are inactivated by the mitochondrial membrane collapse that may occur in pathologic conditions such as ischemia [115]. The PARL and MPP inactivation results in the accumulation of PINK1 on the cytosolic side of the outer mitochondrial membrane, where it phosphorylates the surrounding membrane proteins. Moreover, PINK1 undergoes homodimerization and subsequent autophosphorylation of specific residues [151].

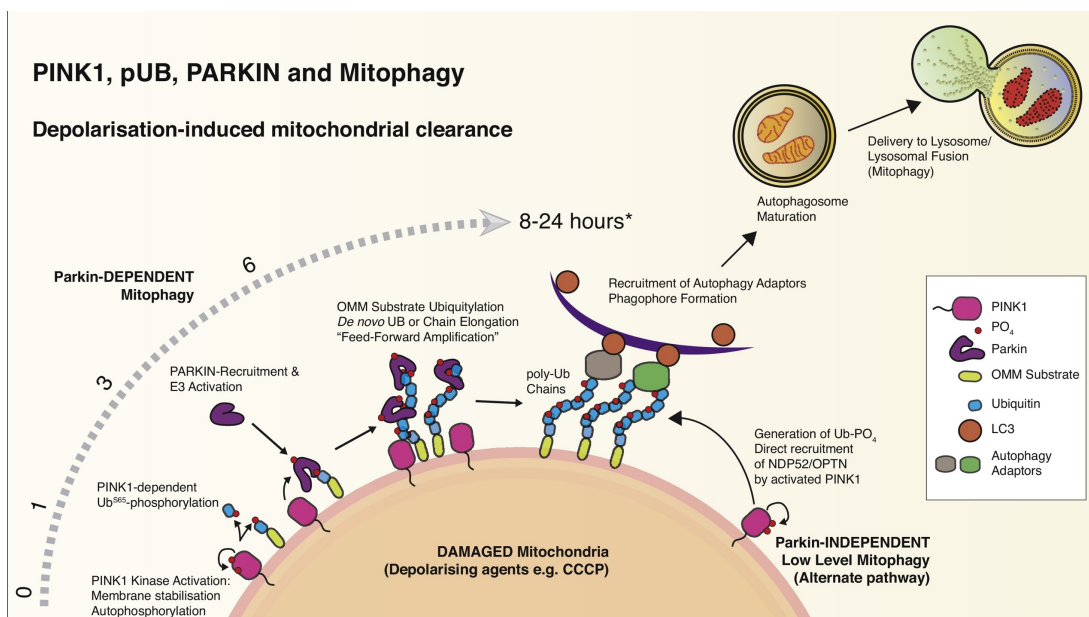


**Figure 11: PINK1 and Parkin mitophagy pathway.**

In these conformations, PINK1 is activated and together with the phosphorylated proteins of the OMM recruit the E3 ubiquitin ligase Parkin. In normal conditions, Parkin is localized in the cytosol in an autoinhibited. Among the PINK1 targets are also included Mnf2 and Parkin itself [152], [153]. While phosphorylated Mnf2 represent a receptor for Parkin anchorage, the E3 ubiquitin ligase is stabilized and activated by the post-translation modification on specific residues and start to ubiquitinate the OMM proteins. Ubiquitin-mediated proteasomal degradation of Mnf2 and Mnf1 is necessary to prevent the fusion of the mitochondrion commissioned to mitophagy [154].



Ubiquitinated proteins of the OMM recruit, in turn, the autophagy adapter proteins, such as NBR1 and p62/SQSTM1 that function as an anchor for the autophagosome nucleation by interacting with the LC3-II, in a zipper-like process [149]. Other molecules are proposed as possible actors in the PINK1/Parkin pathway, but their mechanism of action is still in part unclear.

### **1.6.3.2 BNIP3 and BNIP3L/NIX mediated mitophagy**

In addition to ubiquitinated molecules that act as autophagic receptors, some constitutive proteins of the OMM, such as BNIP3, BNIP3L (or NIX) and FUNDC1 are capable to activate mitophagy [155]. All these proteins contain a motif regulated by phosphorylation at the N-terminus that allow their interaction with the LC3-II and the GABARAP, GABARAPL1 proteins in the membranes of the rising phagosomes. In particular, BNIP3 is anchored to the OMM via its C-terminal transmembrane domain, whereas the N-terminus is facing the cytosol and contains cysteine residues that function as redox sensors [156]. It has suggested that stress insults induce BNIP3 homodimerization and activation by the acting of the N-terminal cysteine residue and the C-terminal transmembrane domain. BNIP3 and NIX promoters contain responsive elements for hypoxia-inducible factors (HIFs), and therefore their expression and activations are potentiated upon chronic hypoxia [157]. Even the FUNDC1 receptor has been reported to activate the mitophagy in hypoxic stress conditions. Moreover, FUNDC1 interacts with both OPA1 and Drp1, coordinating fusion and fission processes during mitophagy [158]. BNIP3 transcription is also positively regulated by RB, NF- $\kappa$ B and oncogenic Ras, factors promoting cell survival and proliferation, whereas its expression is inhibited by p53. Notably, BNIP3 and NIX belong to the Bcl-2 family of pro-apoptotic factors and therefore they also mediate cell death through both apoptosis activation and non-apoptotic mechanisms, depending on the stress conditions and cell types [159]. In consequence, BNIP3 and NIX regulation can determine the cell faith by alternatively inducing cell death or by promoting cell survival through moderate mitophagy [160].

It has been suggested that the induction of mitophagy instead of cell death by BNIP3 depends on its phosphorylation state of the N-terminus.

Moreover, the early autophagic degradation of the organelles exposing death signals is a mechanism to prevent mitochondria-mediated cell death. This pro-survival effect is also supported by the rescue of the anti-apoptotic factors, that translocate from the mitochondria to the endoplasmic reticulum during mitophagy [161]. Experimental evidence also suggested that BNIP3 and NIX pathways can cooperate with PINK1/Parkin machinery. In particular, the Parkin-mediated NIX ubiquitination results in the recruitment of NBR1 on mitochondria, thereby promoting mitophagy [162]. Recent evidence also demonstrated that BNIP3 contributes to the suppression of PINK1 proteolytic cleavage, promoting its accumulation on the OMM [163]. In addition, it has been shown that BNIP3 also recruits Parkin and Drp1 to perform the fission of the mitochondrion from the network, and successively its elimination through mitophagy [164].

## **1.7 Cutaneous malignant melanoma**

Melanoma is a type of solid cancer that arises from the transformation of the melanocytes, which derive from the neural crest progenitors that during the development colonize the skin, eye and several other tissues [165]. The melanocytes evolution is driven by the signalling of the receptor tyrosine kinases (RTK) and by the activity of the microphthalmia-associated transcription factor (MITF) [166]. The main function of melanocytes is to provide the keratinocytes with the melanin, a macromolecule that scatters and absorbs UV radiation, thus protecting the cell nucleus from radiation-induced DNA damages [167]. Melanoma is considered one of the most aggressive and therapy-resistant cancer, also representing the skin tumour with the highest rate of mortality though it accounts for only 1% of all skin malignant tumours [168]. Moreover, the worldwide incidence of cutaneous melanoma progressively increased over the last years, with a higher rate compared to other types of cancers [169]. Indeed, whereas in the past was considered as a rare tumour, in 2012 the skin melanoma turned out to be the 15th most common cancer in the worldwide, with 232,000 new cases estimated and 55,000 related deaths [170]. However, the incidence of cutaneous melanoma varies considerably among the countries depending on the skin phenotype and differences in the sun exposure.

This tumour usually affects young and middle-aged individuals, with a median age of 57 years at diagnosis [171]. It has been registered a linear increase in the incidence after the age of 25 years until the age of 50 years followed by a decrease, especially in the female sex. The major risks for skin melanoma development are family history, the high occurrence of dysplastic nevi, pale skin and light hair, immunosuppression, and ultraviolet radiation exposure [172]. In an ideal model, melanoma develops from a precursor lesion of a naevus that evolves to dysplastic naevus, to melanoma in situ and finally to invasive and metastatic melanoma. However, the scenario is more complex and rarely melanomas pass through every histopathological stage [167]. The melanoma prognosis strongly depends on the reached stage at the diagnosis time. Indeed, early diagnosis and surgical treatment allow a 5-year survival rate approximately of the 98% of patients with localized melanoma [173]. Conversely, this rate radically decreases when the cancer is diagnosed at the regional and invasive stages, falling to 63% and 16% respectively [174]. The melanoma progression is driven by the onset of new somatic mutations that confer additional tumour-related features to the transformed cells. Therefore, the advanced forms of the metastatic melanoma commonly harbour multiple mutations. Coherently, skin melanoma is characterized by the highest mutation rate compared to the other cancer types that also contributes to the occurrence of both intratumor and intertumor heterogeneity [175]. About the 80% of the melanomas carry mutations that potentiate or constitutively activate the MAPK signalling pathway, consisting of the small GTPase Ras that modulates the phosphorylation cascade between RAF-MEK-ERK kinases [176]. This signalling transduction results in the increased expression of the pro-survival and proliferative factors. Almost the 50% of melanomas display gain of function mutations (GOF) in BRAF, a range between 15- 30% GOF in N-RAS, whereas 12-18% have a loss of function of the MAPK-suppressor NF1 [177], [178], [179]. A fourth less representative subtype of melanomas is classified as triple wild-type because none of the previously mentioned mutations occurs [180]. Among the multiple mutations favouring the melanoma progression, recurrent alterations include loss of PTEN and amplifications of AKT3, caused by genomic deletions or by epigenetic silencing, that induce the constitutive activation of the phosphatidylinositol 3-kinase (PI3K) signalling [181], [182].

Other tumour-progression related mutations affect the p53 and RB signalling pathways, resulting in the evasion of the cell cycle checkpoints or apoptotic pathway cell death [172]. Even the alterations of transcription factors and epigenetic regulators have been related to melanoma progression, among which mutations that cause the MITF hyperactivation then promoting cell cycle progression and survival of the melanocytes [183].

### 1.7.1 B-raf signalling and BRAFV600E melanoma

The 90% of melanoma cases with BRAF mutations display the substitution in position 600 of valine for glutamic acid (V600E), whereas V600D and V600R substitutions are less frequent [184]. The BRAF gene encodes the B-raf protein, a serine/threonine kinase of 766 amino acids formed by a C-terminal catalytic domain, and two regulatory portions consisting in a Ras-GTP-binding self-regulatory domain, and the serine-rich hinge region.

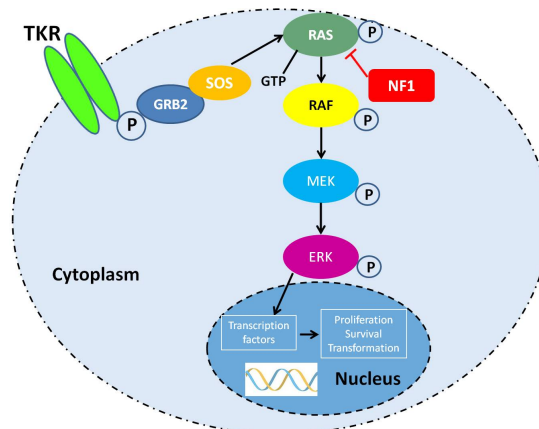


**Figure 12: The MAPK signalling pathway.**

B-raf belongs to the Raf family of the serine/threonine kinase and, together with the isoforms A-raf and C-raf, regulates the MAPK signalling pathway. In basal conditions, wild-type B-raf is in the auto-inhibited conformation, due to the hydrophobic interaction between the glycine-rich P-loop and the activation segment (A-loop) that makes the catalytic domains inaccessible for the ATP necessary for the catalysis.

In physiologic conditions, MAPK signalling is mainly activated by the receptor tyrosine kinases (RTKs) dimerization induced by the binding of the growth factors [185].

The dimerization enables the activation of the receptors by the autophosphorylation of tyrosine residues in their cytosolic domains, which provide the docking sites for the Grb2 protein to recruit SOS at the membrane. Here, SOS protein activates Ras by promoting the exchange of the GDP bound to it with GTP [186]. Activated Ras recruits Raf to the membrane and removes its auto-inhibition loops interaction allowing also the phosphorylation of various activating residues. In this manner, the catalytic site is released, and the full activation is accomplished by allosteric modifications induced by the dimerization of Raf proteins in homo and heterodimers. Raf complexes thus bind to and phosphorylate the kinases MEK1/2, which in turn, phosphorylate ERK1/2 proceeding the phosphorylation cascade that finally induces the expression of gene promoting cell survival and proliferation. On the other hand, the BRAFV600E mutation determines the replacement of a hydrophobic residue, valine, with a polar and hydrophilic one, glutamic acid, which disrupts the hydrophobic interaction between the A-loop and P-loop impeding the auto-inhibition of the protein. This singular aminoacidic substitution generates a BRAF monomer of which catalytic domain is constitutively active with a kinase activity 500-fold higher than its wild-type version, resulting in a detrimental uncontrolled cell proliferation [187].

### **1.7.2 Melanoma treatment**

The choice of the therapeutic approach for melanoma treatment strongly depends on the histopathological stage, the body localization and the genetic profile of a tumour at the diagnosis. Whereas the surgical resection of early-stage melanomas is mostly curative, this approach is rarely effective for advanced stages of cancer [188]. Furthermore, part of the patients undergoing surgical removal displays the subsequent relapse along with tumour dissemination, whereas the 10% of melanoma stages is diagnosed at the late malignant stage [189]. Moreover, nearly the 4% of all melanoma cases manifests as metastases without a detectable primary tumour. Besides surgery, until 2011, the standard treatment for advanced melanoma included chemotherapy with the alkylating agent dacarbazine (DTIC), and high-dose interleukin 2 (IL-2), treatment that showed very low efficacy [190].

In addition, the interferon- $\alpha$ -2b therapy was the only approved adjuvant treatment for patients at high risk of cancer progression. Despite the available therapies, malignant melanoma persisted to be associated with a poor prognosis and only curable at early, pre-metastatic stages. Nevertheless, the research efforts targeted to shed light on the mechanism underlying the melanoma onset and progression allowed the development and approval of new therapeutic agents starting from 2011. In particular, target therapies with BRAF and MEK inhibitors, along with immune checkpoint inhibitor therapies such as the cytotoxic T-lymphocyte-associated antigen 4 (CTLA-4) and the programmed cell death protein 1 (PD-1) blocking antibodies, have strongly improved the patient outcomes. Indeed, statistic reports shows how from 2011 the overall survival for the invasive and metastatic melanomas increased from the 9 months to at least 2 years [191].

### **1.7.2.1 Immunotherapeutic antibodies**

The immunotherapy approach for cancer treatment has been designed based on the evidence that cancer development induces the activation of the immune response [192]. Indeed, chronic inflammation and immune cells are commonly found within the tumour microenvironment and are often linked to antitumoral responses. In this scenario, the T cells infiltrating the cancer mass, after being activated by antigens of the cancer cells, expand earning the capacity to destroy cells displaying these tumour-specific epitopes. This endogenous antitumoral response is limited by the autoregulation of both stimulatory and inhibitory signalling pathways, and escaping mechanisms developed by cancer cells to elude the immune system recognition and activation, resulting in a low efficiency of the cancer eradication immune system mediated. Cancer immunotherapies have been developed to potentiate the endogenous anticancer immune response. One way to do so is to block the physiologic checkpoints of the T-cell mediated response. In particular anti-CTLA-4 antibodies act by blocking the CTLA-4 inhibitory checkpoint receptor, responsible for the cancer immune tolerance by inhibiting the T cell activation [193]. In this manner, anti-CTLA-4 antibodies potentiate the pro-inflammatory T cell cytokine production increasing in this way T cell clonal expansion and infiltration in the tumour mass. The anti-CTLA-4 antibody ipilimumab was approved by the Food and Drugs

Administration (FDA) in 2011 for the treatment of advanced melanoma [168]. Another class of immune checkpoint blockades for the melanoma treatment are the PD-1 blocking antibodies that act by binding and blocking the PD-L1 PD-L2 co-inhibitor molecules of the T cell activation. Among these, nivolumab and pembrolizumab were approved for the treatment of malignant melanoma by the FDA in 2014 and 2015, respectively.

### 1.7.2.2 MAPK pathway-targeted therapy and vemurafenib

The most promising approach for the metastatic melanoma treatment consists of the targeted therapy toward the MAPK pathway [191]. Specific inhibitors have been developed and tested obtaining extraordinary results leading to the FDA approval of the BRAF inhibitors (BRAF-I) vemurafenib (PLX4032) and dabrafenib in 2012 and 2013 respectively, and the MEK inhibitor trametinib in 2013.

Among these, vemurafenib has been selected as the treatment of choice for the metastatic melanoma harbouring the BRAFV600E mutation [194]. PLX4032 functions as ATP-competitor by binding the catalytic domain of BRAF and then blocking the phosphorylation cascade responsible for the uncontrolled proliferation. The vemurafenib therapeutic effects are related to the molecular difference between wild-type and BRAFV600E mutant kinases [195].

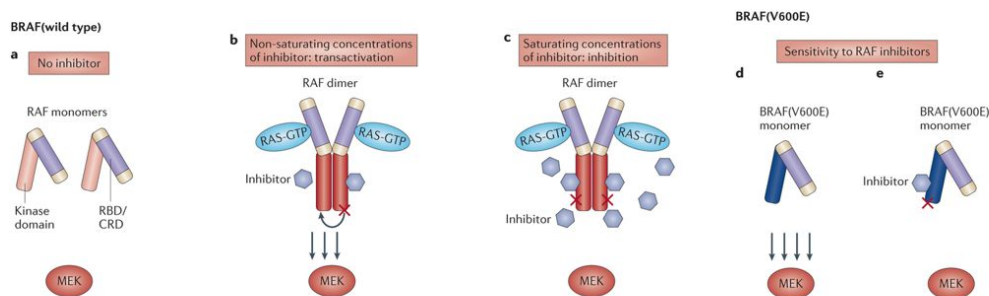


**Figure 13: The RAF inhibitor paradox: action of vemurafenib on BRAF wild-type and BRAFV600E.**

As previously reported, while normal BRAF proteins are enabled by Ras upon specific stimuli and functions as a dimer, BRAFV600E kinases are active as a monomer. Therefore, in basal conditions with normal Ras activity, PLX4032 binds and inactivates BRAFV600E kinases. In these conditions, wild-type B-raf retains its inactive monomeric form, due to the absence of Ras activation. Unfortunately, the therapeutic response to vemurafenib is limited by the potentiation of the ERK signalling, a side effect that may occur upon prolonged or at high-concentration treatment. This phenomenon is usually named “the RAF inhibitor paradox”, and several studies tried to clarify the mechanisms underlying it. Experimental data suggested that saturating the concentration of vemurafenib induces the dimerization and transactivation of both wild-type B-raf kinase in normal cells and mutant B-raf in transformed cells, thus promoting the cell proliferation and transformation [196]. Therefore, BRAF-Is administration must be performed at finely defined concentrations. Reduced effect of the BRAF-Is targeted therapy may also arise from drug resistance mechanisms developed throughout the progression of the tumour and its adaptation to stress and environmental conditions.

### **1.7.2.3 Limitation of the melanoma therapies and drug resistance**

Although immune and target therapies available revolutionized the malignant melanoma treatment, improving the disease management and the outcome, medicine is still far from having a cure for most of the cases. In particular, metastatic melanoma healing failure has been related to both intrinsic and acquired resistance to the treatments. The absence of therapeutic effect since the beginning of the drug administration (primary or intrinsic resistance) is mainly determined by the features originated from the genetic profile of the tumour that varies among the distinct cases. Accordingly, the heterogeneity of the multiple mutations that may drive the melanoma progression reflects the heterogeneity of patient response to therapies. Due to the higher number of melanomas cases intrinsically resistant, immunotherapy approaches displayed a lower response rate but a potential long durable effect due to the lower trend in the development of secondary resistance compared to BRAF inhibitor therapies. Conversely, BRAF-I treatments allow a high rate of benefits achieved in a short period of time in terms of tumour regression,



but frequently the therapeutic effect is only transient. Indeed, after an initial improvement, near the 50% of patients generally have a relapse within 7 months from the beginning of the BRAF-I monotherapy due to acquired resistance, in most cases showing a more aggressive form of cancer [197], [198]. Bearing in mind that the majority of the metastatic melanomas has the BRAFV600E mutation and the vemurafenib exhibits appreciable but time-limited therapeutic effects, several studies focused on the identification of the mechanisms supporting both the intrinsic and acquired resistance to PLX4032, with the purpose of developing secondary drugs to limit the BRAF-Is loss of efficacy [199]. It has been reported that the resistance of BRAFV600E-tumours to BRAF-Is is predominantly driven by the reactivation of the MAPK pathway at a different level, caused by the occurrence of other mutations, among which the gain of function of receptor, tyrosine kinases Ras and MEK, and the loss of function of NF1. However, BRAF-I drug resistance may also arise from the activation of alternative pathways promoting cell survival and proliferation, such as the PI3K/AKT/mTOR pathway. The mutational inactivation of the inhibitory regulator PTEN and RB1 of the PI3K pathway has been related to PLX4032 resistance. The discovery of these molecular mechanisms of drug resistance suggested the use of combined therapies consisting of the administration of BRAF-I together with PI3K/AKT/mTOR pathway inhibitors, leading to satisfying results overcoming the resistance to the MAPK inhibitor monotherapy. The loss of response to vemurafenib may also occur through other several mutational events promoting cell death resistance, uncontrolled proliferation and the cell cycle progression. Though the number of genetic alterations described as favouring the tolerance to BRAF-inhibitor is great, the combinations in which they may occur is even greater. In this view, the management of malignant melanoma has moved toward the administration of personalized therapies, in order to provide the best therapeutic effect and limit the onset of relapse with more aggressive tumour. The growth of both diagnostic technology, drugs development and the acquired knowledge about the melanoma biology led to identifying the combination of the different approaches (immunotherapy, chemotherapy, targeted therapy) as the treatment of choice for the melanoma, selected and combined based on the markers identified in cancer to treat. Even though the dual therapeutic approach allows a better and longer life expectancy for melanoma patients, it is not curative in the majority of the

cases since the complete remission is hampered by resistance onset, even if delayed compared the one occurring with the monotherapy.

### **1.7.3 miRNAs and the plasticity of melanoma**

miRNAs are single stranded small non-coding RNAs of about 19-24 nucleotides in length. They are transcribed in the nucleus and function as post-transcriptional regulators of gene expression by binding the target messenger RNA (mRNA) and inducing its direct degradation or the inhibition of the translation [200]. A single miRNA simultaneously inhibits the expression of several mRNAs and therefore their related proteins, thus it finely regulates essential cellular processes such as differentiation, proliferation and apoptosis. The miRNA expression pattern is crucial for the maintenance of cellular homeostasis and organism development. Qualitative and quantitative dysregulations of miRNAs levels have been related to several human diseases, among which cancer [201]. Around 50% of miRNAs are controlled by a dedicated promoter, whose transcriptional activation is modulated by the intracellular signalling in response to external stimuli. The additional miRNAs are localized within intronic or exonic regions and are synthesized within their transcription units [202]. miRNA synthesis usually begins with transcription of a long pri-miRNA by the nuclear RNA polymerase II or III, then cleaved by the microprocessor complex to form a hairpin-shaped pre-miRNA. Once exported into the cytosol, the pre-miRNA is further processed by the RNase Dicer that creates an imperfect duplex long about 22 nucleotides with a 3' overhang recognized by the Argonaute protein (Ago). Ago selects and isolates one of the duplex's strands and loads it into the RNA-induced silencing complex (RISC) that drives the miRNA in the pairing to the specific mRNA-targets to be regulated.

In the past, miRNAs in cancer were classified as oncogenic (oncomiR) or tumour suppressor, considering their in vitro-ability to inhibit the expression of a specific tumour suppressor or an oncogene protein, respectively. However, it is now widely accepted that each miRNA can induce both oncogenic and tumour suppressive responses, by acting on distinct cellular targets at the same time [203], [204]. Consequently, the miRNA effects on the cancer progression must be considered as the result of the targeting of different

signalling pathways and strongly relies on the genetic and microenvironmental background of the tumour considered. In this view, define the effect and mechanism of action, even just for a miRNA may result tricky, but it may provide an effective strategy to control numerous genes simultaneously as a therapeutic approach to treat multi-mutational genetic diseases, such as melanoma. Many studies proved that the metastatic melanoma resistance is also controlled by the tumour microenvironment crosstalk and by the epigenetic modifications that may occur through miRNAs activity [205]. Indeed, it has been demonstrated that miRNAs contribute to the evolution of the molecular and metabolic plasticity of melanoma, independently from the onset of new genetic mutations. Stress conditions derived from the hostile environment during cancer progression and from therapy selective pressure may modulate miRNAs levels. For example, changes in specific miRNAs levels have been associated with cell death resistance and the activation of the epithelial-mesenchymal transition in melanomas. In this view, miRNAs contribute to the development of heterogenous melanoma masses, that may consist of slow-cycling and apoptosis-resistant cells, and high-proliferative clones that may acquire metastatic features [199]. Different recent studies showed that in melanoma progression the miRNAs expression pattern varies following the development of a tumour throughout the different stages and that melanoma growth and resistance to treatment are eased by the loss of certain miRNAs, and supported by the overexpression of others [206].

Moreover, miRNAs intracellular pattern can also be modified by their delivery via exosomes, small vesicles that contribute to tumour progression throughout the transfer of genetic information, not only between closely localized cells, but also to distant tissues [207]. An overview of the state-of-the-art knowledge about miRNAs dynamics in melanoma biology is provided by Romano and Kwong [208], and Thyagarajan et al. [206] in recent reviews as well as depicted in the Figure 14.

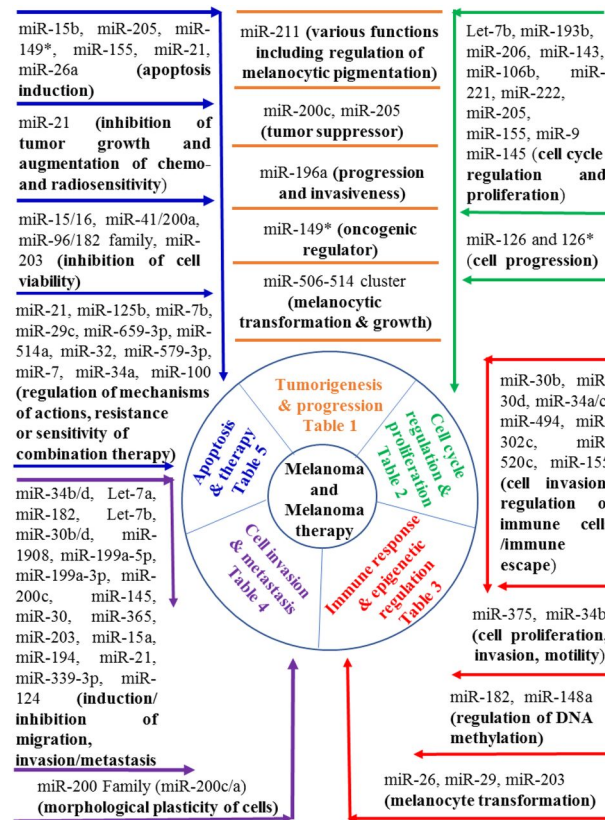


**Figure 14: Schematic representation of miRNAs involved in melanoma progression and therapy.**

So far, about 50 miRNAs have been identified and related to the regulation of melanoma behaviour, along with the recognition and validation of their main molecular targets. The evidence collected highlighted how miRNAs work in the progression and development of resistance in melanoma mainly by dysregulating the signalling of pathways typically involved in malignant transformation.

The complexity of melanoma biology and mechanisms of drug-resistance, along with the exceptional flexibility of these tumours, requires the availability of new therapeutic agents. The identification of new solid targets makes it possible to develop target specific therapy further. The increasing knowledge about the role of miRNAs in melanoma biology make them promising candidates for the development of diagnostic and therapeutic tools.

## **1.8 Intracellular pathways related to cancer progression**

Genetic and epigenetic alterations lead to cell transformation and cancer development promoting to uncontrolled cell proliferation and to disruption of mechanisms controlling cell fate. Several of these mutations affect the physiologic intracellular pathways that control cell cycle progression, cell proliferation, cell motility, apoptosis, and even affecting modification in the tumour microenvironment and the immune response. The hyperactivation of oncogenic signalling pathways together with the inhibition of tumour suppressors signalling, is another mechanism for cancer cells to stand against cancer treatments. In this context, down below are described the pathways frequently mutated in cancers and able to promote drug-resistance: Wnt/ $\beta$ -catenin, TGF-  $\beta$ , Hedgehog and p53.

### **1.8.1 Wnt/ $\beta$ -catenin canonical pathway**

Wnt signalling consists of three different intracellular pathways activated by the binding of the Wnt-protein ligand to the membrane-integrated receptors of the Frizzled family, that transduce the signal to the Dishevelled (Dsh) proteins in the intracellular side. The Wnt pathways are activated by different isoforms of Wnt ligands, Frizzled receptors and Dsh proteins that determine the type of transduction cascade in the cell. While Wnt canonical pathway involves the  $\beta$ -catenin protein, non-canonical pathways are independent from it. The canonical pathway is mainly activated during the embryonic development and it is responsible for the transcription of the genes involved in the body axis determination, cell fate specification, cell migration and proliferation [209]. While during the development the Wnt canonical pathway determines the proper formation of tissues, such as bone, heart and muscle, in the adult is essential for stem cell renewal and tissue homeostasis. Differently, the transduction of the two non-canonical pathways determines the regulation of the planar polarity and shape of the cells by modulating the cytoskeleton and the control of the calcium signalling.

While the Wnt non-canonical pathways are less characterized and their pathological role is still unclear, the Wnt/ $\beta$ -catenin pathway has been linked to several human disorders, such as cancer. In physiological conditions, Wnt canonical pathway is constitutively repressed by continual degradation of the cytoplasmic  $\beta$ -catenin mediated by the destruction complex, which is composed by Axin scaffold protein, APC tumour-suppressor protein, casein kinase 1 CK1, and the glycogen synthase kinase 3 beta GSK-3 $\beta$ . In particular, in the absence of the Wnt ligand, the kinase GSK-3 $\beta$  and CK1 phosphorylate  $\beta$ -catenin, determining its recognition by the  $\beta$ Trcp E3 ubiquitin ligase that carries out the  $\beta$ -catenin ubiquitination and proteasomal-mediated degradation. The  $\beta$ -catenin continuous elimination prevents its action in the nucleus, and genes transcription is thereby inhibited by the DNA-bound T cell factor/lymphoid enhancer factor (TCF/LEF) family of proteins.

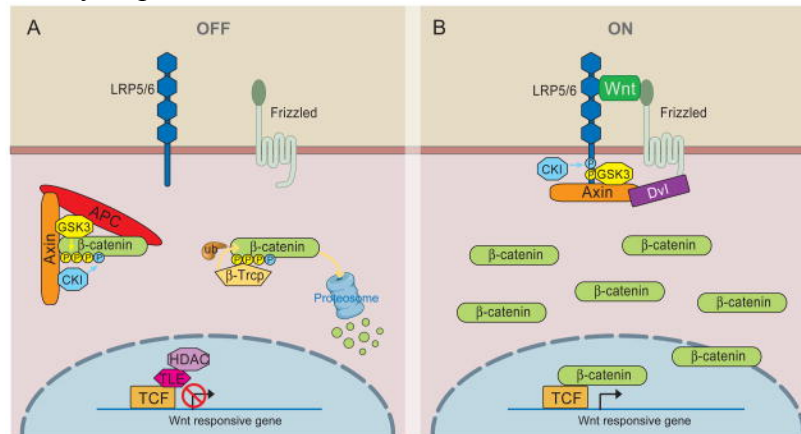


**Figure 15: The Wnt/  $\beta$ -catenin canonical pathway.**

When Wnt ligand binds to the Frizzled receptor (Fz) and its co-receptors LRP6 or LRP5, the formation of the Wnt-Fz-co-receptor complex occurs, resulting in the recruitment of the scaffolding protein Dishevelled (Dsh). The Dsh proteins phosphorylate the co-receptor, leading to the recruitment of the destruction complex to the membrane, an event that causes the inhibition of the  $\beta$ -catenin phosphorylation and degradation. Under these circumstances,  $\beta$ -catenin is stabilized, accumulated and translocated to the nucleus, where it forms complexes with TCF/LEF proteins, activating the expression of the Wnt target genes. Interestingly, the aberrant and increased activation of the Wnt/ $\beta$ -catenin pathway has been linked to the absence of effector T cells within melanoma tumours in humans and mice models [210].

Moreover, clinical studies demonstrated that melanoma patients with lower nuclear levels of  $\beta$ -catenin have a better prognosis when treated with BRAF-inhibitors [211].

### 1.8.2 TGF- $\beta$ pathway

The transforming growth factor- $\beta$  (TGF- $\beta$ ) is a polypeptide ligand that activates a signalling responsible for the control of cellular proliferation and differentiation, wound healing, angiogenesis and also embryonic development [212]. TGF- $\beta$  is synthesized by the cells and released in the extracellular matrix as an inactive homodimer, subsequently activated by proteolysis. The active TGF- $\beta$  homodimer stimulates the signalling by binding the TGF- $\beta$ RII receptor and inducing its hetero-oligomerization with the TGF- $\beta$ RI. Both TGF- $\beta$ RI and TGF- $\beta$ RII contain a serine/threonine-protein kinase domain in the cytosolic terminus, which catalysis is activated following the conformational changes induced by receptors hetero-tetramerization, that induces the reciprocal phosphorylation. In these conditions, active TGF- $\beta$  receptors recruit and phosphorylate the receptor-regulated effector proteins (R-Smads), such as Smad2 and Smad3. Once phosphorylated, the R-Smads form heteromeric complexes with Smad4 and translocate to the nucleus to regulate gene expression [211].

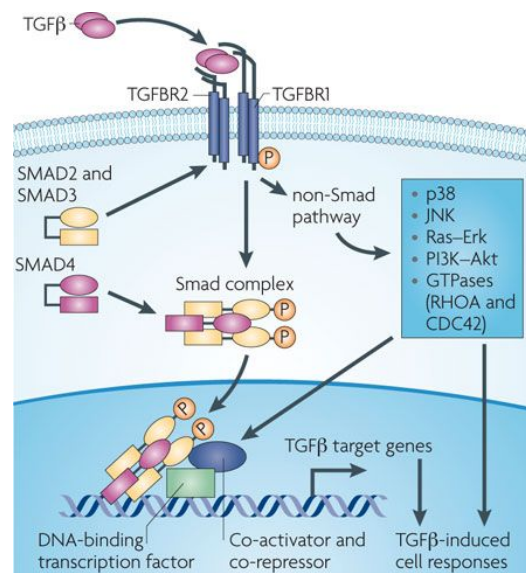


**Figure 16: The TGF- $\beta$  pathway.**

Conversely, the class of the inhibitory Smads (I-Smads) comprising Smad6 and Smad7, antagonize the signalling by interacting with the receptors preventing the phosphorylation of R-Smads or interfering with R-Smad/Smad4 complexing. The transcription of I-Smads is regulated by TGF- $\beta$  a negative feedback loop. TGF- $\beta$  signalling pathway plays two different roles during cancer development depending on the stage of the disease. In particular, in the early phases of the tumorigenesis, TGF- $\beta$  activation may limit cancer progression, acting as a tumour suppressor [213]. Conversely, cancer cells in the late stages commonly acquire the capacity to produce and release a high quantity of TGF- $\beta$  that promotes invasion and metastasis by acting both in autocrine and paracrine manner, inhibiting the immune system anticancer response, and modulating the activity of the cells of the tumour microenvironment [214]. This latter scenario is typical of melanoma in metastatic stages.

### **1.8.3 Hedgehog pathway**

The hedgehog pathway (HH) plays a pivotal role in the embryonic stages, orchestrating cell proliferation and the commitment necessary for tissue, organs morphogenesis and whole organism formation. In the adult, HH activation is restricted to stem and progenitor cells within various organs and it is involved in the regeneration and the maintenance of their homeostasis. In the mammalian, the HH pathway may be activated by the three different proteins, Sonic-Hedgehog (Shh), Indian-Hedgehog (Ihh), and Desert-Hedgehog (Dhh), that have similar functioning, but they show different pattern of expression in different tissues. While Shh is mainly involved in the cell type specification of the neuronal cells and limbs modelling, Ihh drives the skeletal development, mainly by regulating the endochondral ossification during the fetal development [215]. Conversely, Dhh expression and mechanism of action is restricted to the gonads and in particular to Sertoli cells, cells of the testis, granulosa and ovaries cells. In the canonical pathway, the HH proteins initiate the signalling pathway by binding to a surface receptor complex consisting of PTCH1 (twelve-pass membrane protein patched 1) and SMO (G-protein-coupled receptor smoothened). Under physiological conditions, PTCH1 inhibits SMO, keeping it in an unphosphorylated form and inducing its degradation by endocytosis and



lysosomal degradation. When HH ligand binds PTCH1, SMO is hyperphosphorylated and its degradation is prevented. Thus, SMO accumulates on the membrane and with its stabilization the intracellular signal transduction begins.

HH proteins also bind PTCH2 and others accessory proteins in the cellular surfaces, that function as co-receptor helping signal propagation and determining the HH gradient necessary for the correct morphogenesis.

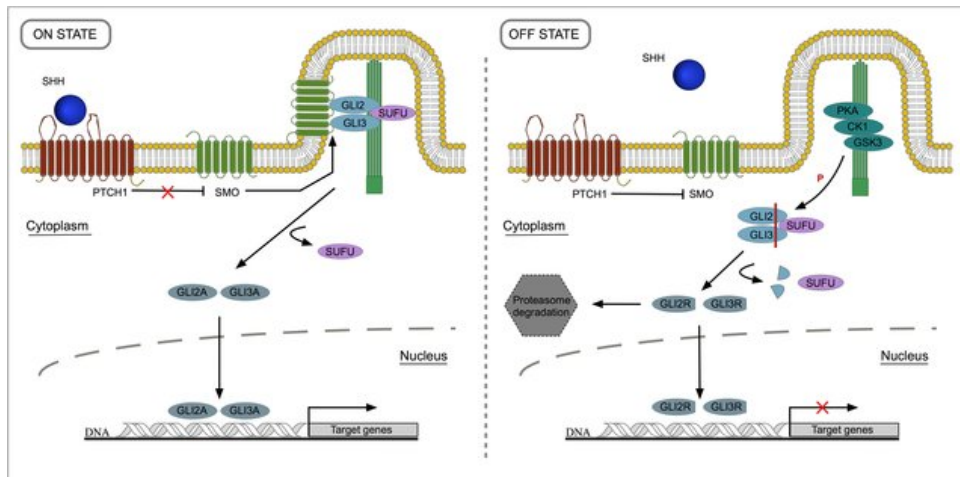


**Figure 17: The Sonic-Hedgehog pathway.**

SMO signal transduction promotes the accumulation of the GLI2 and GLI3 (glioma-associated oncogene family members) transcription factors into the nucleus, where they trigger the expression of the HH target genes, among which GLI1. Therefore, GLI1 protein is transcribed upon pathway stimulation and acts as a transcriptional activator determining a potentiation of the HH signalling. Conversely, GLI2 and GLI3 are constitutively expressed in basal conditions and inactivated by the cleavage of the C-terminus through ubiquitination and partial proteasomal degradation. In the absence of HH ligands, the truncated forms of GLI2 and GLI3 acts as transcriptional inhibitors. The suppressor of fused homolog SUFU prevents GLI2 and GLI3 migration to the nucleus, inhibiting their activity. Upon HH activation, active GLI2 and GLI3 trigger the expression of genes involved in cell cycle progression and proliferation (e.g. cyclin D1 and MYC), in the epithelial to mesenchymal transition (e.g. SNAIL), invasiveness (e.g. osteopontin), stem cell self-renewal (e.g. NANOG, SOX2) and pro-survival proteins (e.g. Bcl-2) [216].

Moreover, the components of the HH pathway may act independently through a non-canonical signalling [217]. Aberrant reactivation and dysregulation of Hedgehog signalling pathways concur in tumorigenesis by potentiating cell proliferation, resistance to cell death, EMT and a plethora of other tumour-related features. Interestingly, the overexpression of GLI1 and GLI2 proteins have been related to acquired resistance to vemurafenib in metastatic melanoma [218].

#### **1.8.4 p53 pathway**

p53 transcription factor is the most important tumour-suppressor in the cells and is activated in response to stress stimuli. In physiologic conditions, p53 is constitutively expressed but its protein levels are kept low by the activity of the specific regulators MDM2 and MDMX, also named MDM4 [219]. In particular, MDM2 is an E3 ubiquitin ligase and forms heterodimers with its regulator MDMX and ubiquitinate p53, determining its nuclear export and proteasomal-mediated degradation. Moreover, the direct binding of MDMX to p53 prevents its activation by blocking the transactivation domain of the transcription factor. In presence of cellular component injury and DNA damage signals, unfavourable environmental conditions, or aberrant signalling of intracellular pathways, several stress receptor mediators can activate p53 through different post-translation modifications such as ubiquitination, methylation, acetylation, or sumoylation, regulating the expression of its target genes involved in the cell-cycle progression and DNA repair mechanism [220]. In case of irreparable damages, p53 can also mediated the activation of the cell death apoptosis. Interestingly, p53 also regulates the transcription of genes essential in cellular senescence, angiogenesis, and autophagy, therefore playing a pivotal role in the maintenance of cell homeostasis. Relevantly, p53 has been found inactivated in almost all transformed cells, either by genetic mutations or by dysregulation of the pathways associated to its activation. In cutaneous melanoma, nearly the 90% of cases are characterized by the inactivation of wild-type p53 [221].

## 2 Aims of the study

Cancer cells are characterized by peculiar intracellular signalling and flexible metabolism compared to normal cells that confer them a great adaptability to the unfavourable environmental conditions encountered during the tumour progression.

As a powerhouse of the cells, mitochondria play a pivotal role in cancer development by modulating their activity in response to the external stimuli and cancer-altered signalling pathways, allowing cell proliferation and survival also in conditions of poor oxygen availability, nutrients limitation, adverse pH and anti-cancer treatments. In this scenario, targeting the mitochondrial processes that drive the flexibility and the metabolic rewiring of transformed cells is now considered a hopeful therapeutic approach for the cancer treatment. For this purpose, research efforts in the last decades have been directed toward the identification of the bioenergetics plasticity mediators in the tumour cells.

Interestingly enough, different experimental data showed overexpression of the endogenous inhibitor of the  $F_1F_0$ -ATP synthase  $IF_1$  in many human cancers and its involvement in mechanisms that give cancer cells a selective advantage. In normal cells,  $IF_1$  is the master negative regulator of ATP hydrolysis mediated by the reversal of the  $F_1F_0$ -ATP synthase, that occurs in the ischemic episodes as a consequence of the mitochondrial electrochemical gradient collapse. Under these conditions,  $IF_1$  exerts an essential protective role by limits the energy consumption ensuring cell homeostasis. While the function of this small evolutionary conserved protein is well defined in normal cells, the role of  $IF_1$  in cancer is still controversial. On the basis of its physiological role, we hypothesized that  $IF_1$  may preserve cancer cell viability in low oxygen conditions typical of the poorly vascularized tumour mass, through the limitation of the ATP consumption by the  $F_1F_0$ -ATP synthase. Indeed, no evidence is available in the literature that clarifies whether the mitochondrial ATP synthase may reverse its activity also in cancer cells, and in case, the necessary conditions to induce the switch from the synthetic activity towards ATP consumption.

In order to address these issues, we previously evaluated the main bioenergetics parameters of osteosarcoma cells expressing IF<sub>1</sub> and silenced for it when exposed to hypoxia (0.5% O<sub>2</sub>) and severe hypoxia (0.1% O<sub>2</sub>). Surprisingly, we found that osteosarcoma cells can synthesize ATP through oxidative phosphorylation even at low oxygen tension, together with the maintenance of high levels of the mitochondrial membrane potential, thus excluding the IF<sub>1</sub> activation. Proved that the reversal of the F<sub>1</sub>F<sub>0</sub>-ATP synthase does not occur even in severe hypoxia, this study aims to investigate whether this phenomenon occurs in cancer cells in a more severe condition represented by anoxia, and to evaluate the eventual contribution of IF<sub>1</sub> on the cellular metabolism in these circumstances. For this purpose, GFP-negative clones stably silenced for IF<sub>1</sub> were produced from the 143B human osteosarcoma cell line, that expresses high levels of the inhibitor. The main bioenergetics parameters of these cellular models were then assessed in anoxia-mimicking conditions, performed by exposing the cells to the uncoupler FCCP. The latter compound functioning as protonophore abolishing the H<sup>+</sup> gradient across the inner mitochondrial membrane, reproducing the  $\Delta\Psi_m$  collapse occurring in ischemic episodes. A second set of osteosarcoma clones stably expressing a red fluorescent protein targeted to the mitochondria was produced and characterized with the aim to evaluate the mitochondrial mass in intact cells exposed to anoxia-mimicking conditions.

Another effect of the great adaptability of transformed cells is the frequent onset of acquired resistance to therapeutics, that represents the most significant challenge in the treatment of several types of cancers, among others cutaneous melanoma, the more aggressive form of skin cancer. Among the factors that influence tumour progression and therapies efficacy, numerous recent studies demonstrated that the dysregulation of miRNAs expression plays a critical role through the epigenetic regulation of oncogenic and tumour-suppressor genes. The characterization of miRNAs, their molecular mechanisms and the identification of their targets, along with their involvement in acquired therapy resistance could drive forward the development of new target therapies and the identification of risk-related biomarkers that may improve the follow-up and treatment of patients affected by melanoma. In this context, the second part of the study was developed during my internship at Children's Hospital Los Angeles, with the particular aim to understand the role of miRNAs in drug resistance towards vemurafenib

in BRAFV600E-mutated metastatic melanoma. The V600E mutation drives the onset and progression of nearly 50% of the melanoma cases, by determining the constitutive activation of the B-raf kinase in the MAPK signalling pathway, leading to the uncontrolled proliferation of the transformed cells. The vemurafenib, also named PLX4032, is a compound developed to specifically target the aberrant signalling of BRAF, found in several types of tumours. However, despite PLX4032 represents the gold standard treatment for the metastatic melanoma, nearly 50% of patients display aggressive cancer relapses due to the acquired resistance to the drug.

For these investigations, the M21 and Colo38 metastatic melanoma cells obtained from patients carrying the BRAFV600E, and the *in vitro* derived M21R and Colo38R cells resistant to PLX4032 were characterized. The first part of the investigation focused on the identification of the intracellular pathways altered in resistant cells that could confer a tumour-related behaviour, and therefore drive the acquired resistance to treatment as a consequence of the miRNAs action. For this purpose, the activation of the main oncogenic and tumour-suppressor pathways related to cancer progression was evaluated and compared in cells sensitive to vemurafenib and resistant cells. Subsequently, with the aim to identify the miRNAs that could determine drug tolerance, the pattern of miRNAs expression of resistant and sensitive melanoma cellular models was characterized and compared. Finally, the effects of the modulation of a first candidate miRNA were assessed in M21 and M21R, in order to evaluate its role in the acquisition of drug-resistance features. Recognize the miRNAs that trigger resistance to vemurafenib and characterize their mechanism of actions may identify novel targets for melanoma treatment aiming to counteract the acquired resistance onset.

# 3 Materials and Methods

## 3.1 Cell cultures

### 3.1.1 Human Osteosarcoma cell lines

Human osteosarcoma 143B cell line was cultured in Dulbecco's Modified Medium (DMEM) supplemented with 10% fetal bovine serum, 25 mM glucose, 4 mM glutamine, and 1 mM, in presence of 100 U/mL penicillin, 100 µg/mL streptomycin, 0.25 µg/mL amphotericin B. The scrambled and IF<sub>1</sub>-silenced derived clones were maintained in complete medium supplemented with puromycin 1 µg/mL. The cell lines were maintained at 37°C in humidified atmosphere with 5% CO<sub>2</sub>, in a cell culture incubator. The experiments were performed seeding the cells in DMEM complete medium, replacing it with fresh medium after 18 hours, in presence of FCCP with, to perform anoxia-mimicking conditions. After 24 or 48 hours of incubation either in normoxia (21% O<sub>2</sub>) or in hypoxia (0.5% O<sub>2</sub>) in the Invivo2 hypoxic work station (Ruskin), cells were collected and assayed. Cell culture reagents were purchased from Gibco (Life Technologies), with exception of glucose, pyruvate and FCCP, provided by Sigma-Aldrich.

### 3.1.2 Human Melanoma cell lines

Human Melanoma cell lines were kindly provided by Dr Soldano Ferrone (PhD, MD), from Harvard University [222]. Briefly, the parental BRAFV600E melanoma cell lines M21 and Colo38 were derived by metastatic lesions of patients with melanoma. Cells were cultured in RPMI-1640 L-glutamine medium (Gibco) supplemented with 10% FBS (Omega Scientific), 100 U/mL penicillin, 100 µg/mL streptomycin (Life Technologies).

Cell lines with acquired vemurafenib resistance, M21R and Colo38R were generated by culturing parental M21 and Colo38 cells in medium with PLX4032 (ChemieTek) for 2 months. The isolated resistant cells M21R and Colo38R were then maintained in presence of 2  $\mu$ M and 5  $\mu$ M vemurafenib, respectively. All cells were cultured at 37°C in a 5% CO<sub>2</sub> humidified atmosphere.

### **3.1.3 Phoenix retrovirus-producer cell line**

The Phoenix cell line ( $\Phi$ -Nx-A) was used to obtain amphotropic retroviruses carrying the vectors for the IF<sub>1</sub>-silencing [223]. The Phoenix cells stably express the Gag, Pol and Env viral proteins necessary for the virus formation and its release in the culture medium. Once transfected with a plasmid, the Phoenix cells package the retroviruses with it. The obtained viruses are capable of infecting mammalian cells and releasing the carried vector but are not able to replicate and exit from the new host. Phoenix cells were maintained in Dulbecco's Modified Medium (DMEM) containing 10% heat-inactivated fetal bovine serum, 25 mM glucose (Sigma), 4 mM glutamine (Sigma), and 1 mM (Sigma), with 100 U/mL penicillin, 100  $\mu$ g/mL streptomycin (Life Technologies). Cell lines were maintained at 37°C in humidified atmosphere with 5% CO<sub>2</sub>.

## **3.2 Bacterial transformation and plasmids purification**

Plasmids of interest were transformed into chemically competent DH5 $\alpha$  *E. coli* (Invitrogen) using the heat shock method. Briefly, vector solutions were added to DH5 $\alpha$  cell resuspensions, carefully flicked to mix and incubated on ice for 30 minutes. Heat shock was then performed placing the mixtures at 42°C for 30 seconds and immediately cooling them down for 2 minutes on ice. Transformed bacteria were then revitalized adding SOC medium (0.5% Yeast Extract 2% Tryptone 10 mM NaCl 2.5 mM KCl 10 mM MgCl<sub>2</sub> 10 mM MgSO<sub>4</sub> 20 mM Glucose) and incubating at 37°C for 1 hour with shaking at 250 rpm. Bacteria were then seeded onto pre-warmed Petri plate, containing solidified LB-agar (Sigma) supplemented with 100  $\mu$ g/mL Ampicillin and incubated for

18 hours at 37°C. Single colonies were then picked up from plates and inoculated in LB-broth in presence of Ampicillin and grown at 37°C with shaking at 250 rpm. Plasmids were finally isolated from bacteria cultures using PureLink™HiPure Plasmid Filter Maxiprep Kit (Invitrogen) following the manufacturer's instructions and quantified through NanoVue spectrophotometer (GE Healthcare's Life Sciences)

### **3.3 Production of stably IF<sub>1</sub>-silenced GFP-negative osteosarcoma clones**

Osteosarcoma GFP-negative clones were obtained via RNA interference, infecting 143B parental cells with the retrovirus carrying the pGFP-V-RS vector, encoding for either a negative-control shRNA (scrambled-TR30013) or shRNA directed to IF<sub>1</sub> (GI325936). The GI325936 plasmid was previously identified as the most efficient for IF<sub>1</sub> silencing in 143B cells[87]. The plasmids were purchased from OriGene Technologies.

#### **3.3.1 Phoenix cell line transfection and collection of viruses**

24 hours prior to transfection,  $\Phi$ -Nx-A cells were seeded in 100 mm Petri dishes, in order to have approximately 80% of confluence at the time of the procedure. The following day, the culture medium was replaced and Phoenix cells were maintained in DMEM complete medium, described above. Phoenix cells were then transfected with 10  $\mu$ g of either TR30013 (scrambled) or GI325936 (shRNA) pGFP-V-RS vector, using the transfection reagent polyethyleneimine (or PEI, Polysciences Inc), with a DNA:PEI ratio of 1:8 (w/w). Transfected cells were incubated for 24 hours at 37°C in a humidified atmosphere with 5% CO<sub>2</sub>. Culture media of transfected  $\Phi$ -Nx cells were then collected in conical tubes and centrifuged at 1500 rpm for 5 minutes to pellet cell debris. Supernatants containing assembled retroviruses were finally filtered through a 45  $\mu$ M filters.



### **3.3.2 143B cell line infection and selection of clones**

Retrovirus packaged with scramble shRNA control or IF<sub>1</sub>-shRNA were used to infect 143B parental cells. 24h before the infection, osteosarcoma cells were seeded in 35 mm Petri dishes at a cell density proper to have almost 70% of confluence at the time of the transduction. The next day, 143B cells were pre-incubated with fresh complete medium supplemented with 8 µg/mL polybrene (Sigma) for 10 minutes at 32°C in a humidified atmosphere with 5% CO<sub>2</sub>. Infections were then performed dispensing the virus supernatants supplemented with polybrene onto cells, and incubating them 5 hours at 32°C and subsequently for 18 hours at 37°C in a humidified atmosphere with 5% CO<sub>2</sub>. Finally, cells were split and selected for stable integration of the shRNAs in the presence of 1µg/mL puromycin. Single colonies were then sub-cloned by limiting dilution and all the clones obtained were assayed for IF<sub>1</sub> expression.

## **3.4 Generation of mtRFP-positive osteosarcoma clones**

Stable clones expressing a red fluorescent protein targeted to mitochondria (RFP) were obtained from 143B parental, scrambled and IF<sub>1</sub>-silenced cells by transfection with the pcDNA3.1-mtRFP plasmid. mtRFP-cell clones were then assayed in order to verify the correlation between fluorescence intensity and cellular mitochondria content.

### **3.4.1 Osteosarcoma cell lines transfection and selection of mtRFP-positive clones**

Transfections were performed as described above, using 2 µg of plasmid DNA, with a DNA:PEI ratio of 1:8 (w/w). After 24h hours, cells were split and cultured with complete medium supplemented with Geneticin G418 0.5 µg/mL (Sigma) to select stable clones. Clones were obtained by limiting dilution and mtRFP expression was subsequently measured by cytometry (Muse cell analyzer Millipore), using excitation wavelength at 532 nm and detection at 576 ± 28 nm.

Data analysis was then performed using Flowing software 3.1 (Cell Imaging Core). Clones with similar mtRFP fluorescence intensity were then selected and maintained in 100 µg/mL G418. mtRFP-fluorescence intensity stability was monitored at each cell culture splitting for at least two weeks.

### **3.4.2 mtRFP-fluorescence intensity fluorometric analysis**

In order to evaluate any intracellular quenching phenomena, mtRFP fluorescence emissions of intact cells were compared to the one measured after cell lysis by using fluorometer (Jasco).

For this purpose, mtRFP cells were resuspended in Hank's Balanced Salt Solution (HBSS) at final concentration either  $2 \times 10^6$  cells/mL or  $4 \times 10^6$  cells/mL and their fluorescence intensity was detected by fluorometer at  $\lambda$  excitation=556 nm and  $\lambda$  emission=575 nm. Same sample was then incubated for 3 minutes with a 0.2 % Triton X-100 (Sigma-Aldrich) solution in HBSS, in order to lyse mitochondria, allowing mtRFP to be free in solution and the fluorescence intensity was recorded.

### **3.5 miRNA mimic and miRNA inhibitor transfection**

The role of miR-425-5p expression in melanoma cells was evaluated through the modulation of its levels by miR-425-5p mimic and inhibitor transient transfection in sensitive and resistant melanoma cells, respectively. miRNA mimics are small, double-stranded RNAs that imitates endogenous miRNAs and allows miRNA functional analysis by up-regulation of miRNA activity.

Conversely, miRNA inhibitors are small, single-stranded RNA molecules designed to specifically bind to and inhibit the endogenous miRNA molecules then down-regulating the miRNA functionality. miR-425-5p mimic, inhibitor and relative negative controls mirVana oligonucleotides were purchased from ThermoFisher. Depending on the assay to perform, 22200 cells/cm<sup>2</sup> cells were seeded in complete medium onto the proper cell culture support, and after 18 hours, cells were transfected with the selected mirVana

oligonucleotide at 50 nM final concentration in culture media. Transfection mixes were prepared in Opti-MEM Reduced Serum Medium (Gibco), using Lipofectamine RNAiMAX transfection reagent (ThermoFisher) and then dispensed onto the cells in a fresh culture medium, according to manufacturer's protocol. To assess the effect of the miRNA increase on the development of BRAF-I resistance, miR-425-5p over-expression in sensitive melanoma cells was performed in culture medium supplemented with PLX4032. Even the miRNA inhibition was performed in melanoma resistant cells maintained in PLX4032, to evaluate the ability of the miR-425-5p decrease to restore the sensitivity to the treatment. Transfection efficiency was checked evaluating the miR-425-5p intracellular levels by quantitative reverse transcription PCR (RT-qPCR).

### **3.6 Cell growth evaluation**

Cell growth of parental, scrambled and IF<sub>1</sub>-silenced clones, were evaluated at 24 hours after exposure of the cells to increasing concentrations of FCCP. In brief, 100000 cells were seeded in 35mm Petri dishes and, after 18 hours, the culture medium was replaced with complete DMEM supplemented with 1  $\mu$ M, 5  $\mu$ M, 10  $\mu$ M, 15  $\mu$ M FCCP. 24 hours later, cells were detached collected and counted. Cell viability was assayed using the trypan blue dye exclusion test. The growth of sensitive and resistant melanoma cells upon PLX4032 treatment was assessed up to 72 hours. For each time point,  $2 \times 10^5$  cells in triplicates were seeded in complete medium, in 6 wells-plate. After 18 hours, the culture medium was replaced with fresh medium supplemented with 2  $\mu$ M and 5  $\mu$ M PLX4032 for M21-M21R and Colo38-Colo38R respectively. Every 24 hours from vemurafenib treatment, cells were detached, collected together with their supernatant counted with Vi-CELL XR 2.03 cell counter and viability analyser (Beckman Coulter, Inc), that automatically performs the trypan blue dye exclusion staining. Data were reported as a total number of viable cells per sample. The evaluation of the growth of melanoma cells after transfection with miRNA-mimic or miRNA-inhibitor was performed with the same method described above. Transfection was performed 24 hours from the seeding, according to the method detailed below.

### **3.7 Cell viability assessment**

The viability of osteosarcoma controls and IF<sub>1</sub>-silenced clone in presence of 10  $\mu$ M and 15  $\mu$ M FCCP was evaluated by cytometry with Muse Count and Viability Assay Kit (Millipore). This kit allows the determination of the viable cells in a sample, due to the different permeability of two fluorescent DNA-binding dyes. The nuclear dye stains all nucleated cells, while the viability dye stains only dying and dead cells. After the incubation in standard or anoxia-mimicking conditions, cells were detached with trypsin, pooled with their culture medium and counted. Samples were then centrifuged, resuspended in the kit reagent following the manufacturer's instructions and incubated at room temperature in the dark for 5 minutes. Stained samples were diluted in HBBS buffer and acquired by the Muse cytometer (Millipore). Data were then analysed with Muse software obtaining live and dead cells populations percentages.

### **3.8 Biochemical assays**

#### **3.8.1 Glucose consumption and lactate release measurements**

Osteosarcoma control cells and IF<sub>1</sub>-silenced clones were grown for 24 hours in the presence of increasing concentration of FCCP, from 1  $\mu$ M up to 15  $\mu$ M, and their glucose consumption and lactate production were determined by spectrophotometric methods. Culture media were collected and residual glucose, lactate released in them were measured with the Glucose Liquid Trinder Method Kit (FAR) and Lactate PAP Fluid Kit (Centronic GmbH) respectively, following manufacturer's instructions. These commercial kits exploit the method firstly described by Tindler in 1969 [224], consisting in the enzymatic conversion of the substance to be quantified, producing hydrogen peroxide (H<sub>2</sub>O<sub>2</sub>). H<sub>2</sub>O<sub>2</sub> then reacts with a chromogen to form a coloured compound photometrically detectable, whose intensity is proportional to the concentration of the substance.

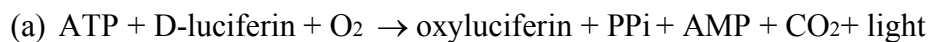
The enzymatic reactions were performed at 37°C and the absorbance was measured at a wave length of 510 nm and 546 nm, for glucose and lactate dosages respectively.

The moles of glucose and lactate were then normalized to the number of cells, and data were expressed as  $\mu\text{mol}/10^6$  cells.

### **3.8.2 Cellular ATP content assay**

The steady-state ATP content of cells after FCCP exposure was evaluated by a luminometric method using a luciferin–luciferase system (ATP bioluminescent assay kit CLS II; Roche).

The luciferase from *Photinus pyralis*, provided by the kit catalyses the following reaction:



Therefore, the light emitted is directly proportional to the ATP content in the sample and can be quantified by introducing an internal standard of a known ATP amount (33pmol). Cells were detached with trypsin, quickly washed in HBSS and resuspended in the buffer (10mM Tris-HCl, 100 mM KCl, 5 mM  $\text{KH}_2\text{PO}_4$ , 1 mM EGTA, 3 mM EDTA, 2 mM  $\text{MgCl}_2$  pH 7.4). Cells were lysed in DMSO to release the intracellular ATP, resuspended in cold water and placed on ice to prevent ATP dissipation. Cellular extracts were immediately assayed by means of following manufacturer's instructions (ATP bioluminescent assay kit CLS II; Roche). Luminescence was detected with the Luminoskan TL Plus (Labsystems) luminometer. Protein contents in the samples were quantified with the Lowry method and the ATP levels were normalized and expressed as nmol/mg protein [225].

### **3.8.3 ADP/ATP ratio assay**

The energetic charge of osteosarcoma control cells and IF<sub>1</sub>-silenced clones, subjected to anoxia-mimicking conditions was estimated by assessing the intracellular ADP/ATP ratio

through a luminometric method. The assay was performed by using ADP/ATP Ratio Assay Kit from Sigma-Aldrich and following the manufacturer's instructions.

Briefly, the kit exploits the luciferin-luciferase method described above for the intracellular ATP measurement (a), followed by a second reaction that converts ADP in quantifiable ATP. The light intensity recorded after the second step represents the bioluminescence produced by the conversion of both intracellular ADP and ATP, and the ADP/ATP is calculated as follows:

$$\frac{(\text{ATP} + \text{ADP luminescence}) - (2^{\circ} \text{ read ATP luminescence})}{(1^{\circ} \text{ read ATP luminescence})}$$

At the time of the assay, cells in culture were detached, quickly washed and resuspended in HBSS to have between 50-90 cells/ $\mu\text{L}$ . 10  $\mu\text{L}$  of this cellular resuspension were then quantified with the kit, following the manufacturer's instructions. Luminescence was recorded with Luminoskan TL Plus (Labsystems) luminometer and ADP/ATP ratio calculated. For each cell line, data were represented as a percentage of the control condition.

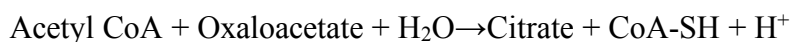
#### **3.8.4 Mitochondrial ATP hydrolysis assay**

The ATPase activity of the  $F_1F_0$ -ATPase complex, in osteosarcoma cells, uncoupled with 1  $\mu\text{M}$  FCCP was evaluated by a luminometric method, in both the presence and the absence of 1.5  $\mu\text{M}$  oligomycin. To limit unspecific ATP hydrolysis and possible ATP synthesis, cells were resuspended in a buffer composed by 0.25 M sucrose, 10 mM HEPES (pH 7.4), 5 mM  $\text{MgCl}_2$ , and 0.1 mM EGTA and supplemented with 4 mM ouabain, 2 mM iodoacetamide, and 25  $\mu\text{M}$  P1,P5-Di(adenosine-5') pentaphosphate (Ap5A). In particular, ouabain inhibited the Na-K-ATPase membrane pumps, that consume ATP, whereas the glycolytic ATP production was prevented with iodoacetamide by blocking D-glyceraldehyde-3-phosphate dehydrogenase. The interconversion of adenine nucleotides ATP, ADP, and AMP by adenylate kinases, was avoided by Ap5A. Briefly, either 143B cells or IF<sub>1</sub>-silenced clone was detached, counted and washed in

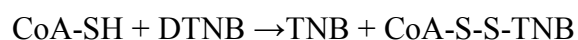
HBSS.  $16 \times 10^6$  cells were then resuspended in the buffer described above, permeabilized by adding digitonin 110  $\mu\text{g}/\text{mL}$  and incubated at 37 °C for 10 minutes. The hydrolytic reaction was then started by adding 1 mM ATP, and 4 minutes later it was stopped by adding 80% dimethyl sulfoxide. The residual ATP was quantified by the luciferin–luciferase method previously described and protein contents in the samples were quantified with the Lowry method. ATPase activities were calculated and expressed as nmol/min/mg protein. Finally, the oligomycin-sensitive ATPase activity of the  $F_1F_0$ -ATPase complex was indirectly obtained as the difference between the total and the oligomycin-insensitive ATPase activity of the cellular sample.

### 3.8.5 Citrate synthase activity assay

Citrate synthase activity was assayed according to the spectrophotometric method described by Trounce et al. [226]. Citrate synthase (CS) is the enzyme that catalyses the initial reaction of the tricarboxylic acid (TCA) cycle and it is widely accepted as a specific marker of the mitochondrial matrix. The reaction catalysed by CS enzyme is the following:



The CS enzymatic activity assay the first reaction is coupled with the following one:



The reduced Coenzyme A (CoA-SH) reduces, in turn, the 5'-dithio-bis-2-nitrobenzoic acid (DTNB), producing the 2-nitro-5-thiobenzoic acid (TNB), a coloured compound quantifiable by spectrophotometer at 412 nm. Considering the stoichiometric relation between the two reactions, TNB rate of accumulation is the index of the citrate synthase activity. Cells were detached, washed in HBSS and resuspended in the following buffer: 10 mM Tris-HCl, 100 mM KCl, 5 mM  $\text{KH}_2\text{PO}_4$ , 1 mM EGTA, 3 mM EDTA, 2 mM

MgCl<sub>2</sub>, (pH 7.4). A fraction of each sample was then diluted in 125 mM Tris-HCl buffer (pH 8) and cells were lysed by incubation with 0.2% Triton X-100. Enzymatic reactions were carried out at 30°C, supplying 1 mM acetyl-coenzyme A, 0.1 mM DTNB and 0.5 mM oxaloacetate and finally absorbances were recorded at 412 nm. Protein concentrations of the samples were determined by the Lowry method and CS activities were calculated and expressed as nmol/min/mg protein.

### **3.9 Flow cytometry assay of mitochondrial membrane potential**

The inner mitochondrial membrane potential ( $\Delta\Psi_m$ ) of cells under uncoupling conditions was measured by flow cytometry loading the cells with tetramethylrhodamine methyl ester (TMRM, Molecular Probes). TMRM is a lipophilic-cationic probe that permeates cellular membranes and accumulates in mitochondria in a  $\Delta\Psi_m$ -dependent manner.

Anoxia was mimicked by culturing cells for 30 minutes or 24 hours in presence of 1  $\mu$ M or 10  $\mu$ M FCCP respectively and staining the cells in either the absence or presence of 0.6  $\mu$ M oligomycin, a concentration that fully inhibits the F<sub>1</sub>F<sub>0</sub>-ATPase complex. The  $\Delta\Psi_m$  was evaluated by incubating cells for 30 min at 37°C in complete medium supplemented with 20 nM TMRM. Cells were then washed twice with HBSS to remove any unincorporated dye, rapidly detached with trypsin and diluted in 10% FBS HBSS solution to have nearly 300000 cells/mL. Samples were finally acquired with MUSE cell analyzer (Millipore), applying 532 nm as a wavelength of excitation while fluorescence emission was measured at 576 $\pm$ 28 nm. Data analysis was performed by the Flowing software 3.1 (Cell Imaging Core).

### **3.10 Fluorescence microscopy**

The  $\Delta\Psi_m$  of osteosarcoma cells and derived clones upon 24 hours of 10  $\mu$ M FCCP treatment was also evaluated by fluorescent microscopy, loading cells with 20nM TMRM.



Furthermore, to assess the reverse hydrolytic activity of the ATP synthase, 1.5  $\mu$ M oligomycin was added before TMRM loading. After the TMRM staining, the cells were washed from the unloaded dye and micrographs at magnification 10x–40x were acquired using a fluorescence inverted microscope Olympus IX50 equipped with a CCD camera, using a specific set of filters: excitation 540 $\pm$ 20 nm and emission 610 $\pm$ 40 nm. Multiple high-power images were acquired with IAS2000 software (Delta Sistemi). At least ten different optic fields were acquired for every experimental condition tested. Fluorescence microscopies of mtRFP-expressing cells were also obtained using instruments and setting reported above. The LC3-YFP fluorescent signal was acquired using the following set of filters: excitation 480 $\pm$ 30 nm and emission 530 $\pm$ 30 nm.

### **3.11 SDS-PAGE and Western blot analysis**

The semiquantitative analysis of the cellular proteins was performed by SDS-PAGE separation and Western blotting. Cells were detached, washed in HBSS and lysed on ice by resuspension in RIPA buffer (50 mM Tris-HCl, 150 mM NaCl, 0.5% sodium deoxycholate, 1% SDS pH 8) in presence of protease inhibitors cocktail and phosphatases inhibitors: 1 mM PMSF, 5 mM sodium fluoride and 1 mM sodium orthovanadate. All the reagents were from Sigma-Aldrich. The protein contents of cellular lysates were quantified by the Lowry method. Samples were then diluted in Bolt LDS Sample Buffer and Bolt Sample Reducing Agent (ThermoFisher) and boiled for 3 minutes, according to the manufacturer's instructions. Equal amounts of proteins lysates (10  $\mu$ g or 20  $\mu$ g) were separated by SDS-PAGE. For this purpose, the samples were loaded in Bolt 4-12% Bis-Tris Plus Gels (Thermofisher) and runs were performed in Bolt MES SDS Running Buffer (Thermofisher) at 150 V for 90 minutes. Resolved proteins were blotted onto a 0.2  $\mu$ m nitrocellulose membranes by the wet method, at 100 V constants for 1.15 hours at 4°C [65]. The efficiency of proteins blotting was evaluated by staining the gels with Coomassie Blue [227]. The blocking of the membranes was performed either with 2% non-fat dry milk (Bio-Rad) or 2% BSA (Sigma) in 0.05% PBS-Tween solution for 1 hour at room temperature, according to the primary antibody manufacturer's instructions.

Nitrocellulose membranes were then incubated with the appropriate diluted primary antibody. The primary antibody specific for IF<sub>1</sub> was purchased from MitoSciences Inc., Eugene. Immunodetection of the OXPHOS complexes subunits was performed according to Sgarbi et al. with a cocktail of antibodies from MitoSciences Inc, Eugene [228]. TOMM20, VDAC1 (porin), BNIP3, p53-HRP conjugated antibodies were from Abcam. Anti-SIRT1 and anti-PGC-1 $\alpha$  antibodies were from Cell Signalling Technologies. Primary antibodies to detected PINK1, Smad2, Smad3 and FBXW11 were provided by Novus Biological. Anti- $\beta$ -actin and anti- $\beta$ -tubulin antibodies were purchased from Sigma Aldrich. Vinculin was from ProteinTech.  $\beta$ -catenin, phospho-Ser9-GSK3  $\beta$  primary antibodies were from Santa Cruz Biotechnology, Inc. The incubations of the primary antibodies were performed according to the manufacturer's instruction. The membranes were then washed in 0.05% PBS-Tween (6 x 5minutes) and then incubated with proper horseradish peroxidase-conjugated secondary antibodies (Life Technologies) 1 hour at room temperature. Chemiluminescent detection was performed with the ECL Western Blotting Detection Reagent Kit (GE Healthcare) using the ChemiDoc MP system equipped with ImageLab software (Bio-Rad) to perform the densitometric scanning of the relative protein intensity.

### **3.12 Evaluation of mtRFP and LC3-YFP colocalization in fluorescence microscopy to asses mitophagy activation**

Mitophagy activation in osteosarcoma cells after 24 hours of exposure to anoxia-mimicking condition was evaluated by fluorescence microscopy in mtRFP-stable clones, transiently over-expressing the LC3 protein fused to a yellow fluorescent protein, carried by the pCMV6-LC3-YFP vector. Upon autophagy induction, cellular LC3-I is modified and converted into LC3-II and integrated into the phagophore membranes, by conjugation with the lipid phosphatidylethanolamine. For this reason, LC3-II could be used as a marker of autophagy activation. The transgenic LC3-YFP as well is conjugated to the autophagosome membranes, resulting in the formation of yellow-fluorescent LC3-puncta in the cytoplasm, visible by fluorescent microscopy.

During mitophagy, mitochondria are selectively degraded within autophagosomes. In the cell lines expressing the mitochondrial red fluorescent protein (mtRFP) and LC3-YFP, mitophagy activation is detectable by the colocalization of the two fluorescent markers, obtained by merging the yellow and red images, acquired sequentially using the proper filters. Colocalizations indicates the presence of the mitochondria inside the assembled autophagosomes and that the mitophagy occurs. For this purpose, the control and IF<sub>1</sub>-silenced clones expressing the mtRFP were seeded in 35mm Petri dishes, in the culture medium already supplemented with the transfection mix, composed by 2 µg of pCMV6-LC3-YFP vector and PEI, in 1:8 DNA:PEI ratio (w/w). 24 hours from the transfection, LC3-YFP expression was checked by fluorescent microscopy and cells were detached, counted and seeded. 200000 and 350000 cells were seeded in 35mm Petri dishes for control and treated conditions, respectively. After 24 hours, culture media were replaced with DMEM complete medium supplemented with 25 µM Chloroquine (CQ). CQ inhibits the endosomal acidification, then arresting autophagy at the step of the autophagosomes fusion with the lysosomes and therefore preventing the degradation of both LC3-YFP and mtRFP markers [226]. Positive controls of mitophagy activation were set up by treating cells with 10 µM deferoxamine (DFO), an iron chelator that inhibits prolyl hydroxylases leading to HIF-1 alpha stabilization [229]. The following day, culture media were removed from plates, replaced with 400 µL of HBSS and fluorescence micrographs of both mtRFP and LC3-YFP channels were acquired from the same optic field, as previously described. Fluorescence images were then processed and merged by using the image deconvolution software AutoDeblur (BioImaging Solutions Inc.)

### **3.13 IC50 calculation by MTT assay**

The half maximal inhibitory concentration (IC<sub>50</sub>), obtained by MTT assay data analysis, was calculated to assess melanoma cells sensitivity to PLX4032 treatment in different experimental conditions. The MTT assay allows to assess cell metabolic activity by evaluating the ability of the mitochondrial NAD(P)H-dependent cellular oxidoreductase

enzymes to metabolize the yellow tetrazolium dye MTT 3-(4,5-dimethylthiazol-2-yl)-2,5-diphenyltetrazolium bromide to formazan, a purple insoluble compound, quantifiable with spectrophotometric method [230]. Considering the rate of cell metabolism an index of the cell viability, the evaluation of the ability of melanoma cells to resist to PLX4032 treatment was performed by assessing with MTT the cytotoxic effect of increasing concentrations of the drug during the time. Testing the cytotoxic effect of the PLX4032 by MTT assay, IC<sub>50</sub> represents the dose of the drug necessary to inhibit the cell metabolism of the 50%. According to this definition, higher values of IC<sub>50</sub> are an index of less sensitivity and more resistance to the vemurafenib anticancer-treatment.

Briefly, cells were seeded in 96 wells plate in the growth medium, and then after 18 hours, the fresh media supplemented with increasing dose of vemurafenib were added. PLX4032 dilutions were prepared freshly by the serial dilution method, in a range of concentration between 31.2 nM to 512  $\mu$ M. Each dose of the drug was tested in triplicate wells. MTT experiments on melanoma cells with increased or reduced levels of miR-425-5p were performed transfecting the cells with miRNA mimic or inhibitor at the same time as culture media replacement, using the method previously described. After 24, 48, 72 hours from the start of the vemurafenib treatment, MTT assay was performed using the Vybrant MTT Cell Proliferation Assay Kit (Thermo Fisher Scientific), following the protocol described below. At each time point, microplates were centrifuged, and culture medium was carefully removed and replaced with 100  $\mu$ L of RPMI without phenol red, supplemented with the proper concentration of PLX4032. 10  $\mu$ L of the 12 mM MTT stock solution was then added to each well and plate were incubated for 4 hours at 37°C in humidified atmosphere with 5% CO<sub>2</sub>. After this incubation, all but 25  $\mu$ L of the medium was removed from each well and then 50  $\mu$ L of DMSO was added to dissolve formazan. Samples were thoroughly mixed and microplates were incubated for an additional 10 minutes at 37°C. The absorbance of each well was detected at 560 nm with GloMax 96 microplate luminometer (Promega). For each PLX4032 concentration, the average signal of the three wells was calculated and the background signal of the medium was subtracted. Corrected values were then normalized to the metabolic activity of the untreated cells, representing the control condition. A non-linear regression analysis was performed with Prism 7 (GraphPad Prism Software), and a sigmoidal dose-response

curve was obtained by plotting Log<sub>10</sub> of drug concentrations on the x-axis and the normalized cell metabolic activities on the y-axis. Finally, the IC<sub>50</sub> values were calculated by interpolation on the dose-response curve by the software.

### **3.14 Dual-luciferase reporter assay**

Dual-luciferase reporter assay (DLR) was performed in melanoma cells to evaluate the activation of oncogenic and tumour-suppressor signalling pathways in different experimental conditions. In the DLR assay, the signalling rates of the pathways were assessed by evaluating the stimulation of the downstream promoter. For this purpose, cells were transfected with vectors carrying multiple repeats of the promoter binding sites, fused to the firefly (*Photinus pyralis*) luciferase reporter gene. Upon pathway activation, molecular effectors bind the repeated sites, stimulating the expression of the reporter gene. Therefore, the quantification of the luciferase activity by luminometric methods provides a measure of the signalling pathway. A vector for the constitutive expression of the sea pansy (*Renilla reniformis*) luciferase was also co-transfected as an internal control and luminescence of firefly luciferase was normalized to the *Renilla* luciferase signal of the same samples. Specificity was checked for each reporter, alternatively transfecting cells with a negative control reporter, non-inducible by molecular effector because of the specific binding sites are mutated. The firefly and sea pansy luciferases display differing biochemical requirements, allowing for the sequential quantitative measurement of both luciferase activities in a single sample. Indeed, firefly luciferase (Fluc) catalysis consists in the oxidation of the luciferin to oxyluciferin, requiring ATP, Mg<sup>2+</sup>, and O<sub>2</sub> [231], while *Renilla* luciferase (Rluc) substrates are O<sub>2</sub> and coelenterazine. Using the DLR reagents, the luminescence of the firefly luciferase can be measured by addition of the luciferin, and this reaction is subsequently quenched while simultaneously activating the luminescence of the *Renilla* luciferase, providing a second reagent. Briefly, the sensitive and resistant melanoma cells were seeded in 12-well plates, after 18 hours the medium was replaced and the co-transfections were performed. Cells were transiently transfected with 1 µg of the reporter vector and 1 µg of pRT-LK control vector, in Opti-MEM Reduced Serum Medium (Gibco), using Lipofectamine transfection reagent

(ThermoFisher). Depending on the experimental design, 50 nM miRNA mimic or inhibitor were also co-transfected with luciferase vectors. After 24 hours, the cells were lysed and the activities of the luciferases were measured using Nano-Glo® Luciferase Assay System reagents (Promega). The Bioluminescence was acquired by GloMax 96 microplate luminometer dual-reagent injector system (Promega).

All vectors used were purchased from Addgene and they are listed below:

M50 Super 8x TOPFlash: Beta-catenin reporter, containing 8 copies of TCF/LEF binding sites fused to firefly luciferase gene

M51 Super 8x FOPFlash: Control of Beta-catenin reporter containing mutated TCF/LEF-binding sites fused to firefly luciferase gene

PG13-luc: p53 reporter carrying 13 copies of the p53-binding consensus sequence fused to firefly luciferase gene

MG15-luc: control of p53 reporter, containing mutant p53 binding sites fused to firefly luciferase gene

SBE4-Luc: firefly luciferase reporter containing four copies of the Smad complex binding site

pRL-TK: vector for the constitutive expression of the *Renilla* luciferase as the internal control of the assay.

Dual luciferase assay to evaluate Sonic-Hedgehog pathway activation was performed with Cignal GLI Reporter (luc) Kit (QIAGEN), following the manufacturer's instruction.

### **3.15 RNA extraction**

Total RNA was extracted from melanoma cells using TRIzol™ Reagent (Invitrogen), according to manufacturer's instruction. In brief, cells were detached and a volume of cellular resuspension corresponding to  $1 \times 10^5$ – $1 \times 10^7$  cells, was collected, washed in PBS and then lysed in 1 mL of TRIzol. Samples were incubated 5 minutes at room temperature to allow complete protein dissociation. 200  $\mu$ L of chloroform was subsequently added, samples were immediately mixed by inversion and incubated at room temperature for 3 minutes. Lysed samples were then centrifuged at 12000 g for 15 minutes at 4°C, to allow phases separation. The upper aqueous phases containing RNA were collected and

dispensed in a new Eppendorf tube containing 500  $\mu$ L of isopropanol. Samples were then mixed by inversion, incubated for 10 minutes at room temperature and centrifuged at 12000 g for 10 minutes at 4°C to precipitate RNA. Pellets were then dried and washed by resuspension in 1 mL of 70% ethanol solution. RNA was then pelleted by centrifugation at 7500 g for 5 minutes at 4°C. Supernatants were discarded and RNA pellets were air dried. Finally, RNA was solubilized in RNAase free water and concentration and purity were measured by the NanoVue Plus spectrophotometer (GE Healthcare Life Science). RNA at higher quality to validate the miRNAs levels in melanoma cell lines by RT-qPCR was obtained from TRizol cellular resuspensions by column purification with RNA-clean up and Concentration kit (Norgen BioTek Corp) following manufacturer's instructions.

### **3.16 miRNAs profiling with Nanostring array**

miRNAs differentially expressed in melanoma cells resistant to vemurafenib with respect to sensitive cells were identified by Nanostring array analysis (Nanostring Technologies), assessing a panel of 800 miRNAs, according to the manufacturer's instruction.

### **3.17 Quantitative reverse transcription PCR**

Two-step reaction quantitative reverse transcription PCR (RT-qPCR) assay was performed to either quantify gene expression (mRNA) or miRNAs levels.

Reagents and protocols used for mRNA and miRNAs RT-qPCR described below. For both assays, 250 ng of RNA were first retrotranscribed into complementary DNA (cDNA) by reverse transcriptase from total RNA using Veriti 96-well Thermal Cycler (ThermoFisher). Obtained cDNA was then used as the template for the qPCR reaction, performed with the CFX96 Touch Real-Time Detection System (Bio-Rad). For each target, the reaction was set up in triplicate. Cycle threshold values (Ct) provided by Real-Time instrument were imported to a Microsoft Excel spreadsheet and relative gene expression (mRNA) or miRNAs levels were calculated by the  $2^{-\Delta\Delta C_t}$  method and expressed as a fold change with respect to the control condition [230].

### **3.17.1 Quantification of miRNAs**

miRNAs single-stranded cDNA was reverse transcribed from total RNA samples using specific miRNA stem-loop primers from the TaqMan MicroRNA Assays and reagents from the TaqMan® MicroRNA Reverse Transcription Kit (Applied Biosystem), following manufacturer's instructions. Thermal cycler was programmed as follows:

Priming: 30 min 16°C

Reverse transcription: 30 min 42°C

Enzyme inactivation: 5 min 85°C

miRNA-specific cDNA was then quantified by Real-Time PCR using TaqMan™ Fast Advanced Master Mix with q-PCR specific primers TaqMan MicroRNA Assays.

The cycling conditions were set as follows:

Uracil N-glycosylase (UNG) enzyme incubation: 50°C for 2 mins

Taq polymerase activation: 95°C for 20 sec

Amplification step (40 cycles):

Denaturation at 95°C for 3 sec

Annealing/elongation with signal acquisition: 60°C 30 sec

The miRNAs expression was normalized to the U6 snRNA endogenous control.

### **3.17.2 Quantification of mRNAs**

The whole RNA was retrotranscribed with random primers approach by using iScript Reverse Transcription supermix for RT-qPCR (Bio-Rad), following the manufacturer's instruction. Thermal cycler protocol was as follows:

Priming 5 min at 25°C

Reverse transcription 20 min at 46°C

RT inactivation 1 min at 95°C



The obtained cDNA was then diluted 1:1 in nucleases free water and used as template in q-PCR reaction. GSK3- $\beta$ ,  $\beta$ -catenin, SMAD2, SMAD3, p53 gene expression analysis were performed setting up q-PCR reactions in iTaq Universal SYBER Green supermix (Bio-Rad) using specific primers. Thermal cycler protocol was as follows:

Polymerase activation and cDNA denaturation: 30 sec at 95°C

Amplification (40 cycles): Denaturation 5 sec at 95°C

annealing, extension and plate read: 30 sec at 60°C

Melt-Curve analysis: from 65°C to 95°C with an increment of 0.5°C for each 5 sec cycle.

The gene expression was normalized to the GADPH housekeeping gene.

### **3.18 Bioinformatic analysis**

Bioinformatic databases were consulted to obtain information about miRNAs identified and confirmed as differently expressed in PLX4032-resistant melanoma cell lines compared to sensitive cells. In particular, for each miRNA, a list of the predicted was obtained by miRWalk database [232].

Genomic targets in common to different miRNAs were identified by calculating the intersection of the lists and drawing Venn Diagram using the web tool provided by Van der Peer Lab (<http://bioinformatics.psb.ugent.be/webtools/Venn/>).

The Human Protein Atlas and the PROGmiRV2 prognostic databases were consulted to obtain statistical information derived from patients about the metastatic melanoma survival and progression in relation to the levels of the predicted target proteins and miRNAs expression levels, respectively [233].

### **3.19 Cell cycle determination**

The distribution of the cellular population in the different cell cycle phases was evaluated via flow cytometry by DAPI staining of fixed cells. In brief, cells were detached, collected, and centrifuged for 10 minutes at 10000 rpm. The cellular pellet was then dried out and suspended in 1 volume of a PBS solution containing the 2% of FBS.

Subsequently, the cells were fixed by adding 20 volumes of ice-cold 70% ethanol in a dropwise manner while mixing with the vortex. Subsequently, cells were stored for two hours on ice and after 18 hours at -20°C. After this incubation, the fixed cells were centrifuged and then the pellet washed two times in the PBS solution containing the 2% of FBS. Afterwards, the cells were resuspended in the DAPI solution at the final concentration 10µg/mL in PBS with 0.1% Triton X-100. DAPI fluorescence was acquired at the flow cytometer, with 405nm laser excitation and detectors at 450 nm. Data obtained were analysed with FlowJo software.

### **3.20 Statistical analysis**

Results were analysed by means of the one-way analysis of variance (ANOVA) with Bonferroni's post-hoc test. Statistical analysis was performed by OriginPro 7.5 software (Origin-Lab Corporation). Data are reported as mean ± SD of at least three independent experiments. A value of  $p \leq 0.05$  was selected to indicate statistical significance.

# 4 Results

## 4.1 Role of IF<sub>1</sub> in the bioenergetics of cancer cells in anoxia

IF<sub>1</sub> expression is increased in several human cancer types, suggesting that this protein contribute to the cancer progression. Based on its physiological role, it has been proposed that IF<sub>1</sub> promote the metabolic plasticity and adaptability typical of the cancer cells, especially in conditions of low or no oxygen availability that may occur in solid tumours. However, whereas its function in normal cells is well defined, IF<sub>1</sub> contribution and mechanisms of action in cancer cells are still unclear.

Experimental evidence previously obtained by our research group revealed that cancer cells, even under severe hypoxia conditions (0.1% O<sub>2</sub>), preserve the mitochondrial membrane potential  $\Delta\Psi_m$  [65]. Consequently, cancer cells do not hydrolyse ATP because the reversal of the ATP synthase does not occur, independently from the IF<sub>1</sub> expression and thus excluding a regulatory contribution of the endogenous inhibitor in hypoxia. With the purpose to find the conditions that may activate IF<sub>1</sub> in tumour cells and to study its role in cancer, here we assessed the bioenergetics of transformed cells in a more severe condition, anoxia, by inducing the  $\Delta\Psi_m$  failure occurring in cells upon total oxygen depletion. To perform our investigation, we used the human 143B osteosarcoma cells that show high IF<sub>1</sub> expression, and we established clones stably silenced for IF<sub>1</sub> (-IF<sub>1</sub>). The anoxia-mimicking conditions were carried out by treating cells for 24 hours with the uncoupler FCCP.

### 4.1.1 Production of IF<sub>1</sub>-silenced and GFP-negative stable clones from 143B cells

Several experimental data showed that the constitutive expression of fluorescent protein reporters in cellular models may induce the modification of protein expression, cells behaviours and also metabolic features, producing non-representative models and thus affecting the results of the investigations [234], [235]. In agreement with this, some of our pilot experiments showed that the GFP-positive cells have a lower tolerance to stress conditions compared to the matching GFP-negative clones, showing a higher rate of mortality [65]. Based on these findings, GFP-negative osteosarcoma clones were obtained by transducing the 143B parental cell line with retroviruses alternatively packaged with the pGFP-V-RS vectors, TR30013 (scrambled) or GI325936 (IF<sub>1</sub> shRNA). Indeed, as shown by the map of the plasmid, the GFP-coding sequence is outside of the LTR region, and thus is not packaged into the viral particles and, in turn, will not be expressed by the transduced cells (Figure 18A).

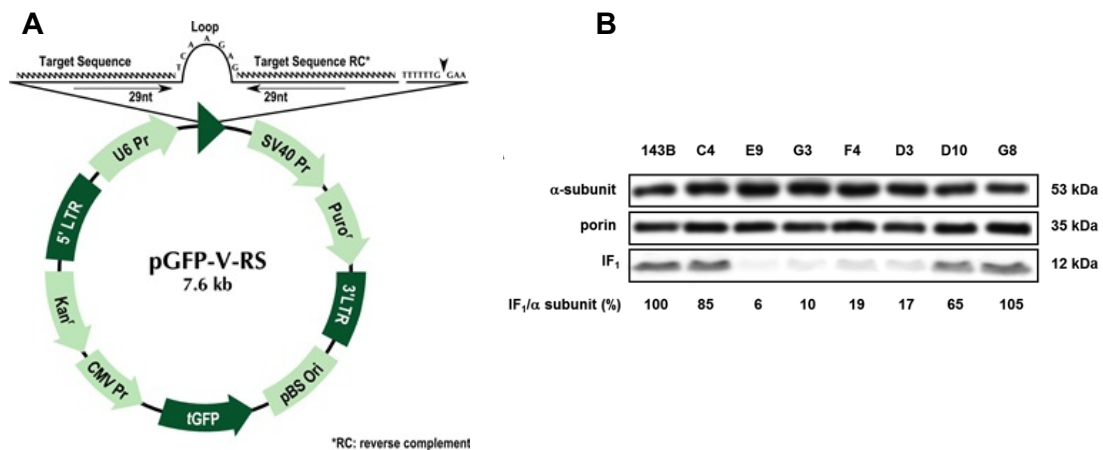


**Figure 18: Screening of osteosarcoma clones GFP negative and stably silenced for IF<sub>1</sub>.** (A) Map of the pGFP-V-RS vector backbone. Cloning site alternatively contains the sequence for non-effective scrambled shRNA or IF<sub>1</sub>-shRNA expression. (B) immunoblot analysis of IF<sub>1</sub> protein levels in parental cells (143B), scrambled clones (C4, D10 and G8) and -IF<sub>1</sub> silenced clones (E9, G3, F4, D3). The α-subunit of the ATP-synthase and the porin VDAC1 were used as mitochondrial loading control. IF<sub>1</sub>-densitometric values were normalized on ATP synthase α-subunit levels and expressed as a percentage with respect to the IF<sub>1</sub> content of the 143B cells (bottom of the panel).

Transduction was carried out as described in the material and methods section. After 24 hours, both the 143B-infected scrambled and the IF<sub>1</sub>-silenced cell populations were assessed by fluorescence microscopy, confirming the total lack of the GFP transduction (data not shown). Indeed, no fluorescence signal was detected, concluding that all the cells of the heterogeneous populations did not express the GFP reporter (-GFP). Finally, the cells were split and cultured in presence of puromycin to select cellular populations stably integrating the vector. Subsequently, single clones were obtained by limiting dilution. Once cultured and expanded, the scrambled and IF<sub>1</sub>-silenced clones were assayed for IF<sub>1</sub> expression by SDS-PAGE separation and protein immunodetection. A great decrease in IF<sub>1</sub> expression was observed in all silenced clones screened, with an average silencing efficiency of about 90% (Figure 18B). The E9 and G3 clones exhibited the best IF<sub>1</sub>-knockdown, with the 6% and 10% of IF<sub>1</sub> residual respect to the 143B parental cells. The cell morphology of all clones isolated was assessed by brightfield microscopy and compared to one of the 143B parental cells. Neither scrambled, nor IF<sub>1</sub>-silenced clones showed morphologic differences with respect to the non-transduced parental cells, concluding that the transfection method did not cause severe alteration of the cell structure. The reliability of so obtained cellular models was biochemical assessed (data not shown). In normal conditions, no variations in the proliferation rate, cellular viability and in the main metabolic parameters (glucose consumption, lactate release, intracellular ATP, CS activity) were observed between control cells (+IF<sub>1</sub>) and -IF<sub>1</sub> silenced clones, as we previously demonstrated with a different set of GFP-positive osteosarcoma clones [65]. In agreement with data already published, in basal conditions, GFP-negative IF<sub>1</sub>-silenced cells displayed a mitochondrial membrane potential  $\Delta\Psi_m$  approximately 30% higher than in the control cells. Proved the fidelity of the newly produced cellular models, the E9 and G3 IF<sub>1</sub>-silenced clones together with the C4 scrambled clone were selected for the experimental investigations. Levels of IF<sub>1</sub> expression were monitored in the cellular models over the time, confirming the stability of the silencing.

#### **4.1.2 Production of osteosarcoma clones stably expressing the mtRFP**

The cellular models stably expressing a red fluorescent protein targeted to the mitochondria were produced from 143B cells and the derived clones, in order to obtain a solid system to monitor both the mitochondrial mass and network of the cells in response to different experimental conditions. For this purpose, 143B cells, C4 scrambled, E9 and G3 IF<sub>1</sub>-silenced clones were transfected with the pcDNA3.1-mtRFP plasmid. 24 hours after the transfection, the cells were split and cultured in presence of the antibiotic G418 to select a cellular population stably expressing the mtRFP. The efficiency of both the transfection and the early selection was evaluated after 24 hours from the split, by checking the expression of the mtRFP through fluorescence flow cytometry. Upon 24 hours of antibiotic selection and therefore 48 hours from the transfection, all the cell populations derived from 143B cells, C4, E9 and G3 clones showed nearly the 30% of cells positive to the mtRFP, with a fluorescence intensity ranging from 20 arbitrary units (A.U.) to 10000 A.U. The left panel of Figure 19A shows an example of the cytofluorimetric assessment of the mtRFP-heterogeneous population obtained by the pcDNA3.1-mtRFP transfection in the 143B parental cell line. Therefore, cells were further cultured in presence of G418, with the purpose of enriching the mtRFP-positive cellular population, testing the cells positivity for mtRFP via flow-cytometry every time cells were split. After four days of selection, all mtRFP-transfect populations displayed around 60% of mtRFP-positive cells (Figure 19A central panel). The cytofluorimetric analysis performed in the following days showed no changes in both the percentage of mtRFP-positive cells and their average fluorescence, suggesting that in this 60% of cells, the expression of the mitochondrial red fluorescent reporter was stable (Figure 19A right panel). Subsequently, single clones mtRFP-positive were obtained from each heterogenous population by limiting dilution, and were expanded in the selective culture medium. Fifteen days after subcloning, single clones showed a proliferation rate identical to one of the non-transfect cell lines. Cytofluorimetric analysis revealed that all the clones isolated had a percentage of mtRFP-positive cells greater than 90%, whereas the average fluorescence intensity varied consistently among the clones, such as from 500 A.U. to 8000 A.U. (Figure 19B).

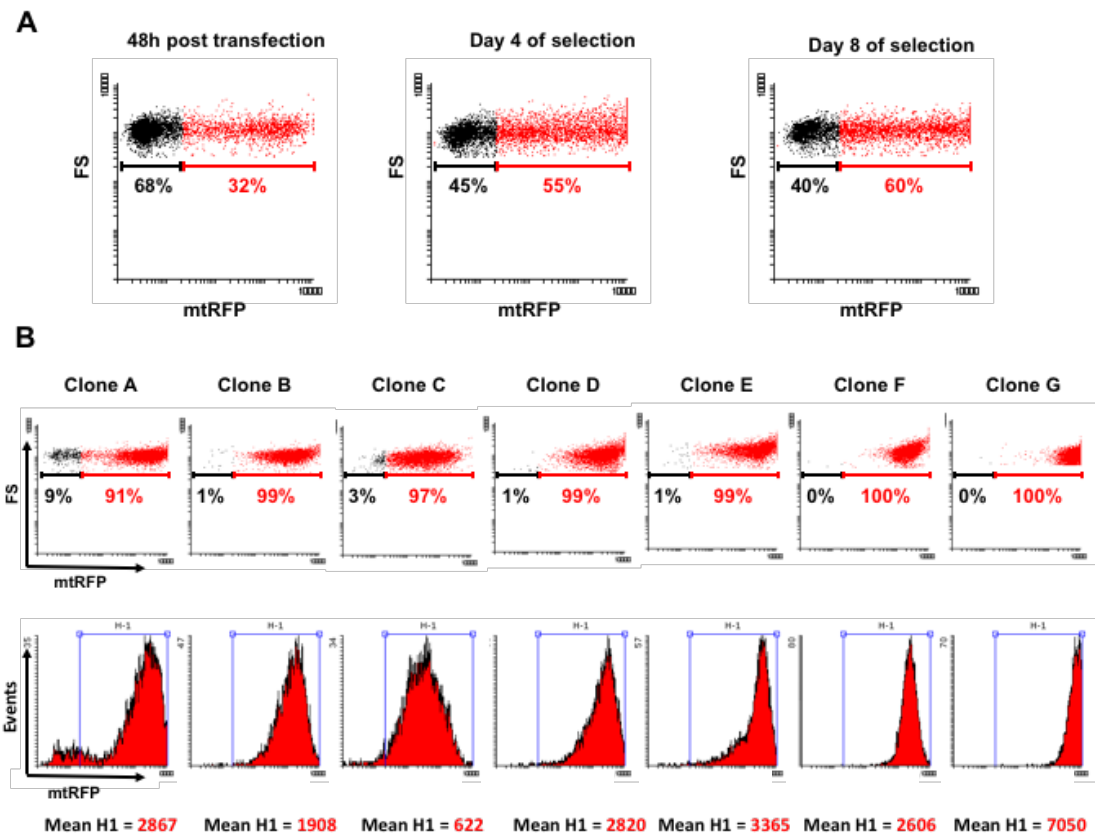


**Figure 19: Example of fluorescence assessment for the isolation of mtRFP clones from 143B cells.** In dotplot graphs, cells size value expressed as forward scatter (FS) are in the y-axis, along the x-axis are the fluorescence intensities of the mtRFP in A.U. (A) left panel: cytofluorimetric analysis of the heterogenous population after 48h from the transfection. Central and right panel: cytofluorimetric evaluation of the cells after 4 and 8 days of selection with G418 antibiotic. (B) analysis of the singles clones obtained by limiting dilution. Top panel: percentage of mtRFP positive cells. Bottom panel: average intensity of the clones.

#### 4.1.2.1 Characterization of mtRFP osteosarcoma clones

##### 4.1.2.1.1 Assessment of the relation between measured fluorescence intensity and quantity of mtRFP expressed

The linearity of the mtRFP fluorescence signal was evaluated in order to highlight the occurrence of quenching phenomena, that may induce the underestimation of the fluorescence intensity and, in turn, the incorrect quantification of the mitochondrial mass.

The quenching phenomena mainly occurs by the energy transfer to other fluorophores or by interaction with quenching molecules in the proximity. Therefore, the fluorescence dissipation may be higher in samples with a high concentration or where the fluorophore is limited to a small cellular compartment, as could also be the mitochondria [236].

For this purpose, the fluorometric assessments were performed with the 143B-Cl.E and 143B-Cl.G mtRFP-clones derived from the 143B parental cells, chosen for the different mean fluorescence intensity: 3598 A.U. and 7050 A.U., respectively (Figure 20A). The 143B cell line was used as negative control for the fluorescence signal (A.U.=20).

The mean fluorescence intensities of samples with either  $1 \times 10^6$  or  $2 \times 10^6$  cells were measured by fluorometry.

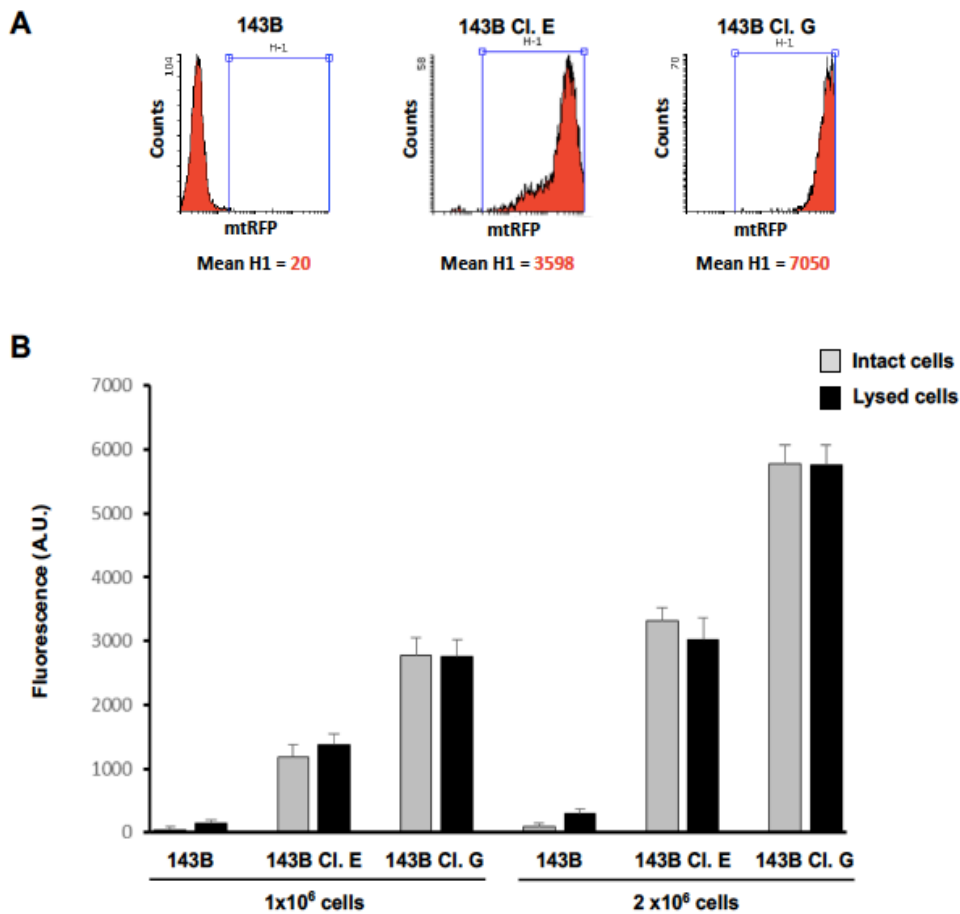


**Figure 20: Evaluation of the relation between mtRFP fluorescence intensity and both mitochondria quantity and concentration in the samples (A) Mean fluorescence intensity of the 143B parental cells and the two derived mtRFP clones 143B Cl.E and the 143B Cl.G. (B) Fluorometric measurement of samples consisting in two different amounts of mtRFP-cells, both intact and lysed.**



Subsequently, the same samples were treated with Triton to lysate both the cells and the mitochondria, and measured again. In lysing condition, the mitochondrial red fluorescence proteins are released in solution thus limiting possible quenching that may occur in the cellular districts. As shown in Figure 20B, the lysed samples showed a mean fluorescence intensity comparable to one of the intact cells, concluding that intracellular quenching phenomena do not occur. Moreover, the relationship between the average fluorescence intensities of 143B Cl.E and 143B Cl.G, determined by flow-cytometry at the beginning, was maintained, independently of the number of cells in the samples ( $1 \times 10^6$  or  $2 \times 10^6$  cells). Furthermore, the linearity of the mtRFP method was strongly confirmed by the doubling of the mean fluorescence intensity of samples containing  $2 \times 10^6$  cells with respect to the values detected in samples with  $1 \times 10^6$  cells of the same clone. Together, these data prove that mtRFP signal was linear and depended on the mtRFP protein content in the samples, also excluding the occurrence of quenching phenomena.

#### **4.1.2.1.2 Monitoring of the mtRFP fluorescence intensity and correlation with citrate synthase activity**

The stability of the mtRFP expression was checked by assessing the average fluorescence intensity of each clone every two days when cells were split, up to 29 days.

In this time frame, all the clones almost maintained the same average fluorescence intensity value, with small but not significant oscillations, independently from the IF<sub>1</sub> expression. Within these 29 days, nearly 10% of standard deviation from the mean fluorescence intensity value was estimated in all clones considered. The fluorescence intensity trend of the 143B Cl.E clone within the 29 days is shown as an example in the Figure 21A. In order to evaluate whether the signal of the mtRFP could be considered index of the cellular mitochondrial content, the fluorescence intensity trend of each clone was compared to its citrate synthase activity (CS) during the normal culture conditions. As previously anticipated, the spectrophotometric determination of the CS enzymatic activity is an assay often used to estimate the cellular mitochondrial content.

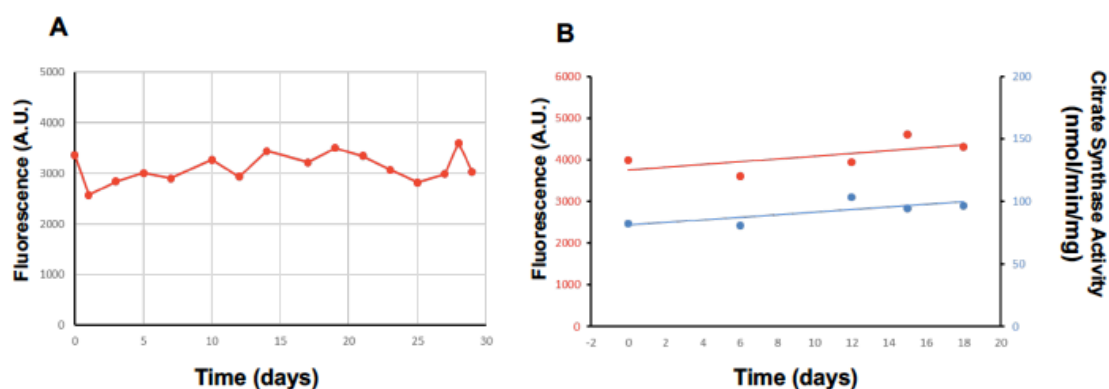


**Figure 21: Time-course monitoring of the 143B-Cl.E** (A) Trend of the average fluorescence intensity within 29 days (B) Correlation between the variation of the mtRFP fluorescence intensity (red line) and the citrate synthase activity (blue line) as a canonical marker of mitochondrial mass within 18 days.

The time course analysis was performed five times over a period of 18 days. For each time point, the cells at 90% of confluence were detached and samples for both cytofluorimetric analysis and CS assay were collected and processed, whereas a fraction was re-seeded for the culturing. To an easy comparison, the mean fluorescence intensity values measured, in A.U., and the citrate synthase activities calculated as nmol/min/mg, were plotted in a double y-axis graph. The data obtained for the 143B clone E are shown as an example in the Figure 21B. Remarkably, all clone analysed displayed moderate oscillations of both parameters during the time, but with a strong correlation between the mtRFP fluorescence and the citrate synthase variations. Therefore, these data indicated that in the isolated stable clones, the mtRFP fluorescence intensity can be taken as an index of the cellular mitochondrial content.

#### 4.1.2.1.3 Assessments of the mtRFP response in conditions inducing variations of the mitochondrial mass

As a further validation of the mtRFP method for the assessment of the mitochondrial mass in intact cells, mtRFP fluorescence intensity was evaluated in response to changes in the cellular mitochondrial content. For this purpose, 143B Cl. E cells were cultured up to 48 hours either in normoxia (21% O<sub>2</sub>) or in hypoxia (0.5% O<sub>2</sub>), a condition that induces a decrease of the mitochondrial mass in osteosarcoma cells, as we previously shown [65]. After 24 hours and 48 hours, the cells were detached and samples collected to assess both mtRFP signal by flow cytometry, and citrate synthase activity.

As shown in Figure 22A, compared to the value obtained in the control conditions, both mtRFP fluorescence intensity and citrate synthase activity showed a decrease of around 15% and 25%, at 24 and 48 hours of exposure to hypoxia, respectively.

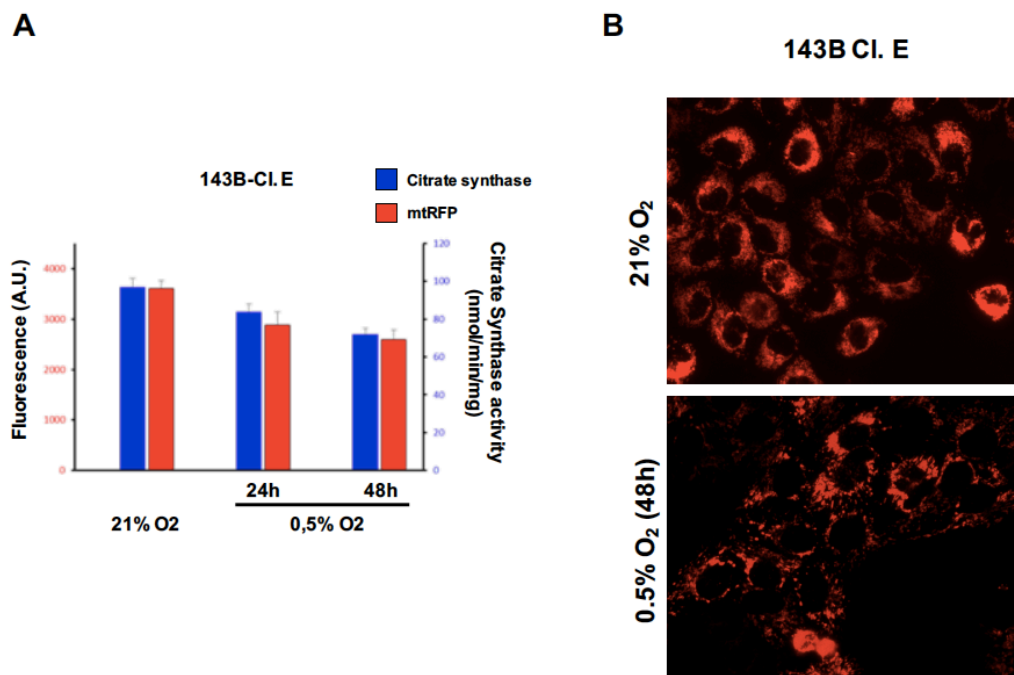


**Figure 22: Mitochondrial mass evaluation of 143B-Cl.E cells after 24h and 48h of exposure to hypoxia (0.5% O<sub>2</sub>)** (A) Correlation between the mean fluorescence intensity values and the citrate synthase activity measured for cells cultured in normal conditions (21% O<sub>2</sub>) and after 24h and 48h of exposure to hypoxia (0.5% O<sub>2</sub>) (B) Fluorescence microscopy images of cells cultured either 48h in control conditions or in anoxia (magnification 20x).

These data again indicate that the mtRFP fluorescence intensity is proportional to the mitochondrial content in the cells. The changes in the mitochondrial mass induced by 48 hours of exposure to low oxygen tension were also directly seen by fluorescence microscopy of adherent cells, as shown in Figure 22B. Conversely, it has been demonstrated in several cell types that resveratrol induces an increase of the mitochondrial mass by stimulating the biogenesis of new organelles [237], [238]. Therefore, 48 hours of treatment with increasing concentrations of resveratrol were performed to induce different levels of mitochondria mass enrichment in the 143B Cl. E cells. In brief, cells were seeded and after 18 hours the medium was replaced with the fresh one, supplemented with resveratrol at final concentration 1  $\mu\text{M}$ , 5  $\mu\text{M}$ , 10  $\mu\text{M}$ , 15  $\mu\text{M}$ , or without it in the control condition. After 48 hours of culturing, fluorescence microscopy images were acquired for each condition, and then cells were detached, collected and processed for the citrate synthase activity assay and the cytofluorimetric assessment of the mtRFP fluorescence intensity. As shown in the Figure 23A, at the increase of the resveratrol concentration used was corresponding the enhancement of both citrate synthase rate and mtRFP fluorescence. Therefore, the intensity of the red fluorescent protein targeted to the mitochondria follows the increase of the mitochondrial content in the cells. While both citrate synthase activity and mtRFP fluorescence showed an increase of the mitochondrial mass of about 10% in the sample with 1  $\mu\text{M}$  resveratrol compared to the control conditions, at the following concentrations the fluorescent marker registered greater increases with respect to the citrate synthase activity. Indeed, the citrate synthase at the resveratrol concentration 5  $\mu\text{M}$  10  $\mu\text{M}$ , 15  $\mu\text{M}$  displayed activity increases of 20%, 30% and 40% respectively, whereas variations of 40%, 55% and 70% were recorded for the mtRFP, with respect to the control condition. This observation suggested that the two approaches may have a different sensitivity to the mitochondrial mass variations. The mitochondrial content enrichment induced by the increasing concentration of resveratrol was also appreciable by fluorescence microscopy, as shown in Figure 23B.

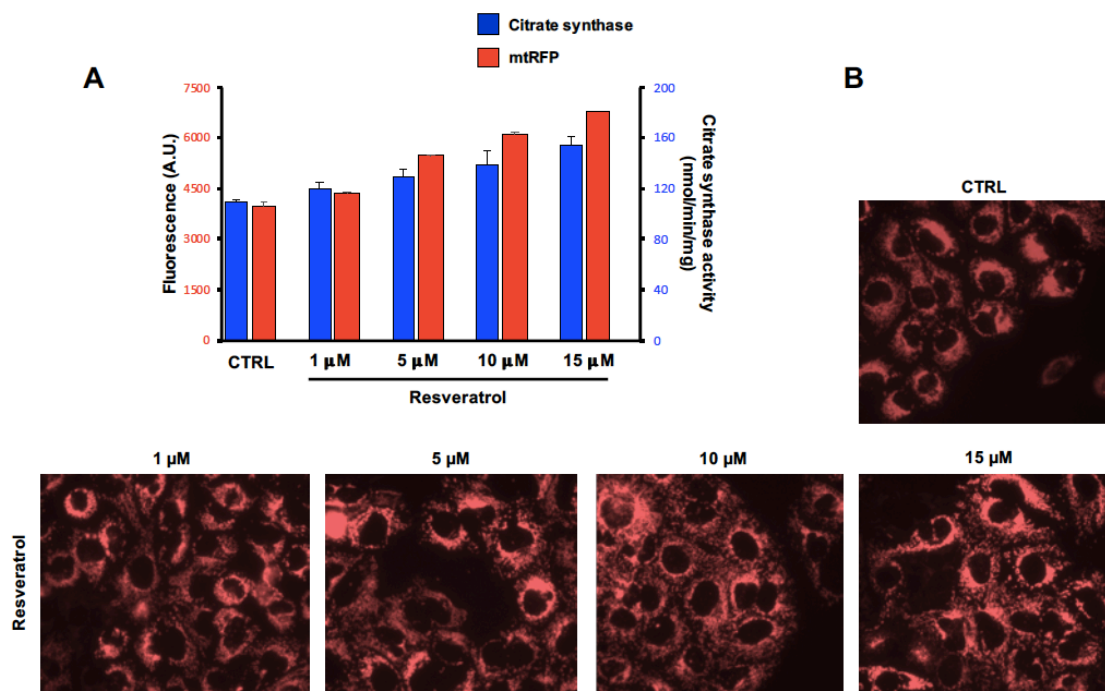


**Figure 23: Mitochondrial mass evaluation in 143B-Cl.E cells after 48h exposure to increasing concentration of resveratrol (A) Correlation between the mean fluorescence intensity values and the citrate synthase activity measured in cells cultured in normal conditions and in medium supplement with resveratrol. (B) Fluorescence microscopy images of cells cultured either 48h in control conditions or in presence of resveratrol (magnification 20x).**

Therefore, the evidence reported above support the use of cellular clones stably expressing the mtRFP to evaluate the mitochondrial mass changes that may occur in response to different experimental conditions, providing the advantage of evaluating this parameter on intact cells.

#### 4.1.2.1.4 Cell growth, CS activity and IF<sub>1</sub> protein levels assessment in mtRFP-clones

The mtRFP clones were analysed for cell growth, citrate synthase activity and IF<sub>1</sub> protein levels, in order to assess whether the features of the original cell lines 143B, E9, G3 and C4 were preserved after the mtRFP transfection and stable selection procedures. The 143B-Cl.E was selected among the clones derived by the 143B parental cell line,

whereas C4-Cl.7 was chosen as scrambled negative control together with the two IF<sub>1</sub>-silenced clones E9-Cl.5 G3-Cl.2. As shown in Figure 24A, the mtRFP clones isolated displayed different mean fluorescence intensities. However, this variability does not affect the usage of the mtRFP method, because the mitochondrial mass can be evaluated within the same clone. Data are expressed as percentage variation of the tested condition respect to the control, allowing the comparison between the clones with different fluorescence intensity. In normal conditions, we previously showed that in human osteosarcoma cells the silencing of IF<sub>1</sub> does not cause changes in cell proliferation, as well as in the activity of citrate synthase compared to the IF<sub>1</sub> expressing cells.

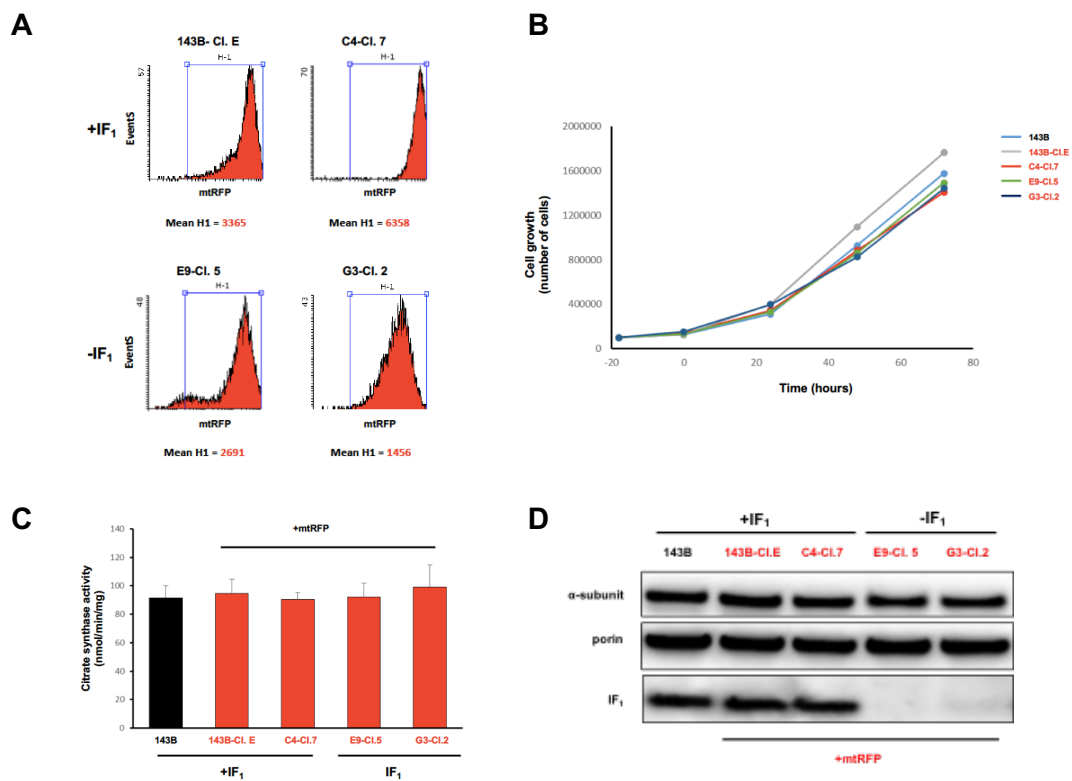


**Figure 24: Assessments of the mtRFP clones 143B-Cl.E, scrambled C4-Cl.7, IF<sub>1</sub> silenced E9-Cl.5 and G3-Cl.2** (A) Flow-cytometry analysis of the mtRFP clones. Mean fluorescence intensities are shown below the graph. (B) Cell growth of 143B parental cells (light blu) and mtRFP clones 143B Cl.E (grey), C4 Cl.7 (red), E9 Cl.5 (green), G3 Cl.2 (blue). (C) Citrate synthase activities expressed as nmol/min/mg of protein. (D) immunoblot analysis of IF<sub>1</sub> protein levels. The  $\alpha$ -subunit of the ATP-synthase and the porin VDAC1 were used as mitochondrial loading control.

According to this observation, cell growth and citrate synthase activity of the mtRFP clones were assessed and compared to 143B parental cells. The cell growth of the mtRFP clones 143B-C1.E, C4-C1.7, E9-C1.5, G3-C1.2 and of the 143B cells was evaluated up to 72 hours, counting the number of cells every 24 hours. As shown in Figure 24B, in normal culture conditions, both mtRFP clones expressing IF<sub>1</sub> (143B-C1.E, C4-C1.7) and the clones silenced for it (E9-C1.5 G3-C1.2) showed a rate of proliferation comparable to the one of 143B parental cell line, concluding that the selection of stable mtRFP clones has not altered the growth behaviour of the cellular models. Moreover, all the mtRFP clones displayed the same citrate synthase activity as the 143B control line, suggesting that also the mitochondrial mass was preserved with the stable expression of the red fluorescent protein (Figure 24C). Levels of IF<sub>1</sub> expression in the mtRFP clones were then assessed by immunodetection of the protein (Figure 24D). The knockdown of IF<sub>1</sub> was confirmed in the E9-C1.5 and G3-C1.2, whereas the control mtRFP clones 143B-C1.E, C4-C1.7 preserved levels of the inhibitor comparable to the 143B parental cell line. Based on these data, the osteosarcoma clones stably expressing the mitochondrial red fluorescent protein were considered a good model for the study of the mitochondrial mass changes in association with the IF<sub>1</sub> expression in cancer cells exposed to stress conditions.

#### **4.1.3 Evaluation of the IF<sub>1</sub> impact on the biology and bioenergetics of osteosarcoma cells in anoxia-mimicking conditions**

Our previous experimental data showed that even severe hypoxia, such as 0.1% O<sub>2</sub>, was not sufficient to abolish the mitochondrial membrane potential  $\Delta\Psi_m$  and force the F<sub>1</sub>F<sub>0</sub>-ATP synthase to reverse its activity to hydrolyse ATP, thus excluding any role played by IF<sub>1</sub> under these conditions [65]. We hypothesized that in cancer cells only severe anoxia may induce the collapse of  $\Delta\Psi_m$  necessary to reverse the ATP synthase and, in turn, to activate the IF<sub>1</sub> inhibition. Therefore, to assess whether IF<sub>1</sub> can preserve cancer cell viability by impeding the ATP deprivation upon anoxic conditions, the uncoupler FCCP was employed to collapse the  $\Delta\Psi_m$  in order to mimic the anoxia condition.

#### 4.1.3.1 Cell growth and viability assays

To investigate a possible protective role of IF<sub>1</sub> in cancer cells in anoxia-mimicking conditions, the GFP-negative IF<sub>1</sub>-silenced clones E9 and G3, the control cells 143B and the scrambled C4 clone were cultured for 24 hours with increasing concentrations of FCCP, and then the growth was assessed. In brief, cells were seeded and after 18 hours the fresh medium was added, supplemented either with FCCP at final concentration 1  $\mu$ M, 5  $\mu$ M, 10  $\mu$ M, or 15  $\mu$ M. After 24 hours of incubation, the cells were detached, collected and counted. As Figure 25A clearly shows, the FCCP induced a reduction of the proliferative capacity of all cells in a dose-dependent manner, without affecting the cell viability. Indeed, the cytofluorimetric assessment of the cell viability with Muse Count and Viability Assay Kit (Millipore), revealed no substantial increases of the cell mortality up to 15  $\mu$ M FCCP, 5% in the control cells and 9% in the IF<sub>1</sub>-silenced cells (Figure 25B). Interestingly, the IF<sub>1</sub>-expressing cells showed a greater capability to proliferate upon increasing concentration of FCCP with respect to the IF<sub>1</sub>-knockdown clones (Figure 25A). Indeed, while control cells proliferated independently from the FCCP concentration, but at reduced rate, the IF<sub>1</sub>-silenced cells significantly arrested their growth at about 10  $\mu$ M FCCP. Collectively, these results provided the first evidence of the protective role of IF<sub>1</sub> in cancer cells in anoxic conditions.



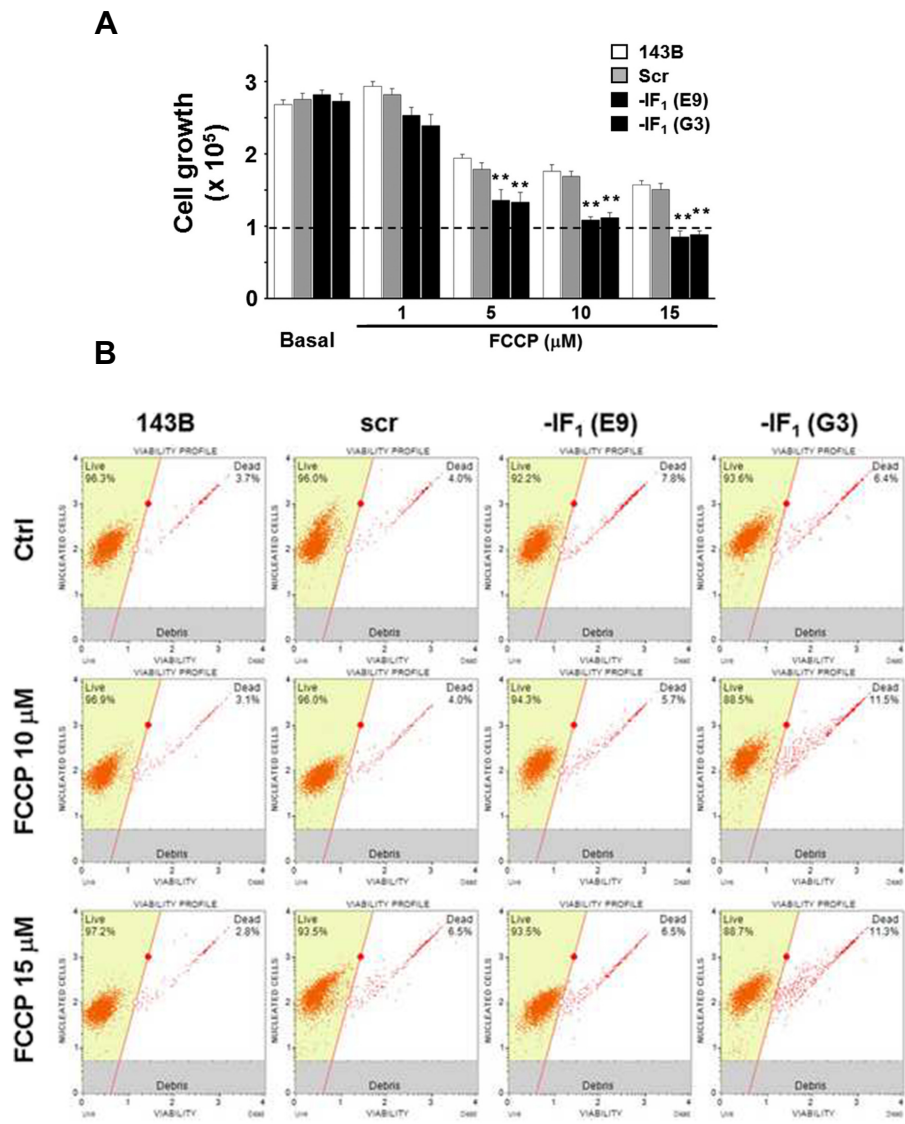


**Figure 25: Growth and viability of IF<sub>1</sub>-expressing cells and IF<sub>1</sub>-silenced clones after 24 hours of culturing in presence of increasing concentration of FCCP. (A) Cell growth analysis. Number of cells is in the y-axis. The dashed line represents the number of cells seeded at the beginning of the experiment. IF<sub>1</sub>-expressing cells showed a greater capability to proliferate upon increasing FCCP doses. (B) Viability of cells cultured for 24 hours in presence of either 10 μM or 15 μM FCCP. In the dot plots, the live-cell population is in the yellow box on the left, whereas dead cells are in the white area on the right. No significant cell-mortality occurs up to 15 μM FCCP, independently from IF<sub>1</sub> expression.**

#### 4.1.3.2 Glycolytic flux assessment and intracellular ATP levels

In order to identify the mechanisms by which IF<sub>1</sub> may favour the proliferation of cancer cells in anoxia by driving the metabolic adaptation, we subsequently focused on the bioenergetic characterization of IF<sub>1</sub>-expressing cells and knockdown clones in anoxia-mimicking conditions. For this purpose, the glycolytic flux and the intracellular steady-state ATP levels were evaluated in osteosarcoma cells upon increasing concentration of FCCP for 24 hours. The experimental conditions were the same as those above. When the incubation time elapsed, the culture supernatants were collected, and both glucose and lactate therein contained were spectrophotometrically quantified and referred to the total number of cells. Notably, we found that the anoxia-mimicking conditions determined a potentiation of glycolysis, represented by the increase of glucose degradation together with production of lactate, in an FCCP dose-dependent manner (Figure 26 A and B). Furthermore, IF<sub>1</sub>-silenced cells showed a greater sensitivity to the FCCP effect, displaying a larger increase in the glycolytic flux at each concentration compared to the control cells. Indeed, when treated with 15  $\mu$ M FCCP, IF<sub>1</sub>-knockdown clones doubled glucose consumption and lactate production compared to the controls.

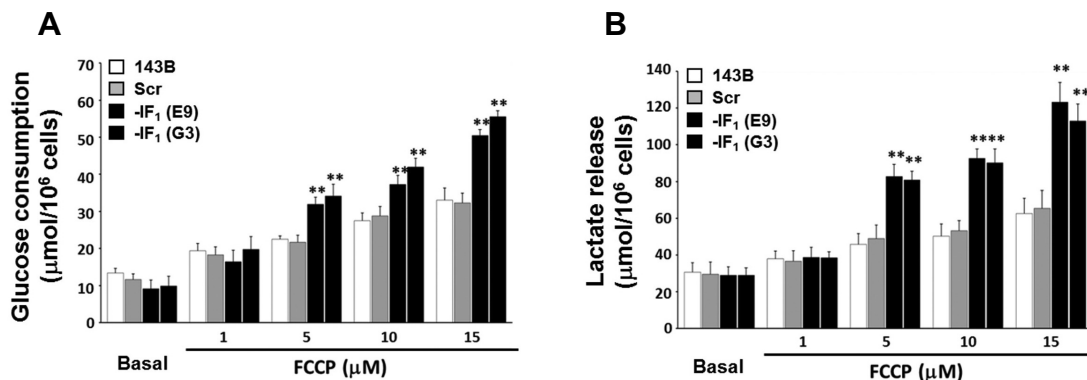


**Figure 26: Glycolytic flux assessment in IF<sub>1</sub>-expressing cells and knockdown clones exposed to increasing concentration of FCCP for 24 hours** (A) Glucose consumption expressed as  $\mu$ mol consumed per  $10^6$  cells. (B) Lactate production expressed as  $\mu$ mol released per  $10^6$  cells. \*\* indicates the statistical significance of data compared to controls, with  $p < 0.01$ . The rise of the glycolytic flux caused by the FCCP increasing concentrations is huger in the IF<sub>1</sub>-silenced cells.

Moreover, for all conditions tested, the glucose consumption and lactate release occurred with a 1:2 stoichiometry, indicating that the totality of consumed glucose was converted into lactate, independently of the expression of the endogenous inhibitor and the FCCCP concentration. Based on the evidence that the energetic metabolism of the osteosarcoma clones was influenced by the IF<sub>1</sub> expression in anoxia-mimicking conditions, we subsequently measured the intracellular content of ATP. The steady-state ATP levels were measured by a luminometric method, after treatment with 10 μM or 15 μM FCCCP for 24 hours. As Figure 27 shows, the uncoupler FCCCP determined a significant decrease of the ATP content in all osteosarcoma cells with a higher reduction in the IF<sub>1</sub>-deprived cells. Indeed, while in the IF<sub>1</sub>-expressing cells the ATP decrease was around 30% when treated at a concentration of FCCCP of 10 μM and 15 μM, IF<sub>1</sub>-silenced cells showed a reduction of about 50% at the lower uncoupler concentration, up to 60% with 15 μM FCCCP. Notably, our data suggest that IF<sub>1</sub> plays a critical role in the energy preservation in cancer cells exposed to the anoxia-mimicking condition.

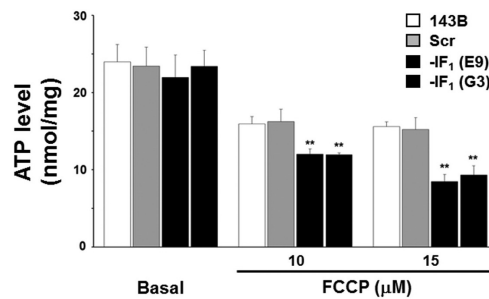


**Figure 27: Steady-state levels of ATP in osteosarcoma cells upon either 10 μM or 15 μM FCCCP exposure for 24 hours.** ATP levels are expressed in nmol of ATP measured/mg of cellular proteins. \*\* indicates the statistical significance of data compared to controls, with p<0.01. Anoxia-mimicking conditions induce a decrease of the steady-state ATP levels, higher in IF<sub>1</sub>-silenced cells.

#### **4.1.3.2.1 Mitochondrial membrane potential evaluation in cell in anoxia-mimicking conditions**

It is extensively described in the literature how IF<sub>1</sub> is activated in normal cells by the collapse of the mitochondrial membrane potential ( $\Delta\Psi_m$ ) that occurs in ischemic episodes. In these conditions, IF<sub>1</sub> acts by limiting the reversal of the F<sub>1</sub>F<sub>0</sub>-ATP synthase, that hydrolyses ATP to sustain the  $\Delta\Psi_m$ . Conversely, the functioning of IF<sub>1</sub> in cancer cells is still uncertain. The data presented above highlight that IF<sub>1</sub> in anoxia-mimicking conditions favours the cellular proliferation and ATP preservation in cancer cells. The latter function seems similar to the role played by IF<sub>1</sub> in normal cells, suggesting that also in cancer cells the inhibitor may influence the maintenance of the  $\Delta\Psi_m$  by regulating the reversal of the ATP synthase. Therefore, we tried to better understand the impact of IF<sub>1</sub> expression on the mitochondrial membrane potential in anoxia-mimicking conditions. Based on the previous results on cell viability, proliferation and ATP levels, the exposure to 10  $\mu$ M FCCP for 24 hours was chosen to compare and characterize the IF<sub>1</sub>-expressing cells and IF<sub>1</sub>-silenced osteosarcoma clones in anoxia-mimicking conditions. After 24 hours under three different conditions, normal culture, FCCP treated, or FCCP and oligomycin treated, cells were loaded with the TMRM, a fluorescent probe that accumulates in the mitochondria in a  $\Delta\Psi_m$ -dependent manner. Subsequently, fluorescence microscopy images were acquired for a first qualitative analysis, and on the same samples flow cytometry was performed for quantitative analysis. As expected, the FCCP induced a huge decrease of the  $\Delta\Psi_m$ , of about -80% in the IF<sub>1</sub>-expressing cells, compared to the basal condition. This massive collapse of the mitochondrial membrane potential was appreciable by both fluorescence microscopy (Figure 28A), and flow cytometry acquisition (Figure 28B and C). Indeed, the almost total absence of TMRM signal in the fluorescence microscopy images of IF<sub>1</sub>-expressing cells (143B and Scr) upon FCCP, pointed out that  $\Delta\Psi_m$  levels were very weak, thus restricting the accumulation of the probe, as also proved by the quantitative analysis. Conversely, in the IF<sub>1</sub>-silenced cells upon anoxia-mimicking conditions, the reduction of the TMRM fluorescence intensity resulted in less than the -20%, compared to the value acquired in basal conditions.

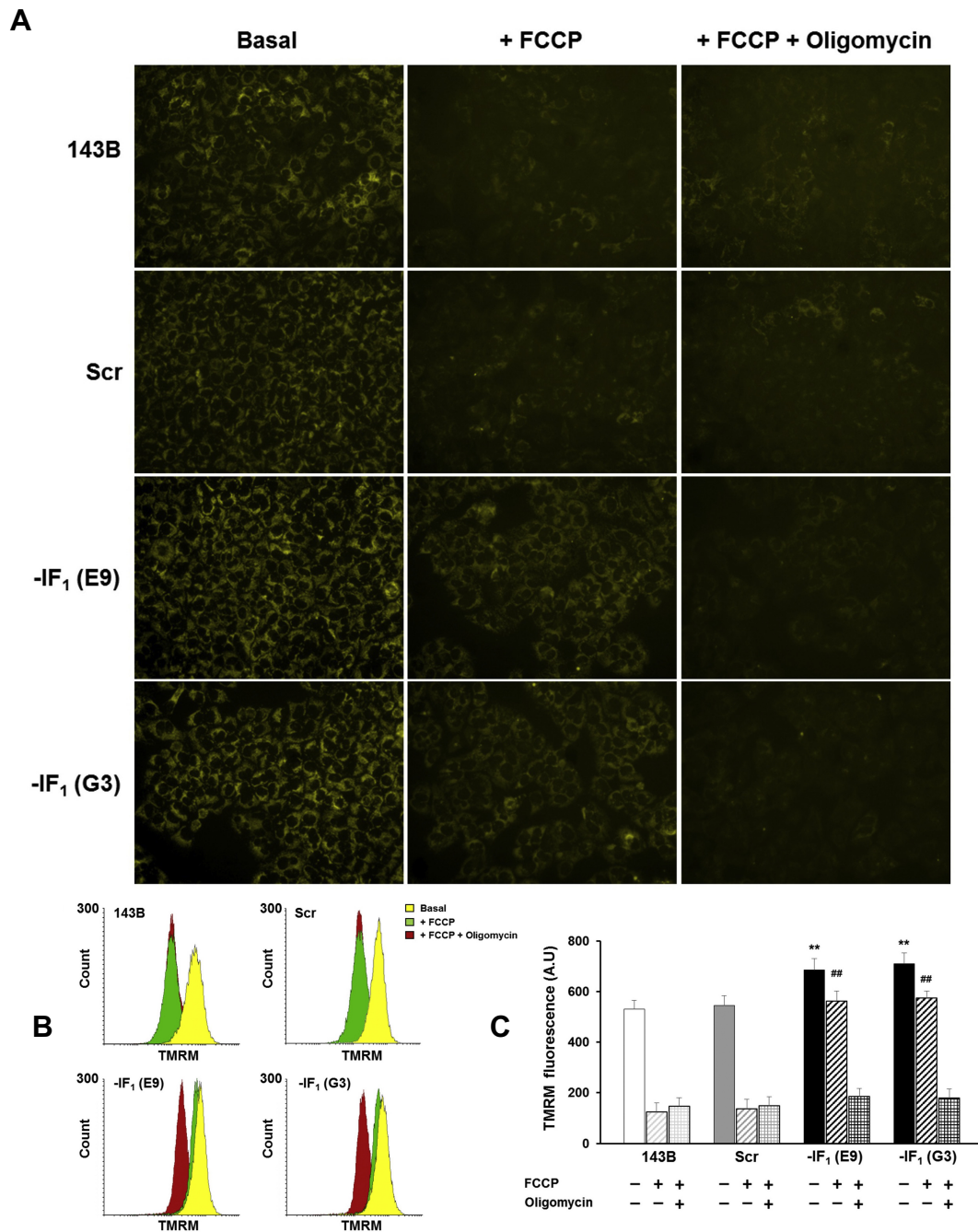


**Figure 28: Mitochondrial membrane potential assessment of osteosarcoma cells after 24 hours of exposure to 10  $\mu$ M FCCP.** Both IF<sub>1</sub>-expressing and IF<sub>1</sub>-silenced clones were cultured either in normal conditions, in presence of FCCP, or FCCP plus oligomycin. (A) Representative fluorescence images of cells stained with TMRM (magnification 10x). (B) Fluorescence distribution of the cells loaded with TMRM in basal condition (yellow), with FCCP (green) or FCCP plus oligomycin (red). Number of Cell acquired is in the y-axis, whereas TMRM fluorescence in the x-axis. (C) Semiquantitative analysis of flow cytometry data. \*\* and ## indicates the statistical significance of the data compared to controls, with  $p < 0.01$ .

To understand whether this  $\Delta\Psi_m$  maintenance in IF<sub>1</sub>-silenced cells was due to the hydrolysis of ATP by the F<sub>1</sub>F<sub>0</sub>-ATP synthase, the activity of the latter complex was inhibited by treating uncoupled cells also with oligomycin. Relevantly, upon both FCCP and oligomycin exposure, TMRM value dropped, reaching the same values of the uncoupled controls. Therefore, these data suggest that under anoxia-mimicking conditions IF<sub>1</sub>-silenced cells sustain the  $\Delta\Psi_m$  through the reverse activity of the F<sub>1</sub>F<sub>0</sub>-ATP synthase, with the consumption of the cytosolic ATP. Although  $\Delta\Psi_m$  was almost abolished in part of the conditions tested, as shown by the TMRM fluorescence intensity (Figure 28), we did not observed any cell mortality. Furthermore, even upon a short exposure to anoxia-like conditions, such as 1  $\mu$ M FCCP for 30 minutes, a collapse of the  $\Delta\Psi_m$  of around -75% was detected by flow cytometry in IF<sub>1</sub>-expressing cells, whereas it was only about 30%-40% in the IF<sub>1</sub>-silenced clones (Figure 29A and B). In the same way as described above, under anoxia-mimicking conditions, when also the oligomycin was added to prevent the ATP-hydrolytic activity of the F<sub>1</sub>F<sub>0</sub>-ATP synthase, the  $\Delta\Psi_m$  of the IF<sub>1</sub>-knockdown cells collapsed and achieved the value of the uncoupled controls, that instead remained unchanged. These data highlight the promptness of IF<sub>1</sub> to exert its protective role even in the early stage of the anoxia-mimicking conditions.

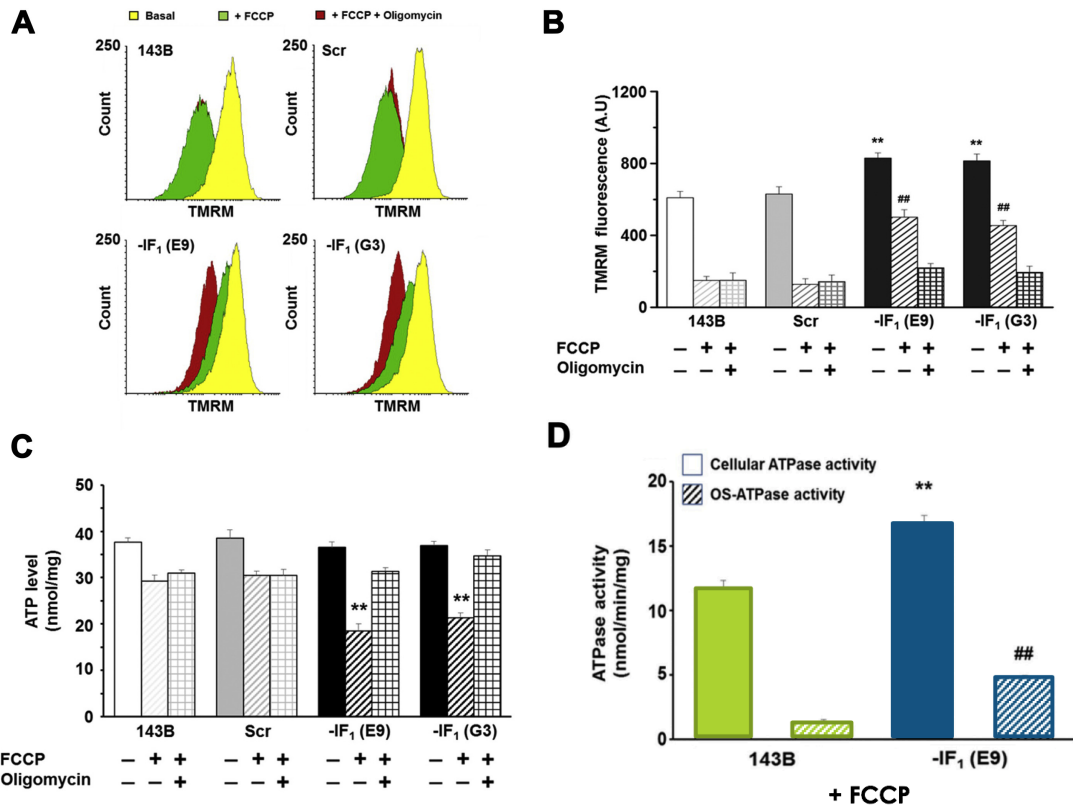


**Figure 29: Assessment of the of osteosarcoma cells after 30 minutes of exposure to 1  $\mu$ M FCCP.** Both IF<sub>1</sub>-expressing and IF<sub>1</sub>-silenced clones were cultured either in normal conditions, in presence of FCCP, or FCCP plus oligomycin. (A) Flow cytometry fluorescence distribution of cells loaded with TMRM in basal condition (yellow), with FCCP (green) or FCCP plus oligomycin (red). (B) Semiquantitative analysis of the  $\Delta\Psi$ m by flow cytometry. (C) Steady-state ATP levels (D) Total and oligomycin-sensitive ATPase activity of both parental cells and the E9 IF<sub>1</sub>-silenced clone. \*\* and ## indicates the statistical significance of the data compared to controls, with  $p < 0.01$ .

#### **4.1.3.3 Steady-state ATP levels and F<sub>1</sub>F<sub>0</sub>-ATP synthase ATPase activity assessments**

To understand whether the  $\Delta\Psi_m$  maintenance in IF<sub>1</sub>-silenced cells was really due to the ATP hydrolysis carried out by the reverse activation of the F<sub>1</sub>F<sub>0</sub>-ATP synthase, ATP steady-state levels were measured in osteosarcoma cells in short-time exposure to anoxia-mimicking conditions (1  $\mu$ M FCCP for 30 minutes). As clearly shown in Figure 29C, FCCP induced the decrease of the intracellular ATP levels in all osteosarcoma cells, with respect to the basal conditions. More interestingly, in anoxia-mimicking conditions, the decrease of the ATP was about 20% in control cells and 45% and IF<sub>1</sub>-silenced clones. Moreover, when oligomycin was added, ATP levels of the -IF<sub>1</sub> clones were similar to the uncoupled controls. Conversely, ATP levels of uncoupled controls cells plus oligomycin were identical to the ones of the cells treated only with FCCP, indicating that IF<sub>1</sub> inhibits completely the ATP-synthases reversed, with maximum efficiency.

Therefore, these data definitively proved that IF<sub>1</sub> expression drives the preservation of intracellular ATP in osteosarcoma cells upon anoxia-mimicking conditions. Moreover, upon FCCP, the lower steady-state ATP levels found in the IF<sub>1</sub>-silenced clones with respect to the control cells, corroborate the hypothesis that in these clones the  $\Delta\Psi_m$  was partially sustained through ATP consumption by the hydrolytic ATP synthase. To confirm this assumption, the fraction of the cellular ATPase activity sensitive to oligomycin, attributable to the F<sub>1</sub>F<sub>0</sub>-ATP synthase, was measured in 143B cells and the IF<sub>1</sub>-silenced clones E9 upon uncoupling conditions. As Figure 29D shows, the oligomycin-sensitive ATPase activity (OS-ATPase activity) was 5-fold lower in controls cells compared to the IF<sub>1</sub>-silenced clones. Indeed, while in the 143B the OS-ATPase activity was less than 10% of the total cellular ATPase activity, the IF<sub>1</sub>-silenced clone was about 30%. Giving the evidence that in IF<sub>1</sub>-silenced cancer cells upon anoxia-mimicking conditions the F<sub>1</sub>F<sub>0</sub>-ATP synthase efficiently hydrolysed ATP, together with the decrease of the steady-state ATP levels and the higher  $\Delta\Psi_m$  compared to the IF<sub>1</sub>-expressing cells, by the opposition it is possible to affirm the role of IF<sub>1</sub>.



Therefore, the data demonstrate that in anoxia-mimicking conditions, IF<sub>1</sub> favours the proliferation of cancer cells by completely inhibiting the hydrolytic activity of the ATP synthase to preserve ATP intracellular levels. Although the  $\Delta\Psi_m$  was almost abolished within 24 hours, the cancer cells expressing IF<sub>1</sub> showed a great viability, suggesting that IF<sub>1</sub> could activate alternative pathways for the cell survival, considering that the prolonged collapse of the mitochondrial membrane potential is usually detrimental to normal cells.

#### **4.1.3.4 Mitochondrial mass assessments**

Considering that the collapse of the mitochondrial membrane potential is widely described as an event that triggers the autophagic degradation of mitochondria, the mitochondrial content in osteosarcoma cells was assessed under anoxia-mimicking conditions. Indeed, as previously described, IF<sub>1</sub>-expressing cells almost completely lose the  $\Delta\Psi_m$ , whereas it is partially preserved in IF<sub>1</sub>-silenced clones upon FCCP. Based on this, we assumed that IF<sub>1</sub>-expressing cells and -IF<sub>1</sub> clones may display differences in the mitochondrial content as the effect of the dissimilar activation of the mitophagy by the  $\Delta\Psi_m$  levels.

For this purpose, a first evaluation of the mitochondrial mass was performed by using osteosarcoma clones stably expressing the red fluorescent protein targeted to the mitochondria. After 24 hours of exposure to 10  $\mu$ M FCCP, fluorescence microscopy images were acquired, and then intact cells were detached, collected and assessed by flow cytometry. Surprisingly, in all osteosarcoma clones, no decreases and no significant variations of the mitochondrial mass were detected in anoxia-mimicking condition with respect to the basal condition, regardless of the IF<sub>1</sub> expression, as shown by both fluorescence microscopy and semi-quantitative flow cytometry analysis (Figure 30). To validate the data obtained, the mitochondrial content was subsequently evaluated in the same conditions in the cellular models negative for both GFP and mtRFP, through the immunodetection of TOMM20 and VDAC1 proteins. These transporters of the outer mitochondrial membrane are commonly used as markers of the mitochondrial mass.

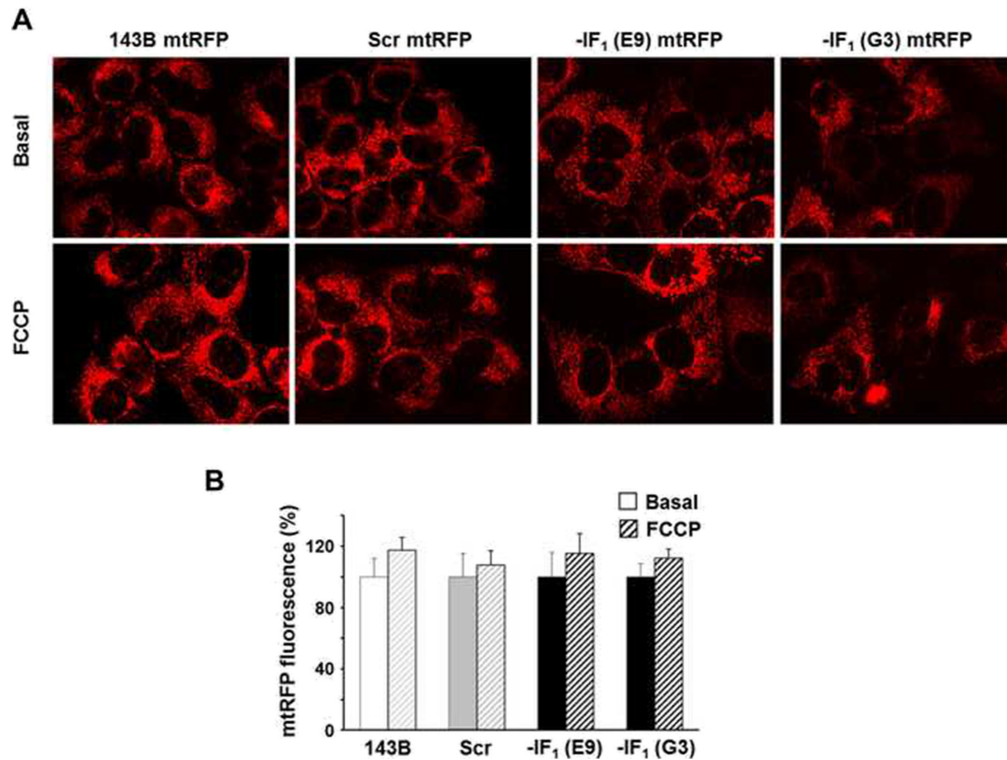


**Figure 30: Mitochondrial mass assessment of mtRFP-osteosarcoma cells cultured 24 hours either in basal conditions or with 10  $\mu$ M FCCP. (A) Representative fluorescence images (magnification 40x). (B) Quantitative analysis of the fluorescence by flow cytometry.**

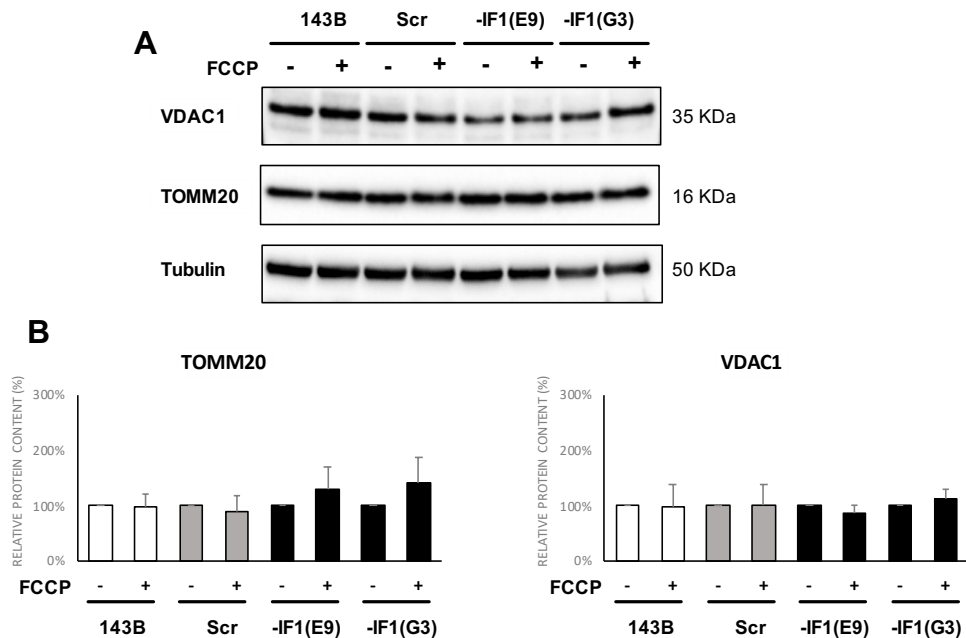


**Figure 31: Mitochondrial mass assessment of osteosarcoma cells cultured 24 hours either in basal conditions or with 10  $\mu$ M FCCP by VDAC1 and TOMM20 protein immunodetection.**

(A) Representative immunodetection of VDAC1 and TOMM20. (B) Semi-quantitative densitometric analysis. TOMM20 and VDAC1 densitometric values were normalized on tubulin and reported as percentage with respect to the basal condition.

In brief, after 24 hours in uncoupling conditions with 10  $\mu$ M FCCP, whole cells lysates were prepared, separated by SDS-page, blotted onto nitrocellulose membranes and the proteins detected with specific antibodies. In agreement with the previous results, no reduction of the expression of both TOMM20 and VDAC1 proteins were detected in anoxia-mimicking conditions compared to the basal condition, in both IF<sub>1</sub>-expressing cells and silenced clones (Figure 31). Unexpectedly, the data collected by the two different methodological approaches highlighted that osteosarcoma cells preserved the mitochondrial mass also after 24 hours of exposure in anoxia-mimicking conditions, independently from the IF<sub>1</sub> expression and thus also regardless the  $\Delta\Psi_m$ .

#### **4.1.3.5 Mitochondrial turnover evaluation**

Despite the obtained evidence pointed out that the steady-state mitochondrial mass levels were not affected by the uncoupling conditions, based on the previous experiments, we hypothesized that the mitophagy might be activated without visible effect on the organelle quantities due to the concomitant activation of the biogenesis process. Indeed, it is well established that both the quality and quantity of mitochondria in a cell result from the balance between the biogenesis processes and organelles elimination through the autophagic degradation, which rates may vary according to different stress conditions [157]. To evaluate the activation of the mitochondrial turnover in anoxia-mimicking conditions, markers of both mitochondrial biogenesis and mitophagy were assessed in IF<sub>1</sub>-expressing and IF<sub>1</sub>-silenced osteosarcoma clones. The  $\Delta\Psi_m$  collapse occurring in anoxia was mimicked with 24 hours of exposure to 10  $\mu$ M FCCP. In particular, the expression of two proteins that positively regulates mitophagy was measured: PINK1, whose accumulation in the IMM upon  $\Delta\Psi_m$  collapse triggers mitophagy, and BNIP3, described to drive mitochondria degradation when the dimeric form is induced by hypoxia [157]. Levels of both PINK1 and BNIP3 were assessed by immunodetection of proteins and semi-quantitative densitometric analysis. Densitometric values of the markers detected in anoxia-mimicking conditions were expressed as a percentage of the levels found in basal condition within the same clone.

As expected, the expression of PINK1 was also detected in normal conditions, due to its involvement in the physiologic process of the mitochondrial turnover. Interestingly, the levels of the mitophagic protein PINK1 were increased about 50% compared to the basal conditions in anoxia-mimicking conditions in the IF<sub>1</sub>-expressing cells. Conversely, the PINK1 levels decreased of about 35% in uncoupled IF<sub>1</sub>-silenced clones, with respect to the basal conditions (Figure 32 A and B). Analysis of the BNIP3 revealed a great expression of this protein in basal conditions in all osteosarcoma cells, but mainly in the inactive monomeric form (Figure 32C). Secondly, upon FCCP treatment, the BNIP3 total levels were strongly decreased in all osteosarcoma cells, compared to the control conditions. However, while the IF<sub>1</sub>- expressing clones preserved nearly the 40% of the inactive BNIP3, the monomer was almost disappeared in the IF<sub>1</sub>-silenced cells in anoxia-mimicking conditions (Figure 32D). Finally, the levels of the BNIP3 dimer, functional to trigger mitophagy, were found sensibly increased in the IF<sub>1</sub>-expressing cells upon FCCP, though the variation occurred in different percentage in 143B and scrambled cells, with an increment of 20% and 70% respectively, compared to the basal conditions. Contrariwise, IF<sub>1</sub>-silenced cells displayed the decrease of the active BNIP3 dimer, about of 40% compared to the control conditions. Therefore, the data collected through the assessment of the mitophagy markers PINK1 and BNIP3 may suggest that, while anoxia-mimicking conditions stimulate mitophagy in IF<sub>1</sub>-expressing cells, the effect is opposite in IF<sub>1</sub>-silenced clones, where the mitochondrial degradation process is reduced respect to the basal conditions. Then, to better define whether the differential activation of BNIP3 and PINK1 could actually lead to altered mitochondria degradation rates, the occurrence of mitophagy was assessed by evaluating the colocalization of the mitochondria in the autophagosomes, by qualitative fluorescence microscopy. For this purpose, osteosarcoma clones stably expressing the mitochondrial red fluorescent protein were transiently transfected with a plasmid for the expression of the LC3 protein fused to the yellow fluorescent protein (YFP), to label the autophagosome.

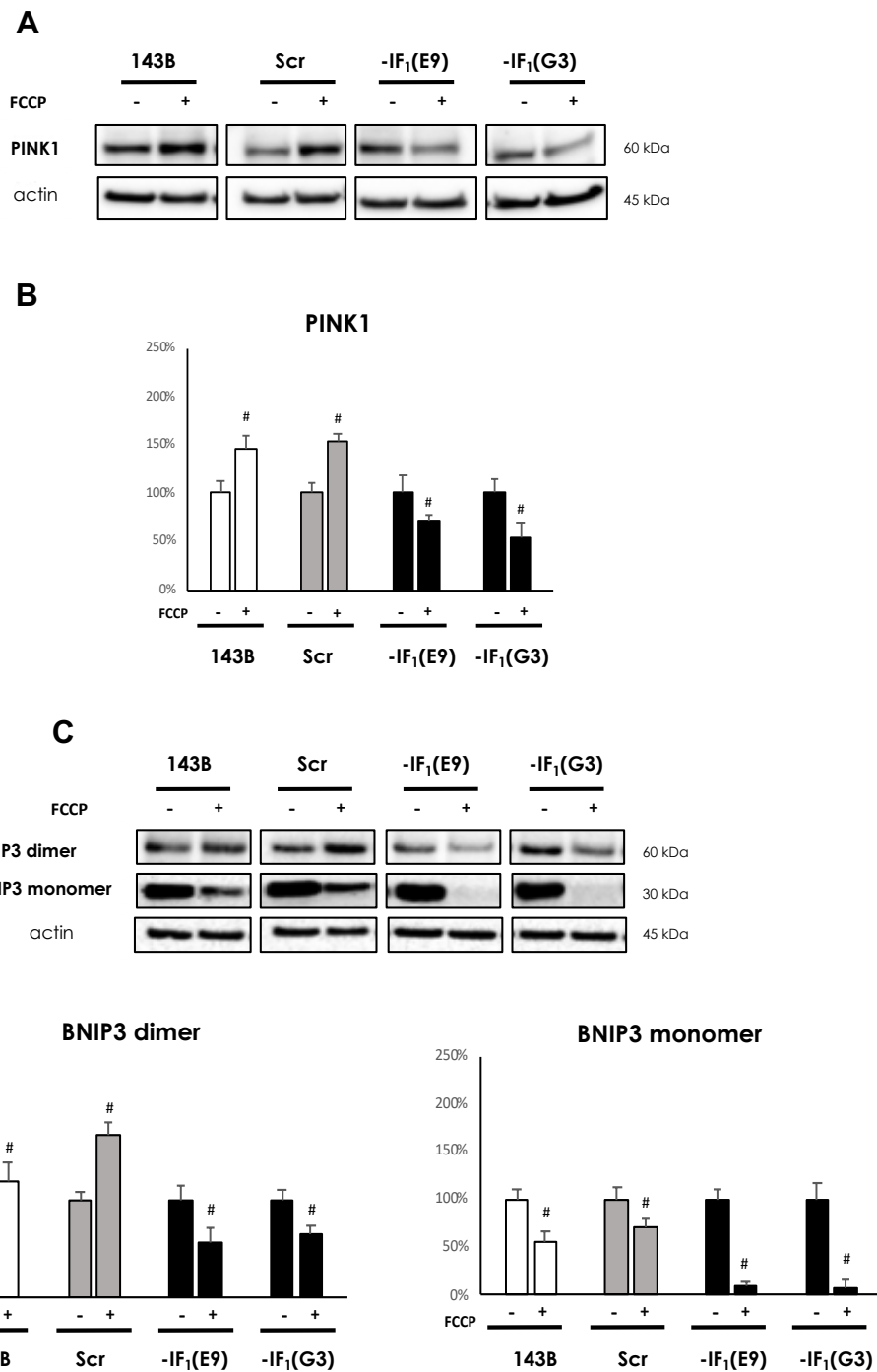


**Figure 32: Evaluation of mitophagy markers: levels of PINK1 and BNIP3 proteins in osteosarcoma cells after 24 hours of 10  $\mu$ M FCCP.** (A) Representative immunodetection of PINK1. (B) Semi-quantitative densitometric analysis of PINK1. (C) Representative immunodetection of BNIP3. BNIP3 acts as a dimer in the mitophagy process. (D) Semi-quantitative densitometric analysis of BNIP3 dimer and BNIP3 monomer. Densitometric values were normalized on the actin levels and reported as percentage with respect to the basal condition. # indicates the statistical significance of the data compared to the controls, with  $p < 0.05$ .

Upon autophagic activation, the endogenous LC3 protein is recruited and conjugated to the membranes of the autophagosome in assembly. Considering the LC3-YFP reporter, in basal condition autophagosome formation slightly occurs and the fluorescence signal is spread in the cytosol. Conversely, the assembled vesicles are visible as fluorescent puncta, due to the different distribution of the LC3 protein. In brief, mtRFP-stable osteosarcoma clones were transiently transfected with the LC3-YFP expression vector, and subsequently exposed to either anoxia-mimicking conditions or cultured in normal conditions. Moreover, positive control samples of the mitophagy activation were set up by culturing the cells in presence of deferoxamine (DFO). Colocalization was assessed by the red and green fluorescence signals from the same optical field, and then merging the two channels. Representative fluorescence images of the experiment are shown in Figure 33. In the left panel is the mitochondrial marker mtRFP in red, in the central panel the autophagic signal of YFP-LC3 in green, and the two merged channels are shown in the right panel, where the colocalization events appear in yellow. As shown in panel A, IF<sub>1</sub>-expressing cells showed a higher assembly of the autophagosomes, but in basal conditions, as suggested by the puncta signals of the LC3, whereas the basal rate of mitophagy was comparable to the one of IF<sub>1</sub>-silenced cells, as indicated by the low occurrence of the colocalization events. However, after 24 hours of deferoxamine treatment, the number of colocalization was increased both in control cells and IF<sub>1</sub>-silenced clones, proving that the cells responded to mitophagic stimuli, and also that mitophagy was detectable with the method used (Figure 33 panel B). Finally, the activation of mitophagy was qualitatively evaluated after 24 hours of exposure to anoxia-mimicking conditions. As clearly shown in panel C, IF<sub>1</sub>-expressing cells showed a huge increase of the colocalization of LC3 and mtRFP signals, suggesting that in these cells mitophagy occurred with a higher rate upon uncoupling conditions. Conversely, in IF<sub>1</sub>-silenced cells the LC3 signal was widespread in the cytosol, with almost the total absence of puncta, indicating that the autophagosomes assembly did not occur, and thus, no colocalization was detected. Therefore, this qualitative analysis suggested that upon anoxia-mimicking condition, the IF<sub>1</sub>-silenced cells reduced the mitophagy rate compared to the basal conditions.

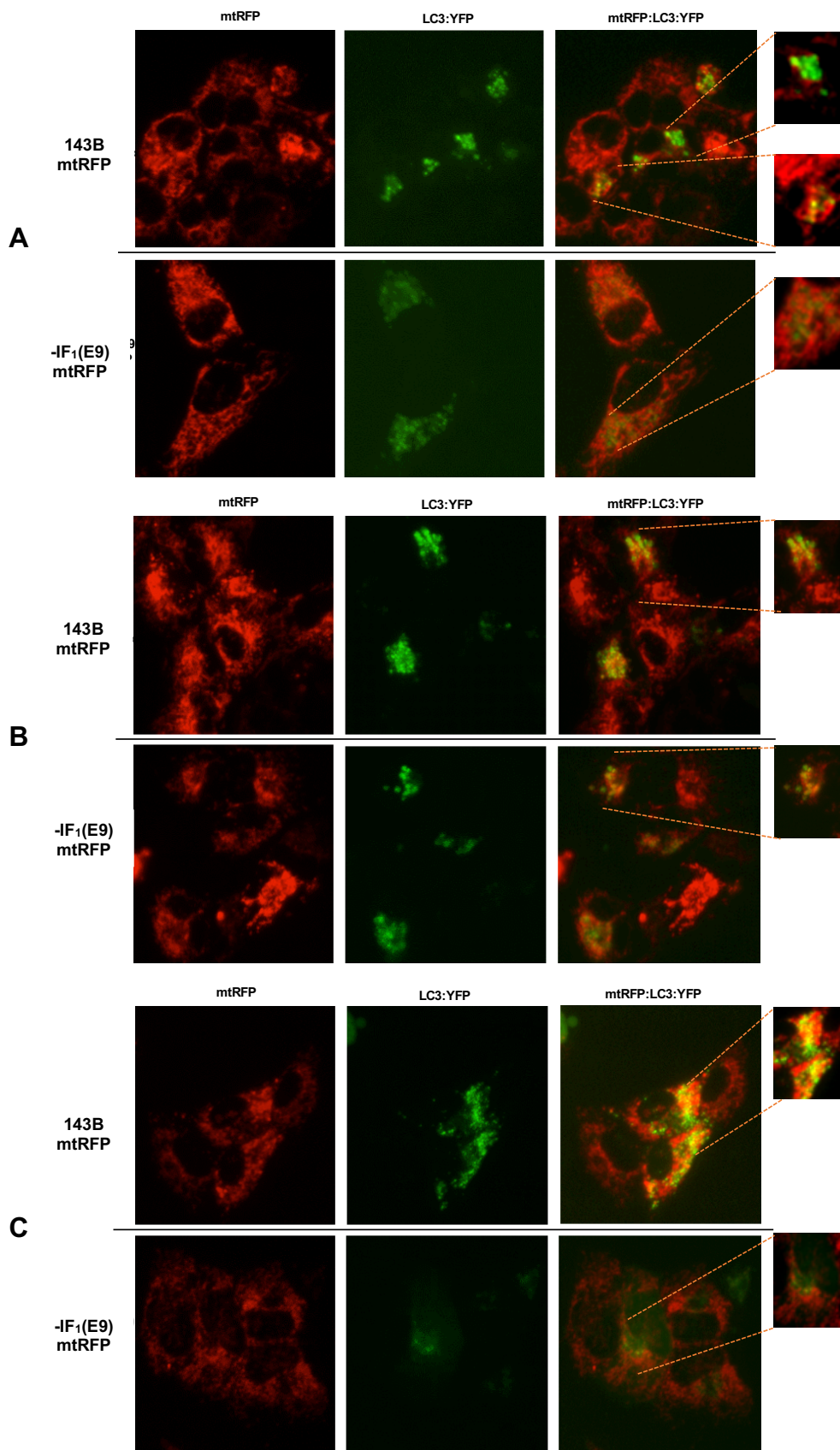


**Figure 33: Evaluation of mitophagy activation by mtRFP and LC3-YFP colocalization in osteosarcoma cells.** Representatives images. (A) Basal conditions (B) Positive control of mitophagy activation, 10  $\mu$ M DFO for 24 hours (C) anoxia-mimicking conditions. 10  $\mu$ M FCCP for 24 hours. (Magnification 40x).

In conclusion, these qualitative data pointed out that in IF<sub>1</sub>-expressing cells the mitophagy rate increased following the BNIP3 and PINK1 activation induced by the anoxia-mimicking conditions. However, considering that no decreases in the mitochondrial mass were detected in osteosarcoma cells upon anoxia-mimicking conditions, the contribution of the mitochondrial biogenesis process was subsequently evaluated by immunodetection of specific biomarkers. In particular, the protein levels of SIRT1 and PGC-1 $\alpha$  were measured in osteosarcoma cells 24 hours after exposure to anoxia mimicking conditions. While PGC-1 $\alpha$  is the main biogenesis regulator by acting as transcriptional co-activator of nuclear genes encoding the mitochondrial proteins, SIRT1 is one of the activators of PGC-1 $\alpha$ , as previously described. As Figure 34 interestingly shows, after 24 hours in uncoupling conditions, in IF<sub>1</sub>-expressing cells both SIRT1 and PGC1- $\alpha$  levels were significantly increased, with an enhancement of nearly 30% and 45-80%, respectively. Conversely, in IF<sub>1</sub>-silenced cells upon FCCP, a decrease of about the 35% was detected in both of mitochondrial biogenesis markers.

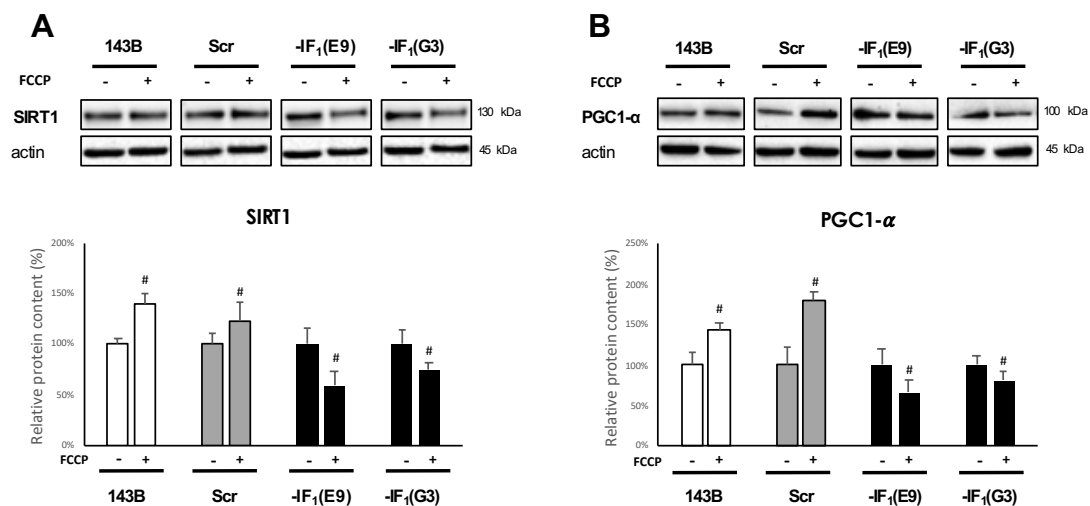


**Figure 34: Evaluation of mitochondrial biogenesis markers: levels of SIRT1 and PGC1- $\alpha$  proteins in osteosarcoma cells after 24 hours of 10  $\mu$ M FCCP. (A) SIRT1 analysis. (B) PGC1- $\alpha$  evaluation. Top panels: representative immunodetection. Bottom panels: semi-quantitative densitometric analysis. Densitometric values were normalized to the actin levels and reported as percentage with respect to the basal condition. # indicates the statistical significance of the data compared to the controls, with  $p < 0.05$ .**



Therefore, these data suggested that upon anoxia-mimicking conditions, the mitochondrial biogenesis is potentiated in IF<sub>1</sub>-expressing cells, whereas in IF<sub>1</sub>-silenced clones is strongly inhibited compared to the basal conditions.

Overall, the evidence collected by the assessment of both mitochondrial biogenesis and mitophagy suggested that in cancer cells exposed to anoxia-mimicking conditions, the expression of IF<sub>1</sub> favours the mitochondrial renewal, whereas the mitochondrial turnover is strongly slowed down in IF<sub>1</sub>-silenced cells. However, in both cases, the steady-state levels of mitochondrial mass are preserved.

#### 4.1.3.6 Cellular energy charge assessment

The autophagic mitochondrial degradation and the generation of new mitochondria are both processes that have a high energy demand and that are strictly controlled in response to the energy status of the cells [130][131]. To evaluate a possible correlation between energy status and mitochondrial turnover rate, the cellular energy charge of the osteosarcoma clones in anoxia-mimicking conditions was assessed by measuring the ADP/ATP ratio, through a luminometric method. Luminescence values recorded for the cells treated with FCCP were reported as a percentage with respect to the basal condition, considered the 100% of ADP/ATP.

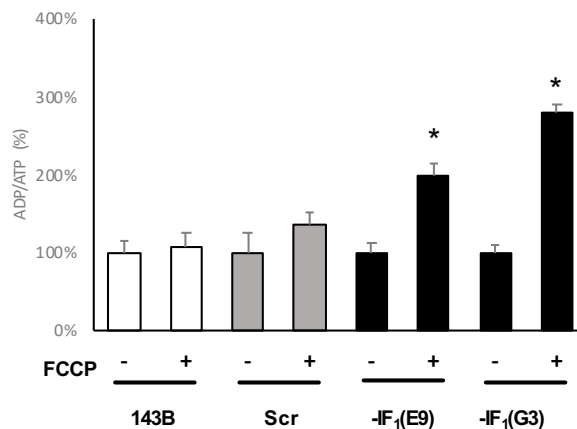


**Figure 35: Assessment of the ADP/ATP ratio as an index of the cellular energy charge in osteosarcoma cells after 24 hours of 10  $\mu$ M FCCP.** # indicates the statistical significance of the data compared to the controls, with  $p < 0.05$

Significantly, the IF<sub>1</sub>-expressing cells showed an ADP/ATP ratio almost preserved in anoxia-mimicking conditions compared to the basal conditions whereas this parameter hugely raised in the IF<sub>1</sub>-silenced cells, indicating a very low cellular energy charge (Figure 35). Indeed, upon uncoupling, the IF<sub>1</sub>-silenced clones E9 and G3 showed an ADP/ATP ratio doubled and triplicated, respectively, compared to the basal condition. Therefore, in cancer cells in anoxia-mimicking conditions, it is supposed that is the preservation of either ATP levels and the cellular energy charge allowed by IF<sub>1</sub> activity to drive the mitochondrial renewal, impossible in -IF<sub>1</sub> cells due to the adverse energy status.

#### 4.1.3.7 OXPHOS complexes and IF<sub>1</sub> protein levels assessment

Despite the mitochondrial mass was preserved in both cases, in anoxia-mimicking conditions the IF<sub>1</sub>-expressing osteosarcoma cells and IF<sub>1</sub>-silenced clones showed substantial differences in the metabolic functions, in term of glycolytic flux, steady-state ATP levels,  $\Delta\Psi_m$ , ATPase activity and energy charge status.

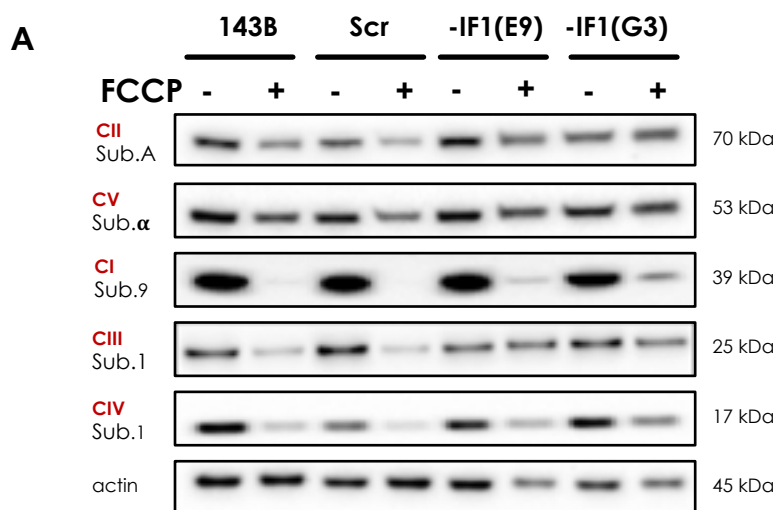
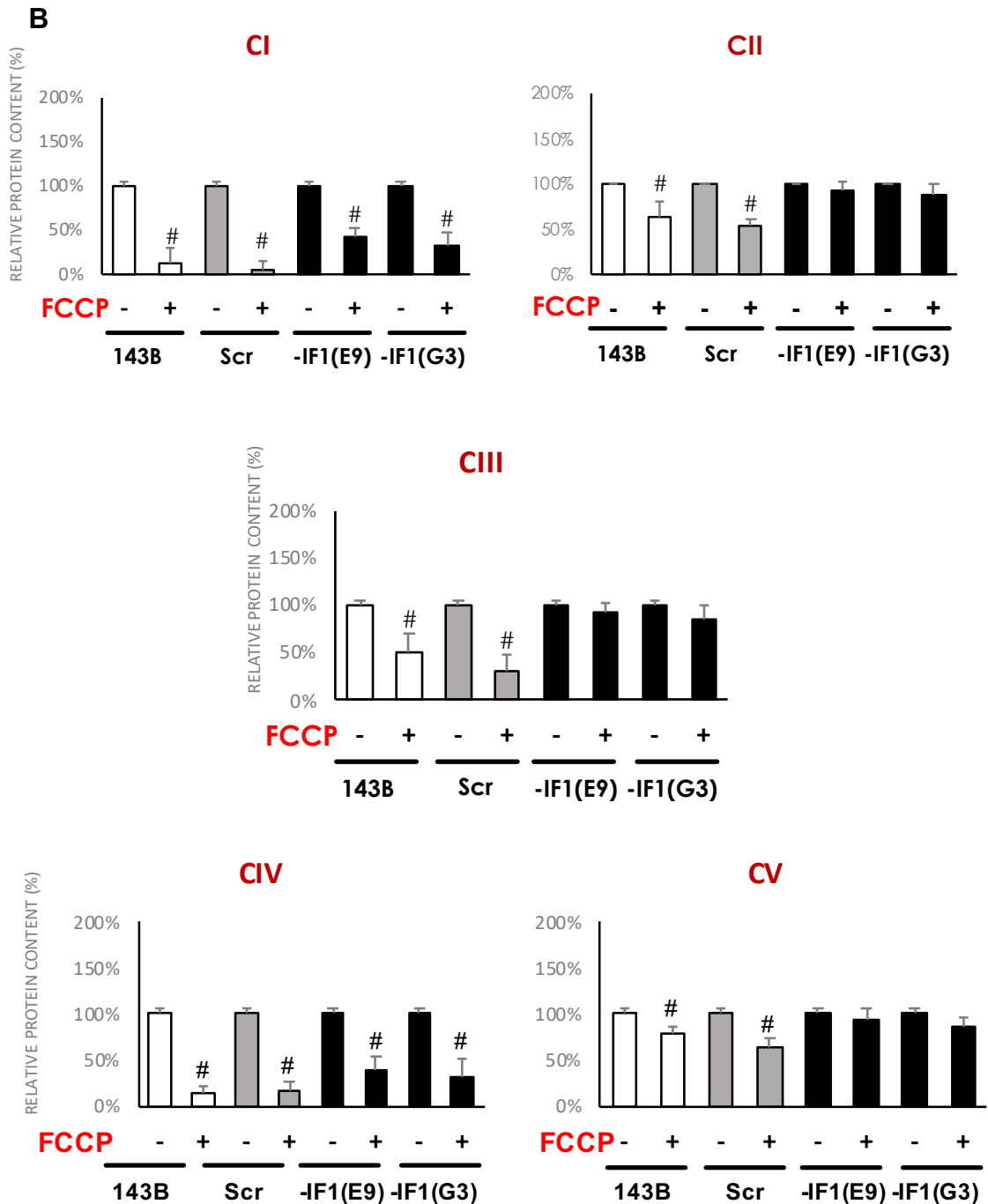


**Figure 36: Assessment of the OXPHOS complexes protein levels in osteosarcoma cells after 24 hours of 10  $\mu$ M FCCP.** (A) Representative immunodetection. (B) Semi-quantitative densitometric analysis. Values were normalized to the actin levels and expressed as percentage change compared to basal condition. # indicates the statistical significance of the data compared to the controls, with  $p < 0.05$ .

Based on this evidence, with the aim to evaluate the impact of the bioenergetic changes on the main mitochondrial function, the cellular content of OXPHOS was assessed by the immunodetection of one subunit for each complex.



As interestingly showed by the Figure 36, after 24 hours of exposure to FCCP, IF<sub>1</sub>-expressing cells displayed a cutback of the expression of all OXPHOS complexes, with decreases of about 90%, 50%, 60%, 85%, 30% for the complexes CI, CII, CIII, CIV, CV, respectively, compared to the basal conditions (Figure 36B). On the contrary, IF<sub>1</sub>-silenced cells surprisingly almost preserved the expression of CII, CIII and CV, whereas a decrease of nearly 65% was estimated for the complexes CI and CIV in uncoupling, with respect to the basal conditions. However, the reduction in the latter complexes in IF<sub>1</sub>-silenced cells was significantly minor compared to ones detected in control cells upon anoxia-mimicking conditions.

Finally, considering that IF<sub>1</sub> in normal cells acts by interacting with the CV, and based on the evidence that with FCCP the levels of the ATP-synthase were decreased of about 30% in IF<sub>1</sub>-expressing cells, the endogenous inhibitor expression was subsequently evaluated in these conditions. As shown in Figure 37, under anoxia-mimicking conditions also the IF<sub>1</sub> expression decreased, but following the same trend of  $\alpha$  and d subunits of F<sub>1</sub>F<sub>0</sub>-ATP synthase, as the qualitative analysis suggested. This observation, suggested that in anoxia-mimicking conditions IF<sub>1</sub> expression is modulated in order to ensure protein levels proportional to its target, the F<sub>1</sub>F<sub>0</sub>-ATP synthase.

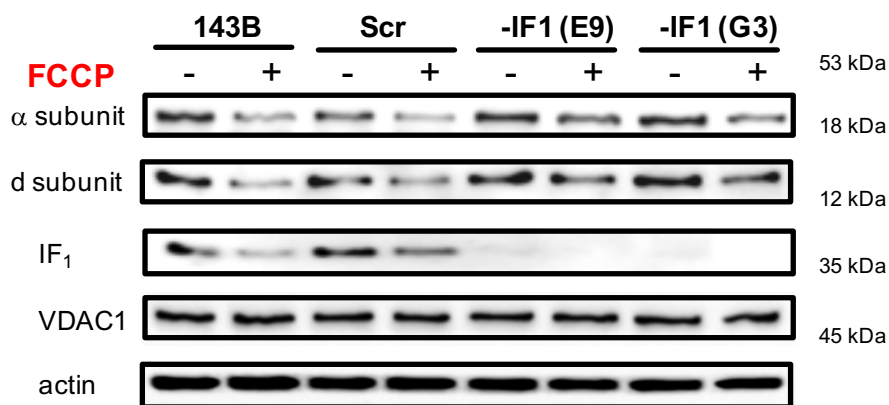


**Figure 37: Qualitative evaluation of the IF<sub>1</sub> expression in relation to the  $\alpha$  and d subunits of F<sub>1</sub>F<sub>0</sub>-ATP synthase, in osteosarcoma cells after 24 hours 10  $\mu$ M FCCP.**

However, the semi-quantitative nature of the immunodetection method did not allow us to be sure about the ratio between IF<sub>1</sub> and ATP-synthase protein levels, suggesting that a different method should be applied to obtain robust data. Therefore, further investigations will be necessary to clarify this aspect.

Overall, the evidence collected proved that IF<sub>1</sub> expression in cancer cells deeply alter their response to anoxia-mimicking conditions, conferring a proliferative advantage by preserving the ATP levels and the cellular energy charge. Moreover, the high rate of mitochondrial turnover highlighted in IF<sub>1</sub>-expressing cells may be a mechanism of cancer cells to overcome the mitochondria-mediated apoptosis upon a prolonged exposure to anoxia, as suggested by some our preliminary data. Therefore, further investigations are ongoing to clarify the effects of IF<sub>1</sub> expression in cancer cells upon prolonged anoxia-mimicking conditions. Moreover, other experiments will be performed to assess the impact of IF<sub>1</sub> expression in cancer cells in conditions of real anoxia.

## **4.2 Role of the miRNAs in the resistance to BRAF-inhibitors in metastatic melanoma**

Cutaneous melanoma is listed as one of the most aggressive and deadly forms of tumours. Whereas early-stage lesions are almost curable, the treatment failure in the late stages of melanoma is the reason for the high rate of mortality. Although the availability of the new therapies from 2012 revolutionized the malignant melanoma treatment improving the survival rate statistics, the failure of the therapies in long-term is still registered in the majority of the cases, with also the occurrence of tumour relapse with dissemination and more aggressive features. Among the mechanism described to drive the onset of the therapy resistance in melanoma, the dysregulation of intracellular pathways usually related to cancer progression plays a central role. Several investigations proved that these signalling alterations occur due to the accumulation of new genetic mutations during the melanoma development, but more interestingly, are also driven by epigenetic modifications. In particular, miRNAs have been described as the master regulators of the gene expression in cancer, and the variation of their pattern levels during the melanoma stage progression has been proved to drive the flexibility and metabolic adaptability typical of these cancers. Based on the increasing experimental evidences collected, miRNAs are nowadays considered suitable candidates for the developing of new targeted therapies for the malignant melanoma, and their estimation as a prognostic biomarker has been proposed.

In this context, this study aimed to clarify the role of miRNAs in the development of resistance to BRAF-inhibitors (BRAFi), a group of drugs for metastatic melanoma targeted therapy marked by the constitutive activation of the MAPK signalling. Among the BRAFi, the vemurafenib (PLX4032) is commonly used for the treatment of the BRAFV600E-mutant metastatic melanoma. The cellular models employed for this purpose were melanoma cells obtained from two patients with BRAFV600E-mutant metastatic melanoma (M21 and Colo38) and the derived vemurafenib resistant clones (M21 and M21R), isolated and kindly provided by Dr Ferrone's research group.

### 4.2.1 Characterization of M21 and M21R melanoma cells

In order to confirm the validity of the cellular models used, we assessed the sensitivity toward vemurafenib (PLX4032) in M21 and M21R cells through MTT assay and the calculation of the half maximal inhibitory concentration (IC<sub>50</sub>). The IC<sub>50</sub> represents the drug concentration necessary to induce a response reduction of 50% *in vitro*. For this purpose, the cells were cultured up to 72 hours in presence of increasing concentrations of vemurafenib, in the range of 31.2 nM to 512  $\mu$ M. Every 24 hours, the cellular metabolic activity of each sample was evaluated by MTT assay, and the data obtained were normalized to the values detected for the cells cultured in the normal medium. Dose-response curves were designed, and the IC<sub>50</sub>s calculated with GraphPad Prism 7 Software, as previously described. As shown in Figure 38, no significant differences were detected between M21 and M21R IC<sub>50</sub> values after 24 hours of exposure to vemurafenib. The comparison of vemurafenib tolerance after 48 hours of treatment was not possible due to the ambiguous dose-response curves obtained for M21 cells, that did not allow the calculation of the IC<sub>50</sub>. Conversely, after 72 hours of PLX4032 exposure, M21R showed an IC<sub>50</sub> of 48.11  $\mu$ M, whereas the value calculated for M21 was only 0.65  $\mu$ M. Therefore, these data confirmed the different sensitivity of M21 and M21R cells to vemurafenib, since the PLX4032 concentration necessary to have the same inhibitory effect in M21R was nearly 75 times higher than the one effective in M21 cells.

Afterwards, the evaluation of the cellular growth of M21 and M21R in presence of 2  $\mu$ M vemurafenib was performed up to 72 hours. 2  $\mu$ M PLX4032 was indicated as the proper concentration to use to growth M21R maintaining a proliferation rate comparable to one of the M21 sensitive cells in normal conditions of culture. Indeed, the growth curves of the M21R cells cultured in presence of 2  $\mu$ M vemurafenib and the M21 in the normal medium were comparable, as shown in Figure 39. Conversely, the growth of M21 cells cultured in medium supplemented with 2  $\mu$ M PLX4032 was almost arrested at 48 hours, with evidence of cell mortality at 72 hours, confirming the sensitivity of the cells to the vemurafenib.

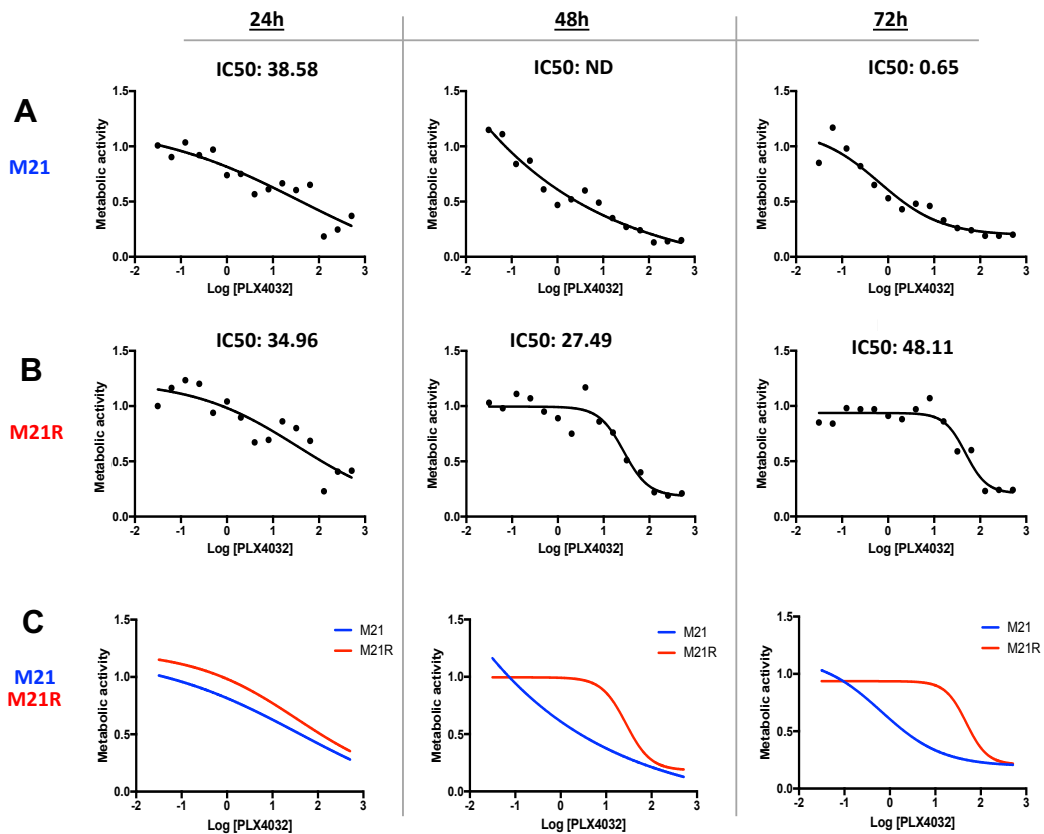


**Figure 38: Evaluation of M21 and M21R sensitivity toward vemurafenib (PLX4032).** Cells were cultured with increasing concentrations of vemurafenib in the range 31.2 nM to 512  $\mu$ M for 24h, 48h and 72h. Cellular metabolic activity was assessed by MTT and the IC50 calculated. Metabolic activity index is in the y-axis, Log of the PLX4032 concentration in the x-axis. IC50 are reported on the top of each graph. (A) Dose-response curves of M21 sensitive cells. (B) Dose-response curves of M21R resistant cells. (C) Merge of M21 and M21R dose-response curve for each time point.

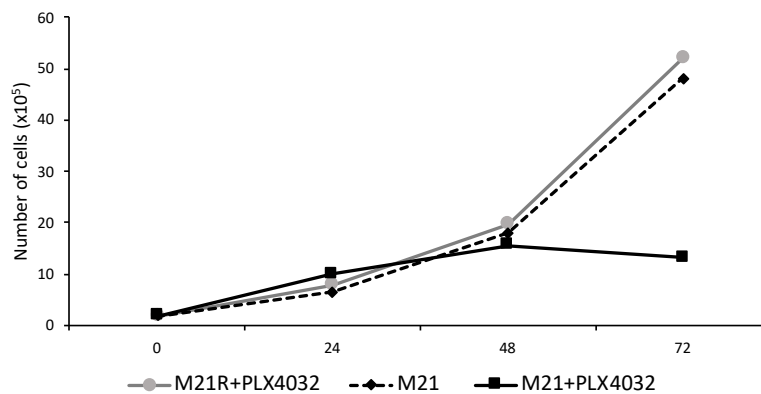


**Figure 39: Growth of M21 and M21R cell in presence of 2  $\mu$ M vemurafenib (PLX4032) up to 72 hours.** M21R cultured with 2  $\mu$ M PLX4032 is the grey line with circles, M21 in normal medium is the black dotted line with rhombus and M21 growth in presence of 2  $\mu$ M PLX4032 is showed in black line and squares.



## **4.2.2 Assessment of the signalling pathways related to cancer progression**

A first set of experiments was performed in order to identify in the resistant cells and the intracellular pathway mainly affected by the action of miRNAs driving the BRAF-I resistance. For this purpose, the activation of Wnt/ $\beta$ -catenin, Sonic-Hedgehog, TGF- $\beta$  and p53 pathways was evaluated in M21 melanoma cells and M21R cells resistant to vemurafenib.

### **4.2.2.1 Wnt/ $\beta$ -catenin signalling pathway**

In physiologic conditions, the Wnt/ $\beta$ -catenin canonical pathway regulates the cell proliferation, migration and cell fate specification necessary during the embryonic development for proper tissues formation and body axis determination [239]. Aberrations in the Wnt signalling have been found in several human cancer types. As previously described, the signalling cascade starts with the binding of the Wnt protein to a Frizzled receptor, whose intracellular signalling leads to the inhibition of the destruction complex that in basal conditions constitutively degrades  $\beta$ -catenin. Therefore,  $\beta$ -catenin accumulates and translocates to the nucleus where it acts as co-activator of TCF/LEF transcription factors, thus enhancing the expression of genes promoting the cell proliferation. With the aim to assess Wnt/ $\beta$ -catenin canonical pathway signalling, the cellular levels and the activation of GSK-3 $\beta$  were evaluated. The GSK-3 $\beta$  serine/threonine kinase is a member of the destruction complex and in normal conditions constitutively phosphorylates the  $\beta$ -catenin, determining its proteasome-mediated degradation and therefore inhibiting the signalling cascade. For this purpose, the GSK-3 $\beta$  transcript levels were quantified through RT-qPCR. In brief, cells were seeded in their proper medium (complete RPMI, supplemented with 2  $\mu$ M PLX4032 for M21R) and after 48 hours were detached, collected and the RNA extracted.

The GSK-3 $\beta$  mRNA retro-transcription and real-time PCR reactions were performed as previously described. The relative gene expression was calculated by the  $2^{-\Delta\Delta C_t}$  method using GADPH as housekeeping gene for normalization. The GSK-3 $\beta$  mRNA levels in M21R cells were reported as a fold change (fc) with respect to M21 cells. As shown in Figure 40A, the vemurafenib resistant M21R cells displayed a small but significant relative decrease in the GSK-3 $\beta$  transcript levels, shown by a fold change of 0.89, that corresponded to a decrease of 26% in the translated protein, as subsequently evaluated by immunodetection (Figure 40 B and C).

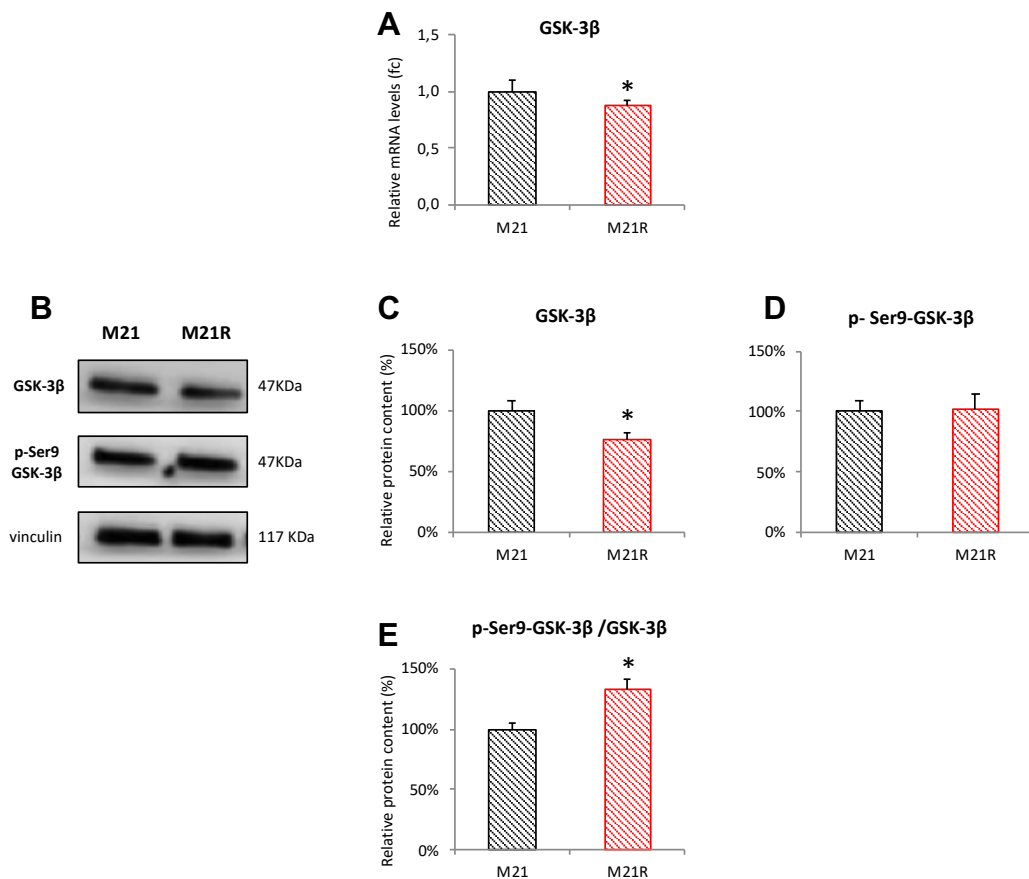


**Figure 40: Assessment of Wnt/ $\beta$ -catenin pathway in M21 and M21R melanoma cells: GSK-3 $\beta$  evaluation.** (A) RT-qPCR assessment of the GSK-3 $\beta$  mRNA levels. (B) Representative immunodetection of the GSK-3 $\beta$  total protein and the inactive form of GSK-3 $\beta$  phosphorylated on Serine 9. Vinculin was used as loading control. (C) Semi-quantitative densitometric analysis of GSK-3 $\beta$  total protein. (D) Semi-quantitative densitometric analysis of p-Ser9-GSK-3 $\beta$ . (E) Calculation of the inactive p-Ser9-GSK-3 $\beta$  percentage on the total GSK-3 $\beta$ . M21R densitometric values were normalized to the vinculin ad expressed as a percentage of to the M21 values. \* indicates the statistical significance of the data compared to controls, with  $p < 0.05$ .

Later, the levels of the inactive GSK-3 $\beta$  were evaluated by immunodetection of the GSK-3 $\beta$  protein phosphorylated on the Serine 9. This post-translation modification was reported to inhibit GSK-3 $\beta$ , enabling  $\beta$ -catenin accumulation and activity. As the panel B and D show, no differences were detected in the quantity of inactive p-Ser9-GSK-3 $\beta$  between sensitive and resistant cells. Accordingly, the percentage of the inactive GSK-3 $\beta$  on the total GSK-3 $\beta$  shown an increase of about 30% in the M21R cells compared to the M21 (Figure 40E). Overall, the data collected suggested that in the vemurafenib resistant cell line the  $\beta$ -catenin disruption complex is less active due to the minor activity of the GSK-3 $\beta$  kinase, compared to the sensitive cells, implying a probable increase in the downstream signalling. In order to prove this assumption, the transcripts and protein levels of the  $\beta$ -catenin were assessed in M21R and M21 cells. In agreement with previous observations, an increase nearly 90% of the  $\beta$ -catenin mRNA levels, together with an huge increment of the protein levels, were measured in M21R cells respect to M21 cells, as shown in Figure 41 A, B, C.  $\beta$ -catenin protein content was almost quadruplicated in the melanoma cells resistant to vemurafenib respect to the control cells. The effect of the  $\beta$ -catenin accumulation on the transcription activation was then evaluated in melanoma cells by the dual-luciferase assay, with the specific reporter containing TCF/LEF binding site repeats fused to the firefly luciferase gene (M50 Super 8x TOPFlash plasmid). In brief, the cells were seeded and after 18 hours co-transfected with the pRTLK control vector, for the constitutive expression of the *Renilla* luciferase and with the TOPFlash plasmid reporter. 24 hours after the transfection, the cells were lysed and the luminescence signal of both luciferases was measured by the luminometer, as previously described. The firefly luciferase luminescence values were normalized to the *Renilla* luciferase signals, and the data of M21R cells were expressed as a percentage of M21 cells value. As shown in Figure 41D, the Wnt/ $\beta$ -catenin signalling was considerably enhanced in the resistant cells, that displayed a transcriptional activation nearly 2.5 times the one measured in the vemurafenib-sensitive cells. The low and almost absent firefly luciferase luminescence in the negative controls proved that the firefly expression occurs only upon specific stimulation of the TCF/LEF binding sites.

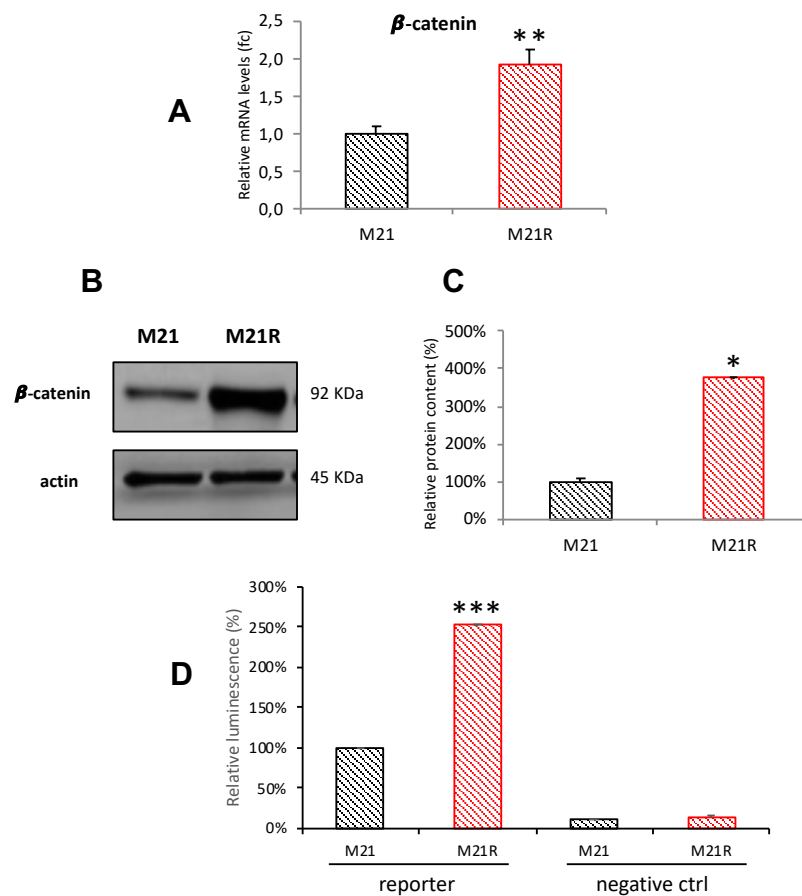


**Figure 41: Assessment of Wnt/β-catenin pathway in M21 and M21R melanoma cells: β-catenin evaluation.** (A) RT-qPCR assessment of the β-catenin mRNA levels. (B) Representative image of the β-catenin protein immunodetection. Actin was used as loading control. (C) Semi-quantitative densitometric analysis of β-catenin protein. M21R densitometric values were normalized to the actin ad expressed as a percentage of the M21 values. (D) Evaluation of the Wnt pathway activation by dual luciferase assay. \* indicate the statistical significance of the data compared to the controls, with \* $p < 0.05$ , \*\* $p < 0.01$  \*\*\* $p < 0.001$ .

Overall, these data proved that in melanoma cells M21R resistant to PLX4032 the β-catenin levels and the signalling of the Wnt canonical pathway are greatly increased compared to the sensitive M21 cells. Interestingly, accumulation of β-catenin has been reported in patients samples during melanoma progression [240]. Moreover, the hyperactivation of the Wnt signalling has been related to acquired resistance to immunotherapy in mice, and to BRAF-inhibitors in other melanoma cellular models [210], [241]. Therefore, the collected data candidate Wnt/β-catenin pathway as a possible target of the miRNAs driving the vemurafenib resistance.

#### 4.2.2.2 TGF- $\beta$ signalling pathway

The activation of the TGF- $\beta$  signalling pathway was evaluated in melanoma cells. In normal conditions, the TGF- $\beta$  signalling covers a wide range of functions by regulating cell cycle progression and cell proliferation, tissues formation and regeneration, but also the programmed cell death and the immune response. Even in cancer cells, the TGF- $\beta$  signalling hyperactivation has dual roles, by acting as a tumour suppressor in early-stages cancers and oppositely by promoting cell survival and oncogenic transformation in advance stages of tumours. The signalling cascade is initiated by the oligomerization of the TGF- $\beta$ R receptors of the type of I and II, activated by the binding of the ligand TGF- $\beta$  as a dimer. Active oligomerized receptors phosphorylate and activate the signalling molecules Smad2 and Smad3 to form the Smad complex with the Smad4 protein and to translocate into the nucleus. By the interaction with DNA-binding transcription factors, co-repressors and co-activators, Smad complex binds promoters of TGF- $\beta$  target genes and regulates their transcription. The mRNAs levels of Smad2 and Smad3 proteins were quantified by RT-qPCR in sensitive and resistant melanoma cells, as previously described for the Wnt pathway analysis. As Figure 42A shows, both Smad2 and Smad3 transcripts resulted increased in the M21R cells compared to the M21, with a fold change of 1.74 and 6.34, respectively. Again, the protein content analysis matched the mRNAs quantification, showing an increment of about 50% of both Smad2 and Smad3 proteins in resistant cells, with respect to the sensitive cells (Figure 42B and C). Once proved the rise of Smads signalling molecules, the TGF- $\beta$  signalling rate was assessed by measuring the downstream transcription activation through dual-luciferase assay with the pSBE4 reporter, in which multiple copies of the Smad complex binding sites were cloned before the coding-sequence of the firefly luciferase. In accord to the previous analysis, TGF- $\beta$ -mediated transcriptional activation in M21R was 2.5 times the one detected in vemurafenib-sensitive M21 cells (Figure 42D). Therefore, the data obtained demonstrated that also the TGF- $\beta$  pathway was up-regulated in the vemurafenib-resistant M21R cells compared to the sensitive melanoma cells M21.

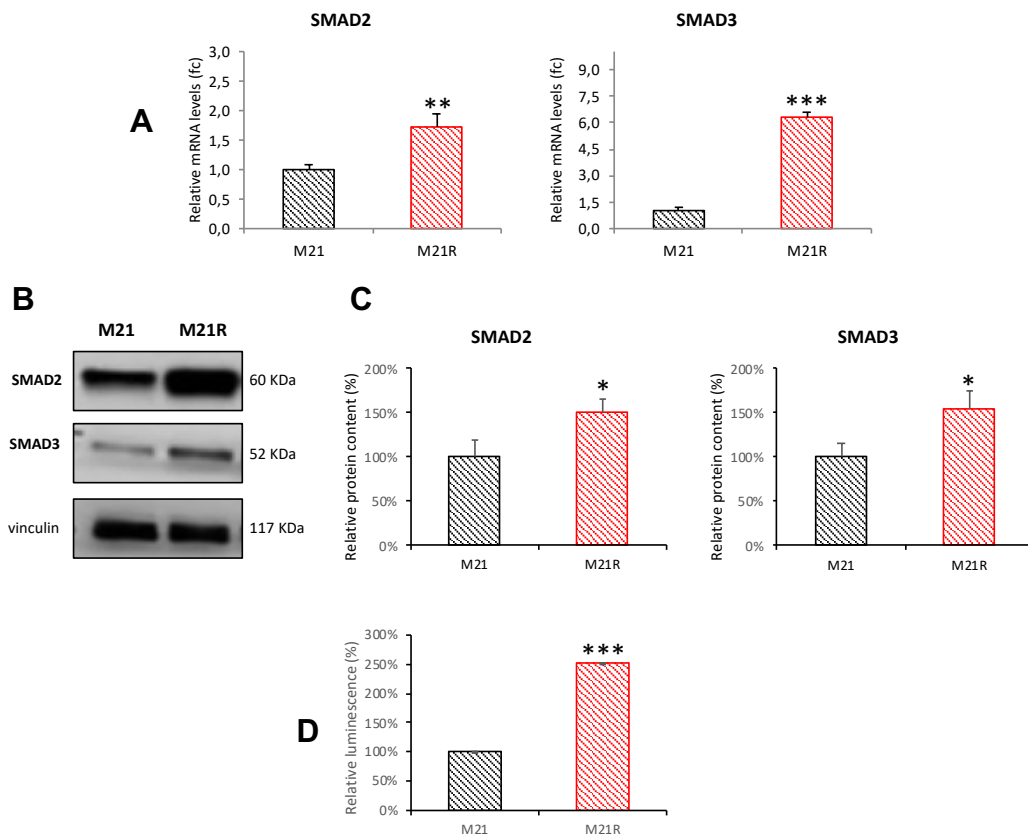


**Figure 42: Evaluation of the TGF- $\beta$  pathway activation in M21 and M21R melanoma cells** (A) RT-qPCR assessment of the SMAD2 and SMAD3 mRNA levels. (B) Representative image of the SMAD2 and SMAD3 proteins immunodetection. Vinculin was used as loading control. (C) Semi-quantitative densitometric analysis of SMAD2 and SMAD3 proteins. M21R densitometric values were normalized to vinculin and expressed as a percentage of the M21 values. (D) Evaluation of the TGF- $\beta$  signalling rate by dual luciferase assay. \* indicate the statistical significance of the data compared to the controls, with \* $p < 0.05$ , \*\* $p < 0.01$  \*\*\* $p < 0.001$ .

Interestingly, the increase of the TGF- $\beta$  pathway signalling has been associated with melanoma progression by inhibiting cancer-specific immune responses, modulating tumour microenvironment and favouring invasion. In particular, it has been demonstrated that transformed melanocytes produce high levels of TGF- $\beta$ , thus stimulating the wild-type pathway in an autocrine/paracrine manner. Therefore, even molecular mediators of the TGF- $\beta$  pathway may be the targets of the miRNAs promoting the acquisition of BRAF-I in metastatic melanoma.

### 4.2.2.3 Sonic-Hedgehog signalling pathway

Afterwards, the activation of the Sonic-Hedgehog (Shh) pathway was evaluated. As previously mentioned, Sonic-Hedgehog signalling is a master regulator of the cell differentiation during the embryonic development, whereas in the adult acts in the tissue regeneration. In basal conditions, the signalling cascade is constitutively repressed by the receptor PTCH1, that promotes SMO degradation by endocytosis. Conversely, the binding of SHH ligand on PTCH1 blocks its inhibitory activity, thus allowing the accumulation of SMO on the surface. In these conditions, SMO starts the intracellular signalling, inducing the translocation of the GLI2 and GLI3 proteins in the nucleus. Here, GLI2 and GLI3 control the transcription of the Shh target genes, among which the GLI1, a transcriptional activator that induces a potentiation of the HH signalling. Interestingly, Ferrone's research group previously reported that M21R melanoma cells display higher levels of GLI1 protein with respect to the M21 cells, suggesting that Shh signalling is potentiated in resistant cells [222]. The same investigation also showed that GLI1 mediated BRAF-I resistance induced the PDGFR- $\alpha$  up-regulation by the reactivation of the MAPK pathway. In order to prove that the increase of GLI1 protein previously observed in resistant cells was due to the enhancement of the Shh signalling, dual luciferase assay was performed to assess the pathway activation rate in M21 and M21R cells. Coherently with the previous investigations, the M21R cells exhibited an increase of Sonic-Hedgehog signalling of about 90% with respect to the M21 cells (Figure 43). The data collected suggested that molecules upstream to GLI1 in the Shh pathway may be the targets of the miRNAs modulating the vemurafenib resistance in the metastatic melanoma. In accordance with this assumption, it has been recently demonstrated that the knockdown of both GLI1 and GLI2 restored the sensitivity to vemurafenib in resistant cellular models, determining both growth arrest and cell senescence [218].

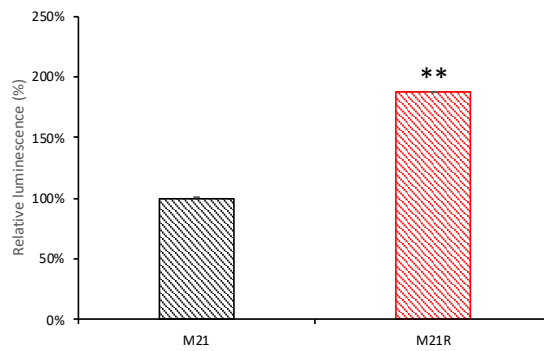


**Figure 43: Assessment of the Sonic-Hedgehog signalling activation in M21 and M21R melanoma cells.** \*\* indicate the statistical significance of the data compared to the controls, with  $p < 0.01$

#### 4.2.2.4 p53 signalling pathway

The activation of the p53 pathway was lastly evaluated in metastatic melanoma cells sensitive and resistant to vemurafenib. As already described, p53 is a nuclear transcription factor that is activated in cells to preserve genomic stability, by regulating the expression of genes involved in the DNA repair process, in the inhibition of the cell cycle progression and finally in the cell death apoptosis, activated if the cellular damages result irreparable. Loss of function and reduced levels of p53 are associated with cancer development and progression. In basal conditions, p53 are maintained low by the MDM2 and MDM4 proteins, that sequester p53 impeding its activity of transcriptional factor and promoting its proteasome-mediated degradation. The increasing of p53 expression and its activation occurs in response to a wide range of stress stimuli by the signalling of the membrane receptors. Interestingly, the RT-qPCR evaluation of p53 mRNA levels, showed a decrease of the transcript, with a fold change of 0.7 in the resistant cells compared to the sensitive, that resulted in the reduction of about 70% of the protein, as assessed by p53 immunodetection (Figure 44 A, B, C). Finally, the reduced levels of p53 correlated to the minor activation of the tumour-suppressor pathway in the M21R cells, with respect to M21 cells, as assessed by dual luciferases assay (Figure 44D).



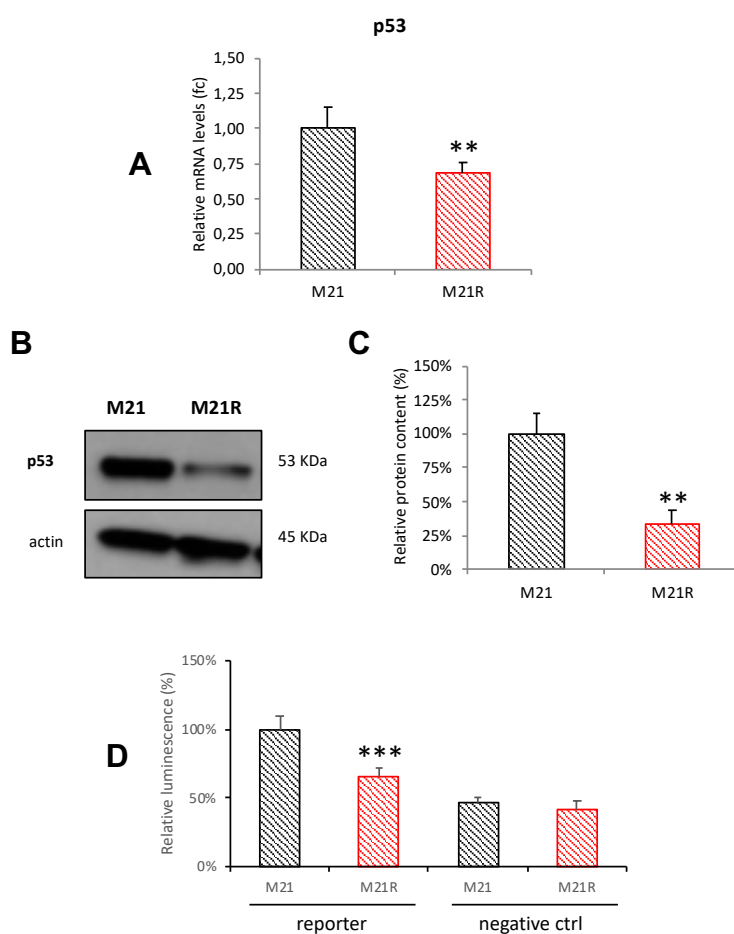


**Figure 44: Assessment of p53 pathway activation in M21 and M21R melanoma cells**  
 (A) RT-qPCR assessment of the p53 mRNA levels. (B) Representative image of the p53 protein immunodetection. Actin was used as loading control. (C) Semi-quantitative densitometric analysis of p53 protein. M21R densitometric values were normalized to actin and expressed as a percentage of the M21 values. (D) Evaluation of the p53 signalling rate by dual luciferase assay. \* indicate the statistical significance of the data compared to the controls, with \*\* $p < 0.01$  \*\*\* $p < 0.001$ .

Overall, the data obtained by the analysis of the cancer-related pathways demonstrated that vemurafenib resistance in M21R melanoma cells was driven by the concomitant activation of several oncogenic pathways (Wnt, TGF- $\beta$ , Shh pathways) together with the inhibition of the p53 tumour-suppressor signalling, highlighting the complexity of the drug-resistance phenomena.

### **4.2.3 Identification of the miRNAs differentially expressed in melanoma cells resistant to vemurafenib**

In order to identify the miRNAs involved in the development of resistance to vemurafenib in metastatic melanoma, miRNAs profiling of sensitive (M21 and Colo38) and resistant cells (M21R and Colo38R) was performed and compared. With this aim, the expression of 800 miRNAs was evaluated by Nanostring array analysis (Nanostring Technologies), and the levels detected in the resistant cells were expressed as a fold change with respect to the values found in the vemurafenib-sensitive cells. As the left panel of Figure 45A shows, a group of 13 miRNAs was identified as up-regulated in both vemurafenib-resistant cell lines, with respect to the sensitive melanoma cells, distinguished by a fold change major of 2. Conversely, 15 miRNAs resulted to be down-regulated (fold change minor of 2) in the M21R and Colo38R cells in comparison to M21 and Colo38, respectively. Subsequently, evaluating the fold change value calculated in M21R cells, the 10 miRNAs most up-regulated and the 10 miRNAs most down-regulated were assessed by RT-qPCR in both M21R and Colo38R cells in order to confirm the data obtained by Nanostring analysis. Notably, only 7 miRNAs within the group of the up-regulated were confirmed by RT-qPCR in both PLX4032-resistant cell lines compared to their sensitive cells (Figure 45B left panel). On the contrary, none of the miRNAs down-regulated was validated in both cells models by RT-qPCR. Reasonably, the poor success of the RT-qPCR for the miRNAs relative levels validation depended on the lower sensitivity of this method compared to the Nanostring array.

**A**

↑	Up-regulated miRNAs	f.c.		↓	Down-regulated miRNAs	f.c.	
		M21R vs M21	Colo38R vs Colo38			M21R vs M21	Colo38R vs Colo38
1	hsa-miR-204-5p	52.86	2.22	1	hsa-miR-499a-5p	-9.69	-3.60
2	hsa-miR-1285-5p	22.64	3.12	2	hsa-miR-203a-5p	-7.21	-9.79
3	hsa-miR-194-5p	13.23	4.23	3	hsa-miR-873-3p	-4.45	-2.54
4	hsa-miR-425-5p	9.22	3.72	4	hsa-miR-1827	-3.83	-3.04
5	hsa-miR-151a-5p	8.49	2.63	5	hsa-miR-543	-3.50	-2.12
6	hsa-miR-4455	6.20	2.19	6	hsa-miR-1973	-3.07	-3.13
7	hsa-miR-149-5p	5.50	2.68	7	hsa-miR-15b-5p	-2.68	-2.27
8	hsa-miR-4516	5.11	2.23	8	hsa-miR-34a-5p	-2.61	-2.86
9	hsa-miR-30a-5p	5.53	2.30	9	hsa-miR-148a-3p	-2.68	-3.39
10	hsa-miR-193b-3p	4.97	2.34	10	hsa-miR-7-5p	-2.46	-44.10
11	hsa-miR-182-5p	4.54	2.11	11	hsa-miR-548m	-2.42	-2.35
12	hsa-miR-625-5p	2.78	6.40	12	hsa-miR-29b-3p	-2.37	-3.20
13	hsa-miR-301a-5p	2.62	2.34	13	hsa-miR-585-3p	-2.33	-2.46
				14	hsa-miR-15a-5p	-2.17	-1.81
				15	hsa-miR-574-5p	-2.19	-2.42

**B**

↑	Up-regulated miRNAs	validation		↓	Down-regulated miRNAs	validation	
		M21R vs M21	Colo38R vs Colo38			M21R vs M21	Colo38R vs Colo38
1	hsa-miR-204-5p	✗	✓	1	hsa-miR-499a-5p	✗	✗
2	hsa-miR-1285-5p	✓	✗	2	hsa-miR-203a-5p	✗	✗
3	<b>hsa-miR-194-5p</b>	✓	✓	3	hsa-miR-873-3p	✓	✗
4	<b>hsa-miR-425-5p</b>	✓	✓	4	hsa-miR-1827	✗	✗
5	<b>hsa-miR-151a-5p</b>	✓	✓	5	hsa-miR-543	✗	✗
6	<b>hsa-miR-4455</b>	✓	✓	6	hsa-miR-1973	✗	✗
7	<b>hsa-miR-149-5p</b>	✓	✓	7	hsa-miR-15b-5p	✗	✗
8	<b>hsa-miR-4516</b>	✓	✓	8	hsa-miR-34a-5p	✗	✓
9	<b>hsa-miR-30a-5p</b>	✓	✓	9	hsa-miR-148a-3p	✓	✗
10	hsa-miR-193b-3p	✓	✗	10	hsa-miR-7-5p	✗	✓

**Figure 45: Identification of miRNAs differentially expressed in PLX4032-resistant and PLX4032-sensitive cells.** (A) Nanostring array analysis results. Lists of the miRNAs found up-regulated (f.c.>2, left panel) and down-regulated (f.c.<2, right panel) in both M21R and Colo38R resistant cells lines compared to M21 and Colo38, respectively. (B) RT-qPCR validation of the miRNAs previously identified by Nanostring analysis. ✓ indicates the validation, ✗ indicates that miRNAs differential expression found with Nanostring was not confirmed by RT-qPCR. A group of 7 miRNAs within the up-regulated was validated in both melanoma models, M21R vs M21 and Colo38 vs Colo38R (in bold).

#### 4.2.4 Assessment of the effect of mir-425-5p levels on the tolerance to vemurafenib in M21 and M21R cells

Afterwards, the list of the probable targets of action for each one of the 7 miRNAs confirmed by RT-qPCR was obtained by the consultation of the miRWalk bioinformatic database. Intriguingly, 3 of these miRNAs were predicted to target the FBXW11 gene, encoding the  $\beta$ TrCP2 protein, an E3 ubiquitin ligase that mediates the ubiquitination and subsequent proteasomal degradation of target proteins, among which GLI2,  $\beta$ -catenin and the MDM2 negative regulator of p53 [242], [243].

These data suggested that the hypothetical reduction of  $\beta$ TrCP2 levels and of its activity, induced by the increase of the miRNAs, could be the explanation for the hyperactivation of Shh, Wnt pathways and p53 signalling inhibition previously observed in M21R cells with respect to M21 cells, as the result of the Gli2,  $\beta$ -catenin and MDM2 accumulation, respectively.

Interestingly, a preliminary assessment of the  $\beta$ TrCP2 levels by immunodetection of the protein, showed a decrease of about 70% in M21R and Colo38R resistant cells with respect to the M21 and Colo38R (Figure 46A).

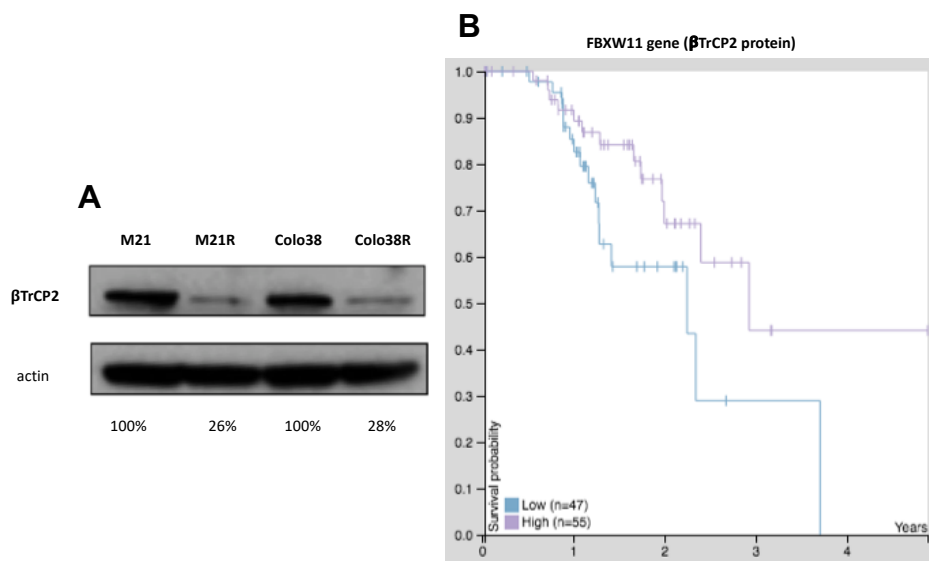


**Figure 46: Assessment of the miRNAs predicted target  $\beta$ TrCP2.** (A) Evaluation of the  $\beta$ TrCP2 levels in M21, M21R, Colo38, Colo38R cell lines by protein immunodetection. Densitometric values of  $\beta$ TrCP2 were normalized to actin, and values detected in resistant cells were expressed as a percentage with respect to the values of the control cells. (B) Kaplan-Meier plot correlating  $\beta$ TrCP2 mRNA levels and melanoma patient survival. Purple line indicates the group of patients with high expression of  $\beta$ TrCP2, whereas the light blue line represents the group of patients with low expression of the protein. Log-rank P value 0.06 (from Human protein atlas)

Moreover, as reported in prognostic databases, survival rate analysis on patients with melanoma showed a partial correlation between the reduced levels of  $\beta$ TrCP2 mRNA and the lower probability of 3-years survival, compared to patients with a higher expression of it, though log-rank P value 0.06 was not significant (Figure 46B).

Consequently, these findings encouraged the study of a first miRNA predicted to target  $\beta$ TrCP2 protein.

Among the three miRNAs sharing  $\beta$ TrCP2 as a possible target, mir-425-5p exhibited the highest variation in M21R cells with respect to the M21 in the Nanostring analysis, with a fold change of 9.22 (Figure 45A). Afterward, the up-regulation of mir-425-5p in resistant cells was confirmed by RT-qPCR, showing a fold change of 1.63 with respect to the sensitive cells (Figure 47A). Notably, as reported in PROGmirV2 database, high levels of mir-425-5p expression have been correlated to a reduced overall survival in patients with metastatic melanoma, compared to patients showing low levels of the miRNAs. Based on these encouraging data, preliminary investigations were performed with the aim to study the role of mir-425-5p in the onset of vemurafenib resistance in metastatic melanoma.

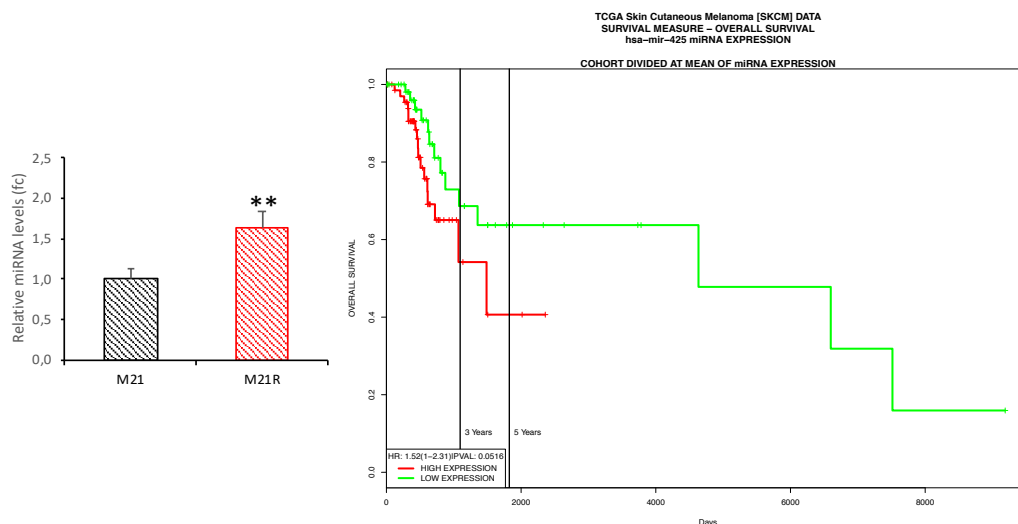


**Figure 47: Assessment of the mir-425-5p.** (A) mir-425-5p levels assessment by RT-qPCR (B) Kaplan-Meier plot correlating the mir-425-5p levels to melanoma patient's survival. The green line indicates the group of patients with low expression of the mir-425-5p, whereas the red line represents the group of patients with high expression of the miRNA. p value: 0.0518 (from PROGmirV2). \*\* indicate the statistical significance of the data compared to the controls, with  $p < 0.01$ .

#### 4.2.4.1 Effect of mir-425-5p overexpression in vemurafenib-sensitive cells

##### 4.2.4.1.1 Cell growth assessment

To assess whether the increase of the mir-425-5p levels could confer resistance to vemurafenib in melanoma, M21 sensitive cells were transiently transfected either with a short RNA mimicking the mir-425-5p or with the scrambled negative control, and the cell growth was evaluated up to 96 hours, in presence of 2  $\mu$ M PLX4032. In brief, cells were seeded and after 18 hours were transfected. Every 24 hours from the transfection, the samples were detached, collected and viable cells were counted using the trypan blue dye exclusion test. Moreover, a portion of each cellular resuspension was collected and processed to extract the total RNA. The levels of mir-425-5p were then monitored at each time point by RT-qPCR, in order to prove the efficiency of the miRNA overexpression method.

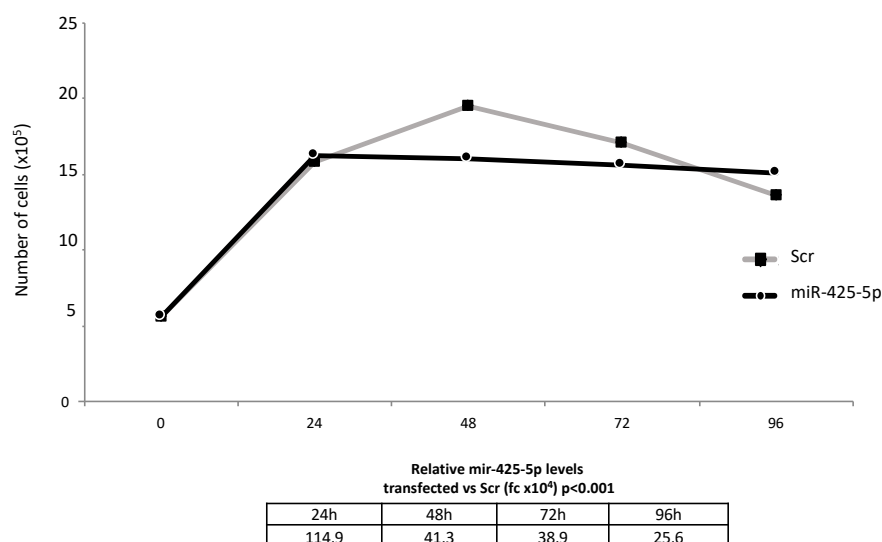


**Figure 48: Cell growth assessment of M21 cells transfected with scrambled negative control or mir-425-5p mimic and cultured up to 96 hours in presence of 2  $\mu$ M PLX4032.**

miRNA over-expression was confirmed by RT-qPCR. The table in the bottom of the panel showed the fold change of mir-425-5p obtained in M21 cells transfected with the miRNA mimic, with respect to the scrambled sample.

The table at the bottom of Figure 31 shows the fold change values of mir-425-5p expression in cells transfected with the miRNA mimic with respect to the scrambled, at each time point.

As shown in Figure 48, in 2  $\mu$ M PLX4032, M21 cells transfected with the scrambled RNA displayed a growth comparable to the one of M21 non-transfected cells (Figure 39). In both cellular types the proliferation almost stopped at 48 hours and subsequently, they started to die. Conversely, the growth of the sensitive cells overexpressing mir-425-5p was hugely slowed down starting from 24 hours, showing a high capacity to tolerate vemurafenib. Indeed, the total number of viable cells was essentially maintained from 24 up to 96 hours of growth in medium supplemented with 2  $\mu$ M PLX4032. Distinctly, these data suggested that melanoma cells overexpressing the mir-425-5p contrast BRAF-inhibitors treatment.

#### **4.2.4.1.2 Cell cycle evaluation**

Based on the differences exhibited in proliferation by M21 sensitive cells overexpressing mir-425-5p with respect to the scrambled control cells, the distribution of the cellular populations in the cell cycle phases was subsequently assessed in the same conditions. The M21 cells sensitive to vemurafenib were seeded, transfected and cultured with medium supplement with 2  $\mu$ M PLX4032 up to 90 hours as previously described. At each time point, cells were detached, collected, fixed in ethanol and stained with the DAPI fluorescent dye. The labelled cells were then acquired by flow cytometry and data analysed by FlowJo software. The levels of mir-425-5p were checked every 24 hours, as previously described (data not shown). As Figure 49 shows, at each time point, the sensitive cells overexpressing the mir-425-5p exhibited a small but reproducible increase in the percentage of cells in the S and G2/M phases, respect to the control cells transfected with the scrambled. In particular, the increment detected in the mir-425-5p overexpressing cells were 2.5%, 6.1%, 3.2%, 4.4% at 24, 48, 72, 96 hours respectively, compared to scrambled cells.

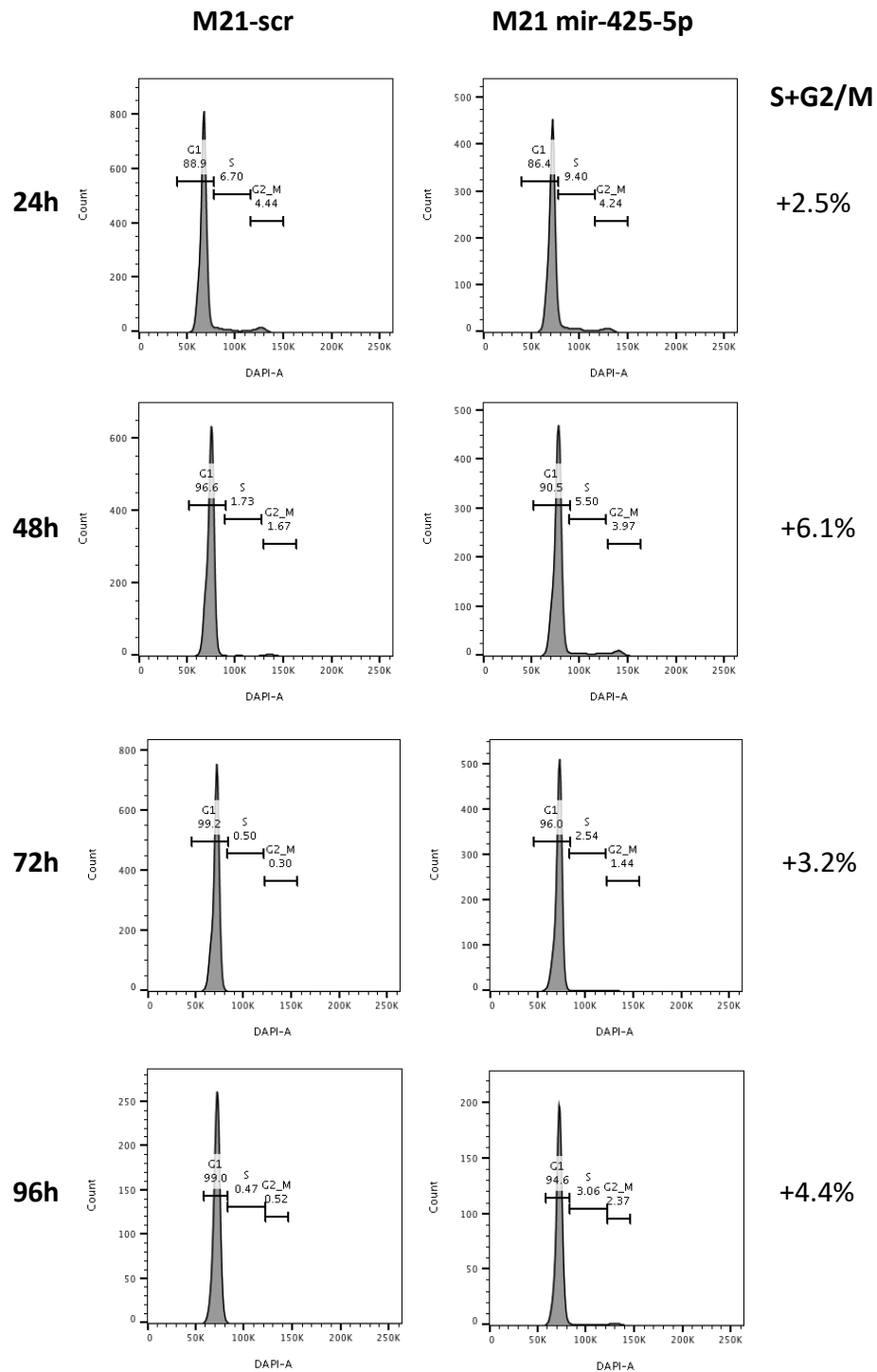


**Figure 49: Cell cycle assessment in M21 cells transfected with scrambled negative control or mir-425-5p mimic, cultured up to 96 hours in presence of 2  $\mu$ M PLX4032.**

In the cytograms, number of cells is in the y-axis, DAPI fluorescence in the x-axis. The total population is separated in three peaks corresponding to G0/G1, S and G2/M phases, highlighted by the horizontal black lines. The percentage of cells in each phase is reported above the corresponding peak. On the right side of the panel, for each time point is reported the percentage increase of cells in S and G2/M phases in M21 overexpressing the mir-425-5p with respect to M21-scrambled.



Therefore, these observations validated the previous hypothesis, suggesting two possible mechanisms of resistance to vemurafenib treatment. In the first scenario, it is possible that the overexpression of the mir-425-5p induces the accumulation of the cells in the S/G2M and their escape to cell death. Alternatively, cells with increased levels of the miRNAs may continue to proliferate at a low rate, renewing and preserving the cellular population upon BRAF-I treatment.

#### 4.2.4.1.3 Metabolic activity assay and IC50 calculation

To further prove the protective effect of the mir-425-5p expression toward vemurafenib, the metabolic activities of M21 cells overexpressing the miRNAs were assessed by MTT assay after 24 hours of exposure to increasing concentrations of vemurafenib. In brief, cells were seeded and after 18 hours were transfected either with mir-425-5p mimic or scrambled RNA, directly in the in medium supplemented with a concentration of PLX4032 in the range from 31.2 nM to 512  $\mu$ M. After 24 hours of incubation, MTT assay was performed as previously described. Absorbance values measured in treated samples were normalized to the signal of the cells cultured in the normal medium.

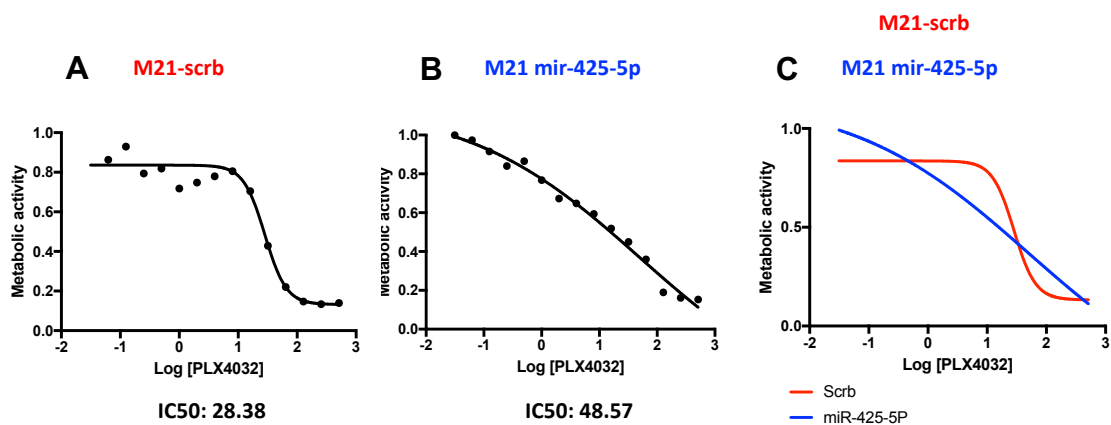


**Figure 50: Metabolic activity assessment and IC50 calculation in M21 sensitive cells transfected either with mir-425-5p mimic or scrambled control and cultured for 24 hours with increasing concentration of PLX4032 (31.2 nM to 512  $\mu$ M).** Metabolic activity index is in the y-axis, Log of the PLX4032 concentration in the x-axis. IC50 are reported under the graphs (A) Dose-response curve of M21 transfected with scrambled RNA. (B) Dose-response curve of cells over-expressing mir-425-5p. (C) Merge of the two dose-response curves. Curve of mir-425-5p-overexpressing cells is in blue, M21 transfected with the control in red.

Notably, at each concentration of PLX4032 tested, M21-scrambled cells exhibited a reduced metabolic activity with respect to the untreated M21-scrambled cells, indicated by a metabolic activity index minor of 0.8 (Figure 50A). Conversely, sensitive cells overexpressing the mir-425-5p exposed at the lower concentrations of PLX4032 preserved a metabolic activity similar to the untreated cells (metabolic activity index ~1) (Figure 50B). More interestingly, melanoma cells overexpressing the miRNAs were less sensitive to higher concentrations of vemurafenib with respect to the control cells, as shown in the merge of the dose-response curve in Figure 50 panel C.

In agreement with previous observations, M21 cells overexpressing mir-425-5p exhibited greater IC<sub>50</sub> values with respect to the M21-scrambled cells, with 48.57  $\mu$ M and 28.38  $\mu$ M IC<sub>50</sub> concentrations, respectively.

Overall, the data collected sustained a positive correlation between increased levels of mir-425-5p and tolerance to vemurafenib.

#### **4.2.4.1.4 Signalling of cancer-related pathways in M21 cells upon mir-425-p overexpression**

To identify the pathway mainly targeted by the mir-425-5p, the activations of Sonic-Hedgehog, p53 and Wnt/ $\beta$ -catenin were assessed by dual luciferase assay in M21 cells upon mir-425-5p overexpression. Notably, as reported above, these cancer-related pathways resulted dysregulated in melanoma cells, that exhibited an increase of both Shh and Wnt oncogenic signalling, together with the lower activation of the p53 tumour-suppressor pathway, with respect to sensitive cells. Moreover, the mir-425-5p was predicted to target  $\beta$ TrCP2 protein, that functions as a negative regulator of GLI2,  $\beta$ -catenin and MDM2, the specific inhibitor of p53. For this purpose, M21 cells were co-transfected with either miRNA mimic or scrambled small RNA and the specific plasmid reporter for the dual luciferase assay. firefly and *Renilla* luminescence signals were acquire after 24 hours from transfection. As the Figure 51 shows, the signalling of all three pathways resulted altered in M21 cells in response to the increase of the mir-425-5p levels.

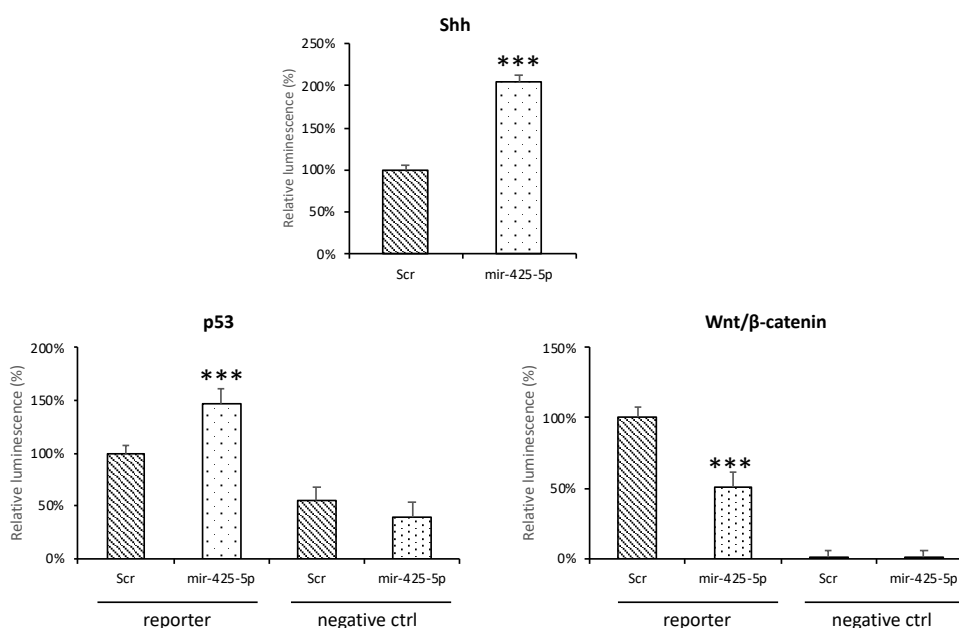


**Figure 51: Evaluation of Sonic-Hedgehog (Shh), p53 and Wnt/β-catenin signalling pathways in M21 sensitive cells overexpressing the mir-425-5p in presence of 2 μM PLX4032.** Luminescence data measured in M21-mir-425-5p cells were expressed as a percentage of the M21-scrb values. \*\*\* indicate the statistical significance of the data compared to the controls, with  $p < 0.001$ .

Shh resulted almost doubled upon miRNA overexpression with respect to the cells transfected with the scrambled control, an event that usually promotes cell proliferation and survival in cells. Conversely, upon mir-425-5p overexpression, p53 signalling increased nearly 50%, whereas Wnt/β-catenin activation was decreased of about 50%, alterations that commonly restrain cell expansion and viability. Overall, these data suggested that mir-425-5p probably mediates the resistance to vemurafenib by enhancing the Sonic-Hedgehog signalling and favouring melanoma progression, overriding the anti-proliferative effect of the p53 and the repression of Wnt signalling. Based on the evidence reported in the literature, it is likely that the counteracting signalling of p53 and Wnt/β-catenin resulted by a negative feedback loop activated in the cells to contrast the abnormal Sonic-Hedgehog transduction.

#### **4.2.4.2 Effect of mir-425-5p inhibition in vemurafenib-resistant melanoma cells**

To stress and underline the important role that mir-425-5p plays in the development of resistance to PLX4032 in melanoma, a set of experiments were performed to evaluate the effects of the mir-425-5p inhibition in M21R cells, in order to highlight possible reversions or reductions of the resistance features. The inhibition of the endogenous levels of mir-425-5p was carried by transient transfection of the specific miRNA inhibitor ( $\alpha$ -mir-425-5p), a small single-stranded RNA that binds and inactivates the complementary target miRNA.

##### **4.2.4.2.1 Cell growth assessment**

For this purpose, the cell growth of M21R transiently inhibited for mir-425-5p expression was assessed up to 72 hours, culturing the cells in medium supplemented with 2  $\mu$ M vemurafenib. In the same manner as previously described, every 24 hours from the transfection the viable cells were counted and the mir-425-5p levels were verified by RT-qPCR. As Figure 52 shows, no alterations in the cell growth were observed in M21R cells transfected with mir-425-5p inhibitor, with respect to the M21R control. Moreover, the RT-qPCR evaluation of the mir-425-5p revealed that the inhibition was nearly abolished at 72 hours from transfection, displaying no significative fold change with respect to the control cells. This evidence suggested that probably the absence of visible effect on the cellular growth was due to the low efficiency of the miRNA inhibition method at long timing. Moreover, the macroscopic effects of the mir-425-5p probably were hidden by the actions of others transforming processes occurring in the melanoma cells.

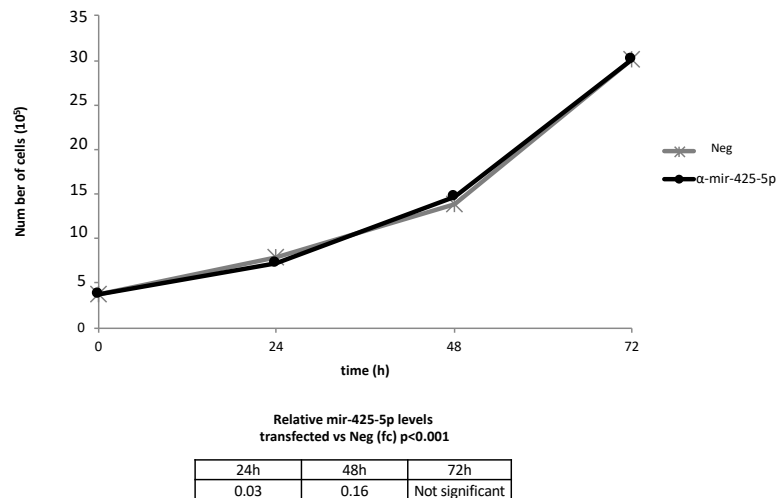


**Figure 52: Cell growth assessment of M21R cells transfected with scrambled negative control or mir-425-5p inhibitor, cultured up to 72 hours in presence of 2  $\mu$ M PLX4032.** miRNA inhibition was confirmed by RT-qPCR. The table in the bottom of the panel showed the fold change of mir-425-5p obtained in M21R cells transfected with the miRNA inhibitor, with respect to the scrambled sample.

#### 4.2.4.2.2 Cell cycle evaluation

Despite the results obtained by the evaluation of the cell growth, the effect of the mir-425-5p inhibition on the cell cycle progression was evaluated in M21R vemurafenib-resistant cells, according to the method described above. Surprisingly, the inhibition of mir-425-5p levels induced a small but reproducible increase of the percentage of cells in the G0/G1 phases, suggesting the inhibition of the cell cycle progression and cellular proliferation (Figure 53). Interestingly, the greater difference in cell cycle distribution was observed at 24 hours, the time point that displayed the highest efficiency of mir-425-5p inhibition, as reported by RT-qPCR (Figure 52). Conversely, the gap between M21R  $\alpha$ -mir-425-5p and M21R-control cells was progressively reduced up to 72 hours, following the recovery of mir-425-5p expression. Therefore, these data suggested that the reduction of mir-425-5p levels in vemurafenib-resistant cells could decrease the tolerance to the treatment.

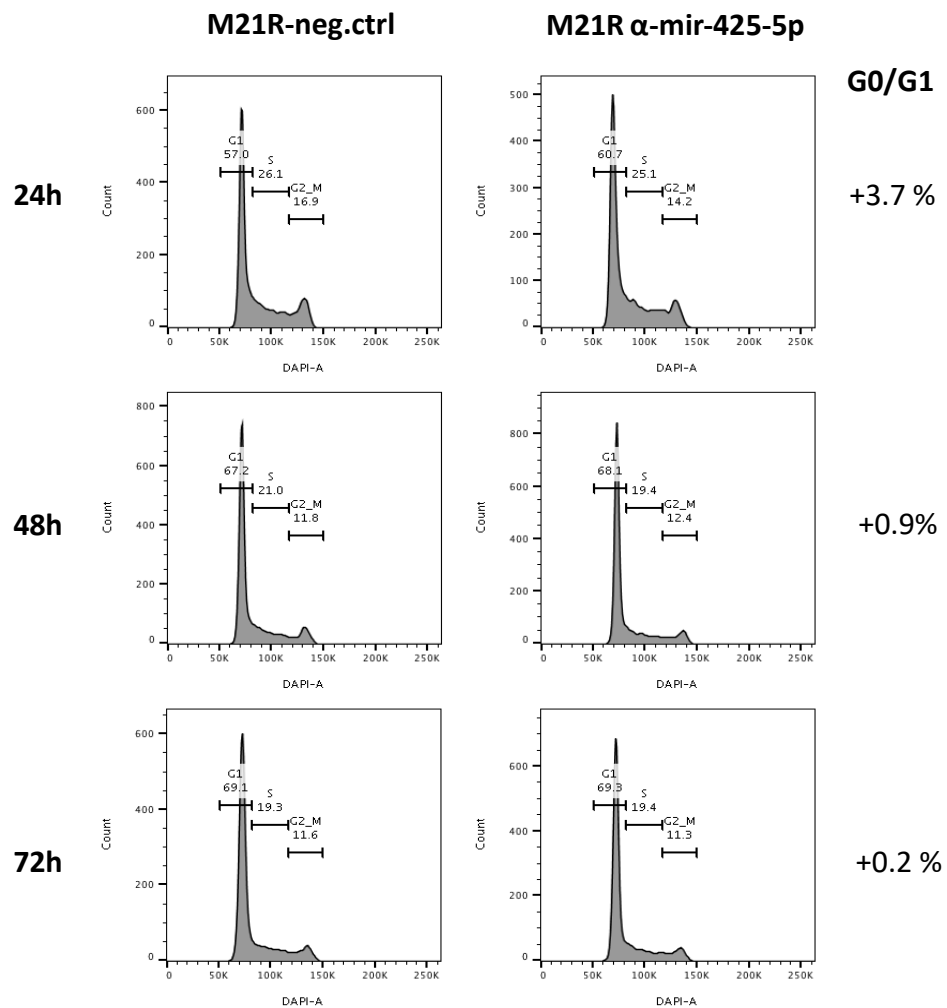


**Figure 53: Cell cycle assessment in M21R cells transfected either with scrambled negative control or  $\alpha$ -mir-425-5p inhibitor, cultured up to 72 hours in presence of 2  $\mu$ M PLX4032.** In the cytograms, number of cells is in the y-axis, DAPI fluorescence intensity in the x-axis. The total population is separated in three peaks corresponding to G0/G1, S and G2/M phases, highlighted by the horizontal black lines. The percentage of cells in each phase is reported above the corresponding peak. On the right side of the panel, for each time point is reported the percentage increase of cells found in G0/G1 phase in M21R inhibited for mir-425-5p expression with respect to M21-scrambled.

#### 4.2.4.2.3. Metabolic activity assay and IC<sub>50</sub> calculation

Based on the last encouraging results, the metabolic activity of M21R cells inhibited for mir-425-5p was assessed by MTT assay after 24 hours of exposure to increasing concentrations of PLX4032. With the same method described above, the culture media with increasing concentrations of vemurafenib were administered to cells at the time of transfection of either  $\alpha$ -mir-425-5p inhibitor or scrambled negative control. After 24 hours, MTT measurements were performed, dose-response curves were plotted and the IC<sub>50</sub> concentrations calculated. Interestingly, the inhibition of the mir-425-5p induced a reduction of the tolerance to vemurafenib in M21R cells with respect to the M21R control cells, as shown in Figure 54. In particular, while M21R transfected cells showed a higher metabolic activity at the lower concentrations of PLX4032, with respect to the untreated cells (metabolic index >1), M21R  $\alpha$ -mir-425-5p cells displayed a decrease in the metabolic activity independently from the drug concentration considered (metabolic index <1). Furthermore, the inhibition of mir-425-5p activity led to the significant drop of the half maximal inhibitory concentration, that was 15.84  $\mu$ M, instead of the 63.09  $\mu$ M obtained in M21R control cells.

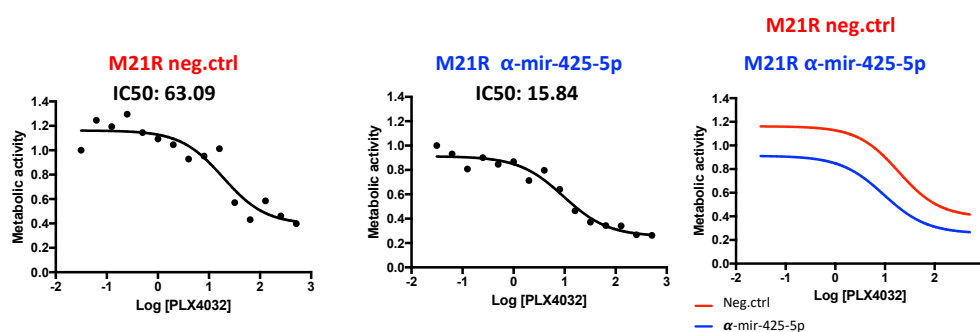


**Figure 54: Metabolic activity assessment and IC<sub>50</sub> calculation in M21R cells transfected either with  $\alpha$ -mir-425-5p inhibitor or scrambled control and cultured for 24 hours with increasing concentrations of PLX4032 (31.2 nM to 512  $\mu$ M). Metabolic activity index is in the y-axis, Log of the PLX4032 concentration in the x-axis. IC<sub>50</sub> are reported above the graphs. (A) Dose-response curve of M21R transfected with the negative control RNA. (B) Dose-response curve of M21R cells transfected with  $\alpha$ -mir-425-5p. (C) Merge of the two dose-response curves. Curve of mir-425-5p-inhibited cells is in blue, M21R transfected with the control in red.**

#### 4.2.4.2.3 Signalling of cancer-related pathways in M21R cells upon mir-425-p inhibition

Finally, the effect of mir-425-5p inhibition on cancer-related signalling pathways was assessed in M21R vemurafenib-resistant cells by dual luciferase assay. As already described, the specific plasmid reporters were transfected together with  $\alpha$ -mir-425-5p or scrambled negative RNA, and luminescence was detected after 24 hours of culture in medium supplemented with 2  $\mu$ M PLX4032. Notably, the inhibition of mir-425-5p activity determined a huge reduction in the activation of the Sonic-Hedgehog signalling, of about the 70% with respect to the control cells (Figure 55). Furthermore, no significant differences were observed in p53 pathway transduction, displaying a low or absent activation of the pathway in both mir-425-5p inhibited and control M21R cells, since the luminescence values detected were comparable to one of the negative controls.

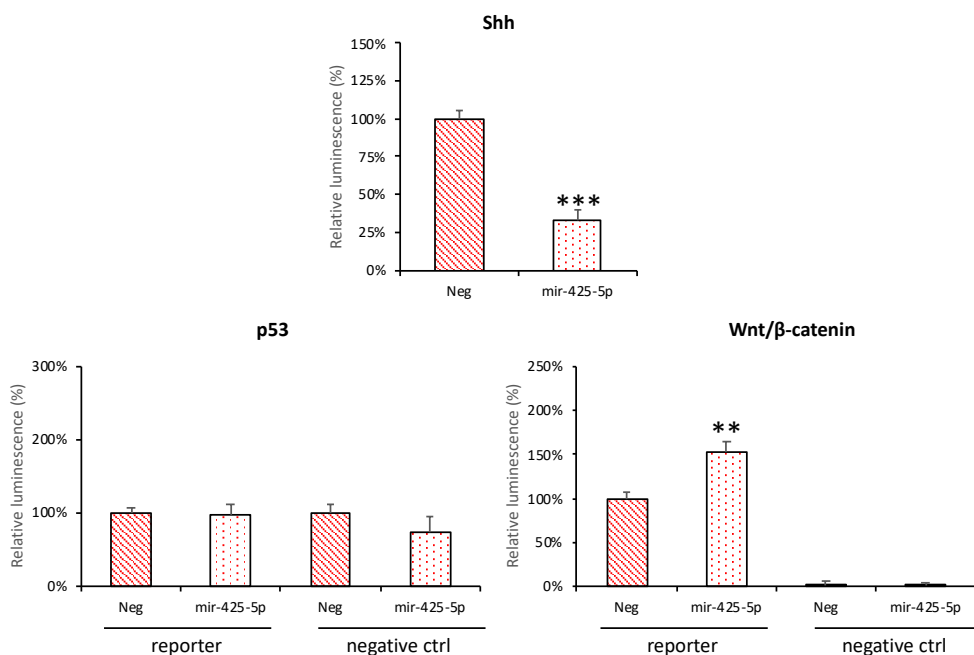


**Figure 55: Evaluation of Sonic-Hedgehog (Shh), p53 and Wnt/ $\beta$ -catenin signalling pathways in M21R cells inhibited for mir-425-5p, in presence of 2  $\mu$ M PLX4032.** Luminescence data measured in M21R-mir-425-5p cells were expressed as a percentage of the M21-scrb values. \* indicate the statistical significance of the data compared to the controls, with \*\* $p < 0.01$  \*\*\* $p < 0.001$ .



Conversely, the Wnt pathway signalling resulted potentiated of 50% upon mir-425-5p inhibition in M21R, with respect to scrambled cells. Therefore, the data collected strongly supported the results previously obtained by studying the effects of the mir-425- 5p over-expression in M21 sensitive cells, pointing out that the miRNA levels positively correlated to Shh pathway signalling rate in metastatic melanoma cells.

Conversely, further investigations are necessary to identify and to confirm the target of action of the mir-425-5p. Based on the evidence collected, others preliminary experiments not part of this work are ongoing with the aim to clarify whether mir-425-5p expression could confer resistance to cell death in vemurafenib-resistant cells. Afterwards, considering that mir-425-5p is proposed to induce a deep modification of the melanoma cell features, also promoting alteration in the metabolic activities, future investigations will have the aim to clarify the impact of this miRNA on the bioenergetics of metastatic melanoma cells. Indeed, it is well established that resistant melanoma cells undergo to a rewiring of the metabolism with respect to the sensitive cells [244]. Characterize the mechanism underlying miRNAs functioning and define their effect on the cellular metabolism, may guide to the identification of new targets for the melanoma therapy, also hypothesizing a combinate approach by targeting both miRNAs and metabolic elements, with the aim to overwhelm the onset of the resistance, to finally ameliorate the prognosis of melanoma patients.

## 5 Discussion

During oncogenesis and cancer progression, the transformed cells are exposed to harsh and unstable environmental conditions, commonly detrimental to the homeostasis and viability of the normal cells. Conversely, cancer cells gain the skills to overcome the poor oxygen afflux, nutrients limitation, and hostile pH conditions that occur in the tumour microenvironment, thanks to the adaptive modification of their cellular metabolism, efficient to drive neoplastic growth.

A pivotal role in the metabolic plasticity of the tumour cells is covered by the mitochondria, that acting as stress sensors modulate their functionality in response to the external stimuli, to provide the energy and the anabolic building blocks necessary to sustain the uncontrolled proliferation. Indeed, it has been well established that not only the mutational events that affect mitochondrial proteins drive oncogenesis, but also the organelles that retain their physiologic asset may be forced by aberrant intracellular signalling pathways to realize the metabolic shift proper to favour cancer development. In particular, a common hallmark of cancer cells is the reprogramming of the energetic metabolism toward the aerobic glycolysis, thus synthesizing ATP preferentially by the glucose fermentation and minimizing oxidative phosphorylation, despite the oxygen availability and the better efficiency of the last process. However, many tumours exhibit the reactivation of OXPHOS during cancer stages progression, an event that resulted to be essential to drive the metastasis. Therefore, these observations suggested that the regulation of the mitochondrial functionality, and in particular of the OXPHOS complexes activity are critical for the metabolic plasticity that drives the cancer progression. Several studies characterized the mechanisms underlying tumour plasticity and cancer metabolic rewiring, in order to identify possible targets for new therapeutic approaches. In this context, the efforts of many research groups focused on the possible role of the endogenous inhibitor of the ATP synthase,  $IF_1$ , in the modulation of the cancer metabolism, since its levels are strongly increased in several types of human cancer [90][96].

Indeed, while the function of IF<sub>1</sub> in normal cells can be considered well established, the implication of IF<sub>1</sub> over-expression in transformed cells is still a matter of debate. In particular, in normal tissues, IF<sub>1</sub> is activated in ischemic episodes, when the F<sub>1</sub>F<sub>0</sub>-ATP synthase reverses its activity and starts to hydrolyse ATP to restore the mitochondrial electrochemical gradient collapsed due to the oxygen unavailability, as final acceptor of the electron transport chain. In these conditions, IF<sub>1</sub> is activated by both  $\Delta\Psi_m$  decrease and matrix acidification and inhibits the ATPase activity of the F<sub>1</sub>F<sub>0</sub>-ATP synthase, thus avoiding ATP depletion to preserve cell viability. Based on its physiological role, it has been hypothesized that IF<sub>1</sub> in cancer cells may favour the metabolic reprogramming by the direct modulation of the ATP synthase activity, both in non-stressing and reduced oxygen tension conditions. Few research groups suggested that IF<sub>1</sub> may promote tumour development in normoxic conditions (21% O<sub>2</sub>) by inhibiting the synthetic activity of the F<sub>1</sub>F<sub>0</sub>-ATP synthase, thus inducing the switch toward aerobic glycolysis [90]. Conversely, we previously demonstrated that in osteosarcoma cells expressing IF<sub>1</sub> in normoxia, the endogenous inhibitor interacts with the ATP synthase, but favouring the ATP synthesis through oxidative phosphorylation [87]. These findings were consistent with data reported by Fujikawa et al. and suggested that the increase of the OXPHOS activity might be the effect of the F<sub>1</sub>F<sub>0</sub>-ATP synthase stabilization, and of the mitochondrial cristae structuring mediated by IF<sub>1</sub> [101].

Based on the knowledge that the ATPase-inhibitory function of IF<sub>1</sub> in normal cells is activated by the  $\Delta\Psi_m$  collapse determined by the oxygen deprivation and acts to block ATP-synthase-mediated ATP hydrolysis, our research group subsequently focused on the study of the IF<sub>1</sub> role in cancer cells in hypoxia. Indeed, no previous evidence was described in the literature about the microenvironment conditions or the cellular dysfunction that may drive the reversal of the ATP synthase activity and therefore the activation of IF<sub>1</sub> in cancer cells. Nevertheless, it is well known that in solid tumours the cells are commonly exposed to low or absent oxygen tension, depending on their distance from the blood vessels, suggesting that IF<sub>1</sub> expression may contribute to cancer cells adaptation to these stress conditions. As reported in our recent paper, with the aim to investigate this aspect, the osteosarcoma cells and IF<sub>1</sub>-silenced clones were exposed to

hypoxia (0.5 % O<sub>2</sub>) and severe hypoxia (0.1% O<sub>2</sub>) [65]. Given the evidence that in osteosarcoma clones previously produced and characterized in normoxia, the GFP expression in the scrambled control cells increased their sensitivity to stress conditions with respect to the 143B parental cells, a new set of GFP-negative cellular models was produced by viral transduction of the scrambled and IF<sub>1</sub>-silencing shRNAs, as described herein. Osteosarcoma clones, produced with transduction method and stably selected, completely lost the GFP expression as expected, but preserved the same biological and bioenergetics features of the GFP-positive osteosarcoma models that we previously employed for the studies of the IF<sub>1</sub> role in normoxia. Furthermore, IF<sub>1</sub>-silencing was and stable in the time with 90-95% transduction efficiency, without modification of the cell morphology and growth behaviour compared to the 143B parental cells, as well as previously observed for the transfection method used for GFP-positive clones production. The experiments carried out in hypoxia with these IF<sub>1</sub>-expressing and IF<sub>1</sub>-silenced clones, surprisingly highlighted that cancer cells synthesize ATP by OXPHOS even when the oxygen tension decreases up to 0.1% O<sub>2</sub>, though with a rate 2.5 times lower than in normoxia, independently from IF<sub>1</sub> expression. Despite the reduction of the cell proliferation and the increase of the glycolytic flux in hypoxia with respect to the basal conditions, the mitochondrial membrane potential  $\Delta\Psi_m$  of the osteosarcoma cells exposed to 0.1% and 0.5% oxygen tension increased in comparison to normoxia. These observations suggested for the first time that in cancer cells, even in severe hypoxia, the F<sub>1</sub>F<sub>0</sub>-ATP synthase does not reverse its activity, and consequently, IF<sub>1</sub> does not inhibit the enzyme due to the high level of  $\Delta\Psi_m$ .

Subsequently, the herein presented investigations were performed exposing cells to anoxia-mimicking conditions, in order to assess whether IF<sub>1</sub> may be activated in cancer cells by the  $\Delta\Psi_m$  collapse and if the endogenous inhibitor can protect cells from energy depletion, as it happens in mammalian cells in ischemic episodes. In particular, the  $\Delta\Psi_m$  abolishment occurring in anoxia was reproduced keeping the cells for 24 hours in presence of the uncoupler FCCP. Interestingly, we showed that, in our cancer model, IF<sub>1</sub> expression favour the cell proliferation in anoxia-mimicking conditions, with respect to clones stably silenced for IF<sub>1</sub>, where growth is almost arrested. Moreover, while in basal conditions IF<sub>1</sub>-expressing cells and IF<sub>1</sub>-silenced clones displayed the same glycolic flux,

the exposure to the uncoupler induced an increase of the glucose consumption and lactate release in both cell models, but it is more obvious in IF<sub>1</sub>-silenced cells. Simultaneously, we proved that in anoxia-mimicking conditions the steady-state ATP levels were significantly decreased in all cellular models, but largely in IF<sub>1</sub>-silenced clones. As expected, these data showed that upon anoxia-mimicking conditions the cancer cells boost the ATP glycolysis to obtain energy. However, the major glycolytic flux, together with the lower ATP levels found in IF<sub>1</sub>-silenced clones compared to control cells in FCCP, suggested that in these cells the increased glycolysis rate try to counteract the ATP drop caused by the ATP synthase reverse activity, though with a not complete efficiency. Notably, these observations are consistent with the results obtained by Fujikawa et al. through the real-time study of Hela cells stably silenced for IF<sub>1</sub>, in short-time (10 minutes) of exposure to the uncoupler CCCP [3].

Additionally, we demonstrated that the  $\Delta\Psi_m$  collapse induces the reversal of the F<sub>1</sub>F<sub>0</sub>-ATP synthase also in cancer cells, and even more interesting that IF<sub>1</sub> is activated in uncoupling conditions and fully blocks the ATPase activity. Indeed, we found that ATP levels of IF<sub>1</sub>-expressing cells in anoxia-mimicking conditions were almost identical to those found in the same cells with the F<sub>1</sub>F<sub>0</sub>-ATP synthase fully inhibited by oligomycin treatment, together with FCCP. The effects of the IF<sub>1</sub> activity on the  $\Delta\Psi_m$  were clearly visible by fluorescence microscopy of TMRM-stained cells upon uncoupling conditions, showing that IF<sub>1</sub>-expressing cells were almost completely depolarized, whereas IF<sub>1</sub>-silenced clones largely preserved the mitochondrial membrane potential, in an ATP-synthase dependent manner, as demonstrated by the FCCP co-treatment with oligomycin. Moreover, the contribution of the F<sub>1</sub>F<sub>0</sub>-ATP synthase hydrolytic activity in the  $\Delta\Psi_m$  maintenance was further confirmed by the increase of the oligomycin-sensitive ATPase activity found in the IF<sub>1</sub>-silenced clone, that was 5-fold higher than in 143B parental cells expressing IF<sub>1</sub>. The data just discussed and reported in our recent paper were also confirmed with cellular models derived from the HEK-293, a human embryonic kidney transformed cell line that displayed 4-fold higher levels of IF<sub>1</sub> compared to the 143B osteosarcoma cells [65].

It is also noteworthy that, upon FCCP treatment, the  $\Delta\Psi_m$  collapse in IF<sub>1</sub>-expressing cells occurred in a very short time, as demonstrated by TMRM staining and steady-state ATP levels assessment in osteosarcoma cells exposed for 30 minutes to 1  $\mu$ M FCCP. Even so, IF<sub>1</sub>-expressing cells were still viable after 24 hours of uncoupling, as shown by the viability assay of control cells after a day of growth in presence either 10  $\mu$ M or 15  $\mu$ M FCCP. Indeed, it is well established that the  $\Delta\Psi_m$  collapse may induce either the cell death mediated by cytochrome-c release from the organelles, or the selective degradation of mitochondria through autophagy [114]. Therefore, intrigued by the absence of cell death, both in uncoupled IF<sub>1</sub>-expressing cells and IF<sub>1</sub>-silenced clones with low steady-state ATP levels, we further investigated the effects of the anoxia-mimicking conditions on the cellular mitochondrial mass. From the GFP-negative cellular models we produced osteosarcoma clones stably expressing the mtRFP, a red fluorescent protein target to the mitochondria, in order to assess the mitochondria content in intact and viable cells, by flow cytometry and fluorescence microscopy. We demonstrated that in this cellular model the mtRFP fluorescence intensity was linear to the mitochondrial content, and not affected by quenching phenomena. Moreover, the mtRFP expression in osteosarcoma clones resulted stable even after a year of cell culture, and the fluorescence intensity followed the physiologic oscillations of the mitochondrial mass, as shown by the comparison with citrate synthase activity assay. The mtRFP method of mitochondrial mass detection was also validated by comparing the fluorescence signal and the citrate synthase activities of cells exposed to conditions known to induce either the reduction (hypoxia) or the increase (resveratrol) of the mitochondrial mass. Subsequently, we demonstrated that the mtRFP expression does not alter the growth and the main biochemical features of the osteosarcoma cells with respect to the GFP-negative clones of origin. In conclusion, the mtRFP-expressing osteosarcoma clones turned out to be great tools to study the mitochondrial mass variations in different experimental conditions, concerning IF<sub>1</sub> expression, even in the long run, thanks to the stable expression of the fluorescent reporter. Therefore, mtRFP-positive osteosarcoma cells were employed for the study of the mitochondrial mass of osteosarcoma cells expressing IF<sub>1</sub> and -IF<sub>1</sub> clones exposed to anoxia-mimicking conditions for 24 hours.

The flow cytometry and fluorescence microscopy analysis of mtRFP-clones surprisingly did not show decreases or significant changes in the mitochondrial mass of all cellular models assessed, with respect to the basal conditions, independently from IF<sub>1</sub> expression, and, hence, from  $\Delta\Psi_m$  levels. This result was further confirmed by protein immunodetection of the mitochondrial mass markers TOMM20 and VDAC1, that did not show significant variations in IF<sub>1</sub>-expressing and IF<sub>1</sub>-silenced cells cultured in presence of FCCP, with respect to normal conditions. Therefore, we showed that the steady-state levels of mitochondrial mass are maintained in cancer cells after 24 hours of anoxia-mimicking conditions, independently from IF<sub>1</sub> and, in turn, from the intracellular ATP content and the mitochondrial membrane potential levels.

Taking into account of these unexpected results and knowing that the mitochondrial content in the cells depends on the balance between several mitochondrial turnover processes, we evaluated the rate of both mitochondrial biogenesis and organelles degradation throughout autophagy. The activation of the latter process, also termed mitophagy, was assessed by the protein levels detection of PINK1 and BNIP3 dimer, that act as receptors for the autophagosomes nucleation and are reported to be exposed on the outer mitochondrial membrane in response to  $\Delta\Psi_m$  collapse and decreased oxygen levels, respectively. Interestingly, we found that both the positive regulators of mitophagy were increased in IF<sub>1</sub>-expressing cells in FCCP, with respect to the basal conditions. Therefore, upon-anoxia mimicking conditions, cancer cells expressing IF<sub>1</sub> enhance the mitophagy, a result quite expected due to the prolonged  $\Delta\Psi_m$  collapse occurring in the cells in these conditions, despite no reduction in the mitochondrial mass. Conversely, we observed that PINK1 and BNIP3 dimer protein levels were reduced in IF<sub>1</sub>-silenced clones exposed to FCCP, suggesting the inhibition of the mitochondria degradation, despite no increase of the mitochondrial content. Moreover, we found out that PINK1 and BNIP3 differential activations modulated the mitochondria autophagic degradation in anoxia-mimicking conditions. This confirmation was obtained by the fluorescence microscopy evaluation of the mitochondria colocalization within the autophagosomes in mtRFP clones transiently expressing the LC3-YFP protein. The fluorescence images clearly showed the increase of the mitochondria sequestered within the autophagosomes in IF<sub>1</sub>-expressing cells exposed to FCCP, with respect to the basal conditions. Oppositely, IF<sub>1</sub>-silenced cells

exhibited almost the complete absence of mitophagic events in anoxia-mimicking conditions. Our observations were consistent with the RNA interference studies performed by Lefebvre et al. that identified IF<sub>1</sub> as essential for the mitophagy activation mediated by the PINK1/Parkin pathway [109]. Furthermore, our evidence suggested that IF<sub>1</sub> activity may be relevant also for the mitophagy mediated by BNIP3 dimerization. Based on these findings proving the impairment of the mitophagy, and considering that no variations in the mitochondria content were observed, both in control cells and in IF<sub>1</sub>-silenced clones, we hypothesized that a compensatory activation of the mitochondrial biogenesis process could occur in the cells exposed to anoxia-mimicking conditions. This assumption was confirmed by the protein levels evaluation of PGC-1 $\alpha$ , the transcriptional co-activator of the mitochondria biogenesis genes, and its positive regulator SIRT1. Indeed, while a significant increase of both mitochondrial biogenesis markers was observed in IF<sub>1</sub>-expressing cells, under anoxia-mimicking conditions.

On the other hand, IF<sub>1</sub>-silenced cells showed the reduction of these proteins at translation level. These data suggested that in cancer cells expressing IF<sub>1</sub> in uncoupling conditions, the potentiation of the mitochondria degradation through autophagy is counterbalanced by the production of new organelles through the biogenesis process. Conversely, in the absence of the inhibitor, the  $\Delta\Psi_m$  preservation seems to function as a signal for the mitochondria maintenance, and thus neither the mitophagy nor the biogenesis is stimulated. Subsequently, considering that the mitochondria turnover process require energy and is modulated in response to cellular energy charge, the ADP/ATP ratio was assessed. Consistently with our previous findings, we observed that IF<sub>1</sub>-expressing cells almost preserved the energy charge in uncoupling conditions. Conversely, IF<sub>1</sub>-silenced cells showed a huge increase in the ADP/ATP ratio, indicating a very low cellular energy status. These data suggested that the different rate of mitochondrial turnover in IF<sub>1</sub>-expressing cells and IF<sub>1</sub>-silenced clones may depend on the different cellular energy charge balance and also on the total ATP available.

Finally, driven by the consistent changes in the main bioenergetic parameters between control cells and IF<sub>1</sub>-silenced clones, we evaluated the OXPHOS complexes expression, through the proteins immunodetection in cells exposed to anoxia-mimicking conditions for 24 hours. Interestingly, while the IF<sub>1</sub>-expressing cells showed a consistent decrease in



the protein levels of all OXPHOS complexes, the IF<sub>1</sub>-silenced cells displayed a greater preservation of them. However, it is possible that the maintenance of the complexes in IF<sub>1</sub>-silenced cells upon FCCP is actually an effect of the stationary condition induced by the inhibition of the mitochondria degradation. Conversely, the low levels of OXPHOS expressed in controls cells may be due to the impairment between the rapid mitochondrial membrane formation and degradation, and the synthesis, import and assembly of the complexes into them, due to the high rate of the mitochondrial turnover in these cells upon uncoupling. This hypothesis is consistent with proteomic studies reporting that OXPHOS complexes have a degradation rate comparable to the mitochondria turnover [147]. Interestingly, IF<sub>1</sub> levels in anoxia-mimicking conditions seem to follow the decrease of the ATP synthase, its functional target. This observation suggested that the endogenous inhibitor action is allowed by the finely regulation of its expression in response to the stress conditions.

To sum up, all our data pointed out that in cancer cells the collapse of the mitochondrial membrane potential induces the reversal of the ATP synthase to maintain  $\Delta\Psi_m$ , and the consequent activation of the endogenous inhibitor IF<sub>1</sub>, as it happens in normal mammalian cells upon ischemia. Moreover, our findings proved that IF<sub>1</sub> overexpression in cancer cells has a protective role, by allowing cellular proliferation and the preservation of both ATP levels and the cellular energy charge, events that promote a high mitochondrial turnover rate in cells in anoxia-mimicking conditions. The forced renewal of the mitochondrial mass induced by IF<sub>1</sub> could be a mechanism for cancer cells to escape from the cell death mediated by the release of pro-apoptotic factor from the mitochondria, that are eliminated and replaced before the detrimental event. This hypothesis is corroborated by our preliminary experiments, showing that IF<sub>1</sub>-expressing cells maintain a better viability after 48 hours of exposure to anoxia-mimicking conditions, compared to IF<sub>1</sub>-silenced cells that activate cell apoptosis.

Interestingly, another research group proposed that IF<sub>1</sub> may exert an anti-apoptotic role by impeding the mitochondrial cristae remodelling prevents the apoptosis completion [106]. Further investigations are ongoing to study in depth the effect of IF<sub>1</sub> expression in cancer cells exposed to prolonged anoxia-mimicking conditions and to clarify the functioning of the endogenous inhibitor IF<sub>1</sub> in real anoxia conditions.

Proving that IF<sub>1</sub> acts as a mediator of metabolic plasticity and cell death escape mechanism in true anoxia, and elucidating the mechanism underlying these effects, may open a great perspective for the cancer treatment, considering IF<sub>1</sub> as a promising target for the development of new therapeutic approach.

The ability of cancer cells to defeat harsh and unstable environmental conditions by the cellular reprogramming is also accountable to drive acquired drug resistance to cancer therapy in several types of tumours. Among these, cutaneous melanomas display high aggressiveness and a high rate of mortality that have been correlated to the plasticity and mutability behaviours gained by these tumours, affecting the efficacy of the classical cancer therapies. The study of the mechanisms underlying melanoma biology and of the progressive acquisition of cancer-related traits allowed the identification of new targets and the development of innovative therapeutic approaches for the melanoma treatment. The approval of both immunotherapy and target therapy drugs from 2012, statistically improved the overall survival of the metastatic melanoma patients. However, these therapies are not showing a curative effect in most of the cases. Indeed, events of secondary resistance have been reported in the majority of the melanoma patients, with tumour relapses with even more severe and disseminating features. Interestingly, recent investigation pointed out that the progressive acquisition of transforming characteristic in melanoma cells is not only due to the accumulation of new mutations in the genome, but it is also driven by epigenetic modifications. Notably, it is widely demonstrated the involvement of the small non-coding RNAs in the transcriptional regulation of the genes driving the cancer progression [201]. In particular, qualitative and quantitative dysregulations of specific miRNAs have been related to melanoma transformation and progression by promoting cell survival, epithelial-mesenchymal transition, cell cycle progression, metastasis, altered immune response and metabolic rewiring in melanoma cells. The increasing evidence of miRNAs role as master regulators of adaptability, typical of the melanoma cells, led to consider them as promising therapeutic targets. Moreover, it has been reported that miRNAs pattern of expression is progressively altered within the stages of melanoma progression, suggesting the possible prognostic value of the miRNAs profiling analysis in patients.

In this context, this study was developed during my fellowship at Children's Hospital of Los Angeles, with the aim to identify and characterize the miRNAs involved in drug-resistance towards vemurafenib in BRAFV600E-mutated metastatic melanoma. Indeed, almost 50% of the melanoma cases carries the V600E substitution in the BRAF gene, that constitutively activates the MAPK signalling pathway, with the effect of an uncontrolled cell proliferation. The standard treatment for these types of melanoma are the BRAF-inhibitor drugs, among which the vemurafenib (PLX4032) was approved by the FDA in 2012.

The cellular models employed for the study were the M21 and Colo38 cells, obtained from patients with BRAFV600E-mutated metastatic melanoma, and the derived vemurafenib-resistant cell line M21R and Colo38R. Firstly we focused our attention on the identification of the molecular pathways dysregulated in M21R resistant melanoma cells compared to M21 sensitive cells, that could be associable to cancer progression and therefore targeted by the miRNA driving the acquired resistance toward PLX4032. For this purpose, the activation of the Wnt/ $\beta$ -catenin, TGF- $\beta$ , Sonic-Hedgehog and p53 signalling pathways was evaluated by assessing the mRNA and protein levels of the main signalling molecules by RT-qPCR and immunodetection respectively, and by evaluating the signalling rate through the dual luciferase assay. Interestingly, we proved that all three oncogenic pathways analysed were hugely up-regulated in the vemurafenib-resistant cells with respect to the cells sensitive to the treatment, whereas the tumour-suppressor pathway p53 was concomitantly inhibited. In particular, we detected a decrease in the mRNA and protein levels of the kinase GSK-3 $\beta$ , the negative regulator of the Wnt/ $\beta$ -catenin. Moreover, M21R cells displayed the increase of the inactive form p-ser9-GSK-3 $\beta$  respect to the total GSK-3 $\beta$  protein. Coherently, the increase of  $\beta$ -catenin transcript and protein levels were observed in resistant cell lines compared to sensitive cells, resulting in the boost of the Wnt/ $\beta$ -catenin downstream signalling, as demonstrated by the dual luciferase assay. These findings are consistent with literature data, reporting that the hyperactivation of the Wnt/ $\beta$ -catenin signalling pathway is related to BRAF-inhibitors resistance in other types of melanoma cellular models, and it drives immunotherapy resistance in melanoma mouse models [210], [241]. Interestingly,  $\beta$ -catenin protein levels were found increased in melanoma patients during cancer progression [240].

In the same way, the analysis of the Smad2 and Smad3 proteins of the TGF- $\beta$  pathway revealed a significant increase of these signalling molecules, detectable both at mRNAs and proteins levels, resulting in the hyperactivation of the downstream responsive elements in M21R vemurafenib-resistant cells with respect to the M21 sensitive cells. Interestingly, it has been reported that transformed melanocytes release high levels of TGF- $\beta$ , stimulating the signalling in an autocrine/paracrine loop with an inhibitory effect on the immune-response and favouring the invasiveness of the cells [246]. By dual luciferase assay, we proved that also Sonic-Hedgehog signalling pathway was potentiated in M21R cells with respect to M21. This evidence confirmed the hypothesis of the Shh reactivation previously formulated by Sabbatino et al. based on the observation of GLI1 accumulation detected M21R, with respect to M21 cells [222]. Finally, we showed how in vemurafenib-resistant cells p53 anti-tumour pathway was strongly repressed compared to vemurafenib-sensitive cells, as proved by the reduced mRNA and protein levels of p53 and by the dual-luciferase assay specific for p53 signalling.

Overall, our analysis of the cancer-related pathways highlighted how the resistant melanoma cells undergo a profound alteration of the intracellular signalling, potentiating oncogenic pathways, such as Wnt/ $\beta$ -catenin, TGF- $\beta$  and Sonic-Hedgehog, on one hand while shutting down p53 tumour-suppressor pathway on the other, promoting in this way cancer progression and invasion.

Our data did not allowed us to identify a preferential pathway targeted by the miRNAs responsible for the drug-resistance onset, therefore, we extend our analysis to all the pathways found dysregulated in vemurafenib-resistant cells. The identification of the potential miRNAs determining the development of drug resistance towards vemurafenib was performed by comparing the pattern of expression of 800 miRNAs between sensitive and resistant metastatic melanoma cells, through Nanostring array (Nanostring Technologies). In particular, we discovered a group of 13 miRNAs up-regulated and 15 down-regulated in both M21R and Colo38R vemurafenib-resistant cells with respect to M21 and Colo38 sensitive melanoma cells. This result suggested that, despite the heterogeneity of the melanoma tumours, some miRNAs may ubiquitously drive the drug-resistance onset, representing good targets for therapies intending to counteract the onset of tolerance toward vemurafenib.

Subsequently, by RT-qPCR validation and bioinformatic analysis, we identified a group of 3 miRNAs up-regulated in resistant cells all predicted to target the FBXW11 gene, encoding  $\beta$ TrCP2. This protein is an E3 ubiquitin ligase that mediates the proteasomal degradation of cellular proteins, among which GLI2,  $\beta$ -catenin and MDM2, the specific inhibitor of p53, thus representing a good target of action for the miRNAs candidates to carry out resistance onset through upregulation. Notably, we found that  $\beta$ TrCP2 protein levels were decreased nearly 70% in both PLX4032-resistant cells with respect to the sensitive cells. The data collected led us to hypothesize that the increased levels of the 3 miRNAs identified could repress the expression of  $\beta$ TrCP2, whose reduced activity may result in the accumulation of GLI2,  $\beta$ -catenin and MDM2 thus inducing the hyperactivation of Shh and Wnt/ $\beta$ -catenin and the inhibition of the p53 pathways, respectively, in agreement with our previous observation. Moreover, prognostic databases correlated the  $\beta$ TrCP2 low expression with the reduced overall survival of patients. Consequently, we focused on the study of the mir-425-5p, the most up-regulated of the three miRNAs taken into account in the M21R cell line with respect to M21, whose target was predicted to be  $\beta$ TrCP2. Interestingly, the first set of experiments highlighted that the induction of mir-425-5p over-expression confers to M21 sensitive cells tolerance to vemurafenib. In particular, we found that mir-425-5p upregulation protects M21 from cells death. Coherently, we proved that mir-425-5p overexpression determine a small but significant increase of the cell cycle progression. These findings suggested that mir-425-5p confers resistance to vemurafenib by promoting the development of a cellular population able to proliferate at a low rate even in presence of the drug. Moreover, the dose-response curve obtained by MTT assay showed that when mir-425-5p is increased in M21 cells, the IC50 increase, indicating the lower sensitivity to the higher concentration of vemurafenib. Interestingly, mir-425-5p overexpression seems to correlate with a higher metabolic activity of M21 cells with respect to the control cells, as suggested by the MTT assay. Further demonstrations of the involvement of mir-425-5p in the development of vemurafenib resistance were provided by inhibiting the miRNA levels in the M21R melanoma cells. Indeed, the evaluation of the same parameter reported above, showed the partial restoration of the sensitivity toward PLX4032 in resistant cells inhibited for mir-425-5p expression.

Finally, our data suggested that mir-425-5p confers resistance toward vemurafenib by increasing the Sonic-Hedgehog signalling, but further investigations are necessary to identify and confirm the direct target of the miRNA. Consistently with our findings, miR-425-5p has been reported to promote tumorigenicity and aggressiveness in hepatocellular carcinoma, gastric and breast cancers, and more interestingly it is reported to modulate chemosensitivity of colorectal cancer cells to 5-fluorouracil and oxaliplatin treatments [247], [248], [249], [250], [251]. In contradiction to our findings, that propose mir-425-5p as an oncomiR in melanoma and also to the data reported in prognostic databases, Liu et al. suggested that mir-425 may acts as a tumour-suppressor, limiting cell proliferation and metastasis and inducing apoptosis of melanoma cells. However, in their paper is not specified which arm of the mir-425 double-stranded precursor is considered, whether the mir-425-5p or the mir-425-3p. Concretely, it is demonstrated that the complementary strands of the miRNA precursor may exert opposite effects on cell proliferation, apoptosis, migration. For example, while increased levels of mir-425-5p promote chemoresistance in hepatocellular carcinoma, elevated levels of mir-425-3p oppositely sensitize cells to the treatment in the same cancer type [252].

Therefore, as an additional proof of the role of mir-425-5p in the onset of drug-resistance toward PLX4032, new experiments are ongoing to assess the effect of mir-425-5p modulation in Colo38 and Colo38R melanoma cells. Consolidated the role of mir-425-5p in the acquired resistance to BRAF-inhibitors, future investigations will be performed to study the impact of this miRNA on the metabolism of the metastatic melanoma cells. Indeed, it is well demonstrated that melanoma cells resistant to therapy deeply change their metabolic features with respect to the sensitive cells [244]. Moreover, increasing evidence suggested that miRNAs act as the main regulator of the metabolic switch and adaptability of melanoma cells in stress conditions [208]. To define the mechanisms of miRNAs action and determine their impact on the cellular bioenergetics, may contribute to the identification of new targets for the melanoma therapy. Moreover, the combine therapeutic strategy targeting both metabolic components and miRNAs may help to counteract the onset of drug resistance, representing a good chance to improve the prognosis of melanoma patients.



# 6 Bibliography

- [1] P. Siekevitz, "Powerhouse of the Cell," *Scientific American*, vol. 197. Scientific American, a division of Nature America, Inc., pp. 131–144, 1957.
- [2] M. W. Gray, "Mitochondrial evolution.," *Cold Spring Harbor perspectives in biology*, vol. 4, no. 9, p. a011403, Sep. 2012.
- [3] L. Ernster and G. Schatz, "Mitochondria: a historical review.," *The Journal of Cell Biology*, vol. 91, no. 3, p. 227s LP-255s, Dec. 1981.
- [4] I. Scott and R. J. Youle, "Mitochondrial fission and fusion.," *Essays in biochemistry*, vol. 47, pp. 85–98, 2010.
- [5] M. Liesa and O. S. Shirihai, "Mitochondrial Dynamics in the Regulation of Nutrient Utilization and Energy Expenditure," *Cell Metabolism*, vol. 17, no. 4, pp. 491–506, 2013.
- [6] L. Contreras, I. Drago, E. Zampese, and T. Pozzan, "Mitochondria: The calcium connection," *Biochimica et Biophysica Acta (BBA) - Bioenergetics*, vol. 1797, no. 6, pp. 607–618, 2010.
- [7] H. Vakifahmetoglu-Norberg, A. T. Ouchida, and E. Norberg, "The role of mitochondria in metabolism and cell death," *Biochemical and Biophysical Research Communications*, vol. 482, no. 3, pp. 426–431, 2017.
- [8] S. W. G. Tait and D. R. Green, "Mitochondria and cell signalling," *Journal of Cell Science*, vol. 125, no. 4, p. 807 LP-815, Feb. 2012.
- [9] D. C. Wallace, "Bioenergetic Origins of Complexity and Disease," *Cold Spring Harbor Symposia on Quantitative Biology*, vol. 76, no. 0, pp. 1–16, Jan. 2011.
- [10] D. Hanahan and R. A. Weinberg, "Hallmarks of cancer: the next generation.," *Cell*, vol. 144, no. 5, pp. 646–74, Mar. 2011.
- [11] S. Vyas, E. Zaganjor, and M. C. Haigis, "Mitochondria and Cancer.," *Cell*, vol. 166, no. 3, pp. 555–566, Jul. 2016.
- [12] W.-X. Zong, J. D. Rabinowitz, and E. White, "Mitochondria and Cancer.," *Molecular cell*, vol. 61, no. 5, pp. 667–676, Mar. 2016.
- [13] W. Kühlbrandt, "Structure and function of mitochondrial membrane protein complexes," *BMC Biology*, vol. 13, no. 1, p. 89, 2015.
- [14] D. M. Walther and D. Rapaport, "Biogenesis of mitochondrial outer membrane proteins," *Biochimica et Biophysica Acta (BBA) - Molecular Cell Research*, vol. 1793, no. 1, pp. 42–51, 2009.
- [15] N. Wiedemann, A. E. Frazier, and N. Pfanner, "The protein import machinery of



- mitochondria.,” *The Journal of biological chemistry*, vol. 279, no. 15, pp. 14473–6, Apr. 2004.
- [16] J. M. Herrmann and J. Riemer, “The Intermembrane Space of Mitochondria,” *Antioxidants & Redox Signaling*, vol. 13, no. 9, pp. 1341–1358, Nov. 2010.
- [17] F. Palmieri, “Mitochondrial carrier proteins.,” *FEBS letters*, vol. 346, no. 1, pp. 48–54, Jun. 1994.
- [18] A. M. Distler, J. Kerner, and C. L. Hoppel, “Proteomics of mitochondrial inner and outer membranes,” *PROTEOMICS*, vol. 8, no. 19, pp. 4066–4082, Oct. 2008.
- [19] M. Zick, R. Rabl, and A. S. Reichert, “Cristae formation—linking ultrastructure and function of mitochondria,” *Biochimica et Biophysica Acta (BBA) - Molecular Cell Research*, vol. 1793, no. 1, pp. 5–19, 2009.
- [20] S. Cogliati, J. A. Enriquez, and L. Scorrano, “Mitochondrial Cristae: Where Beauty Meets Functionality.,” *Trends in biochemical sciences*, vol. 41, no. 3, pp. 261–273, Mar. 2016.
- [21] V. M. Gohil and M. L. Greenberg, “Mitochondrial membrane biogenesis: phospholipids and proteins go hand in hand.,” *The Journal of cell biology*, vol. 184, no. 4, pp. 469–72, Feb. 2009.
- [22] G. Paradies, V. Paradies, V. De Benedictis, F. M. Ruggiero, and G. Petrosillo, “Functional role of cardiolipin in mitochondrial bioenergetics,” *Biochimica et Biophysica Acta (BBA) - Bioenergetics*, vol. 1837, no. 4, pp. 408–417, 2014.
- [23] I. O. Mazunin, S. A. Levitskii, M. V. Patrushev, and P. A. Kamenski, “Mitochondrial matrix processes,” *Biochemistry (Moscow)*, vol. 80, no. 11, pp. 1418–1428, Nov. 2015.
- [24] A. M. D’Erchia *et al.*, “Tissue-specific mtDNA abundance from exome data and its correlation with mitochondrial transcription, mass and respiratory activity,” *Mitochondrion*, vol. 20, pp. 13–21, 2015.
- [25] C. M. Gustafsson, M. Falkenberg, and N.-G. Larsson, “Maintenance and Expression of Mammalian Mitochondrial DNA,” *Annual Review of Biochemistry*, vol. 85, no. 1, pp. 133–160, Jun. 2016.
- [26] N.-G. Larsson *et al.*, “Mitochondrial transcription factor A is necessary for mtDNA maintenance and embryogenesis in mice,” *Nature Genetics*, vol. 18, no. 3, pp. 231–236, Mar. 1998.
- [27] “Animal Mitochondrial DNA: Structure and Evolution,” *International Review of Cytology*, vol. 141, pp. 173–216, Jan. 1992.
- [28] M. Falkenberg, N.-G. Larsson, and C. M. Gustafsson, “DNA Replication and Transcription in Mammalian Mitochondria,” *Annual Review of Biochemistry*, vol. 76, no. 1, pp. 679–699, Jun. 2007.
- [29] R. Gilkerson *et al.*, “The mitochondrial nucleoid: integrating mitochondrial DNA into cellular homeostasis.,” *Cold Spring Harbor perspectives in biology*, vol. 5, no. 5, p.

a011080, May 2013.

- [30] H. A. L. Tuppen, E. L. Blakely, D. M. Turnbull, and R. W. Taylor, "Mitochondrial DNA mutations and human disease," *Biochimica et Biophysica Acta (BBA) - Bioenergetics*, vol. 1797, no. 2, pp. 113–128, Feb. 2010.
- [31] M. Pinto and C. T. Moraes, "Mechanisms linking mtDNA damage and aging.," *Free radical biology & medicine*, vol. 85, pp. 250–8, Aug. 2015.
- [32] D. C. Wallace and D. Chalkia, "Mitochondrial DNA genetics and the heteroplasmy conundrum in evolution and disease.," *Cold Spring Harbor perspectives in biology*, vol. 5, no. 11, p. a021220, Nov. 2013.
- [33] C. Wirth, U. Brandt, and C. Hunte, "Structure and function of mitochondrial complex I," *Biochimica et Biophysica Acta (BBA) - Bioenergetics*, vol. 1857, no. 7, pp. 902–914, Jul. 2016.
- [34] G. Cecchini, "Function and Structure of Complex II of the Respiratory Chain," *Annual Review of Biochemistry*, vol. 72, no. 1, pp. 77–109, Jun. 2003.
- [35] A. R. Crofts, "The Cytochrome  $bc_1$  Complex: Function in the Context of Structure," *Annual Review of Physiology*, vol. 66, no. 1, pp. 689–733, Mar. 2004.
- [36] M. Wikström and V. Sharma, "Proton pumping by cytochrome c oxidase – A 40 year anniversary," *Biochimica et Biophysica Acta (BBA) - Bioenergetics*, vol. 1859, no. 9, pp. 692–698, Sep. 2018.
- [37] S. J. R. Heales, M. E. Gegg, and J. B. Clark, "Oxidative phosphorylation: Structure, function, and intermediary metabolism," *International Review of Neurobiology*, vol. 53, pp. 25–56, Jan. 2002.
- [38] P. MITCHELL, "Coupling of Phosphorylation to Electron and Hydrogen Transfer by a Chemi-Osmotic type of Mechanism," *Nature*, vol. 191, no. 4784, pp. 144–148, Jul. 1961.
- [39] D. Poburko, J. Santo-Domingo, and N. Demaurex, "Dynamic regulation of the mitochondrial proton gradient during cytosolic calcium elevations.," *The Journal of biological chemistry*, vol. 286, no. 13, pp. 11672–84, Apr. 2011.
- [40] C. von Ballmoos, A. Wiedenmann, and P. Dimroth, "Essentials for ATP Synthesis by  $F_1F_0$  ATP Synthases," *Annual Review of Biochemistry*, vol. 78, no. 1, pp. 649–672, Jun. 2009.
- [41] A. Wiedenmann, P. Dimroth, and C. von Ballmoos, " $\Delta\psi$  and  $\Delta pH$  are equivalent driving forces for proton transport through isolated  $F_0$  complexes of ATP synthases," *Biochimica et Biophysica Acta (BBA) - Bioenergetics*, vol. 1777, no. 10, pp. 1301–1310, Oct. 2008.
- [42] J. E. Walker, "The ATP synthase: the understood, the uncertain and the unknown," *Biochemical Society Transactions*, vol. 41, no. 1, pp. 1–16, Feb. 2013.
- [43] J. E. Walker *et al.*, "Primary structure and subunit stoichiometry of  $F_1$ -ATPase from bovine mitochondria.," *Journal of molecular biology*, vol. 184, no. 4, pp. 677–701, Aug.

1985.

- [44] J. P. Abrahams, A. G. W. Leslie, R. Lutter, and J. E. Walker, "Structure at 2.8 Å resolution of F1-ATPase from bovine heart mitochondria," *Nature*, vol. 370, no. 6491, pp. 621–628, Aug. 1994.
- [45] R. J. Devenish, M. Prescott, G. M. Boyle, and P. Nagley, "The Oligomycin Axis of Mitochondrial ATP Synthase: OSCP and the Proton Channel," *Journal of Bioenergetics and Biomembranes*, vol. 32, no. 5, pp. 507–515, 2000.
- [46] C. von Ballmoos, G. M. Cook, and P. Dimroth, "Unique Rotary ATP Synthase and Its Biological Diversity," *Annual Review of Biophysics*, vol. 37, no. 1, pp. 43–64, Jun. 2008.
- [47] J. Weber, "ATP synthase--the structure of the stator stalk.," *Trends in biochemical sciences*, vol. 32, no. 2, pp. 53–6, Feb. 2007.
- [48] R. J. Devenish, M. Prescott, and A. J. W. Rodgers, "The Structure and Function of Mitochondrial F1F0-ATP Synthases," in *International review of cell and molecular biology*, vol. 267, 2008, pp. 1–58.
- [49] J. Habersetzer *et al.*, "Human F1F0 ATP Synthase, Mitochondrial Ultrastructure and OXPHOS Impairment: A (Super-)Complex Matter?," *PLoS ONE*, vol. 8, no. 10, p. e75429, Oct. 2013.
- [50] P. Paumard *et al.*, "The ATP synthase is involved in generating mitochondrial cristae morphology.," *The EMBO journal*, vol. 21, no. 3, pp. 221–30, Feb. 2002.
- [51] R. K. Nakamoto, J. A. Baylis Scanlon, and M. K. Al-Shawi, "The rotary mechanism of the ATP synthase.," *Archives of biochemistry and biophysics*, vol. 476, no. 1, pp. 43–50, Aug. 2008.
- [52] I. Wittig and H. Schagger, "Structural organization of mitochondrial ATP synthase," *Biochimica et Biophysica Acta (BBA) - Bioenergetics*, vol. 1777, no. 7–8, pp. 592–598, Jul. 2008.
- [53] R. J. Devenish, M. Prescott, and A. J. W. Rodgers, "The Structure and Function of Mitochondrial F1F0-ATP Synthases," *International Review of Cell and Molecular Biology*, vol. 267, pp. 1–58, Jan. 2008.
- [54] A. I. Jonckheere, J. A. M. Smeitink, and R. J. T. Rodenburg, "Mitochondrial ATP synthase: architecture, function and pathology.," *Journal of inherited metabolic disease*, vol. 35, no. 2, pp. 211–25, Mar. 2012.
- [55] H. Noji, R. Yasuda, M. Yoshida, and K. Kinosita, "Direct observation of the rotation of F1-ATPase," *Nature*, vol. 386, no. 6622, pp. 299–302, Mar. 1997.
- [56] S. J. Morana, C. M. Wolf, J. Li, J. E. Reynolds, M. K. Brown, and A. Eastman, "The involvement of protein phosphatases in the activation of ICE/CED-3 protease, intracellular acidification, DNA digestion, and apoptosis.," *The Journal of biological chemistry*, vol. 271, no. 30, pp. 18263–71, Jul. 1996.

- [57] F. I. Ataulakhanov and V. M. Vitvitsky, "What determines the intracellular ATP concentration.," *Bioscience reports*, vol. 22, no. 5–6, pp. 501–11.
- [58] B. Kadenbach, R. Ramzan, L. Wen, and S. Vogt, "New extension of the Mitchell Theory for oxidative phosphorylation in mitochondria of living organisms," *Biochimica et Biophysica Acta (BBA) - General Subjects*, vol. 1800, no. 3, pp. 205–212, Mar. 2010.
- [59] G. J. Grover, P. A. Marone, L. Koetzner, and D. Seto-Young, "Energetic signalling in the control of mitochondrial F1F0 ATP synthase activity in health and disease," *The International Journal of Biochemistry & Cell Biology*, vol. 40, no. 12, pp. 2698–2701, Jan. 2008.
- [60] R. Acin-Perez, E. Salazar, M. Kamenetsky, J. Buck, L. R. Levin, and G. Manfredi, "Cyclic AMP produced inside mitochondria regulates oxidative phosphorylation.," *Cell metabolism*, vol. 9, no. 3, pp. 265–76, Mar. 2009.
- [61] M. Hüttemann, I. Lee, L. Samavati, H. Yu, and J. W. Doan, "Regulation of mitochondrial oxidative phosphorylation through cell signaling," *Biochimica et Biophysica Acta (BBA) - Molecular Cell Research*, vol. 1773, no. 12, pp. 1701–1720, Dec. 2007.
- [62] E. W. Yamada and N. J. Huzel, "Calcium-binding ATPase inhibitor protein of bovine heart mitochondria. Role in ATP synthesis and effect of Ca<sup>2+</sup>," *Biochemistry*, vol. 28, no. 25, pp. 9714–8, Dec. 1989.
- [63] G. I. Belogradov, "Recent advances in structure-functional studies of mitochondrial factor B," *Journal of Bioenergetics and Biomembranes*, vol. 41, no. 2, pp. 137–143, Apr. 2009.
- [64] M. Campanella *et al.*, "Regulation of Mitochondrial Structure and Function by the F1F0-ATPase Inhibitor Protein, IF1," *Cell Metabolism*, vol. 8, no. 1, pp. 13–25, 2008.
- [65] G. Sgarbi, S. Barbato, A. Costanzini, G. Solaini, and A. Baracca, "The role of the ATPase inhibitor factor 1 (IF1) in cancer cells adaptation to hypoxia and anoxia," *Biochimica et Biophysica Acta - Bioenergetics*, vol. 1859, no. 2, pp. 99–109, 2018.
- [66] J. García-Bermúdez and J. M. Cuezva, "The ATPase Inhibitory Factor 1 (IF1): A master regulator of energy metabolism and of cell survival," *Biochimica et Biophysica Acta - Bioenergetics*, vol. 1857, no. 8, pp. 1167–1182, 2016.
- [67] G. Cannino, F. Ciscato, I. Masgras, C. Sánchez-Martín, and A. Rasola, "Metabolic Plasticity of Tumor Cell Mitochondria," *Frontiers in Oncology*, vol. 8, p. 333, Aug. 2018.
- [68] P. E. Porporato, N. Filigheddu, J. M. B.-S. Pedro, G. Kroemer, and L. Galluzzi, "Mitochondrial metabolism and cancer," *Cell Research*, vol. 28, no. 3, pp. 265–280, Mar. 2018.
- [69] O. WARBURG, "On the origin of cancer cells.," *Science (New York, N.Y.)*, vol. 123, no. 3191, pp. 309–14, Feb. 1956.
- [70] P. S. Ward and C. B. Thompson, "Metabolic Reprogramming: A Cancer Hallmark Even Warburg Did Not Anticipate," *Cancer Cell*, vol. 21, no. 3, pp. 297–308, Mar. 2012.

- [71] K. C. Patra and N. Hay, "The pentose phosphate pathway and cancer," *Trends in Biochemical Sciences*, vol. 39, no. 8, pp. 347–354, Aug. 2014.
- [72] B. J. Altman, Z. E. Stine, and C. V. Dang, "From Krebs to clinic: glutamine metabolism to cancer therapy," *Nature Reviews Cancer*, vol. 16, no. 10, pp. 619–634, Oct. 2016.
- [73] G. Solaini, G. Sgarbi, and A. Baracca, "Oxidative phosphorylation in cancer cells," *Biochimica et Biophysica Acta (BBA) - Bioenergetics*, vol. 1807, no. 6, pp. 534–542, Jun. 2011.
- [74] S. J. Yeung, J. Pan, and M.-H. Lee, "Roles of p53, Myc and HIF-1 in Regulating Glycolysis — the Seventh Hallmark of Cancer," *Cellular and Molecular Life Sciences*, vol. 65, no. 24, pp. 3981–3999, Dec. 2008.
- [75] F. Di Lisa and P. Bernardi, "Mitochondrial function as a determinant of recovery or death in cell response to injury.," *Molecular and cellular biochemistry*, vol. 184, no. 1–2, pp. 379–91, Jul. 1998.
- [76] D. A. Harris and A. M. Das, "Control of mitochondrial ATP synthesis in the heart.," *The Biochemical journal*, vol. 280 ( Pt 3), no. Pt 3, pp. 561–73, Dec. 1991.
- [77] M. E. PULLMAN and G. C. MONROY, "A NATURALLY OCCURRING INHIBITOR OF MITOCHONDRIAL ADENOSINE TRIPHOSPHATASE.," *The Journal of biological chemistry*, vol. 238, pp. 3762–9, Nov. 1963.
- [78] G. Van Heeke *et al.*, "Recombinant bovine heart mitochondrial F1-ATPase inhibitor protein: Overproduction in Escherichia coli, purification, and structural studies," *Biochemistry*, vol. 32, no. 38, pp. 10140–10149, Sep. 1993.
- [79] "Protonic inhibition of the mitochondrial adenosine 5'-triphosphatase in ischemic cardiac muscle. Reversible binding of the ATPase inhibitor protein to the mitochondrial ATPase during ischemia," *Journal of Molecular and Cellular Cardiology*, vol. 19, no. 7, pp. 661–668, Jul. 1987.
- [80] N. Ichikawa, C. Ando, and M. Fumino, "Caenorhabditis elegans MAI-1 protein, which is similar to mitochondrial ATPase inhibitor (IF1), can inhibit yeast F0F1-ATPase but cannot be transported to yeast mitochondria," *Journal of Bioenergetics and Biomembranes*, vol. 38, no. 2, pp. 93–99, Oct. 2006.
- [81] B. NORLING, C. TOURIKAS, B. HAMASUR, and E. GLASER, "Evidence for an endogenous ATPase inhibitor protein in plant mitochondria. Purification and characterization," *European Journal of Biochemistry*, vol. 188, no. 2, pp. 247–252, Mar. 1990.
- [82] E. Cabezón, I. Arechaga, P. Jonathan, G. Butler, and J. E. Walker, "Dimerization of bovine F1-ATPase by binding the inhibitor protein, IF1.," *The Journal of biological chemistry*, vol. 275, no. 37, pp. 28353–5, Sep. 2000.
- [83] M. J. van Raaij, J. P. Abrahams, A. G. Leslie, J. E. Walker, A. Leslie, and J. Walker, "The structure of bovine F1-ATPase complexed with the antibiotic inhibitor aurovertin B.," *Proceedings of the National Academy of Sciences*, vol. 93, no. 14, pp. 6913–6917, Jul.

1996.

- [84] E. Cabezón, M. G. Montgomery, A. G. W. Leslie, and J. E. Walker, “The structure of bovine F1-ATPase in complex with its regulatory protein IF1,” *Nature Structural & Molecular Biology*, vol. 10, no. 9, pp. 744–750, Sep. 2003.
- [85] E. Cabezon, P. J. Butler, M. J. Runswick, and J. E. Walker, “Modulation of the oligomerization state of the bovine F1-ATPase inhibitor protein, IF1, by pH,” *The Journal of biological chemistry*, vol. 275, no. 33, pp. 25460–4, Aug. 2000.
- [86] “Dimerization of F0F1ATP synthase from bovine heart is independent from the binding of the inhibitor protein IF1,” *Biochimica et Biophysica Acta (BBA) - Bioenergetics*, vol. 1556, no. 2–3, pp. 133–141, Dec. 2002.
- [87] S. Barbato, G. Sgarbi, G. Gorini, A. Baracca, and G. Solaini, “The inhibitor protein (IF1) of the F1F0-ATPase modulates human osteosarcoma cell bioenergetics,” *The Journal of biological chemistry*, vol. 290, no. 10, pp. 6338–48, Mar. 2015.
- [88] “Proteomic analysis of F1F0-ATP synthase super-assembly in mitochondria of cardiomyoblasts undergoing differentiation to the cardiac lineage,” *Biochimica et Biophysica Acta (BBA) - Bioenergetics*, vol. 1827, no. 7, pp. 807–816, Jul. 2013.
- [89] \*,‡,§ José J. García, ‡ Edgar Morales-Ríos, ‡ and Paulina Cortés-Hernández, and J. S. Rodríguez-Zavala‡, “The Inhibitor Protein (IF1) Promotes Dimerization of the Mitochondrial F1F0-ATP Synthase‡,” 2006.
- [90] L. Sánchez-Cenizo *et al.*, “Up-regulation of the ATPase Inhibitory Factor 1 (IF1) of the Mitochondrial H<sup>+</sup>-ATP Synthase in Human Tumors Mediates the Metabolic Shift of Cancer Cells to a Warburg Phenotype,” *Journal of Biological Chemistry*, vol. 285, no. 33, pp. 25308–25313, Aug. 2010.
- [91] F. Bosetti, G. Yu, R. Zucchi, S. Ronca-Testoni, and G. Solaini, “Myocardial ischemic preconditioning and mitochondrial F1F0-ATPase activity,” *Molecular and Cellular Biochemistry*, vol. 215, no. 1/2, pp. 31–38, 2000.
- [92] W. Rouslin, C. W. Broge, and I. L. Grupp, “ATP depletion and mitochondrial functional loss during ischemia in slow and fast heart-rate hearts,” *American Journal of Physiology-Heart and Circulatory Physiology*, vol. 259, no. 6, pp. H1759–H1766, Dec. 1990.
- [93] W. Rouslin and C. W. Broge, “Regulation of the mitochondrial adenosine 5'-triphosphatase in situ during ischemia and in vitro in intact and sonicated mitochondria from slow and fast heart-rate hearts,” *Archives of biochemistry and biophysics*, vol. 280, no. 1, pp. 103–11, Jul. 1990.
- [94] W. ROUSLIN and C. W. BROGE, “Why the Mitochondrial ATPase Inhibitor IF1 Fails to Inhibit the Mitochondrial ATPase in Situ in Fast Heart-Rate Mammalian and Avian Hearts,” *Annals of the New York Academy of Sciences*, vol. 671, no. 1 Ion-Motive AT, pp. 505–506, Nov. 1992.
- [95] W. Rouslin, G. D. Frank, and C. W. Broge, “Content and binding characteristics of the mitochondrial ATPase inhibitor, IF1 in the tissues of several slow and fast heart-rate

- homeothermic species and in two poikilotherms,” *Journal of Bioenergetics and Biomembranes*, vol. 27, no. 1, pp. 117–125, Feb. 1995.
- [96] M. Sánchez-Aragó *et al.*, “Expression, regulation and clinical relevance of the ATPase inhibitory factor 1 in human cancers,” *Oncogenesis*, vol. 2, no. 4, pp. e46–e46, Apr. 2013.
- [97] Y.-X. Gao *et al.*, “ATPase inhibitory factor 1 expression is an independent prognostic factor in non-small cell lung cancer.,” *American journal of cancer research*, vol. 6, no. 5, pp. 1141–8, 2016.
- [98] T. Yin, L. Lu, Z. Xiong, S. Wei, and D. Cui, “ATPase inhibitory factor 1 is a prognostic marker and contributes to proliferation and invasion of human gastric cancer cells,” *Biomedicine & Pharmacotherapy*, vol. 70, pp. 90–96, Mar. 2015.
- [99] R. Song *et al.*, “Reciprocal activation between ATPase inhibitory factor 1 and NF- $\kappa$ B drives hepatocellular carcinoma angiogenesis and metastasis,” *Hepatology*, vol. 60, no. 5, pp. 1659–1673, Nov. 2014.
- [100] P. Vaupel, F. Kallinowski, and P. Okunieff, “Blood flow, oxygen and nutrient supply, and metabolic microenvironment of human tumors: a review.,” *Cancer research*, vol. 49, no. 23, pp. 6449–65, Dec. 1989.
- [101] M. Fujikawa, H. Imamura, J. Nakamura, and M. Yoshida, “Assessing actual contribution of IF1, inhibitor of mitochondrial FoF1, to ATP homeostasis, cell growth, mitochondrial morphology, and cell viability.,” *The Journal of biological chemistry*, vol. 287, no. 22, pp. 18781–7, May 2012.
- [102] L. Formentini, M. Sánchez-Aragó, L. Sánchez-Cenizo, and J. M. Cuezva, “The mitochondrial ATPase inhibitory factor 1 triggers a ROS-mediated retrograde prosurvival and proliferative response.,” *Molecular cell*, vol. 45, no. 6, pp. 731–42, Mar. 2012.
- [103] J. Zhang *et al.*, “ROS and ROS-Mediated Cellular Signaling,” *Oxidative Medicine and Cellular Longevity*, vol. 2016, pp. 1–18, Feb. 2016.
- [104] M. Campanella, A. Seraphim, R. Abeti, E. Casswell, P. Echave, and M. R. Duchon, “IF1, the endogenous regulator of the F1Fo-ATP synthase, defines mitochondrial volume fraction in HeLa cells by regulating autophagy,” *Biochimica et Biophysica Acta (BBA) - Bioenergetics*, vol. 1787, no. 5, pp. 393–401, May 2009.
- [105] G. Sgarbi, G. Gorini, F. Liuzzi, G. Solaini, and A. Baracca, “Hypoxia and IF<sub>1</sub> Expression Promote ROS Decrease in Cancer Cells.,” *Cells*, vol. 7, no. 7, Jun. 2018.
- [106] D. Faccenda *et al.*, “Control of Mitochondrial Remodeling by the ATPase Inhibitory Factor 1 Unveils a Pro-survival Relay via OPA1.,” *Cell reports*, vol. 18, no. 8, pp. 1869–1883, Feb. 2017.
- [107] D. Faccenda, C. H. Tan, A. Seraphim, M. R. Duchon, and M. Campanella, “IF1 limits the apoptotic-signalling cascade by preventing mitochondrial remodelling,” *Cell Death & Differentiation*, vol. 20, no. 5, pp. 686–697, May 2013.
- [108] H. Tanton *et al.*, “F1Fo-ATP Synthase Inhibitory Factor 1 in the Normal Pancreas and in

- Pancreatic Ductal Adenocarcinoma: Effects on Bioenergetics, Invasion and Proliferation,” *Frontiers in Physiology*, vol. 9, p. 833, Jul. 2018.
- [109] V. Lefebvre *et al.*, “Genome-wide RNAi screen identifies ATPase inhibitory factor 1 (ATPIF1) as essential for PARK2 recruitment and mitophagy,” *Autophagy*, vol. 9, no. 11, pp. 1770–1779, Nov. 2013.
- [110] L. D. Zorova *et al.*, “Mitochondrial membrane potential,” *Analytical Biochemistry*, vol. 552, pp. 50–59, Jul. 2018.
- [111] T. E. Gunter and D. R. Pfeiffer, “Mechanisms by which mitochondria transport calcium,” *American Journal of Physiology-Cell Physiology*, vol. 258, no. 5, pp. C755–C786, May 1990.
- [112] D. B. Zorov *et al.*, “The mitochondrion as Janus Bifrons,” *Biochemistry (Moscow)*, vol. 72, no. 10, pp. 1115–1126, Oct. 2007.
- [113] T. Briston *et al.*, “Mitochondrial permeability transition pore: sensitivity to opening and mechanistic dependence on substrate availability,” *Scientific Reports*, vol. 7, no. 1, p. 10492, Dec. 2017.
- [114] J. J. Lemasters *et al.*, “The mitochondrial permeability transition in cell death: a common mechanism in necrosis, apoptosis and autophagy.,” *Biochimica et biophysica acta*, vol. 1366, no. 1–2, pp. 177–96, Aug. 1998.
- [115] S. M. Jin, M. Lazarou, C. Wang, L. A. Kane, D. P. Narendra, and R. J. Youle, “Mitochondrial membrane potential regulates PINK1 import and proteolytic destabilization by PARL,” *The Journal of Cell Biology*, vol. 191, no. 5, pp. 933–942, Nov. 2010.
- [116] D. B. Zorov, M. Juhaszova, and S. J. Sollott, “Mitochondrial reactive oxygen species (ROS) and ROS-induced ROS release.,” *Physiological reviews*, vol. 94, no. 3, pp. 909–50, Jul. 2014.
- [117] D. Mokranjac and W. Neupert, “Energetics of protein translocation into mitochondria,” *Biochimica et Biophysica Acta (BBA) - Bioenergetics*, vol. 1777, no. 7–8, pp. 758–762, Jul. 2008.
- [118] H. Terada, “Uncouplers of oxidative phosphorylation.,” *Environmental health perspectives*, vol. 87, pp. 213–8, Jul. 1990.
- [119] R. J. Kessler *et al.*, “Uncouplers and the molecular mechanism of uncoupling in mitochondria.,” *Proceedings of the National Academy of Sciences of the United States of America*, vol. 74, no. 6, pp. 2241–5, Jun. 1977.
- [120] J. M. Herrmann, S. Longen, D. Weckbecker, and M. Depuydt, “Biogenesis of Mitochondrial Proteins,” Springer, New York, NY, 2012, pp. 41–64.
- [121] C. Handschin and B. M. Spiegelman, “PGC-1 Coactivators and the Regulation of Skeletal Muscle Fiber-Type Determination,” *Cell Metabolism*, vol. 13, no. 4, p. 351, Apr. 2011.



- [122] M. Uldry, W. Yang, J. St-Pierre, J. Lin, P. Seale, and B. M. Spiegelman, “Complementary action of the PGC-1 coactivators in mitochondrial biogenesis and brown fat differentiation.,” *Cell metabolism*, vol. 3, no. 5, pp. 333–41, May 2006.
- [123] V. K. Mootha *et al.*, “Erra and Gabpa/b specify PGC-1 $\alpha$ -dependent oxidative phosphorylation gene expression that is altered in diabetic muscle,” *Proceedings of the National Academy of Sciences of the United States of America*, vol. 101, no. 17, p. 6570 LP-6575, Apr. 2004.
- [124] J. E. Dominy and P. Puigserver, “Mitochondrial biogenesis through activation of nuclear signaling proteins.,” *Cold Spring Harbor perspectives in biology*, vol. 5, no. 7, p. a015008, Jul. 2013.
- [125] J. S. Chang, P. Huypens, Y. Zhang, C. Black, A. Kralli, and T. W. Gettys, “Regulation of NT-PGC-1 $\alpha$  Subcellular Localization and Function by Protein Kinase A-dependent Modulation of Nuclear Export by CRM1,” *Journal of Biological Chemistry*, vol. 285, no. 23, pp. 18039–18050, Jun. 2010.
- [126] K. Aquilano, P. Vigilanza, S. Baldelli, B. Pagliei, G. Rotilio, and M. R. Ciriolo, “Peroxisome Proliferator-activated Receptor  $\gamma$  Co-activator 1 $\alpha$  (PGC-1 $\alpha$ ) and Sirtuin 1 (SIRT1) Reside in Mitochondria,” *Journal of Biological Chemistry*, vol. 285, no. 28, pp. 21590–21599, Jul. 2010.
- [127] M. Monsalve, Z. Wu, G. Adelmant, P. Puigserver, M. Fan, and B. M. Spiegelman, “Direct coupling of transcription and mRNA processing through the thermogenic coactivator PGC-1.,” *Molecular cell*, vol. 6, no. 2, pp. 307–16, Aug. 2000.
- [128] C. A. Virbasius, J. V. Virbasius, and R. C. Scarpulla, “NRF-1, an activator involved in nuclear-mitochondrial interactions, utilizes a new DNA-binding domain conserved in a family of developmental regulators.,” *Genes & development*, vol. 7, no. 12A, pp. 2431–45, Dec. 1993.
- [129] R. C. Scarpulla, R. B. Vega, and D. P. Kelly, “Transcriptional integration of mitochondrial biogenesis,” *Trends in Endocrinology & Metabolism*, vol. 23, no. 9, pp. 459–466, Sep. 2012.
- [130] C. Cantó and J. Auwerx, “PGC-1 $\alpha$ , SIRT1 and AMPK, an energy sensing network that controls energy expenditure.,” *Current opinion in lipidology*, vol. 20, no. 2, pp. 98–105, Apr. 2009.
- [131] D. G. Hardie, “AMP-activated/SNF1 protein kinases: conserved guardians of cellular energy,” *Nature Reviews Molecular Cell Biology*, vol. 8, no. 10, pp. 774–785, Oct. 2007.
- [132] A. Brunet *et al.*, “Stress-Dependent Regulation of FOXO Transcription Factors by the SIRT1 Deacetylase,” *Science*, vol. 303, no. 5666, pp. 2011–2015, Mar. 2004.
- [133] H. Vaziri *et al.*, “hSIR2(SIRT1) functions as an NAD-dependent p53 deacetylase.,” *Cell*, vol. 107, no. 2, pp. 149–59, Oct. 2001.
- [134] F. Picard *et al.*, “Erratum: Sirt1 promotes fat mobilization in white adipocytes by repressing PPAR- $\gamma$ ,” *Nature*, vol. 429, no. 6993, pp. 771–776, Jun. 2004.

- [135] P. J. Adhietty, G. Uguccioni, L. Leick, J. Hidalgo, H. Pilegaard, and D. A. Hood, "The role of PGC-1 $\alpha$  on mitochondrial function and apoptotic susceptibility in muscle," *American Journal of Physiology-Cell Physiology*, vol. 297, no. 1, pp. C217–C225, Jul. 2009.
- [136] R. J. Youle and A. M. van der Bliek, "Mitochondrial fission, fusion, and stress.," *Science (New York, N.Y.)*, vol. 337, no. 6098, pp. 1062–5, Aug. 2012.
- [137] S. Hoppins, L. Lackner, and J. Nunnari, "The Machines that Divide and Fuse Mitochondria," *Annual Review of Biochemistry*, vol. 76, no. 1, pp. 751–780, Jun. 2007.
- [138] K. Nakada *et al.*, "Inter-mitochondrial complementation: Mitochondria-specific system preventing mice from expression of disease phenotypes by mutant mtDNA," *Nature Medicine*, vol. 7, no. 8, pp. 934–940, Aug. 2001.
- [139] M. Yoneda, T. Miyatake, and G. Attardi, "Complementation of mutant and wild-type human mitochondrial DNAs coexisting since the mutation event and lack of complementation of DNAs introduced separately into a cell within distinct organelles.," *Molecular and cellular biology*, vol. 14, no. 4, pp. 2699–712, Apr. 1994.
- [140] R. Rossignol, R. Gilkerson, R. Aggeler, K. Yamagata, S. J. Remington, and R. A. Capaldi, "Energy substrate modulates mitochondrial structure and oxidative capacity in cancer cells.," *Cancer research*, vol. 64, no. 3, pp. 985–93, Feb. 2004.
- [141] Y. Matsushima and L. S. Kaguni, "Matrix proteases in mitochondrial DNA function," *Biochimica et Biophysica Acta (BBA) - Gene Regulatory Mechanisms*, vol. 1819, no. 9–10, pp. 1080–1087, Sep. 2012.
- [142] M. Karbowski and R. J. Youle, "Regulating mitochondrial outer membrane proteins by ubiquitination and proteasomal degradation.," *Current opinion in cell biology*, vol. 23, no. 4, pp. 476–82, Aug. 2011.
- [143] W. Voos and K. Röttgers, "Molecular chaperones as essential mediators of mitochondrial biogenesis," *Biochimica et Biophysica Acta (BBA) - Molecular Cell Research*, vol. 1592, no. 1, pp. 51–62, Sep. 2002.
- [144] A. Sugiura, G.-L. McLelland, E. A. Fon, and H. M. McBride, "A new pathway for mitochondrial quality control: mitochondrial-derived vesicles," *The EMBO Journal*, vol. 33, no. 19, pp. 2142–2156, Oct. 2014.
- [145] N. Mizushima and M. Komatsu, "Autophagy: Renovation of Cells and Tissues," *Cell*, vol. 147, no. 4, pp. 728–741, Nov. 2011.
- [146] I. Tanida, T. Ueno, and E. Kominami, "LC3 and Autophagy," Humana Press, 2008, pp. 77–88.
- [147] N. G. Lipsky and P. L. Pedersen, "Mitochondrial turnover in animal cells. Half-lives of mitochondria and mitochondrial subfractions of rat liver based on [<sup>14</sup>C]bicarbonate incorporation.," *The Journal of biological chemistry*, vol. 256, no. 16, pp. 8652–7, Aug. 1981.

- [148] G. Twig *et al.*, “Fission and selective fusion govern mitochondrial segregation and elimination by autophagy,” *The EMBO Journal*, vol. 27, no. 2, pp. 433–446, Jan. 2008.
- [149] A. Stotland and R. A. Gottlieb, “Mitochondrial quality control: Easy come, easy go,” *Biochimica et Biophysica Acta - Molecular Cell Research*, vol. 1853, no. 10, pp. 2802–2811, 2015.
- [150] A. W. Greene *et al.*, “Mitochondrial processing peptidase regulates PINK1 processing, import and Parkin recruitment.,” *EMBO reports*, vol. 13, no. 4, pp. 378–85, Apr. 2012.
- [151] K. Okatsu *et al.*, “PINK1 autophosphorylation upon membrane potential dissipation is essential for Parkin recruitment to damaged mitochondria,” *Nature Communications*, vol. 3, no. 1, p. 1016, Jan. 2012.
- [152] A. Kazlauskaitė *et al.*, “Phosphorylation of Parkin at Serine65 is essential for activation: elaboration of a Miro1 substrate-based assay of Parkin E3 ligase activity.,” *Open biology*, vol. 4, no. 3, p. 130213, Mar. 2014.
- [153] L. A. Kane *et al.*, “PINK1 phosphorylates ubiquitin to activate Parkin E3 ubiquitin ligase activity.,” *The Journal of cell biology*, vol. 205, no. 2, pp. 143–53, Apr. 2014.
- [154] M. E. Gegg, J. M. Cooper, K.-Y. Chau, M. Rojo, A. H. V. Schapira, and J.-W. Taanman, “Mitofusin 1 and mitofusin 2 are ubiquitinated in a PINK1/parkin-dependent manner upon induction of mitophagy,” *Human Molecular Genetics*, vol. 19, no. 24, pp. 4861–4870, Dec. 2010.
- [155] C. Ploumi, I. Daskalaki, and N. Tavernarakis, “Mitochondrial biogenesis and clearance: a balancing act,” *The FEBS Journal*, vol. 284, no. 2, pp. 183–195, Jan. 2017.
- [156] Å. B. Gustafsson, “Bnip3 as a Dual Regulator of Mitochondrial Turnover and Cell Death in the Myocardium,” *Pediatric Cardiology*, vol. 32, no. 3, pp. 267–274, Mar. 2011.
- [157] A. H. Chourasia, M. L. Boland, and K. F. Macleod, “Mitophagy and cancer,” *Cancer & Metabolism*, vol. 3, no. 1, p. 4, Dec. 2015.
- [158] M. Chen *et al.*, “Mitophagy receptor FUNDC1 regulates mitochondrial dynamics and mitophagy,” *Autophagy*, vol. 12, no. 4, pp. 689–702, Apr. 2016.
- [159] J. Zhang and P. A. Ney, “Role of BNIP3 and NIX in cell death, autophagy and mitophagy,” *Cell Death & Differentiation*, vol. 16, no. 7, pp. 939–946, Jul. 2009.
- [160] Y. Zhu *et al.*, “Modulation of Serines 17 and 24 in the LC3-interacting Region of Bnip3 Determines Pro-survival Mitophagy versus Apoptosis,” *Journal of Biological Chemistry*, vol. 288, no. 2, pp. 1099–1113, Jan. 2013.
- [161] S. Saita, M. Shirane, and K. I. Nakayama, “Selective escape of proteins from the mitochondria during mitophagy,” *Nature Communications*, vol. 4, no. 1, p. 1410, Dec. 2013.
- [162] F. Gao *et al.*, “The mitochondrial protein BNIP3L is the substrate of PARK2 and mediates mitophagy in PINK1/PARK2 pathway,” *Human Molecular Genetics*, vol. 24, no. 9, pp.

2528–2538, May 2015.

- [163] T. Zhang *et al.*, “BNIP3 Protein Suppresses PINK1 Kinase Proteolytic Cleavage to Promote Mitophagy.,” *The Journal of biological chemistry*, vol. 291, no. 41, pp. 21616–21629, Oct. 2016.
- [164] Y. Lee, H.-Y. Lee, R. A. Hanna, and Å. B. Gustafsson, “Mitochondrial autophagy by Bnip3 involves Drp1-mediated mitochondrial fission and recruitment of Parkin in cardiac myocytes.,” *American journal of physiology. Heart and circulatory physiology*, vol. 301, no. 5, pp. H1924-31, Nov. 2011.
- [165] R. L. Mort, I. J. Jackson, and E. E. Patton, “The melanocyte lineage in development and disease,” *Development*, vol. 142, no. 4, pp. 620–632, Feb. 2015.
- [166] J. Y. Lin and D. E. Fisher, “Melanocyte biology and skin pigmentation,” *Nature*, vol. 445, no. 7130, pp. 843–850, Feb. 2007.
- [167] A. H. Shain and B. C. Bastian, “From melanocytes to melanomas,” *Nature Reviews Cancer*, vol. 16, no. 6, pp. 345–358, Jun. 2016.
- [168] B. Domingues, J. M. Lopes, P. Soares, and H. Pópulo, “Melanoma treatment in review.,” *ImmunoTargets and therapy*, vol. 7, pp. 35–49, 2018.
- [169] Z. Ali, N. Yousaf, and J. Larkin, “Melanoma epidemiology, biology and prognosis.,” *EJC supplements : EJC : official journal of EORTC, European Organization for Research and Treatment of Cancer ... [et al.]*, vol. 11, no. 2, pp. 81–91, Sep. 2013.
- [170] J. Ferlay *et al.*, “Cancer incidence and mortality worldwide: Sources, methods and major patterns in GLOBOCAN 2012,” *International Journal of Cancer*, vol. 136, no. 5, pp. E359–E386, Mar. 2015.
- [171] M. Rastrelli, S. Tropea, C. R. Rossi, and M. Alaibac, “Melanoma: epidemiology, risk factors, pathogenesis, diagnosis and classification.,” *In vivo (Athens, Greece)*, vol. 28, no. 6, pp. 1005–11, Nov. 2014.
- [172] J. A. Lo and D. E. Fisher, “The melanoma revolution: from UV carcinogenesis to a new era in therapeutics.,” *Science (New York, N.Y.)*, vol. 346, no. 6212, pp. 945–9, Nov. 2014.
- [173] A. Niezgoda, P. Niezgoda, and R. Czajkowski, “Novel Approaches to Treatment of Advanced Melanoma: A Review on Targeted Therapy and Immunotherapy.,” *BioMed research international*, vol. 2015, p. 851387, Jun. 2015.
- [174] R. L. Siegel, K. D. Miller, and A. Jemal, “Cancer statistics, 2016,” *CA: A Cancer Journal for Clinicians*, vol. 66, no. 1, pp. 7–30, Jan. 2016.
- [175] T. M. Grzywa, W. Paskal, and P. K. Włodarski, “Intratumor and Intertumor Heterogeneity in Melanoma,” *Translational Oncology*, vol. 10, no. 6, pp. 956–975, Dec. 2017.
- [176] B. Govindarajan *et al.*, “Malignant transformation of melanocytes to melanoma by constitutive activation of mitogen-activated protein kinase kinase (MAPKK) signaling.,” *The Journal of biological chemistry*, vol. 278, no. 11, pp. 9790–5, Mar. 2003.

- [177] M. Colombino *et al.*, “BRAF/NRAS mutation frequencies among primary tumors and metastases in patients with melanoma,” *Journal of clinical oncology : official journal of the American Society of Clinical Oncology*, vol. 30, no. 20, pp. 2522–9, Jul. 2012.
- [178] J.-H. Lee, J.-W. Choi, and Y.-S. Kim, “Frequencies of BRAF and NRAS mutations are different in histological types and sites of origin of cutaneous melanoma: a meta-analysis,” *British Journal of Dermatology*, vol. 164, no. 4, pp. 776–784, Apr. 2011.
- [179] M. Kiuru and K. J. Busam, “The NF1 gene in tumor syndromes and melanoma,” *Laboratory investigation; a journal of technical methods and pathology*, vol. 97, no. 2, pp. 146–157, 2017.
- [180] R. Cancer Genome Atlas Network *et al.*, “Genomic Classification of Cutaneous Melanoma,” *Cell*, vol. 161, no. 7, pp. 1681–96, Jun. 2015.
- [181] J. M. Stahl *et al.*, “Deregulated Akt3 Activity Promotes Development of Malignant Melanoma,” *Cancer Research*, vol. 64, no. 19, pp. 7002–7010, Oct. 2004.
- [182] M. Stark and N. Hayward, “Genome-Wide Loss of Heterozygosity and Copy Number Analysis in Melanoma Using High-Density Single-Nucleotide Polymorphism Arrays,” *Cancer Research*, vol. 67, no. 6, pp. 2632–2642, Mar. 2007.
- [183] L. A. Garraway *et al.*, “Integrative genomic analyses identify MITF as a lineage survival oncogene amplified in malignant melanoma,” *Nature*, vol. 436, no. 7047, pp. 117–122, Jul. 2005.
- [184] P. A. Ascierto *et al.*, “The role of BRAF V600 mutation in melanoma,” *Journal of Translational Medicine*, vol. 10, no. 1, p. 85, Jul. 2012.
- [185] M. Cargnello and P. P. Roux, “Activation and function of the MAPKs and their substrates, the MAPK-activated protein kinases,” *Microbiology and molecular biology reviews : MMBR*, vol. 75, no. 1, pp. 50–83, Mar. 2011.
- [186] H. Lavoie and M. Therrien, “Regulation of RAF protein kinases in ERK signalling,” *Nature Reviews Molecular Cell Biology*, vol. 16, no. 5, pp. 281–298, May 2015.
- [187] P. T. C. Wan *et al.*, “Mechanism of activation of the RAF-ERK signaling pathway by oncogenic mutations of B-RAF,” *Cell*, vol. 116, no. 6, pp. 855–67, Mar. 2004.
- [188] H. Tsao, L. Chin, L. A. Garraway, and D. E. Fisher, “Melanoma: from mutations to medicine,” *Genes & Development*, vol. 26, no. 11, pp. 1131–1155, Jun. 2012.
- [189] G. Leonardi *et al.*, “Cutaneous melanoma: From pathogenesis to therapy (Review),” *International Journal of Oncology*, vol. 52, no. 4, pp. 1071–1080, Feb. 2018.
- [190] M. Winder and A. Virós, “Mechanisms of Drug Resistance in Melanoma,” Springer, Berlin, Heidelberg, 2017, pp. 1–18.
- [191] J. J. Luke, K. T. Flaherty, A. Ribas, and G. V. Long, “Targeted agents and immunotherapies: optimizing outcomes in melanoma,” *Nature Reviews Clinical Oncology*, vol. 14, no. 8, pp. 463–482, Apr. 2017.

- [192] P. H. Pandya, M. E. Murray, K. E. Pollok, and J. L. Renbarger, “The Immune System in Cancer Pathogenesis: Potential Therapeutic Approaches,” *Journal of immunology research*, vol. 2016, p. 4273943, 2016.
- [193] Y. K. Chae *et al.*, “Current landscape and future of dual anti-CTLA4 and PD-1/PD-L1 blockade immunotherapy in cancer; lessons learned from clinical trials with melanoma and non-small cell lung cancer (NSCLC),” *Journal for ImmunoTherapy of Cancer*, vol. 6, no. 1, p. 39, Dec. 2018.
- [194] G. Bollag *et al.*, “Vemurafenib: the first drug approved for BRAF-mutant cancer,” *Nature Reviews Drug Discovery*, vol. 11, no. 11, pp. 873–886, Nov. 2012.
- [195] A. A. Samatar and P. I. Poulikakos, “Targeting RAS–ERK signalling in cancer: promises and challenges,” *Nature Reviews Drug Discovery*, vol. 13, no. 12, pp. 928–942, Dec. 2014.
- [196] P. I. Poulikakos, C. Zhang, G. Bollag, K. M. Shokat, and N. Rosen, “RAF inhibitors transactivate RAF dimers and ERK signalling in cells with wild-type BRAF,” *Nature*, vol. 464, no. 7287, pp. 427–430, Mar. 2010.
- [197] A. Hauschild *et al.*, “Dabrafenib in BRAF-mutated metastatic melanoma: a multicentre, open-label, phase 3 randomised controlled trial,” *The Lancet*, vol. 380, no. 9839, pp. 358–365, Jul. 2012.
- [198] P. B. Chapman *et al.*, “Improved Survival with Vemurafenib in Melanoma with BRAF V600E Mutation,” *New England Journal of Medicine*, vol. 364, no. 26, pp. 2507–2516, Jun. 2011.
- [199] J. L. Manzano *et al.*, “Resistant mechanisms to BRAF inhibitors in melanoma,” *Annals of translational medicine*, vol. 4, no. 12, p. 237, Jun. 2016.
- [200] A. Eulalio, E. Huntzinger, and E. Izaurralde, “Getting to the root of miRNA-mediated gene silencing,” *Cell*, vol. 132, no. 1, pp. 9–14, Jan. 2008.
- [201] S. Barbato, G. Solaini, and M. Fabbri, “MicroRNAs in Oncogenesis and Tumor Suppression,” in *International review of cell and molecular biology*, vol. 333, 2017, pp. 229–268.
- [202] N. Tétreault and V. De Guire, “miRNAs: Their discovery, biogenesis and mechanism of action,” *Clinical Biochemistry*, vol. 46, no. 10–11, pp. 842–845, Jul. 2013.
- [203] L. P. Lim *et al.*, “Microarray analysis shows that some microRNAs downregulate large numbers of target mRNAs,” *Nature*, vol. 433, no. 7027, pp. 769–773, Feb. 2005.
- [204] M. Selbach, B. Schwanhäusser, N. Thierfelder, Z. Fang, R. Khanin, and N. Rajewsky, “Widespread changes in protein synthesis induced by microRNAs,” *Nature*, vol. 455, no. 7209, pp. 58–63, Sep. 2008.
- [205] G. M. Fischer, Y. N. Vashisht Gopal, J. L. McQuade, W. Peng, R. J. DeBerardinis, and M. A. Davies, “Metabolic strategies of melanoma cells: Mechanisms, interactions with the tumor microenvironment, and therapeutic implications,” *Pigment Cell & Melanoma Research*, vol. 31, no. 1, pp. 11–30, Jan. 2018.

- [206] A. Thyagarajan, A. Shaban, and R. P. Sahu, “MicroRNA-Directed Cancer Therapies: Implications in Melanoma Intervention,” *Journal of Pharmacology and Experimental Therapeutics*, vol. 364, no. 1, p. 1 LP-12, Jan. 2018.
- [207] A. Gajos-Michniewicz, M. Duechler, and M. Czyz, “MiRNA in melanoma-derived exosomes,” *Cancer Letters*, vol. 347, no. 1, pp. 29–37, May 2014.
- [208] G. Romano and L. N. Kwong, “miRNAs, Melanoma and Microenvironment: An Intricate Network.,” *International journal of molecular sciences*, vol. 18, no. 11, Nov. 2017.
- [209] Z. Steinhart and S. Angers, “Wnt signaling in development and tissue homeostasis,” *Development*, vol. 145, no. 11, p. dev146589, Jun. 2018.
- [210] S. Spranger, R. Bao, and T. F. Gajewski, “Melanoma-intrinsic  $\beta$ -catenin signalling prevents anti-tumour immunity,” *Nature*, vol. 523, no. 7559, pp. 231–235, Jul. 2015.
- [211] J. L. Wrana and L. Attisano, “The Smad pathway,” *Cytokine & Growth Factor Reviews*, vol. 11, no. 1–2, pp. 5–13, Apr. 2000.
- [212] M. Morikawa, R. Derynck, and K. Miyazono, “TGF- $\beta$  and the TGF- $\beta$  Family: Context-Dependent Roles in Cell and Tissue Physiology,” *Cold Spring Harbor Perspectives in Biology*, vol. 8, no. 5, p. a021873, May 2016.
- [213] V. Syed, “TGF- $\beta$  Signaling in Cancer,” *Journal of Cellular Biochemistry*, vol. 117, no. 6, pp. 1279–1287, Jun. 2016.
- [214] N. S. Nagaraj and P. K. Datta, “Targeting the transforming growth factor- $\beta$  signaling pathway in human cancer,” *Expert Opinion on Investigational Drugs*, vol. 19, no. 1, pp. 77–91, Jan. 2010.
- [215] G. B. Carballo, J. R. Honorato, G. P. F. de Lopes, and T. C. L. de S. e Spohr, “A highlight on Sonic hedgehog pathway,” *Cell Communication and Signaling*, vol. 16, no. 1, p. 11, Dec. 2018.
- [216] B. Stecca and A. Ruiz i Altaba, “Context-dependent Regulation of the GLI Code in Cancer by HEDGEHOG and Non-HEDGEHOG Signals,” *Journal of Molecular Cell Biology*, vol. 2, no. 2, pp. 84–95, Apr. 2010.
- [217] E. A. Barnes, M. Kong, V. Ollendorff, and D. J. Donoghue, “Patched1 interacts with cyclin B1 to regulate cell cycle progression,” *The EMBO Journal*, vol. 20, no. 9, pp. 2214–2223, May 2001.
- [218] F. Faião-Flores *et al.*, “Targeting the hedgehog transcription factors GLI1 and GLI2 restores sensitivity to vemurafenib-resistant human melanoma cells,” *Oncogene*, vol. 36, no. 13, pp. 1849–1861, Mar. 2017.
- [219] S. L. Harris and A. J. Levine, “The p53 pathway: positive and negative feedback loops,” *Oncogene 2005 24:17*, vol. 24, no. 17, p. 2899, Apr. 2005.
- [220] A. Mandinova and S. W. Lee, “The p53 pathway as a target in cancer therapeutics: obstacles and promise.,” *Science translational medicine*, vol. 3, no. 64, p. 64rv1, Jan.

2011.

- [221] N. F. Box, T. O. Vukmer, and T. Terzian, "Targeting p53 in melanoma.," *Pigment cell & melanoma research*, vol. 27, no. 1, pp. 8–10, Jan. 2014.
- [222] F. Sabbatino *et al.*, "PDGFR $\alpha$  up-regulation mediated by sonic hedgehog pathway activation leads to BRAF inhibitor resistance in melanoma cells with BRAF mutation.," *Oncotarget*, vol. 5, no. 7, pp. 1926–41, Apr. 2014.
- [223] W. S. Pear, M. L. Scott, and G. P. Nolan, "Generation of High-Titer, Helper-Free Retroviruses by Transient Transfection," in *Gene Therapy Protocols*, New Jersey: Humana Press, pp. 41–58.
- [224] P. Trinder, "Determination of blood glucose using an oxidase-peroxidase system with a non-carcinogenic chromogen.," *Journal of clinical pathology*, vol. 22, no. 2, pp. 158–61, Mar. 1969.
- [225] J. H. Waterborg and H. R. Matthews, "The Lowry Method for Protein Quantitation," in *Proteins*, New Jersey: Humana Press, 1984, pp. 1–4.
- [226] T. Shintani and D. J. Klionsky, "Autophagy in health and disease: a double-edged sword.," *Science (New York, N.Y.)*, vol. 306, no. 5698, pp. 990–5, Nov. 2004.
- [227] J. L. Brunelle and R. Green, "Coomassie Blue Staining," *Methods in Enzymology*, vol. 541, pp. 161–167, Jan. 2014.
- [228] G. Sgarbi *et al.*, "Mitochondria hyperfusion and elevated autophagic activity are key mechanisms for cellular bioenergetic preservation in centenarians," *Aging*, vol. 6, no. 4, pp. 296–310, Apr. 2014.
- [229] M. Safran and W. G. Kaelin, "HIF hydroxylation and the mammalian oxygen-sensing pathway," *Journal of Clinical Investigation*, vol. 111, no. 6, pp. 779–783, Mar. 2003.
- [230] T. Mosmann, "Rapid colorimetric assay for cellular growth and survival: Application to proliferation and cytotoxicity assays," *Journal of Immunological Methods*, vol. 65, no. 1, pp. 55–63, 1983.
- [231] D. S. McNabb, R. Reed, and R. A. Marciniak, "Dual Luciferase Assay System for Rapid Assessment of Gene Expression in *Saccharomyces cerevisiae*," *Eukaryotic Cell*, vol. 4, no. 9, p. 1539 LP-1549, Sep. 2005.
- [232] H. Dweep and N. Gretz, "miRWalk2.0: a comprehensive atlas of microRNA-target interactions," *Nature Methods*, vol. 12, p. 697, Jul. 2015.
- [233] C. P. Goswami and H. Nakshatri, "PROGmiR: a tool for identifying prognostic miRNA biomarkers in multiple cancers using publicly available data.," *Journal of clinical bioinformatics*, vol. 2, no. 1, p. 23, Dec. 2012.
- [234] J. Yang *et al.*, "The Impact of GFP Reporter Gene Transduction and Expression on Metabolomics of Placental Mesenchymal Stem Cells Determined by UHPLC-Q/TOF-MS.," *Stem cells international*, vol. 2017, p. 3167985, 2017.



- [235] J. V. F. Coumans, D. Gau, A. Poljak, V. Wasinger, P. Roy, and P. Moens, “Green fluorescent protein expression triggers proteome changes in breast cancer cells,” *Experimental cell research*, vol. 320, no. 1, pp. 33–45, Jan. 2014.
- [236] “Quenching of Fluorescence,” in *Principles of Fluorescence Spectroscopy*, Boston, MA: Springer US, 2006, pp. 277–330.
- [237] S.-K. Kim *et al.*, “Resveratrol Induces Hepatic Mitochondrial Biogenesis Through the Sequential Activation of Nitric Oxide and Carbon Monoxide Production,” *Antioxidants & Redox Signaling*, vol. 20, no. 16, pp. 2589–2605, Jun. 2014.
- [238] L. A. Meira Martins *et al.*, “The Interplay Between Apoptosis, Mitophagy and Mitochondrial Biogenesis Induced by Resveratrol Can Determine Activated Hepatic Stellate Cells Death or Survival,” *Cell Biochemistry and Biophysics*, vol. 71, no. 2, pp. 657–672, Mar. 2015.
- [239] T. Zhan, N. Rindtorff, and M. Boutros, “Wnt signaling in cancer,” *Oncogene*, vol. 36, no. 11, pp. 1461–1473, Mar. 2017.
- [240] T. Sinnberg *et al.*, “ $\beta$ -Catenin signaling increases during melanoma progression and promotes tumor cell survival and chemoresistance,” *PloS one*, vol. 6, no. 8, p. e23429, 2011.
- [241] T. Sinnberg *et al.*, “A Nexus Consisting of Beta-Catenin and Stat3 Attenuates BRAF Inhibitor Efficacy and Mediates Acquired Resistance to Vemurafenib,” *EBioMedicine*, vol. 8, pp. 132–149, Jun. 2016.
- [242] N. Bhatia *et al.*, “Gli2 Is Targeted for Ubiquitination and Degradation by  $\beta$ -TrCP Ubiquitin Ligase,” *Journal of Biological Chemistry*, vol. 281, no. 28, pp. 19320–19326, Jul. 2006.
- [243] A. W. Lau, H. Fukushima, and W. Wei, “The Fbw7 and betaTRCP E3 ubiquitin ligases and their roles in tumorigenesis,” *Frontiers in bioscience (Landmark edition)*, vol. 17, pp. 2197–212, Jun. 2012.
- [244] B. I. Ratnikov, D. A. Scott, A. L. Osterman, J. W. Smith, and Z. A. Ronai, “Metabolic rewiring in melanoma,” *Oncogene*, vol. 36, no. 2, pp. 147–157, Jan. 2017.
- [245] M. Fujikawa, H. Imamura, J. Nakamura, and M. Yoshida, “Assessing actual contribution of IF1, inhibitor of mitochondrial FoF1, to ATP homeostasis, cell growth, mitochondrial morphology, and cell viability,” *Journal of Biological Chemistry*, vol. 287, no. 22, pp. 18781–18787, 2012.
- [246] A. Busse and U. Keilholz, “Role of TGF- $\beta$  in Melanoma,” *Current Pharmaceutical Biotechnology*, vol. 12, no. 12, pp. 2165–2175, Dec. 2011.
- [247] F. Fang, T. Song, T. Zhang, Y. Cui, G. Zhang, and Q. Xiong, “MiR-425-5p promotes invasion and metastasis of hepatocellular carcinoma cells through SCAI-mediated dysregulation of multiple signaling pathways,” *Oncotarget*, vol. 8, no. 19, pp. 31745–31757, May 2017.

- [248] Z. ZHANG *et al.*, “microRNA-425-5p is upregulated in human gastric cancer and contributes to invasion and metastasis in vitro and in vivo,” *Experimental and Therapeutic Medicine*, vol. 9, no. 5, pp. 1617–1622, May 2015.
- [249] G. Di Leva *et al.*, “Estrogen Mediated-Activation of miR-191/425 Cluster Modulates Tumorigenicity of Breast Cancer Cells Depending on Estrogen Receptor Status,” *PLoS Genetics*, vol. 9, no. 3, p. e1003311, Mar. 2013.
- [250] I. Cristóbal, J. Madoz-Gúrpide, F. Rojo, and J. García-Foncillas, “Potential therapeutic value of miR-425-5p in metastatic colorectal cancer.,” *Journal of cellular and molecular medicine*, vol. 20, no. 11, pp. 2213–2214, 2016.
- [251] Y. Zhang *et al.*, “MicroRNA-425-5p regulates chemoresistance in colorectal cancer cells via regulation of Programmed Cell Death 10,” *Journal of Cellular and Molecular Medicine*, vol. 20, no. 2, pp. 360–369, Feb. 2016.
- [252] V. Vaira *et al.*, “MicroRNA-425-3p predicts response to sorafenib therapy in patients with hepatocellular carcinoma,” *Liver International*, vol. 35, no. 3, pp. 1077–1086, Mar. 2015.

# 7 Images Sources

**Figure 1:** (A).Mitochondrion (biology)-Images|Britannica.com. Available at: <https://www.britannica.com/science/mitochondrion/images-videos/media/386130/17869>. (B) 1.8.2 Applications and skills: 8.2.2 Perspectives on mitochondria and chloroplasts. Available at: [https://www.philpoteducation.com/mod/book/view.php?id=805&chapterid=1076#](https://www.philpoteducation.com/mod/book/view.php?id=805&chapterid=1076#/).

**Figure 2:** van der Laan, M., Bohnert, M., Wiedemann, N. & Pfanner, N. Role of MINOS in mitochondrial membrane architecture and biogenesis. *Trends in Cell Biology* 22, 185–192 (2012).

**Figure 3:** Nadege, B. Mitochondria: from bioenergetics to the metabolic regulation of carcinogenesis. *Frontiers in Bioscience Volume*, 4015 (2009).

**Figure 4:** KEGG PATHWAY: Oxidative phosphorylation - Homo sapiens (human) Available at: [https://www.genome.jp/kegg-bin/show\\_pathway?hsa00190](https://www.genome.jp/kegg-bin/show_pathway?hsa00190)

**Figure 5:** Taurino, F. & Gnoni, A. Systematic review of plasma-membrane ecto-ATP synthase: A new player in health and disease. *Experimental and Molecular Pathology* 104, 59–70 (2018).

**Figure 6:** Available at: <http://6e.plantphys.net/ch/12/wt12.04/wt1104a.png>

**Figure 7:** Faccenda, D. & Campanella, M. Molecular regulation of the mitochondrial F1Fo-ATP synthase: Physiological and pathological significance of the Inhibitory Factor 1 (IF1). *International Journal of Cell Biology* (2012). doi:10.1155/2012/367934

**Figure 8:** De Castro, I. P., Martins, L. M. & Tufi, R. Mitochondrial quality control and neurological disease: An emerging connection. *Expert Reviews in Molecular Medicine* 12, (2010).

**Figure 9:** Stotland, A. & Gottlieb, R. A. Mitochondrial quality control: Easy come, easy go. *Biochimica et Biophysica Acta - Molecular Cell Research* 1853, 2802–2811 (2015).

**Figure 10:** Cai, Q. & Tammineni, P. Alterations in Mitochondrial Quality Control in Alzheimer's Disease. *Frontiers in Cellular Neuroscience* 10, (2016).

**Figure 11:** McWilliams, T. G. & Muqit, M. M. PINK1 and Parkin: emerging themes in mitochondrial homeostasis. *Current Opinion in Cell Biology* 45, 83–91 (2017).

**Figure 12:** Available at: <https://medivizor.com/blog/wp-content/uploads/2016/05/image5.jpeg>.

**Figure 13:** Samatar, A. A. & Poulidakos, P. I. Targeting RAS-ERK signalling in cancer: Promises and challenges. *Nature Reviews Drug Discovery* 13, 928–942 (2014).

**Figure 14:** Thyagarajan, A., Shaban, A. & Sahu, R. P. MiRNA directed cancer therapies: Implications in melanoma intervention. *Journal of Pharmacology and Experimental Therapeutics* jpet.117.242636 (2017). doi:10.1124/jpet.117.242636

**Figure 15:** MacDonald, B. T., Tamai, K. & He, X. Wnt/ $\beta$ -Catenin Signaling: Components, Mechanisms, and Diseases. *Developmental Cell* 17, 9–26 (2009).

**Figure 16:** Ikushima, H. & Miyazono, K. TGF $\beta$  2 signalling: A complex web in cancer progression. *Nature Reviews Cancer* 10, 415–424 (2010).

**Figure 17:** Fernandes-Silva, H., Correia-Pinto, J. & Moura, R. Canonical Sonic Hedgehog Signaling in Early Lung Development. *Journal of Developmental Biology* 5, 3 (2017).